# Monitoring of real time cGMP dynamics in hypoxic injury and atrial fibrillation to better understand and treat cardiovascular disease

Doctoral Thesis

University of Hamburg

Faculty of Mathematics, Informatics and Natural Sciences

Department of Chemistry

Submitted by

## Nadja Irene Bork

Hamburg, March 2020

Die vorliegende Arbeit „Monitoring of real time cGMP dynamics in hypoxic injury and atrial fibrillation to better understand and treat cardiovascular disease" wurde am Institut für Experimentelle Herz-Kreislaufforschung des Universitätsklinikums Hamburg-Eppendorf im Zeitraum 01. April 2016 – 31. März 2020 angefertigt.

# List of Publications

**Bork NI**, Molina CE, Nikolaev VO. cGMP signalling in cardiomyocyte microdomains. Biochem Soc Trans. 2019;47(5):1327-1339.

Stathopoulou K, Schobesberger S, **Bork NI**, Sprenger JU, Perera RK, Sotoud H, Geertz B, David JP, Christ T, Nikolaev VO, Cuello F. Divergent off-target effects of RSK N-terminal and C-terminal kinase inhibitors in cardiac myocytes. Cell Signal. 2019;63:109362.

Ruthenbeck A, Marangoni E, Diercks BP, Krüger A, Froese A, **Bork NI**, Nikolaev VO, Guse AH, Meier C. Membrane-Permeable Octanoyloxybenzyl-Masked cNMPs As Novel Tools for Non-Invasive Cell Assays. Molecules. 2018;23(11).

Jungen C, Scherschel K, **Bork NI**, Kuklik P, Eickholt C, Kniep H, Klatt N, Willems S, Nikolaev VO, Meyer C. Impact of Intracardiac Neurons on Cardiac Electrophysiology and Arrhythmogenesis in an Ex Vivo Langendorff System. J Vis Exp. 2018(135).

Wright PT, Bhogal NK, Diakonov I, Pannell LMK, Perera RK, **Bork NI**, Schobesberger S, Lucarelli C, Faggian G, Alvarez-Laviada A, Zaccolo M, Kamp TJ, Balijepalli RC, Lyon AR, Harding SE, Nikolaev VO, Gorelik J. Cardiomyocyte Membrane Structure and cAMP Compartmentation Produce Anatomical Variation in beta2AR-cAMP Responsiveness in Murine Hearts. Cell Rep. 2018;23(2):459-469.

**Bork NI**, Nikolaev VO. cGMP Signaling in the Cardiovascular System-The Role of Compartmentation and Its Live Cell Imaging. Int J Mol Sci. 2018;19(3).

**Bork NI**, Nikolaev VO. Receptor-Cyclic Nucleotide Microdomains in the Heart. In: Nikolaev V, Zaccolo M, editors. Microdomains in the Cardiovascular System. Cham: Springer International Publishing; 2017. p. 3-15.

Perera RK, Fischer TH, Wagner M, Dewenter M, Vettel C, **Bork NI**, Maier LS, Conti M, Wess J, El-Armouche A, Hasenfuss G, Nikolaev VO. Atropine augments cardiac contractility by inhibiting cAMP-specific phosphodiesterase type 4. Sci Rep. 2017;7(1):15222.

Frankenreiter S, Bednarczyk P, Kniess A, **Bork NI**, Straubinger J, Koprowski P, Wrzosek A, Mohr E, Logan A, Murphy MP, Gawaz M, Krieg T, Szewczyk A, Nikolaev VO, Ruth P, Lukowski R. cGMP-Elevating Compounds and Ischemic Conditioning Provide Cardioprotection Against Ischemia and Reperfusion Injury via Cardiomyocyte-Specific BK Channels. Circulation. 2017;136(24):2337-2355.

Straubinger J, Boldt K, Kuret A, Deng L, Krattenmacher D, **Bork N**, Desch M, Feil R, Feil S, Nemer M, Ueffing M, Ruth P, Just S, Lukowski R. Amplified pathogenic actions of angiotensin II in cysteine-rich LIM-only protein 4-negative mouse hearts. FASEB J. 2017;31(4):1620-1638.

Jungen C, Scherschel K, Eickholt C, Kuklik P, Klatt N, **Bork N**, Salzbrunn T, Alken F, Angendohr S, Klene C, Mester J, Klöcker N, Veldkamp MW, Schumacher U, Willems S, Nikolaev VO, Meyer C. Disruption of cardiac cholinergic neurons enhances susceptibility to ventricular arrhythmias. Nat Commun. 2017;8:14155.

Sprenger JU, **Bork NI**, Herting J, Fischer TH, Nikolaev VO. Interactions of Calcium Fluctuations during Cardiomyocyte Contraction with Real-Time cAMP Dynamics Detected by FRET. PLoS One. 2016;11(12):e0167974.

Straubinger J, Schöttle V, **Bork N**, Subramanian H, Dunnes S, Russwurm M, Gawaz M, Friebe A, Nemer M, Nikolaev VO, Lukowski R. Sildenafil Does Not Prevent Heart Hypertrophy and Fibrosis Induced by Cardiomyocyte Angiotensin II Type 1 Receptor Signaling. J Pharmacol Exp Ther. 2015;354(3):406-416.

Yang W, Burkhardt B, Fischer L, Beirow M, **Bork N**, Wönne EC, Wagner C, Husen B, Zeilinger K, Liu L, Nussler AK. Age-dependent changes of the antioxidant system in rat livers are accompanied by altered MAPK activation and a decline in motor signaling. EXCLI J. 2015;14:1273-1290.

# Contents

# List of Tables

# List of Figures

# List of Abbreviations

| | |
|---|---|
| AAD | Antiarrhythmic drug |
| AC | Adenylyl cyclase |
| ACE | Angiotensin converting enzyme |
| AF | Atrial fibrillation |
| $\alpha$MHC | $\alpha$-Myosin heavy chain |
| AMP | Adenosine monophosphate |
| ANP | Atrial natriuretic peptide |
| APD | Action potential duration |
| APS | Ammonium persulfate |
| AT1 | Angiotensin II type 1 |
| ATP | Adenosine triphosphate |
| $\beta$AR | $\beta$-Adrenergic receptor |
| bp | Base pair |
| BDM | 2,3-Butandione monoxime |
| BFP | Blue fluorescent protein |
| BK channel | $Ca^{2+}$-activated $K^+$ channel |
| BNP | Brain natriuretic peptide |
| BPM | Beats per minute |
| BSA | Bovine serum albumin |
| $Ca^{2+}$ | Calcium |
| CaMKII | $Ca^{2+}$/calmodulin-dependent protein kinase II |
| cAMP | 3',5'-cyclic adenosine monophosphate |
| CBP | CREB-binding protein |
| CFP | Cyan fluorescent protein |
| cGMP | 3',5'-cyclic guanosine monophosphate |
| CHX | Cycloheximide |
| CMOS | Complementary metal oxide semiconductor |
| cMyBP-C | Cardiac myosin binding protein C |
| CNG | Cyclic-nucleotide-gated channel |
| CNP | C-type natriuretic peptide |
| $CO_2$ | Carbon dioxide |
| CREB | cAMP-responsive element-binding protein |
| CVD | Cardiovascular disease |
| D2 | Dimer2 |
| DAD | Delayed after depolarization |

| | |
|---|---|
| DAG | Diacylglycerol |
| DCM | Dilated cardiomyopathy |
| $ddH_2O$ | Double-distilled $H_2O$ |
| DMEM | Dulbecco's Modified Eagle's Medium |
| DMSO | Dimethyl sulfoxide |
| E | Efficiency |
| EAD | Early after depolarization |
| ECC | Excitation-contraction coupling |
| EDTA | Ethylenediaminetetraacetic acid |
| EGTA | Ethyleneglycoltetraacetic acid |
| eNOS | Endothelial NOS |
| ESC | European Society of Cardiology |
| FCS | Fetal calf serum |
| FIH | Factor-inhibiting HIF |
| FRET | Förster resonance energy transfer |
| GC | Guanylyl cyclase |
| GC-1 | $NO\text{-}GC\alpha_1\beta_1$ |
| GC-2 | $NO\text{-}GC\alpha_2\beta_1$ |
| GFP | Green fluorescent protein |
| GHS | Globally harmonized system of classification and labelling of chemicals |
| GMP | Guanosine monophosphate |
| gp | Guinea pig |
| GTP | Guanosine triphosphate |
| H/R | Hypoxia/reoxygenation |
| HCN | Hyperpolarization-activated cyclic nucleotide gated channels |
| HEPES | 4-(2-hydroxyethyl)-1-piperazineethanesulfonic acid |
| HIF | Hypoxia-inducible factor |
| HIF-$1\alpha$ | Hypoxia-inducible factor $1\alpha$ |
| HIF-$1\beta$ | Hypoxia-inducible factor $1\beta$ |
| HIF-2 | Hypoxia-inducible factor 2 |
| HIF-3 | Hypoxia-inducible factor 3 |
| HRE | Hypoxia responsible elements |
| HRP | Horseradish peroxidase |
| $I_{Ca,L}$ | LTCC current |
| IBMX | 3-Isobutyl-1-Methylxanthine |
| ICM | Ischemic cardiomyopathy |
| IHD | Ischemic heart disease |

| | |
|---|---|
| IMDM | Iscove Modified Dulbecco Media |
| iNOS | Inducible NOS |
| IP$_3$ | Inositol 1,4,5-triphosphate |
| IRAG | IP$_3$-receptor associated cGMP kinase substrate |
| ITS | Insulin-transferrin selenium |
| LA | Left atrium |
| LDH | Lactate dehydrogenase |
| LED | Light emitting diode |
| LTCC | L-type calcium channel |
| LV | Left ventricle |
| LVEDD | Left ventricular end-diastolic diameter |
| LVEF | Left ventricular ejection fraction |
| MEM | Minimum essential medium |
| Mg$^{2+}$ | Magnesium |
| miRNA | MicroRNA |
| ms | Mouse |
| MOI | Multiplicity of infection |
| N$_2$ | Nitrogen |
| NCBI | National centre for biotechnology information |
| NCX | Na$^+$/Ca$^{2+}$ exchanger |
| NEP | Neprilysin |
| NKA | Na$^+$/K$^+$-ATPase |
| NKH 477 | 6-[3-(dimethylamino)propionyl]-forskolin |
| NF-$\kappa$B | Nuclear factor $\kappa$B |
| nNOS | Neuronal NOS |
| NO | Nitric oxide |
| NO-GC | Nitric oxide-stimulated guanylyl cyclase, also known as soluble GC, sGC |
| NOS | Nitric oxide synthase |
| NP | Natriuretic peptide |
| NP-GC | Membrane bound guanylyl cyclase, also known as pGC |
| NT-proBNP | N-terminal pro BNP |
| O$_2$ | Oxygen |
| ODQ | 1H-[1,2,4]oxa-diazolo[4,3-a]quinoxalin-1-one |
| o.n. | Over night |
| PBS | Phosphate buffered saline |
| PCR | Polymerase chain reaction |
| PDE | Phosphodiesterase |

| | |
|---|---|
| PDE1 | Phosphodiesterase 1 |
| PDE2 | Phosphodiesterase 2 |
| PDE3 | Phosphodiesterase 3 |
| PDE5 | Phosphodiesterase 5 |
| PDE9 | Phosphodiesterase 9 |
| PEG 8000 | Polyethylene Glycol 8000 |
| PFU | Plaque-forming unit |
| PHD | Prolyl hydroxylase |
| PKA | Protein kinase A |
| PKG | Protein kinase G, also known as cGK |
| PKG I$\alpha$ | PKG-type I$\alpha$ |
| PKG I$\beta$ | PKG-type I$\beta$ |
| PKG II | PKG-type II |
| PLM | Phospholemman |
| PLN | Phospholamban, also known as PLB |
| $PO_2$ | Partial pressure of oxygen |
| pVHL | von Hippel-Lindau E3 ubiquitin ligase |
| qRT PCR | Quantitative reverse transcriptase polymerase chain reaction |
| r | Distance between donor and acceptor in FRET |
| $R_0$ | Förster radius |
| RA | Right atrium |
| rb | Rabbit |
| RFP | Red fluorescent protein |
| RGS | Regulator of G-protein signalling |
| Rluc | *Renilla* luciferase |
| ROS | Reactive oxygen species |
| RT | Room temperature |
| rpm | Rotations per minute |
| RV | Right ventricle |
| RyR2 | Ryanodine receptor |
| $S_0$ | Singlet state |
| $S_1$ | Excited state |
| Sapp | T-Sapphire |
| SDS | Sodium dodecyl sulfate |
| SDS PAGE | SDS polyacrylamide gel electrophoresis |
| SEM | Standard error of the mean |
| SERCA2a | Sarcoplasmic reticulum $Ca^{2+}$-ATPase |

| | |
|---|---|
| SNAP | S-Nitroso-N-acetyl-DL-penicillamine |
| SOD | Sodium deoxycholate |
| SR | Sinus rhythm |
| T-tubule | Transverse tubule |
| TAE buffer | Tris-acetate-EDTA buffer |
| TEMED | Tetramethylethylenediamine |
| TG | Transgenic |
| TnC | Troponin C |
| TnI | Troponin I |
| TRIS | Tris-(hydroxymethyl)-aminomethan |
| UKE | University Medical Centre Hamburg-Eppendorf |
| VASP | Vasodilator-stimulated protein |
| WT | Wildtype |
| YFP | Yellow fluorescent protein |

# Zusammenfassung

Die Entwicklung neuer Behandlungsmöglichkeiten für Herz-Kreislauf-Erkrankungen ist das Hauptziel der kardiovaskulären Forschung. 3',5'-Cyclisches Guanosinmonophosphat (cGMP) ist ein Second Messenger, der für seine kardioprotektive Funktion im Herz-Kreislauf-System bekannt ist. In dieser Arbeit wurde die Rolle von cGMP in zwei häufig vorkommenden Herz-Kreislauf-Erkrankungen untersucht, Hypoxie/Reoxygenierung und Vorhofflimmern.

Ein Hauptmerkmal vieler Herz-Kreislauf-Erkrankungen sind Verletzungen durch Hypoxie/Reoxygenierung. Über die Rolle von cGMP während Hypoxie/Reoxygenierung ist bisher allerding nur wenig bekannt. In diesem Teil der Arbeit wurden Förster Resonanz Energie Transfer (FRET)-basierte cGMP Messungen verwendet, um die cGMP Signalkaskade während Hypoxie/Reoxygenierung zu analysieren. Hypoxie/Reoxygenierung in adulten ventrikulären Maus Kardiomyozyten führte zu einem Anstieg der basalen cGMP Spiegel. Dieser Anstieg wurde durch Protein-Instabilität der Phosphodiesterase 3A (PDE3A) verursacht, was zu einer Reduzierung des cGMP-Abbaus führte. Darüber hinaus wurde das Redoxgleichgewicht der für die basale cGMP Produktion verantwortlichen Stickstoffmonoxid (NO) stimulierten Guanylatcyclase (NO-GC) in Richtung der oxidierten, NO-unsensitiven Form verschoben. Diese grundlegenden Befunde aus einem *In-vitro* Hypoxie/Reoxygenierung-Modell konnten in einem *Ex-vivo* Ganzherz-Langendorff-Anoxie-Modell sowie in einem *In-vivo* Ischämie/Reperfusion-Modell validiert werden. cGMP Messungen in humanen ventrikulären Kardiomyozyten zeigten die Reproduzierbarkeit dieser Befunde im Menschen. Dies macht das Potenzial der cGMP Signalkaskade als Angriffspunkt für die Behandlung von Verletzungen durch Hypoxie/Reoxygenierung in der Klinik deutlich.

Da die verfügbaren Behandlungsmöglichkeiten bei Vorhofflimmern sehr begrenzt sind, ist die Entwicklung neuer molekularer Ziele dringend erforderlich. In diesem Teil der Arbeit wurden FRET-basierte cGMP Messungen in humanen Kardiomyozyten aus linken und rechten Vorhöfen von Patienten im Sinus Rhythmus oder mit Vorhofflimmern verwendet, um herauszufinden, ob die cGMP Signalkaskade ein potenzielles therapeutisches Ziel für die Behandlung von Vorhofflimmern darstellt. Sowohl NO-GC als auch die von natriuretischen Peptiden stimulierte Guanylatcyclase (NP-GC) sind an der cGMP Synthese beteiligt. Während NO-GC Stimulation zu einem identischen cGMP Anstieg in Kardiomyozyten aus allen Bedingungen führte, war er nach NP-GC Stimulation unterschiedlich. PDE1, PDE2, PDE3 und PDE5 sind am Abbau von cGMP in atrialen Kardiomyozyten beteiligt. Während der cGMP Anstieg nach PDE3 Inhibition in allen Bedingungen gleich war, hatte die Inhibition von PDE2 und PDE5 unterschiedliche Auswirkungen. Die Daten liefern grundlegende Einblicke in die Regulation der cGMP-Signalkaskade in atrialen Kardiomyozyten sowohl unter gesunden als auch unter Krankheitsbedingungen. Sie machen das Potenzial der cGMP Signalkaskade als therapeutisches Ziel bei der Behandlung von Vorhofflimmern deutlich.

# Abstract

The development of new cardioprotective strategies to treat cardiovascular diseases (CVDs) is the major goal of cardiovascular research. The second messenger 3',5'-cyclic guanosine monophosphate (cGMP) is known for its cardioprotective role in the cardiovascular system. In this work, the cardioprotective role of cGMP was investigated in two common CVD conditions, hypoxia/reoxygenation injury and atrial fibrillation (AF).

Hypoxia/reoxygenation injury is considered as one major characteristic of many CVDs. However, little is known about the role of cGMP dynamics during hypoxia/reoxygenation. In this part of the work, Förster resonance energy transfer (FRET)-based cGMP measurements were used in order to analyse real time cGMP dynamics during hypoxia/reoxygenation. Hypoxia/reoxygenation injury caused a significant increase in basal cGMP levels in adult ventricular mouse cardiomyocytes. This was due to protein instability of phosphodiesterase 3A (PDE3A), which led to a reduction of cGMP degradation. Furthermore, the redox equilibrium of the nitric oxide (NO)-stimulated guanylyl cyclase (NO-GC), which is responsible for basal cGMP production, was shifted towards the oxidized, NO-insensitive form. These basic findings from an *in vitro* model of hypoxic injury could be validated in an *ex vivo* whole heart Langendorff model of anoxic injury as well as in an *in vivo* open chest model of ischemia/reperfusion injury, which demonstrates the physiological relevance of the results. FRET-based cGMP measurements in human ventricular cardiomyocytes made it possible to show the reproducibility of these findings in the human situation. This shows the potential of using the cGMP signalling cascade as a therapeutic target in the treatment of hypoxia/reoxygenation injury in the clinics.

Currently available treatment options for AF are limited and new molecular targets are urgently needed. In this part of the work, FRET-based cGMP imaging was used in human atrial cardiomyocytes of right (RA) and left atria (LA) of patients in sinus rhythm (SR) and with AF in order to figure out whether the cGMP signalling cascade could be a potential therapeutic target for the treatment of AF. The data demonstrate that both, NO-GC and natriuretic-peptide-stimulated GC (NP-GC) are involved in cGMP generation in human atrial cardiomyocytes. However, whereas the cGMP increase upon NO-GC stimulation was equal in cardiomyocytes of RA and LA of patients in SR and with AF, the cGMP increase upon NP-GC stimulation was different. Furthermore, it could be shown that PDE1, PDE2, PDE3, and PDE5 are involved in cGMP degradation. Whereas inhibition of PDE3 increased cGMP levels equally in all conditions, the effects of PDE2 and PDE5 inhibition were different. The data provide fundamental insights into the regulation of the cGMP signalling cascade in human atrial cardiomyocytes under healthy and disease conditions and demonstrate the potential of the cGMP signalling cascade as a therapeutic target in the treatment of AF.

# 1. Introduction

## 1.1 Cardiovascular diseases

### 1.1.1 Cardiovascular diseases worldwide

Cardiovascular diseases (CVDs) are the leading cause of death worldwide. In 2017, an estimated 17.8 million people died of CVDs [1, 2]. A recent report from the European Society of Cardiology (ESC) shows that despite the big efforts on cardiovascular research CVDs remain the main cause of death in the ESC countries (Figure 1.1) [3].
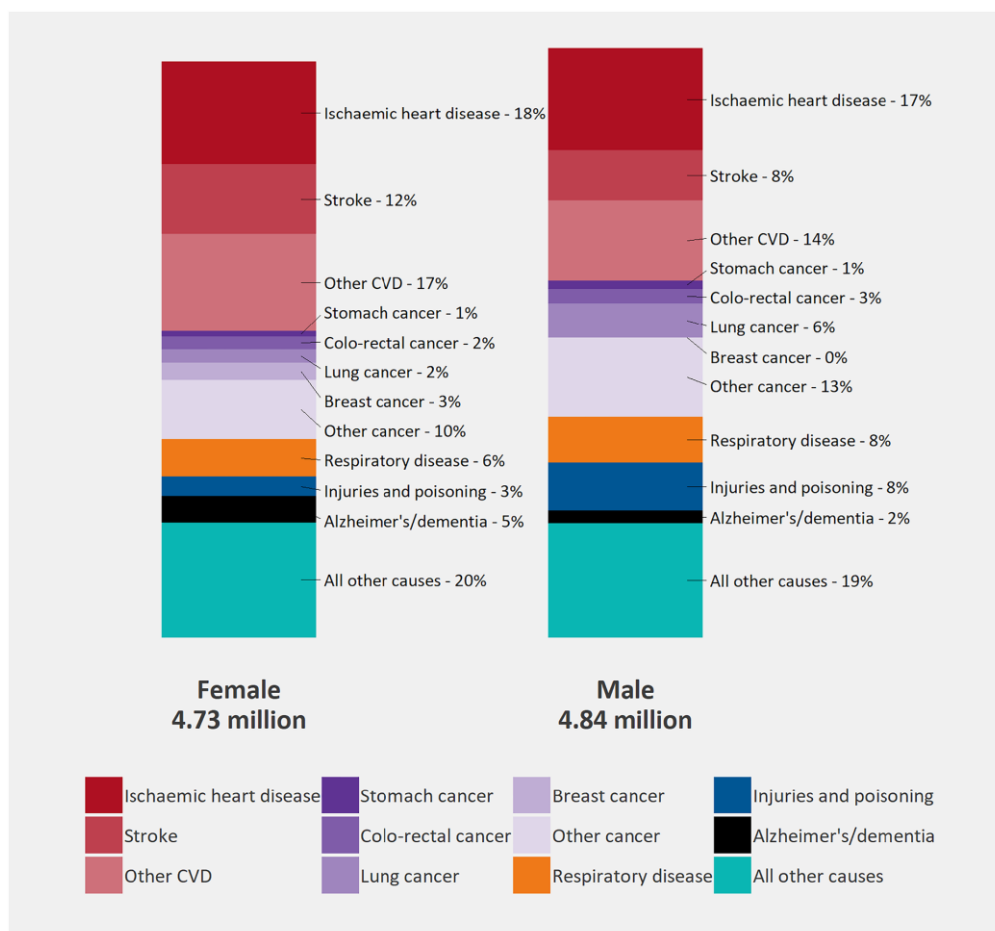
**Figure 1.1:** **Main causes of death for females and males of all age groups in Europe.** Cardiovascular diseases (CVDs) remain the leading cause of death in Europe. Among CVDs, ischemic heart disease is the most common cause of death in both female and male, followed by stroke. Figure adapted from [3].

### 1.1.2 Characterization of cardiovascular diseases

CVDs include many different diseases. They can be divided in several main types which will be described shortly in the following [4]. Ischemic heart disease (IHD), also known as coronary heart disease, is the most common CVD and the main cause of death among CVDs

followed by stroke [3, 5]. IHD describes heart problems caused by narrowed arteries, mostly due to atherosclerosis. IHD can culminate in myocardial infarction or sudden cardiac death [6, 7]. Plaque formation can also lead to other CVDs. Peripheral arterial disease occurs when the arteries outside the heart and the brain become narrowed or obstructed most commonly due to systemic atherosclerosis which is a high risk for heart attack and ischemic stroke [6, 8, 9]. Bulge formation in the aorta, classified as aneurysm when the bulge grows to 50 percent or greater than the normal size of the vessel, pose a major risk for aortic rupture when it remains untreated [6].

Diseases with structural defects of the heart also belong to CVDs. Congenital heart disease is a term that covers all significant structural heart defects which are present at birth. Abnormal structure of cardiac chambers, valves, or the great vessels in those patients alters the normal pattern of blood flow. Patients with congenital heart disease may develop cardiac complications such as arrhythmias, heart failure, and valve insufficiency, even after surgical correction of the structural abnormalities [6, 10]. Valvular heart diseases are congenital or acquired defects in one or more heart valves either leading to stenosis because the valves do not open properly any more or regurgitation caused by valve leakage leading to backflow [11, 12].

Heart failure is a multifactorial, systemic CVD. Systolic failure occurs when the heart muscle is weak, diastolic failure is caused by a stiff heart muscle which is unable to relax normally. In heart failure, structural, neurohumoral, cellular, and molecular mechanisms are activated and act as a network to maintain physiological function of the heart. Cardiomyopathy is one of many causes of heart failure [6, 13, 14].

Inflammatory heart diseases also belong to the CVDs, they include myocarditis, pericarditis, and endocarditis. Amongst others, they can be triggered by viruses, bacteria, fungi, and parasites [15, 16].

Another type of CVD are cardiac arrhythmias, among which atrial fibrillation (AF) is the most common sustained heart rhythm disorder [17, 18].

Medications that treat CVDs e.g. drugs to lower blood pressure, are amongst the most cost-effective interventions available to health systems. Still the total global costs of CVDs are increasing. The World Heart Federation has estimated, that by 2030 the total global costs of CVDs is set to rise from approximately USD 863 billion in 2010 to alarming USD 1044 billion [3]. Also the mortality from CVDs has been increasing since 2007 worldwide [19]. During the last decades, many efforts have been focused on CVD research in order to better understand the mechanisms leading to CVDs and to improve the treatment options (Figure 1.2).
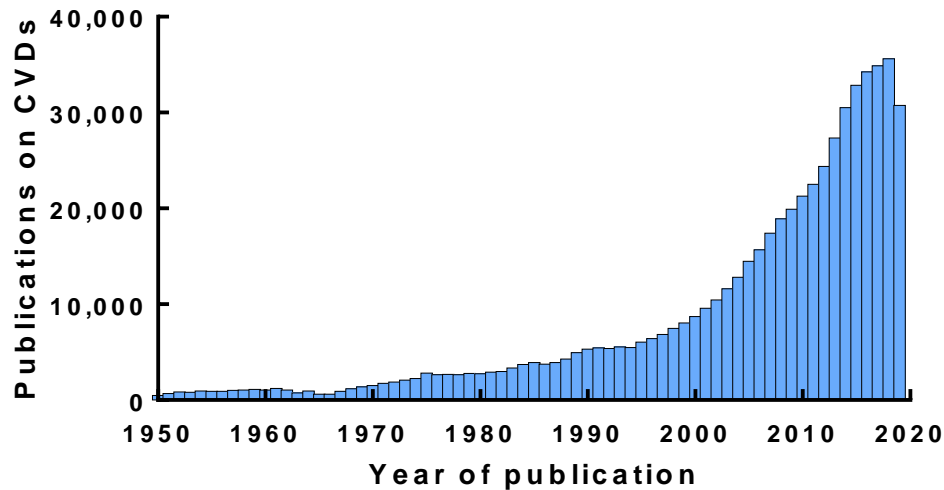
**Figure 1.2:** **Publications on cardiovascular diseases (CVDs) per year.** The number of publications on CVDs increased exponentially during the last years. However, the mortality from CVDs is still increasing worldwide. PubMed search: Cardiovascular [all fields] AND disease [all fields].

The development of new therapeutic strategies for better and more efficient treatment of CVDs is essential in order to reduce mortality rate from CVDs and the annual burden.

### 1.1.3 Hypoxia and its role in cardiovascular diseases

Hypoxia describes the imbalance between the amount of oxygen ($O_2$) supplied to a cell and the amount of $O_2$ required by those cell for proper metabolism, leading to pathological consequences [20, 21, 22]. It is correlated with the pathology of many CVDs, including IHD which is the most common CVD. Other CVDs in which hypoxia is an important risk factor are heart failure, peripheral arterial disease, congenital heart disease, valvular heart disease, hypertension, and cardiomyopathy [21, 23, 24, 25, 26]. Therefore, it is of great interest to elucidate the mechanisms leading to hypoxia for treating those CVDs.

Myocardial hypoxia has different reasons: i) reduction or interruption of the coronary blood flow inducing ischemic hypoxia, ii) a sufficient perfusion but a decrease in the partial pressure of oxygen ($PO_2$) in the arterial blood causing systemic hypoxia, iii) a decrease in the $O_2$ transport capacity of the blood causing anaemic hypoxia, and iv) reduced intracellular utilization of $O_2$ inducing histotoxic hypoxia [20].

The reduction of $O_2$ supply in the heart causes a switch from aerobic to anaerobic metabolism. Thereby the capacity of cardiomyocytes to generate energy from adenosine triphosphate (ATP) and creatine phosphate becomes severely reduced [20, 27]. Impaired calcium ($Ca^{2+}$) handling with simultaneous loss of $Ca^{2+}$ homeostasis [28, 29], reactive oxygen

species (ROS) accumulation and loss of osmotic control lead to contractile dysfunction, membrane disruption, and finally cardiac cell death [20, 30, 31].

How cells adapt to changes in levels of $O_2$ has long been unknown. In 2019, William Kaelin, Peter Ratcliffe and Gregg Semenza were awarded the Nobel Prize in Physiology or Medicine for the identification of the molecular machinery that regulates the activity of genes in response to varying levels of $O_2$, the so called hypoxia-inducible factor (HIF) machinery [32]. Under normoxic conditions, HIF-$\alpha$ protein is hydroxylated through an oxygen dependent process by prolyl hydroxylases (PHDs). Proline-hydroxylated HIF-$\alpha$ is then recognized by the von Hippel-Lindau E3 ubiquitin ligase (pVHL) and degraded through the ubiquitin-proteasome system. Additionally, HIF-$\alpha$ can be asparagine-hydroxylated by factor-inhibiting HIF (FIH) which inhibits its interaction with transcriptional activators such as p300 or 3',5'-cyclic adenosine monophosphate (cAMP)-responsive element-binding protein (CREB)-binding protein (CBP) (Figure 1.3). Under hypoxic conditions, however, HIF-$\alpha$ protein is stabilized and translocates to the nucleus, forming a heterodimer complex with HIF-1$\beta$. This complex activates the transcription of hypoxia-inducible genes by binding to hypoxia responsive elements (HREs) [26, 33, 34] (Figure 1.3).
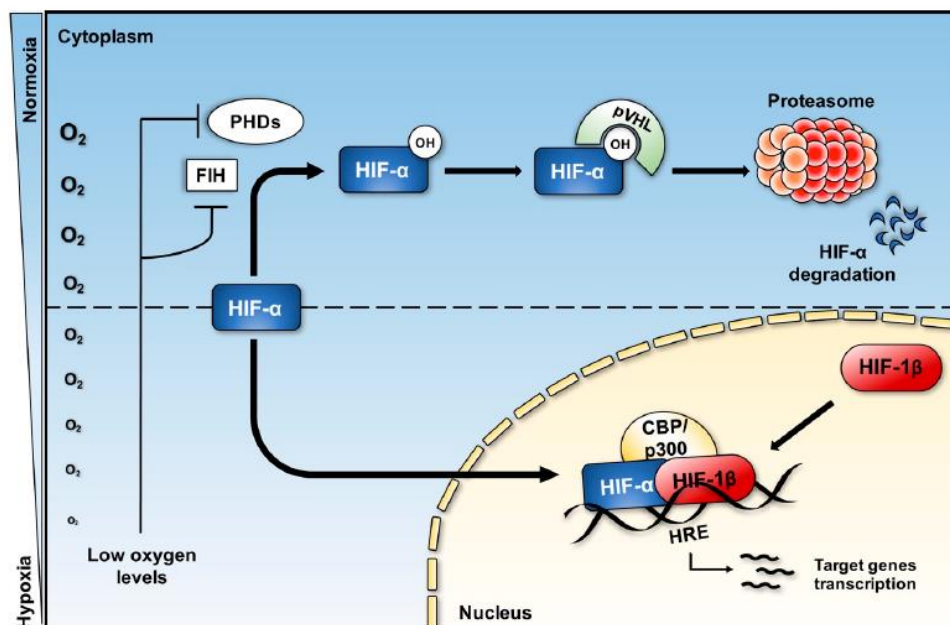


**Figure 1.3:** **Activation of hypoxia-inducible factor (HIF) pathway in response to hypoxia.** Under normoxic conditions, HIF-$\alpha$ protein is hydroxylated by prolyl hydroxylases (PHDs) leading to binding of the von Hippel-Lindau E3 ubiquitin ligase (pVHL) and subsequent degradation through the ubiquitin-proteasome system. The factor-inhibiting HIF (FIH) can also hydroxylate HIF-$\alpha$ at an asparagine residue which is important in the transactivation domain, thereby preventing its interaction with transcriptional activators such as p300 or 3',5'-cyclic adenosine monophosphate (cAMP)-responsive element-binding protein (CREB)-binding protein (CBP). Under hypoxic conditions, HIF-$\alpha$

protein is stabilized, translocates to the nucleus and forms a heterodimer complex with HIF-1$\beta$, thereby activating the transcription of hypoxia-inducible genes by binding to hypoxia responsive elements (HREs). Figure adapted from [35].

In response to hypoxia, HIF induces the expression of hundreds of genes, which can be categorized according to different biological functions such as metabolism or anti-apoptosis [24, 36, 37]. For example, it can shift the cellular energy metabolism from oxidative phosphorylation towards glycolysis and activate the transcription of genes encoding for glucose transporters and glycolytic enzymes in order to maintain ATP levels under hypoxic conditions. Moreover, it inhibits the mitochondrial oxidative metabolism, thereby reducing ROS generation [24, 36, 38, 39].

Another major transcription factor responding to cellular stress including hypoxia is nuclear factor $\kappa$B (NF-$\kappa$B) [40, 41]. However, the mechanisms by which NF-$\kappa$B is activated under low oxygen conditions are still unclear [35, 42], but it seems that there is a positive regulatory loop between NF-$\kappa$B and HIF-1 [37].

In the literature, hypoxia and ischemia are often used interchangeably, despite they are very different conditions. Whereas hypoxia describes only the disparity for $O_2$, ischemia is the combination of a decline in the supply of $O_2$ and the significant reduction in the clearance of metabolites, leading to an intracellular drop in pH [20, 22].

### 1.1.4 Atrial fibrillation

AF belongs to the CVDs and is the most common sustained heart rhythm disorder. It affects approximately 33.5 million people annually worldwide and is associated with substantial morbidity and mortality [17, 43]. AF is a highly dynamic condition, involving episodes of sinus rhythm (SR) punctuated by periods of arrhythmia [17]. Current guidelines to classify AF are based on pattern and duration of the arrhythmia. AF is classified as paroxysmal AF when it terminates spontaneously or with medical intervention within seven days. If it lasts longer than seven days, it is classified as persistent AF, and continuing for more than one year is defined as long-standing persistent or permanent AF [44, 45].

The molecular mechanisms underlying AF are not well understood. However, it is well accepted that the fundamental mechanisms of AF are an initiating trigger such as ectopic activity and a vulnerable substrate to promote re-entries and maintain the arrhythmia. Ectopic activity can be caused by delayed after depolarizations (DADs), which in turn are caused by abnormal diastolic $Ca^{2+}$ leak from the sarcoplasmic reticulum through the Ryanodine receptor (RyR2), or by early after depolarizations (EADs), which can occur when the action potential

duration (APD) is prolonged and inward cell membrane $Ca^{2+}$ currents recover from inactivation and allow $Ca^{2+}$ to move into the cell. Reentry requires appropriate tissue properties, a so called vulnerable substrate. A vulnerable substrate is characterized by structural remodelling such as atrial dilatation and fibrosis or electrical remodelling capable of maintaining the arrhythmia [46, 47, 48] (Figure 1.4).
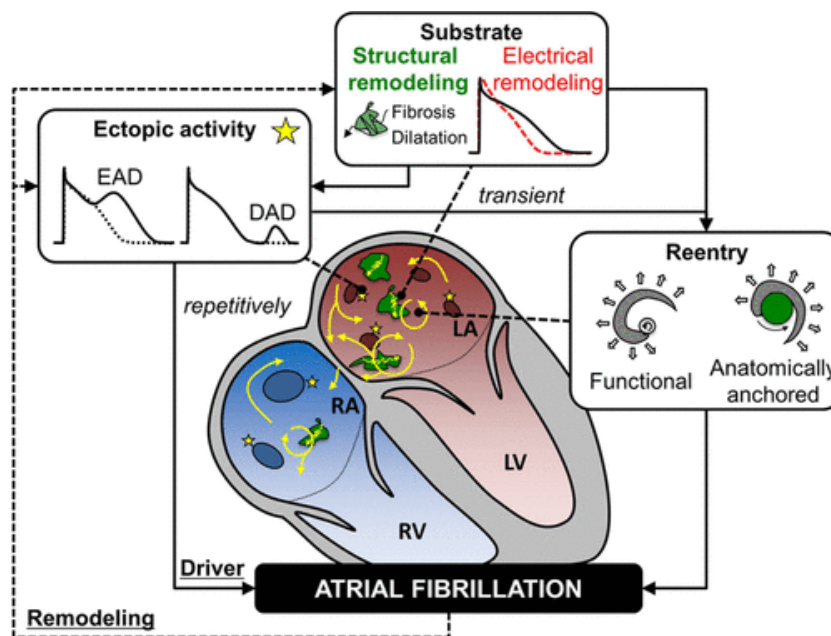


**Figure 1.4:** **Fundamental mechanisms of atrial fibrillation (AF).** AF needs an initiating trigger such as ectopic beats arising from early and delayed after depolarizations (EADs, DADs) and a vulnerable substrate to promote re-entries and maintain the arrhythmia. Structural remodelling of the atria such as dilatation and fibrosis or electrical remodelling such as short effective refractory periods are vulnerable substrates to maintain AF. LA, left atrium; LV, left ventricle; RA, right atrium; RV, right ventricle. Figure adapted from [17].

Antiarrhythmic drugs (AADs) are one of the currently available treatment options for AF. However, AADs have moderate efficacy and the potential to provoke ventricular arrhythmia. Therefore, they should be used with caution [17, 49, 50]. Another treatment option are ablation approaches, which have been shown to be a much more effective therapeutic option. However, catheter ablation is not a benign procedure and can cause many major adverse events. Working precisely in catheter ablation is very difficult and it is not easy to ensure that all ectopic points are removed during the procedure. Even if catheter ablation was successful, there is no guarantee that no new ectopic points will appear [17, 51]. Since currently available AF treatment options remain limited in efficacy [17, 52], intense research on AF during the last 20 years has identified different molecular targets and mechanisms which could be potential targets for AF therapy. Ion channels, atrial $Ca^{2+}$-handling proteins, several transcription factors, and components of the myofilaments are some of these

potential targets [17]. Combating oxidative stress and inflammation could be also an interesting and poorly understood way to treat AF. Another approach is the use of microRNAs (miRNAs) to inhibit protein translation and promote mRNA degradation of several targets [17, 52]. Second messengers such as 3',5'-cyclic adenosine monophosphate (cAMP), $Ca^{2+}$, and 3',5'-cyclic guanosine monophosphate (cGMP) are other promising potential targets to treat AF.

## 1.2 Second messengers in the heart

### 1.2.1 Function of second messengers in the heart

Second messengers are small signalling molecules. Upon binding of the so called "first messengers" like hormones or neurotransmitters to their corresponding receptors, second messenger production is stimulated. Once produced, the second messenger diffuses rapidly to its protein targets, and alters their activities as a response to the information received by the specific receptor [53, 54]. Second messengers can be divided into four classes: i) cyclic nucleotides like cAMP, cGMP, and other soluble molecules that signal within the cytosol, ii) lipid and lipid-derived messengers such as diacylglycerol (DAG) and inositol 1,4,5-triphosphate ($IP_3$) that signal within membranes, iii) ions, such as $Ca^{2+}$, and Magnesium ($Mg^{2+}$), signalling between cellular compartments, and iv) gases, and free radicals, which can signal throughout the cell and even to neighbouring cells [53].

The main second messengers in the heart involved in cardiac signalling pathways are $Ca^{2+}$, cAMP, and cGMP. They are key factors in the regulation of contraction-relaxation and modulation of cardiac gene expression.

$Ca^{2+}$ is the major factor regulating excitation-contraction coupling (ECC), which means the translation of electrical excitation into contractile function. For proper cardiac function systolic and diastolic [$Ca^{2+}$] must be tightly regulated [55, 56, 57]. Membrane depolarization during an action potential opens voltage-sensitive L-type calcium channels (LTCCs) in the surface membrane and transverse tubules (T-tubules) of the cardiomyocytes and a small amount of $Ca^{2+}$ enters the cell. This causes a $Ca^{2+}$-induced $Ca^{2+}$-release from the sarcoplasmic reticulum *via* RyR2. This increase in [$Ca^{2+}$] initiates cardiomyocyte contraction. $Ca^{2+}$ binding to troponin C (TnC) results in myofilament activation and cell shortening. For relaxation to occur, $Ca^{2+}$ must be removed from the cytoplasm. Therefore, RyR2s close, $Ca^{2+}$ is pumped back into the sarcoplasmic reticulum through the sarcoplasmic reticulum $Ca^{2+}$-ATPase (SERCA2a), and out of the cell through $Na^+/Ca^{2+}$ exchanger (NCX). Phospholamban (PLN) is

a regulator of SERCA2a activity. It inhibits SERCA2a when dephosphorylated [55, 56, 58]. The highly coordinated process of the ECC can be fine-tuned by two $Ca^{2+}$-regulatory proteins, $Ca^{2+}$/calmodulin-dependent protein kinase II (CaMKII) and cAMP-dependent protein kinase A (PKA) [56]. The serine/threonine kinase CaMKII is activated in response to increased $Ca^{2+}$ signals by $Ca^{2+}$/calmodulin binding. It can phosphorylate LTCC [59], PLN [60], RyR2 [61], cardiac $Na^+$ channels [62], and probably SERCA2a [56, 58], thereby modifying their activities.

cAMP is the second messenger responsible for the "fight or flight" mechanism. Thus, sympathetic stimulation of β-adrenergic receptors (β-ARs) by norepinephrine or epinephrine activates adenylyl cyclase (AC) which produces cAMP. cAMP then activates PKA which has key phosphorylation targets in the ECC system such as LTCCs, RyR2s, PLN and troponin I (TnI), thereby exerting positive chronotropic, inotropic and lusitropic effects [56, 57, 63, 64, 65].

cGMP is a much less studied second messenger. cGMP signalling often exerts opposite effects on cardiac contraction, in part as consequences of cAMP-cGMP crosstalk [66] but also because of the opposing effects of protein kinase G (PKG) and PKA-mediated phosphorylation on target proteins. cGMP is therefore considered as the "myocardial brake" [66, 67, 68]. PKG, as well as PKA, can both increase SERCA2a activity by phosphorylation of PLN, leading to an increase in cytosolic $Ca^{2+}$ re-uptake [69, 70]. Additionally, both kinases can phosphorylate TnI which decreases the sensitivity of TnC for $Ca^{2+}$ [71, 72] (Figure 1.5). However, unlike PKA, PKG does not simultaneously enhance the release of $Ca^{2+}$ from the sarcoplasmic reticulum. Furthermore PKG is able to reduce $Ca^{2+}$ influx by directly inhibiting LTCCs [73] (Figure 1.5).
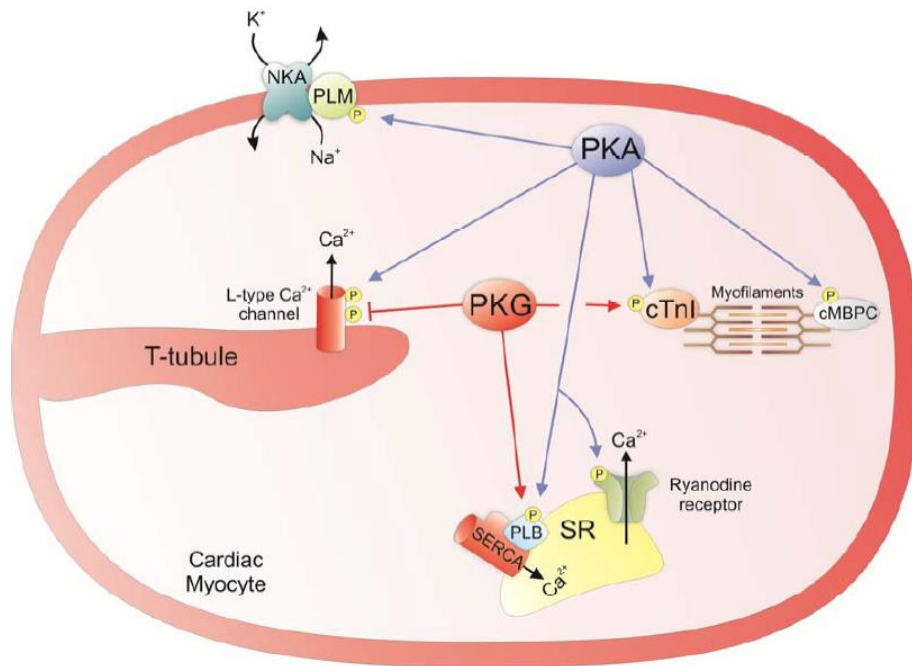
**Figure 1.5:** **Phosphorylation targets of protein kinase A (PKA) and protein kinase G (PKG) involved in contractility regulation of cardiomyocytes.** Both, PKA and PKG can phosphorylate phospholamban (PLN or PLB), leading to an increase of $Ca^{2+}$ re-uptake in the sarcoplasmic reticulum through sarcoplasmic reticulum $Ca^{2+}$-ATPase (SERCA2a). Additionally, both kinases phosphorylate cardiac Troponin I (cTnI), thereby decreasing the sensitivity of Troponin C (TnC) for $Ca^{2+}$. However, whereas PKA increases sarcoplasmic reticulum $Ca^{2+}$ release *via* phosphorylation of Ryanodine receptor (RyR2) and increases inward $Ca^{2+}$ flow through L-type $Ca^{2+}$ channel (LTCC) phosphorylation, PKG can reduce cellular $Ca^{2+}$ intake by directly inhibiting LTCCs. The activity of $Na^+/K^+$-ATPase (NKA) is also regulated by PKA. Phosphorylation of the associated protein phospholemman (PLM) increases the cellular export of $Na^+$. Cardiac myosin binding protein C (cMyBP-C) is another target of PKA. Basal phosphorylation is necessary for maintaining thick-filament orientation, dynamic regulation, and contractile mechanics. Figure adapted from [73].

Phosphodiesterases (PDEs) are enzymes which can hydrolyse cyclic nucleotides to their monophosphates, cGMP to guanosine monophosphate (GMP) and cAMP to adenosine monophosphate (AMP), by hydrolysis of the 3'-phosphate bond [74]. As a result, they are also involved in the tight spatio-temporal regulation of the second messengers cAMP and cGMP in the cell.

The role of cGMP as a second messenger in the heart will be discussed in detail in the following section.

## 1.2.2 The cGMP signalling pathway in the cardiovascular system

The unique second messenger cGMP is involved in the regulation of many physiological processes in the cardiovascular system including the regulation of hypertrophy and fibrosis during cardiac remodelling [75, 76], as well as the regulation of cardiac contractility [77, 78], and vascular tone [79, 80]. Dysregulation at any level of the cGMP signalling cascade can result in severe pathologies [81, 82].

Since its discovery more than 50 years ago [83] numerous studies have been done, investigating the role of cGMP in the heart. cGMP is present in all major cardiac cell types, cardiomyocytes, cardiac fibroblasts, endothelial cells, and vascular smooth muscle cells [75, 82].

The cGMP signalling cascade is composed by cGMP generating guanylyl cyclases (GCs), cGMP degrading PDEs, and cGMP effector proteins like PKG (Figure 1.6).
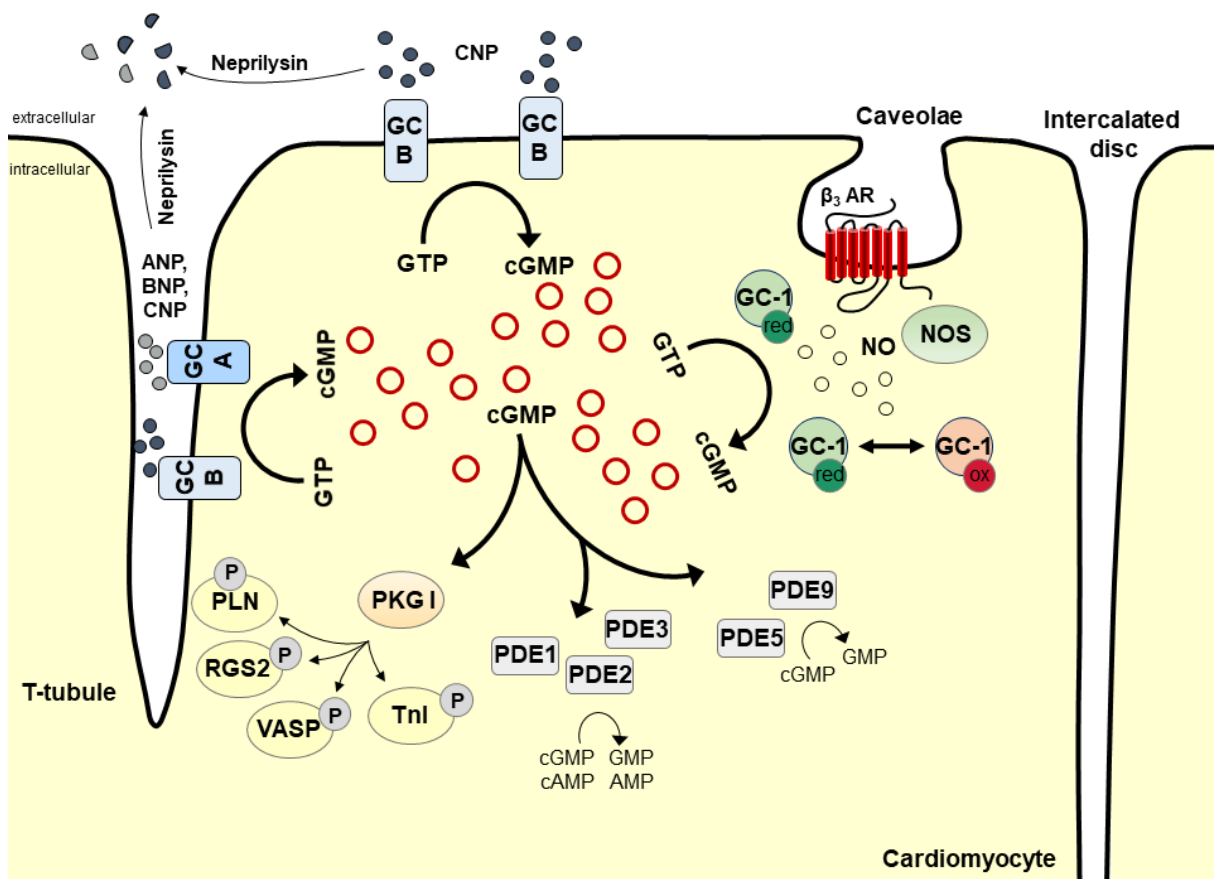


**Figure 1.6:    cGMP signalling cascade.**   3',5'-cyclic guanosine monophosphate (cGMP) is generated from guanosine triphosphate (GTP) by two different types of guanylyl cyclases (GCs). Membrane bound guanylyl cyclases (NP-GCs) are the receptors for the natriuretic peptides (NPs). Atrial natriuretic peptide (ANP) and brain natriuretic peptide (BNP) stimulate GC-A, C-type natriuretic peptide (CNP) stimulates GC-B. NPs can be degraded by Neprilysin. Nitric oxide (NO)-stimulated GCs (NO-GCs) are the "soluble" GCs, with GC-1 being present in cardiomyocytes. GC-1 is stimulated by NO which is generated from L-Arginine by NO synthases (NOS). GC-1 can be present in the cell in a reduced (red) or oxidized (ox) state. cGMP is degraded to guanosine monophosphate (GMP) by

phosphodiesterases (PDEs). PDE5 and PDE9 are cGMP specific, whereas other PDEs (PDE1, PDE2, and PDE3) are dual-substrate specific and degrade both cGMP and 3',5'-cyclic adenosine monophosphate (cAMP). The most important cGMP effector protein is protein kinase G (PKG). PKG I is present in cardiomyocytes and has several phosphorylation targets in the cell like phospholamban (PLN), regulator of G-protein signalling 2 (RGS2), vasodilator-stimulated protein (VASP), and Troponin (TnI).

*1.2.2.1 cGMP synthesis by guanylyl cyclases*

GCs synthesize cGMP from guanosine triphosphate (GTP). They were described first in 1969 by three different groups [84, 85, 86]. Two different types of GCs can generate cGMP: i) Membrane-bound GCs (NP-GCs), also known as particulate GCs (pGCs), are activated by natriuretic peptides (NPs). Atrial natriuretic peptide (ANP) and brain natriuretic peptide (BNP) activate guanylyl-cyclase A (GC-A), C-type natriuretic peptide (CNP) activates guanylyl-cyclase B (GC-B) [87]. ii) Nitric oxide (NO)-sensitive GCs (NO-GCs), also known as soluble GCs (sGCs), are stimulated by NO [88].

Seven NP-GCs, GC-A to GC-G, have been identified in mammalian cells. They all share the same structure, consisting of an extracellular ligand binding domain, a short transmembrane region, and a C-terminal cyclase domain [89, 90]. In cardiomyocytes, two cGMP synthesizing NP-GCs have been identified, GC-A and GC-B. Additionally, the so called "clearance receptor" NPRC has been shown to be expressed in cardiomyocytes. NPRC lacks the C-terminal catalytic domain but is still able to bind NPs, thereby controlling extracellular NP concentration by internalisation and degradation [87, 89, 90].

Mammalian cardiac NPs are ANP, BNP, CNP, and osteocrin/musclin [87, 91, 92]. ANP is produced in cardiomyocytes of the atria, BNP in the ventricular cardiomyocytes. Both are released in response to stretch to their respective cardiac chambers [93, 94]. CNP is mainly found in the central nervous system and endothelial cells but it was also found to be expressed in all four chambers of the heart [95]. Circulating ANP, BNP, and CNP reduce pre- and after-load in normal and failing hearts by plasma sequestration from vascular compartments and stimulation of renal natriuresis and diuresis [96]. Additionally, they can counter regulate many of the pathophysiological influences of the renin-angiotensin-aldosterone system by blocking it [93, 97]. ANP and BNP can also have direct cardioprotective effects on the heart and moderate cardiac remodelling by preventing hypertrophic growths of the cardiomyocytes [93, 98, 99, 100, 101, 102]. CNP has also been shown to prevent cardiac remodelling by attenuating hypertrophic growth of cardiomyocytes and supressing collagen formation [103]. Plasma concentrations of BNP or its prohormone N-terminal pro BNP (NT-proBNP) are commonly used as a biomarker in heart failure [104]. Osteocrin/musclin binds to the clearance receptor NPRC with high affinity, but not to GC-A

and GC-B, thereby blocking NPRC mediated degradation of NPs, potentiating their effect [87, 105]. Neprilysin is a membrane bound endopeptidase, that cleaves and inactivates NPs [106].

NO-GC is typically found as heterodimer consisting of a larger $\alpha$-subunit ($\alpha_1$ or $\alpha_2$) and a smaller haem-containing $\beta$-subunit ($\beta_1$ or $\beta_2$) [107]. NO-GC$\alpha_1\beta_1$ (GC-1) is the most prevalent heterodimer in the heart while NO-GC$\alpha_2\beta_1$ (GC-2) is mainly found in brain tissue [108, 109]. Despite differences in the primary structure of $\alpha_1$ and $\alpha_2$ subunits, kinetic properties and sensitivity towards NO are indistinguishable [109, 110]. The two isoforms GC-1 and GC-2 also play an important role in the central nervous system, where GC-1 is involved in the presynaptic signalling, whereas GC-2 regulates postsynaptic signalling. Homodimers of $\alpha$ or $\beta$ subunits can be formed as well and have been described for $\beta_1$ [111], $\beta_2$ [112] and $\alpha_1$ [113]. The haem moiety of NO-GC is crucial for NO binding. It can only bind NO in the reduced state, the oxidized state is insensitive to NO [114]. NO is generated from L-arginine by NO synthases (NOSs) [115]. Three different isoforms have been identified, the neuronal NOS (nNOS), the endothelial NOS (eNOS), and the inducible NOS (iNOS). All can be expressed in cardiomyocytes modulating cardiac function [115, 116].

### 1.2.2.2 cGMP degradation by phosphodiesterases

PDEs are the only enzymes that degrade 3',5'-cyclic nucleotides [117]. They hydrolyse them to their monophosphates, cGMP to GMP and cAMP to AMP, by hydrolysis of the 3'-phosphate bond [74]. PDE activity has been described first shortly after the discovery of cAMP [118, 119]. Up to date 21 genes encoding for PDEs have been identified. They can be subdivided into 11 super-families, PDE1 – PDE11, based on their C-terminal catalytic domain [117]. Alternative splicing and the use of alternative transcriptional start sites leads to more than 60 different isoforms [74, 120, 121]. PDEs differ in their kinetic properties, as well as in modes of regulation, intracellular localization, cellular expression, and inhibitor sensitivities [117, 120, 121, 122].

In the heart, at least seven PDE families have been described, PDE1-5, 8, and 9 [123]. Recently, a novel role of PDE10 in the regulation of cardiac remodelling and heart failure has been discovered [124]. Cardiac PDEs differ in their cyclic nucleotide specificity. While PDE1, 2, 3, and 10 are dual-substrate PDEs and can hydrolyse both cyclic nucleotides, cAMP and cGMP [124, 125, 126], PDE4 and 8 hydrolyse only cAMP [127, 128], whereas PDE5 and 9 are cGMP-specific PDEs [67, 129, 130].

Different kinetic properties, localisation, and expression of the PDEs in the heart lead to a complex regulatory network. PDE1 is a $Ca^{2+}$/Calmodulin-stimulated PDE [131, 132]. Dual substrate PDEs underpin a crosstalk between cAMP and cGMP. While PDE2 is known as

"cGMP-simulated PDE", PDE3 is known as the "cGMP-inhibited PDE" [66, 120, 133]. The N-terminal GAF domains of PDE2 can bind cGMP, leading to a concomitant increase in the hydrolytic activity [134, 135]. For PDE3, the hydrolysis rate of cAMP ($V_{max}$) is nearly 10-fold higher than the $V_{max}$ for cGMP, and therefore cGMP can act as an inhibitor of cAMP hydrolysis. [120]. PDE3 has a very high affinity for cGMP ($K_M$ = 0.02 µM). Under conditions with very low cGMP levels like in cardiomyocytes, the PDE3 family is very important for controlling cellular cGMP levels [120] and PDE3 has been shown to be the main PDE responsible for basal cGMP degradation in murine cardiomyocytes [136].

The biological roles of each PDE isoform are distinct due to its unique expression pattern at the level of tissue, cell type, and subcellular compartment [117].

*1.2.2.3 cGMP effector activation*

Besides the dual substrate PDEs PDE2, and PDE3, leading to a crosstalk between cGMP and cAMP, one important effector target of cGMP is PKG, also known as cGK. Three isoforms, PKG-type I$\alpha$ (PKG I$\alpha$), PKG-type I$\beta$ (PKG I$\beta$), and PKG-type II (PKG II) have been identified. PKG I$\alpha$ is expressed in cardiomyocytes [137, 138].

PKG has several phosphorylation targets in the cell. As already mentioned above (section 1.2.1), some of its targets are involved in the regulation of the ECC. PKG can phosphorylate PLN [69] leading to an increased sarcoplasmic reticulum $Ca^{2+}$-reuptake through SERCA2a. Additional phosphorylation of TnI decreases the affinity of TnC for $Ca^{2+}$ [72, 139]. Direct inhibition of LTCC by PKG reduces the cellular intake of $Ca^{2+}$ [73]. By modifying various targets in the ECC, PKG can blunt contraction and enhance relaxation [67].

Additionally, PKG is involved in the regulation of vascular tone. One PKG target is the regulator of G protein signalling (RGS) protein. RGS proteins are GTPase activating proteins that inhibit signalling by heterotrimeric G proteins [140]. In the heart, PKG can activate RGS2 and RGS4 through phosphorylation and mediate vascular smooth muscle regulation [141, 142, 143]. Other PKG substrates involved in smooth muscle regulation include the regulatory myosin-binding subunit of myosin phosphatase [144], $Ca^{2+}$-activated $K^+$ channels (BK) [145], and IP$_3$-receptor associated cGMP kinase substrate (IRAG) [146]. Phosphorylation of all these targets contributes to a reduction of intracellular $Ca^{2+}$ concentration or alteration in $Ca^{2+}$ sensitisation causing a decrease in smooth muscle tone [147]. Vasodilatory-stimulated phosphoprotein (VASP) is a thin filament actin-binding protein and target substrate of PKG which has been shown to be involved in vascular relaxation as well [82, 148].

A family of the voltage-gated channels, the cyclic nucleotide-gated channels (CNGs) are another downstream target of cGMP. In the heart, hyperpolarization-activated cyclic-

nucleotide-gated (HCN) channels are involved in sinus node regulation [149, 150]. Other CNGs play an important role in vision and olfaction [151].

cGMP signalling is regulated in so called "microdomains". Microdomains are regulated by subcellular pools of PDEs, differentially distribution of cGMP generating receptors and PKG molecules. They ensure spatial and temporal control of cGMP signalling and provide functional specificity to cGMP-dependent downstream signalling events [96, 152].

### 1.2.3 cGMP as cardioprotective second messenger in the heart

*1.2.3.1 Cardioprotective functions of cGMP*

It is well accepted that cGMP acts as a cardioprotective second messenger in the heart. The cardioprotective role of cGMP was shown in numerous studies in different animal- and disease-models. The possibility to intervene at many points in the cGMP signalling cascade, like cGMP generation, degradation, and effector activation, offers a wide range of possible therapeutic targets.

The cardioprotective role of NP-GCs was demonstrated in multiple GC-A overexpression and disruption studies [79, 80, 99, 100] . Cardiomyocyte-restricted overexpression of GC-A could attenuate cardiomyocyte remodelling by acting as a negative regulator of cardiomyocyte size [100]. Mice deficient in GC-A were mildly hypertensive and showed increased cardiac hypertrophy and fibrosis [79, 80], and cardiomyocyte specific GC-A deletion resulted in the development of cardiac hypertrophy [99]. However, clinical trials using the BNP analogue nesiritide for the treatment of acute decompensated heart failure were not successful [153, 154]. A possible explanation for this could be the downregulation and decreased sensitivity of GC-A receptors during heart failure [155]. Nevertheless, BNP-guided therapy, which means choosing medical treatment based on the BNP plasma levels, could improve the outcome in heart failure in the STARS-BNP Multicentre Study [156] and in the BATTLESCARRED study [157]. GC-B was also shown to be involved in cardioprotection. CNP administration could inhibit endothelin-1 induced cardiomyocyte hypertrophy *in vitro* [158] and attenuated cardiac remodelling after myocardial infarction *in vivo* through its antifibrotic and antihypertrophic action [103]. Angiotensin II induced cardiac hypertrophy, fibrosis, and contractility dysfunction could be also attenuated by CNP administration [159]. The use of Neprilysin inhibitors to increase NP levels by inhibition of NP breakdown is another promising strategy to improve the pathophysiology of heart failure [106]. Sacubitrilat administration to murine ventricular cardiomyocytes that have been put under catecholaminergic stress resulted in a strong reduction of the arrhythmogenic $Ca^{2+}$ leak from the sarcoplasmic reticulum without affecting the systolic $Ca^{2+}$ release [160]. Neprilysin inhibition has also already shown promising results

in the clinics. In the PARADIGM-HF study simultaneous inhibition of Neprilysin and angiotensin II receptors by sacubitril/valsartan significantly reduced morbidity and mortality in heart failure patients compared to sole interference with the renin-angiotensin system [161, 162, 163].

Another potential target to increase cardioprotective cGMP levels is NO-GC. The use of NO donors like glyceryl trinitrate or sodium nitroprusside to stimulate cGMP production is mostly used to treat acute angina pectoris attacks in patients. However, the problem with the use of NO donors is that they have a narrow therapeutic window and do not allow a constant and long-lasting cGMP stimulation [81, 164]. More recently, two new classes of drugs have been developed to increase NO-GC activity, the so called NO-GC stimulators and NO-GC activators. While stimulators increase the activity of the NO-sensitive, haem-containing NO-GC, activators can increase the activity of the oxidized and/or haem-free NO-GC [75, 164]. Activation of NO-GC was shown to be cardioprotective in many different models. In an *in vitro* model of endothelin-1 induced hypertrophy in neonatal rat cardiomyocytes, administration of the NO-GC activator BAY 58-2667 could elicit protective, antihypertrophic, cardiomyocyte-selective effects [165]. An ischemia-reperfusion model in rat hearts, could show that infarct size was attenuated when either NO-GC stimulator Bay 41-2272, or NO-GC activator Bay 60-2770 was given during early reperfusion [166]. Recently, another study demonstrated the important role of cardiomyocyte NO-GC for cardioprotective signalling by cGMP elevating agents following acute myocardial infarction. Basal infarct sizes were significantly reduced by administration of the NO-GC activator cinaciguat in wildtype mice, whereas infarct sizes in cardiomyocyte-specific NO-GC knockout mice could not be reduced with this agent [167]. The same group also demonstrated that cGMP elevating compounds provide cardioprotection against ischemia-reperfusion injury *via* cardiomyocyte-specific BK channels, a downstream target of PKG [168].

Targeting PDEs in order to reach cGMP-dependent cardioprotection is another attempt which has been investigated by multiple groups. The role of PDE5 inhibition in cardioprotection is perhaps the most frequently studied and many animal studies showed promising cardioprotective results for the use of PDE5 inhibitors. In mice exposed to chronic pressure overload induced by transverse aortic constriction, chamber and myocyte hypertrophy was clearly improved by oral administration of the PDE5 inhibitor Sildenafil. Additionally, already pre-established hypertrophy could be reversed by Sildenafil administration, restoring chamber function back to normal [169]. A further study claimed that this cardioprotective role of Sildenafil in mice with chronic pressure overload is caused by cGMP-mediated PKG activation *via* PDE5 inhibition [170], and a mouse model of hypertension-mediated pressure overload demonstrated that the initial antihypertrophic and cardioprotective effects of PDE5 inhibitors are mediated *via* the PKG target protein RGS2

[142]. However, until now, it is highly discussed in the field, whether PDE5 is expressed in murine cardiomyocytes or not. Some groups clearly demonstrated that PDE5 protein is not detectable in murine cardiomyocytes [137, 171, 172]. Then, the question is, how can PDE5 inhibition have cardioprotective effects, when PDE5 is not expressed in murine cardiomyocytes? One possible explanation could be, that Sildenafil treatment affects other cell types, such as for example fibroblasts. cGMP can diffuse through gap junctions [173] and cGMP produced in fibroblasts can enter cardiomyocytes through this gap junctions [174]. Another possible explanation could be the inhibition of other PDEs, which are present in cardiomyocytes, by higher doses of Sildenafil. PDE1C is known to be such a PDE and it is expressed in cardiomyocytes at high levels [75, 137]. This could also explain, why clinical trials failed using Sildenafil to improve cardiac function. Two clinical trials, the RELAX trial and the SIDAMI trial showed little or no cardioprotective effect of Sildenafil treatment in patients with heart failure [175, 176]. In these studies, the used pharmacological concentration of Sildenafil was not high enough to inhibit PDE1C, which might explain the unexpected outcome [75].

Targeting PDEs other than PDE5 in order to increase cardioprotective cGMP levels was also done during the last years. PDE9 is a cGMP specific PDE which has been suggested as a potential therapeutic target. PDE9A inhibition could reverse pre-established heart disease *in vivo* in a mouse model of transverse aortic constriction [130]. Targeting dual-substrate PDEs have shown promising results as well. Mice with global deletion of PDE1C were protected against pathological cardiac remodelling such as myocardial hypertrophy, apoptosis, cardiac fibrosis, and loss of contractile function induced by transverse aortic constriction [177]. Broad PDE1 inhibition with the PDE1-selective inhibitor IC86340 was also effective. It could suppress cardiomyocyte hypertrophy *in vitro* [178] as well as *in vivo* [179]. Selective pharmacological inhibition of PDE2 with Bay 60-7550 could attenuate the pathogenesis of experimental heart failure in a mouse model of abdominal aortic constriction and this effect was promoted by cGMP signalling [180].

PKG exerts the physiological effects of cGMP in the cardiovascular system. However, direct small molecular activators of PKG still have to be developed as drug therapy [82]. Knock-in mice expressing the redox-dead PKG I$\alpha^{C42S}$ were protected against pressure overload induced pathological cardiac remodelling in a model of chronic transaortic constriction [181].

An overview of the potential therapeutic targets in the cGMP signalling cascade is shown in Figure 1.7.
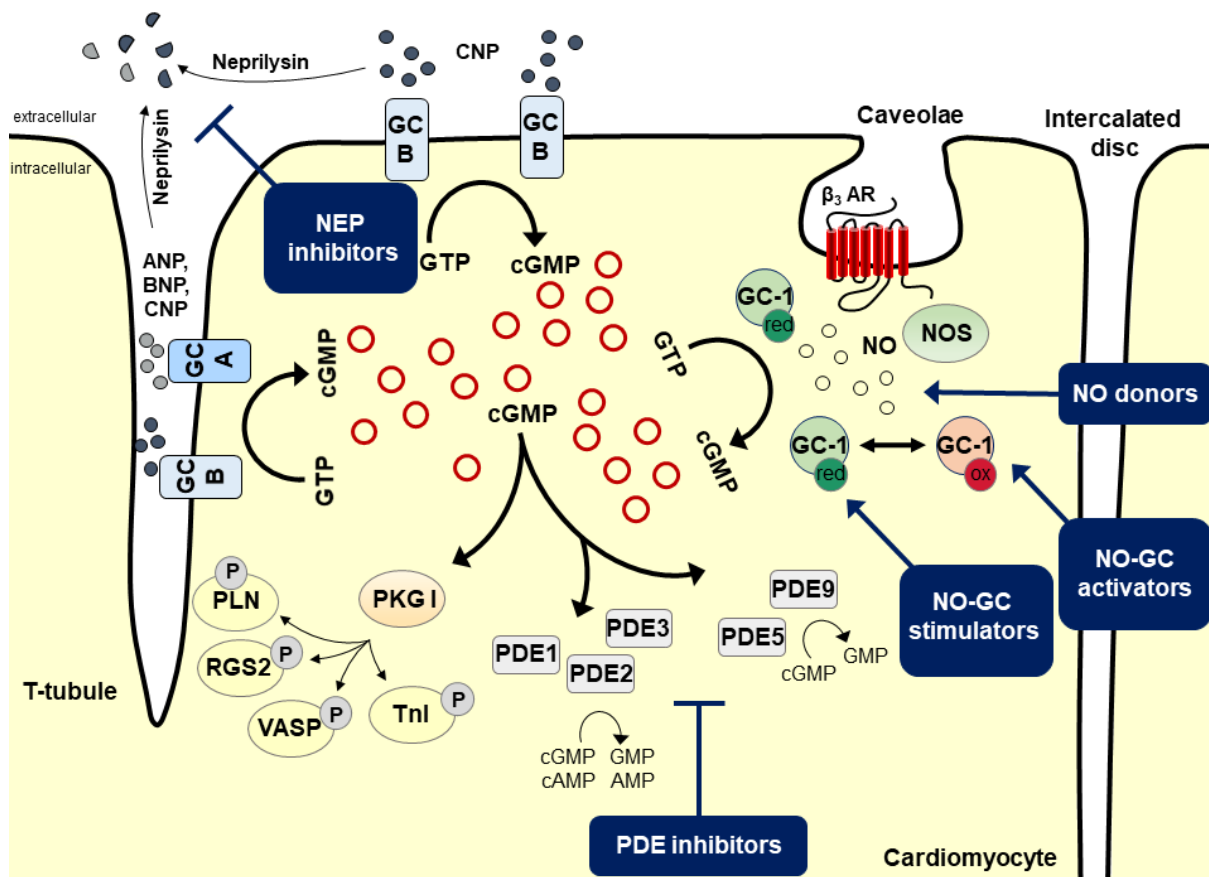
**Figure 1.7:** **Potential cardioprotective therapeutic targets in the cGMP signalling cascade.**
The possibility to intervene at many levels in the cGMP signalling cascade, like cGMP generation, degradation, and effector activation, offers a wide range of possible therapeutic targets. NEP inhibitors, NO donors, NO-GC stimulators and activators, as well as PDE inhibitors act on different points in the cGMP signalling cascade and have been shown to be cardioprotective. ANP, atrial natriuretic peptide; BNP, brain natriuretic peptide; cAMP, 3',5'-cyclic adenosine monophosphate; cGMP, 3',5'-cyclic guanosine monophosphate; CNP, C-type natriuretic peptide; GC, guanylyl cyclase; GMP, guanosine monophosphate; GTP, guanosine triphosphate; NEP, Neprilysin; NO, nitric oxide; NO-GC, NO-stimulated GC; NOS, NO synthase; NP, natriuretic peptide; NP-GC, membrane bound guanylyl cyclase; PDE, phosphodiesterase; PKG, protein kinase G ; PLN, phospholamban; RGS2, regulator of G-protein signalling 2; TnI, Troponin I; VASP, vasodilator-stimulated protein.

*1.2.3.2 Role of cGMP in hypoxia/reoxygenation injury*

As already mentioned above, multiple studies have been done in different animal models, demonstrating that increasing cGMP levels during myocardial ischemia/reperfusion injury using e.g. NO-GC stimulators/activators or PDE inhibitors provide cardioprotection against ischemia/reperfusion injury [166, 167, 182, 183].

However, not much is known about the specific role of cGMP signalling during hypoxic injury alone. Hypoxia is a key risk factor in many different CVDs and not necessarily associated

with ischemia. Therefore, it is important to elucidate the potential cardioprotective effect of cGMP on hypoxic injury alone to target hypoxia in many different CVDs.

Some attempts have been made in the past to investigate cGMP levels during hypoxic injury. However, those studies which have been mostly done in hypoxic whole-heart Langendorff models show contradictory results. Whereas in a Langendorff-perfused rat heart model, 10 min of anoxia showed an increase in cGMP levels during the end of this 10 min period [184], 30 min of hypoxia [185] or 40 min of hypoxia, followed by 90 min reoxygenation [186] showed a decrease in cGMP content. Studies from single cell models showed the same contradictory results. While in one study two hours of hypoxia in adult rat cardiomyocytes led to a significant increase in cGMP levels compared to controls [187], 30/60 min of anoxia caused no significant alteration in cGMP levels in adult rat cardiomyocytes in another study [188].

In order to figure out whether the cGMP signalling cascade might be a good therapeutic target for hypoxic injury, more studies are urgently needed.

### 1.2.3.3 Role of cGMP in atrial fibrillation

Not much is known about the role of cGMP in AF. Some studies showed an increase in plasma cGMP and ANP levels in AF. In a dog model, AF- induction with aconitine led to a significant increase in cGMP levels, whereas cAMP levels remained unchanged. Bringing the dogs back to SR with atropine treatment returned cGMP plasma levels back to normal. In the same study, the authors also showed that cGMP levels were significantly higher in patients with AF [189, 190]. Other studies, in which cGMP levels were measured using radioimmunoassay, showed that cGMP as well as ANP levels were markedly increased in patients with paroxysmal AF during arrhythmia [191, 192, 193]. One possible explanation could be that increased ANP and cGMP plasma levels might be a compensatory mechanism of cardiac dysfunction [194].

Mapping of an AF locus to chromosome 1p36-p35 in a family of 11 clinically affected AF members could identify a heterogenous frameshift mutation in the gene encoding for ANP, *NPPA*. This frameshift mutation abolished the normal stop codon resulting in a 12 amino acid extension of ANP. This mutant ANP was still active but more resistant to proteolytic degradation than the wildtype ANP and subjects with this mutation showed very high concentrations of mutant ANP. An isolated rat heart model in which hearts were perfused either with ANP or with mutant ANP, could show shortened action potentials when perfused with mutant ANP. This indicates that this mutant ANP form creates a possible substrate for the treatment of AF patients and shows that perturbation of the ANP-cGMP pathway can result in cardiac electrical instability [195]. A recently published study created two transgenic

mouse lines expressing either the human wild-type *NPPA* gene or the human mutant *NPPA* gene found by Hodgson-Zingman and colleagues [195]. They could show that the mice expressing the mutant *NPPA* showed remodelling of cardiac $Na^+$, $Ca^{2+}$, and $K^+$ channels creating an electrophysiologic substrate for re-entrant AF. Plasma cGMP levels were increased in mice expressing mutant *NPPA* [196]. Another AF-associated human variant in the *NPPA* gene (p.Ile138Thr) was shown to cause inflammation, fibroblast activation, and atrial fibrosis, leading to AF in knock-in rats. This gene variant inhibits the interaction between ANP and its receptor GC-A. Reduced intracellular cGMP levels and mutant ANP induce differentiation of cardiac fibroblasts to myofibroblasts and promote fibrosis [197].

Pitx2 is a transcription factor that plays a critical role in directing cardiac asymmetric morphogenesis [198]. The *PITX2* gene has been shown to be associated with the pathology of AF and single nucleotide variants on the human chromosome 4q25, 170 kb distal to the *PITX2* gene, have been shown to be associated with an increased risk of familial AF [199]. *PITX2* expression can be increased [200] or decreased [201] in atrial samples of AF patients compared to SR samples. *PITX2* targets multiple genes, however one main target is *NPPA*. Pitx2c markedly activates *NPPA* promoter, increases *NPPA* gene transcription, and augments ANP production. Thereby it can regulate LTCC current ($I_{Ca,L}$) by a post-translational mechanism involving ANP [198].

Abundance of epicardial adipose tissue is associated with AF, however origin and factors involved in epicardial adipose tissue expansion are still unknown. Recently, it could be shown that atrial epicardial adipose tissue derives from adult atrial epicardial cells *via* epithel-to-mesenchymal transition. ANP promotes adipogenic differentiation by cGMP activation, showing a crosstalk between epicardial adipose tissue expansion and mechanical function of atrial myocardium [202].

Several studies investigated the effect of NO in AF. A pig model of AF showed a marked decrease in eNOS expression and NO bioviability in AF [203]. Atrial-specific up-regulation of microRNA-31 (miRNA-31) in goat and human AF was shown to deplete nNOS by accelerating mRNA decay and alteration of nNOS subcellular location. Silencing of miRNA-31 in atrial myocytes from patients with AF could restore nNOS and normalize action potential duration [204]. Another study investigated the impact of NO signalling on calcium influx in human right atrial myocytes and its relation to AF. Therefore, the authors measured $I_{Ca,L}$ with voltage-clamp technique. In cardiomyocytes from patients in SR, $I_{Ca,L}$ increased with increasing concentrations of the NO-donor SNAP. PDE3 inhibition with Cilostamide enhanced $I_{Ca,L}$ to similar extent as SNAP. When cAMP was elevated by PDE3 inhibition or βAR stimulation with Isoprenaline, SNAP reduced $I_{Ca,L}$, pointing to cGMP-cAMP cross-regulation. In AF, the stimulatory effect of SNAP on $I_{Ca,L}$ was attenuated, while its inhibitory effect on isoprenaline- or Cilostamide-stimulated current was preserved [205].

Clearly, more studies are needed in the future to investigate whether cGMP is a suitable therapeutic target for AF.

## 1.3 Tools for cGMP detection, Förster resonance energy transfer

In order to investigate cGMP as a therapeutic target, tools for cGMP detection are indispensable. Various technical approaches have been used in the past to study the cGMP signalling cascade. Radioimmunoassay, enzyme-linked immunosorbent assay, or Immunoblot are classical biochemical techniques that can be used to study cGMP signalling. However, despite being quite sensitive and specific, all these techniques require high amounts of cells or tissues that need to be disrupted. Furthermore, analysis of real time dynamics under physiologically relevant conditions is impossible using those techniques [206].

Electrophysiological patch-clamp recording of CNG channels made it possible to monitor real time cGMP dynamics in living cells with very high resolution [207, 208]. However, spatial resolution with this technique is limited to subsarcolemmal microdomains and the measurements are technically quite challenging [152, 209].

One state-of-the-art technique which has been intensively used during the last years to study cyclic nucleotide dynamics is Förster resonance energy transfer (FRET). FRET is a quantum mechanical phenomenon, which was discovered by the German physicist Theodor Förster in 1948 [210]. It is a non-radiative, distance-dependent energy transfer from a donor fluorophore to an acceptor fluorophore [211]. For FRET to occur certain conditions must be fulfilled: i) the donor-acceptor distance must be less than 10 nm; ii) the fluorophores must be appropriately oriented in space; and iii) the donor emission spectrum must overlap at least 30% with the acceptor excitation spectrum [211, 212, 213]. An example for such overlap of the emission spectrum of green fluorescent protein (GFP) and the excitation spectrum of red fluorescent protein (RFP) is shown in Figure 1.8 (Figure 1.8 B).

The efficiency (E) of FRET is dependent on the distance ($r$) between the donor and the acceptor and can be described with the following equation, where $R_0$, also called Förster radius, is the distance at which half of the energy is transferred [210, 211].

$$E = \frac{1}{1 + \left(\frac{r}{R_0}\right)^6}$$

The Jablonski diagram, which is shown in Figure 1.8 (Figure 1.8 A), explains the effect of FRET. The absorption of a photon by the donor fluorophore raises an electron from the singlet state ($S_0$) to an excited state ($S_1$). When the electron drops back to ground level, the energy that is released from this relaxation of the donor is taken up partially by an acceptor, leading to the excitation of an acceptor electron and further to emission of a photon as the acceptor electron falls back from the $S_1$ state to the ground level $S_0$ (Figure 1.8 A) [214].
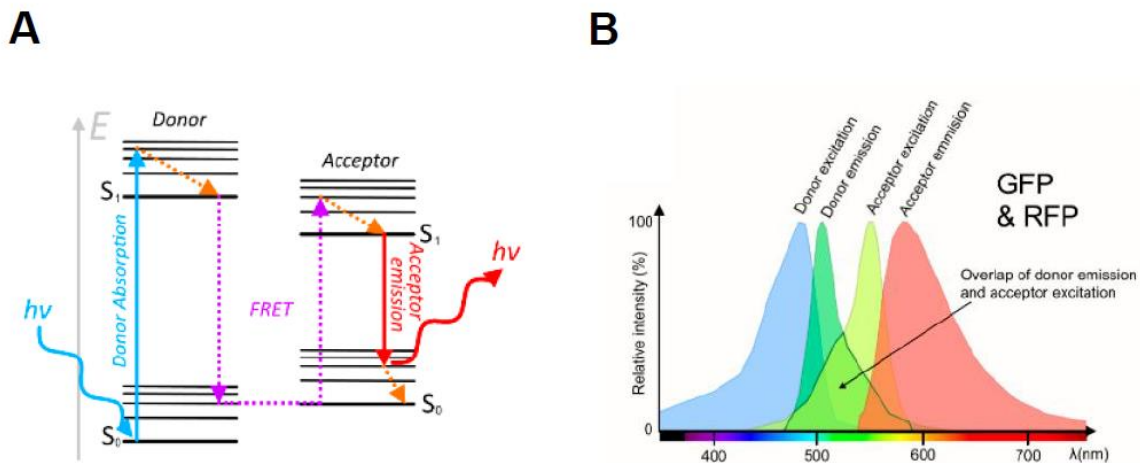


**Figure 1.8:** **Principles of Förster resonance energy transfer (FRET).** **A)** Jablonski diagram explaining the effect of FRET. Absorption of a photon by the donor fluorophore raises an electron from the singlet state ($S_0$) to the excited state ($S_1$). The energy that is released from the relaxation of the donor is taken up partially by an acceptor, leading to excitation of an acceptor electron and further to the emission of a photon by the acceptor as the acceptor electron falls back from the $S_1$ state to the ground level $S_0$. **B)** Overlap of the donor emission and acceptor excitation spectrum of green fluorescent protein (GFP) and red fluorescent protein (RFP). The spectra must overlap at least 30% to allow FRET. Figures adapted from [214].

Since the early 2000's several FRET-based as well as fluorescent non-FRET biosensors have been developed for cGMP measurements, which are summarized in Table 1.1. All these sensors have different sensitivities, selectivities, and dynamic ranges, making each of them useful for different types of cells and tissues.

The challenges to measure cGMP in adult cardiomyocytes are the very low basal cGMP levels (~10 nM) [136], and the fact that basal cAMP levels (~1 µM) are more than 100-times higher than cGMP levels in adult cardiomyocytes [215]. The first sensor making it possible to measure real time cGMP dynamics in living adult cardiomyocytes was the biosensor red-cGES-DE5. It consists of the PDE5A GAF-A domain flanked by the two fluorophores T-Sapphire and Dimer2. It has a very high cGMP sensitivity ($EC_{50}$ = 40 nM), and a high selectivity for cGMP over cAMP (> 1000-fold) [136, 216, 217] (Figure 1.9). Two other recently developed FRET sensors which are suitable for the use in adult cardiomyocytes are Yellow

*Pf*PKG and Red *Pf*PKG. They consist of the cyclic nucleotide binding domain D of *Plasmodium falciparum* PKG flanked by the fluorophores cyan fluorescent protein (CFP) and Venus (Yellow *Pf*PKG) or T-Sapphire and Dimer2 (Red PfPKG) [218].

**Table 1.1: FRET-based and non-FRET cGMP biosensors.** BFP, blue fluorescent protein; cAMP, 3',5'-cyclic adenosine monophosphate; CFP, cyan fluorescent protein; cGMP, 3',5'-cyclic guanosine monophosphate; GFP, green fluorescent protein; PDE, phosphodiesterase; PKG, protein kinase G; Rluc, *Renilla* luciferase; YFP, yellow fluorescent protein**.**

| Name and EC$_{50}$ | Design | Properties | References |
|---|---|---|---|
| **FRET-based cGMP biosensors** | | | |
| **CGY-Del1**, EC$_{50}$ = 20 nM | CFP and YFP fused to N- and C-terminal ends of PKG I$\alpha$ | Single chain, low cGMP/cAMP selectivity | [219], [220] |
| **cGES-GKIB**, EC$_{50}$ = 5 µM | Binding domain from PKG-I flanked by YFP and CFP | Single chain, rather slow kinetics, not enough selectivity between cAMP and cGMP | [220] |
| **Cynget-1 and Cynget-2**, EC$_{50}$:1.5/1.9 µM | CFP and YFP fused to N- and C-terminal ends of PKG I$\alpha$, with truncated N-terminus | Single chain, better cGMP/cAMP selectivity, relatively low sensitivity and temporal resolution | [221], [222] |
| **cGI family (cGi-500/3000/6000)**, EC$_{50}$: 500/3000/6000 nM | Both cGMP binding domains of PKG I fused to CFP and YFP | Single chain, small size, moderate selectivity and sensitivity, high dynamic range, fast kinetics | [223], [224], [225] |
| **cGES-DE2, cGES-DE5**, EC$_{50}$: 0.9/1.5 µM | Single cGMP binding (GAF domains) from PDE2 or PDE5 fused to CFP and YFP (PDE2A GAF-B domain; PDE5A GAF-A domain) | Single chain, fast kinetics, moderate sensitivity, small size | [220], [226] |
| **PDE5-GAF A+B sensor**, EC$_{50}$ = 0.3 µM | PDE5 GAF A + B domain flanked with CFP and YFP | Single chain, highly selective for cGMP, very slow binding and dissociation kinetics to low cGMP concentrations | [224], [227] |
| **PDE2-GAF sensor**, EC$_{50}$ = 0.04 µM | PDE2A GAF A+B domains flanked by CFP and YFP | High affinity for cGMP, very low cAMP/cGMP selectivity | [227] |

| | | | |
|---|---|---|---|
| **Red-cGES-DE5**, $EC_{50} = 40$ nM | PDE5A GAF-A domain, flanked with T-Sapphire and Dimer 2 | High selectivity for cGMP over cAMP (> 1000-fold), high affinity for cGMP, fast kinetics | [216], [136], [217], [228] |
| **Yellow *Pf*PKG**, **Red *Pf*PKG**, $EC_{50}$: 23 nM/30 nM | Cyclic nucleotide binding domain D of *Plasmodium falciparum* PKG flanked with the fluorophores CFP and Venus (Yellow *Pf*PKG) or T-Sapphire and Dimer2 (Red *Pf*PKG) | Single chain; Yellow *Pf*PKG: high affinity, large dynamic range; Red *Pf*PKG: high affinity, lower dynamic range than yellow *Pf*PKG (28%) | [218] |
| **<sup>T</sup>hPDE5<sup>VV</sup>**, $EC_{50} = 0.32$ µM | PDE5A GAF-A domain (similar to cGES-DE5) flanked with mTurquoise and mVenus | High specificity for cGMP over cAMP, better reversibility than cGi500 | [229] |
| **Non-FRET cGMP biosensors** | | | |
| **GAF-BRET sensor**, $EC_{50} = 30$ nM | PDE5 GAF-A domains as fusions between GFP and Rluc | Single Chain, good cGMP selectivity, slow kinetics | [230] |
| **FlincGs (FlincG1-3)**, $EC_{50}$: 0.17 – 0.89 µM | Both cGMP binding domains from PKG I fused to circular permuted GFP | Single chain, good dynamic range, rapid kinetics, moderate cGMP/cAMP selectivity | [231]. [232], [233] |
| **Cyngus**, $EC_{50} = 1$ µM | Unicolor fluorescent sensor, PDE5A GAF-A domain sandwiched between sREACh and mTagBFP | Single chain, good selectivity for cGMP over cAMP (400-fold), fast kinetics, change in fluorescence signal small | [234] |
| **Green cGull**, $EC_{50} = 1.09$ µM | cGMP binding domain of PDE5A (GAF-A) inserted in the vicinity of Citrine | High dynamic range, moderate sensitivity | [235] |

As already mentioned above, only two types of cGMP biosensors which are capable of measuring cGMP dynamics in adult cardiomyocytes are available until now, the sensors red-cGES-DE5 [216] (Figure 1.9) and Yellow *Pf*PKG or Red *Pf*PKG [218]. The principle of the FRET sensor red-cGES-DE5 is shown in Figure 1.9.
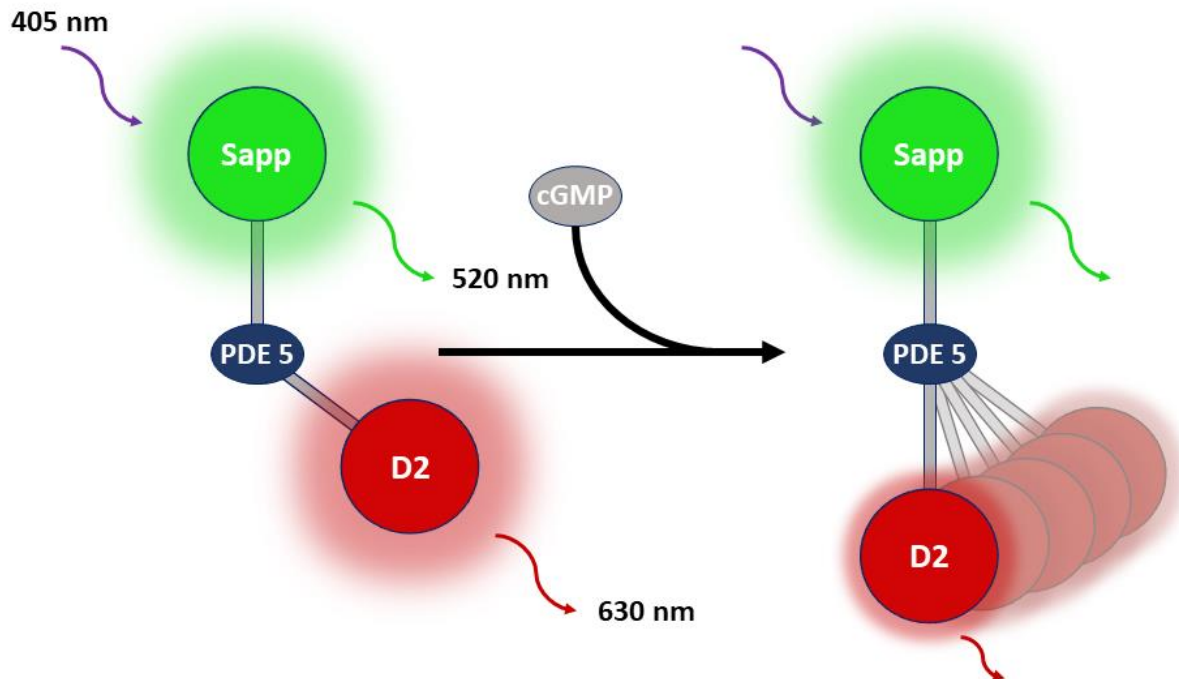


**Figure 1.9:** **Principle of the FRET-based cGMP biosensor red-cGES-DE5.** The biosensor consists of the GAF-A domain of phosphodiesterase 5A (PDE5), flanked by the donor fluorophore T-Sapphire (Sapp) and the acceptor fluorophore Dimer2 (D2). Excitation of the donor fluorophore T-Sapphire with light of 405 nm, leads to an emission of 520 nm light. When donor and acceptor fluorophores are at close proximity to each other (<10 nm), Förster resonance energy transfer (FRET) can occur. By FRET, energy is transferred from the donor to the acceptor fluorophore, which results in emission of the acceptor at 630 nm. 3',5'-cyclic guanosine monophosphate (cGMP) binding to the PDE5 GAF-A domain leads to a conformational change of the sensor, increasing the distance between donor and acceptor fluorophores and a decrease of FRET.

A few years ago, our group has generated a transgenic mouse line with cardiomyocyte-specific expression of the red-cGES-DE5 biosensor. The cardiomyocyte-specific expression in these mice was reached by expressing the red-cGES-DE5 biosensor under the cardiac muscle-specific α-myosin heavy chain (αMHC) promoter [136] (Figure 1.10).
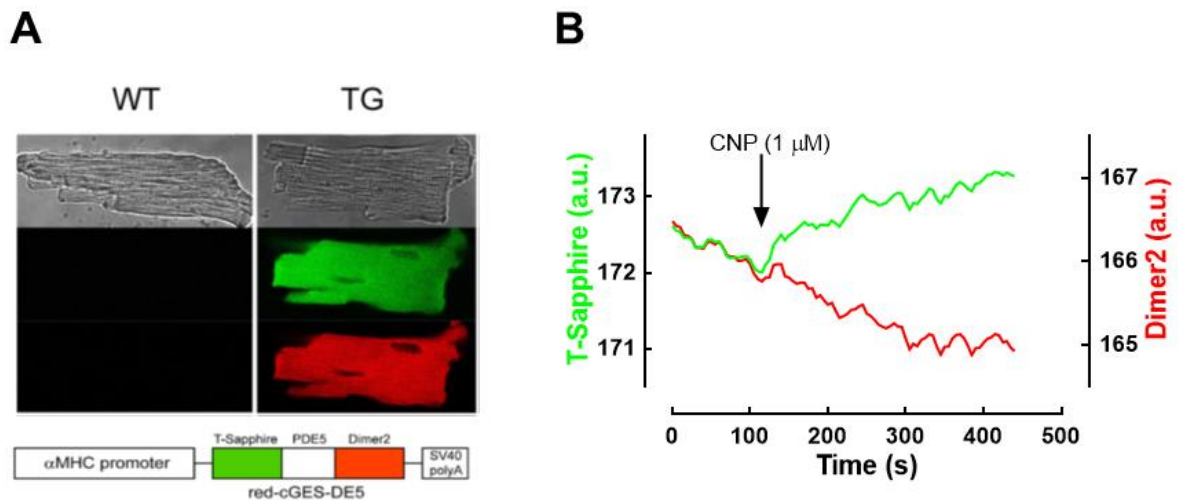
**Figure 1.10:  Red-cGES-DE5 transgenic mice.  A)** Confocal images of wildtype (WT) and transgenic (TG) cardiomyocytes in T-Sapphire and Dimer2 channels and schematic presentation of the sensor sequence. The 3',5'-cyclic guanosine monophosphate (cGMP) binding domain of PDE5, flanked by the two fluorophores T-Sapphire and Dimer2, was expressed under control of the cardiac muscle-specific α-myosin heavy chain (αMHC) promoter. Figures adapted from [136]. **B)** Exemplary FRET trace, showing the change in fluorescence of the two fluorophores T-Sapphire and Dimer2 upon stimulation with C-type natriuretic peptide (CNP, 1 µM).

## 1.4 Aim of this thesis

The development of new cardioprotective strategies to treat CVDs is the major goal of cardiovascular research. The second messenger cGMP is known for its cardioprotective role in the cardiovascular system and the cGMP signalling cascade offers many potential therapeutic targets. In this work, the cardioprotective role of cGMP was investigated in two different disease models, hypoxic injury and AF.

### 1.4.1 Changes in mouse and human cardiomyocyte cGMP dynamics during hypoxic injury

Hypoxia is considered as one major characteristic of many CVDs. However, until now, not much is known about the role of cGMP dynamics in hypoxic injury.

In this part of the work, different models of hypoxic injury in mouse and human cardiomyocytes were used to answer four major questions:

- What is the effect of hypoxic injury on the cGMP signalling cascade?

- What are direct cardiomyocyte-specific effects of hypoxic injury on cGMP signalling and what are indirect effects such as cell-cell contact and influence of other cell types?
- Can results generated from mouse cardiomyocytes be reproduced in human cardiomyocytes?
- Is there a potential therapeutic target in the cGMP signalling cascade which can be used to protect from hypoxic injury?

### 1.4.2 cGMP signalling in the human atrium and its role in atrial fibrillation

This part of the work investigated the effect of the cardioprotective second messenger cGMP in AF. Since currently available treatment options for AF are limited, new molecular targets are urgently needed. Mice are not a good model for AF, therefore, human tissue samples were used in this part of the work.

The aim was to establish real time cGMP imaging in human atrial cardiomyocytes in order to characterize the cGMP signalling cascade in cardiomyocytes of right (RA) and left human atria (LA) of patients in SR and with AF.

Major questions were:

- Does cGMP signalling play a role in human atrial cardiomyocytes?
- What are the differences in cGMP signalling between cardiomyocytes from RA and LA?
- How is cGMP signalling altered in AF?
- What are the specific roles of different GCs for cGMP generation and which PDEs are involved in cGMP degradation in RA and LA from patients in SR and with AF?

# 2. Material and Methods

## 2.1 Material

### 2.1.1 Mouse lines

The mouse lines used in this work are listed in Table 2.1.

**Table 2.1:**     **Mouse lines.**

| Mouse line | Genetic background | Origin |
| --- | --- | --- |
| Red-cGES-DE5 | C57/BL6 | Prof. Viacheslav Nikolaev [136] |
| CM NO-GC$^{-/fl}$ | C57/BL6 | Prof. Robert Lukowski [167] |
| Red-cGES-DE5 x CM NO-GC$^{-/fl}$ | C57/BL6 | Prof. Robert Lukowski |
| CAG-Epac1-camps | FVB/N1 | Prof. Viacheslav Nikolaev [236] |

### 2.1.2 Eukaryotic cell lines

The eukaryotic cell lines used in this work are listed in Table 2.2.

**Table 2.2:**     **Eukaryotic cell lines.**

| Cell line | Manufacturer | Catalogue number |
| --- | --- | --- |
| HEK293A | Invitrogen | R705-07 |

### 2.1.3 Plasmids

Plasmids used in this work are listed in Table 2.3.

**Table 2.3:**     **Plasmids.**

| Plasmid | Vector | Origin |
| --- | --- | --- |
| T-Sapphire | pcDNA3.0 | Dr. Oliver Griesbeck, MPI Martiensried |
| ECFP | pECFP-N1 | Clontech |

**2.1.4 DNA Oligonucleotides**

*2.1.4.1 DNA oligonucleotides for PCR, qRT PCR, and TaqMan PCR*

In this work, DNA oligonucleotides were used for polymerase chain reaction (PCR), quantitative reverse transcriptase polymerase chain reaction (qRT PCR), and TaqMan polymerase chain reaction (TaqMan PCR). DNA Oligonucleotides were purchased from Eurofins Genomics (Ebersberg) and are listed in Table 2.4.

**Table 2.4:    DNA Oligonucleotides.**

| DNA Oligonucleotide | Sequence (5'-3') | Application |
|---|---|---|
| GAPDH forward | 5'-CGTCCCGTAGACAAAATGGT -3' | qRT PCR |
| GAPDH reverse | 5'-GAATTTGCCGTGAGTGGAGT -3' | qRT PCR |
| GUCY1A1 forward | 5'-CCCCTGGTCAGGTTCCTAAG-3' | qRT PCR |
| GUCY1A1 reverse | 5'-GGAGACTCCCTTCTGCATTCT-3' | qRT PCR |
| GUCY1B1 forward | 5'-CTGCTGGTGATCCGCAATTAT-3' | qRT PCR |
| GUCY1B1 reverse | 5'-GATGGTATCATAGCCAGACTCCT-3' | qRT PCR |
| HIF-1$\alpha$ forward | 5'- TCAAGTCAGCAACGTGGAAG -3' | qRT PCR |
| HIF-1$\alpha$ reverse | 5'- TATCGAGGCTGTGTCGACTG-3' | qRT PCR |
| IL2p32 forward | 5'-TCACATCCAGTTCTATGCTGGT-3' | TaqMan PCR |
| IL2p32 reverse | 5'-CAAGGAAACTGGGAACATGAA-3' | TaqMan PCR |
| NPR1 forward | 5'-TGGAGACACAGTCAACACAGC-3' | qRT PCR |
| NPR1 reverse | 5'-CCGAAGACAAGTGGATCCTG-3' | qRT PCR |
| NPR2 forward | 5'-TGTTTGGTGTTTCCAGTTTCC-3' | qRT PCR |
| NPR2 reverse | 5'-AGTTCTTCCCAGCGAATGC-3' | qRT PCR |
| PDE1A forward | 5'-TATGTCCCTGATACTCCATGCAG-3' | qRT PCR |
| PDE1A reverse | 5'-TGGAAGCCCTAATTCAGCTTCT-3' | qRT PCR |
| PDE1C forward | 5'-TACCGATTTCTGCACTTGTCTC-3' | qRT PCR |
| PDE1C reverse | 5'-TCTGTCAGCCAGTTTGCTACT-3' | qRT PCR |
| PDE2A forward | 5'-TCATGACCTGGACCACAGAG-3' | qRT PCR |
| PDE2A reverse | 5'-TAGCAATGGCTTGAGCAAAGTG-3' | qRT PCR |
| PDE3A forward | 5'-TGTTTGAAGACATGGGGCTCT-3' | qRT PCR |
| PDE3A reverse | 5'-TAGAACATCGGTGGCATGGATT-3' | qRT PCR |
| PDE5A forward | 5'-TGAGGTTCTTTGCAGGTGGAT-3' | qRT PCR |

| | | |
|---|---|---|
| PDE5A reverse | 5'-CAGAGCAGCAAACATGCACT-3' | qRT PCR |
| redDE5 forward | 5'-TGACAGACAGATCCCTCCTAT-3' | PCR |
| redDE5 reverse | 5'-GGATGCTCAGGTAGTGGTT-3' | PCR |
| redDE5 forward | 5'-TGAAGTTCGAGGGCGACAC-3' | TaqMan PCR |
| redDE5 reverse | 5'-GTTGTACTCCAGCTTGTGCC-3' | TaqMan PCR |

### 2.1.4.2 Universal probes for TaqMan PCR

Universal TaqMan PCR probes used in this work were pre-labelled with a reporter fluorophore (FAM) and a dark quencher dye. They were purchased from Sigma Aldrich (St. Louis). Universal probes for TaqMan PCR are listed in Table 2.5.

**Table 2.5:    Universal probes for TaqMan PCR.**

| Probe | Gene | Catalogue number |
|---|---|---|
| Probe #32 | Housekeeping gene IL32 | 04687655001 |
| Probe #161 | Target gene red-cGES-DE5 | 04694481001 |

### 2.1.5 Antibodies

In this work, primary and secondary antibodies were used for Immunoblot analysis of isolated mouse ventricular cardiomyocytes, mouse ventricular tissue samples, human ventricular tissue samples, and human atrial tissue samples.

### 2.1.5.1 Primary antibodies

Primary antibodies used in this work are listed in Table 2.6.

**Table 2.6:    Primary antibodies.** gp, guinea pig; ms, mouse; o.n., overnight; rb, rabbit; RT, room temperature.

| Primary Antibody | Dilution, incubation conditions, species | Manufacturer, catalogue number |
|---|---|---|
| Anti-GAPDH | 1:160.000 in 5% milk; 1 h RT; ms | Bio Trend #5G4 |
| Anti-GC-B | 1:2.500 in 2% milk; 4°C o.n.; gp | Kind gift from H. Schmidt |
| Anti-Calsequestrin | 1:5.000 in 3% BSA; 1 h RT; rb | Thermo Scientific PA1-913 |
| Anti-NO-GC$\alpha_1$ | 1:2.000 in 3% milk; 4°C o.n.; rb | Kind gift from A. Friebe |

| | | |
|---|---|---|
| Anti-NO-GCβ$_1$ | 1:2.000 in 3% milk; 4°C o.n.; rb | Kind gift from A. Friebe |
| Anti-PDE1C | 1:1.000 in 5% milk; 4°C o.n.; rb | Kind gift from C. Yan |
| Anit-PDE2A | 1:500 in 3% BSA; 4°C o.n.; rb | Fabgennix #PD2A-101AP |
| Anti-PDE3A | 1:1.000 in 3% milk; 4°C o.n.; rb | Kind gift from C. Yan |
| Anti-PKG | 1:1.000 in 5% milk; 4°C o.n.; rb | Cell Signalling #3248S |

*2.1.5.2 Secondary antibodies*

In this work, horseradish peroxidase (HRP)-conjugated secondary antibodies were used. Antibodies were diluted in the same buffer as the corresponding primary antibody (Table 2.6). Secondary antibodies are listed in Table 2.7.

**Table 2.7:** **Secondary antibodies.** Antibodies were diluted in the same buffer as the corresponding primary antibody. RT, room temperature.

| Secondary Antibody | Dilution, incubation conditions | Manufacturer, catalogue number |
|---|---|---|
| Goat anti-mouse | 1:5.000; 1 h RT | Biorad #170-5047 |
| Goat anti-rabbit | 1:5.000; 1 h RT | Biorad #170-5046 |
| Goat anti-guinea pig | 1:5.000; 1 h RT | Merck #AP108P |

**2.1.6 Chemicals**

Chemicals used in this work are listed in Table 2.8.

**Table 2.8:** **Chemicals.**

| Chemical | Manufacturer | Catalogue number |
|---|---|---|
| Acrylamide (Rotiphorese Gel 40) | Carl Roth | 3029.1 |
| Agarose universal peqGold | VWR | 35-1010 |
| Agarose, Plaque GP | Biozym | 840101 |
| Ammonium persulfate (APS) | Sigma Aldrich | A3678-25G |
| Ampuwa water | Fresenius, Kabi Pac | 40 676.00.00 |
| Atrial natriuretic peptide (ANP) human | Calbiochem | 05-23-0300 |

| | | |
|---|---|---|
| BAY 41-2772 | Sigma Aldrich | B8810 |
| BAY 58-2667, Cinaciguat | Axon medchem | 2172 |
| BAY 60-2770 | Sigma Aldrich | SML2281 |
| Bay 60-7550 | Chem Cruz | sc 396772 |
| β-Mercaptoethanol | Sigma Aldrich | M6250-100ML |
| Blebbistatin | Sigma Aldrich | B0560 |
| Bovine serum albumin (BSA) | Sigma Aldrich | A6003-25G |
| Bromphenolblue | Carl Roth | A512.1 |
| 2,3-Butandione monoxime (BDM) | Sigma Aldrich | B0753-25G |
| $CaCl_2$ x 2 $H_2O$ | Sigma Aldrich | C8108-500G |
| C-type natriuretic peptide (CNP) | Calbiochem | 05-23-0310 |
| Cilostamide | Santa Cruz | sc 201180A |
| CsCl | Sigma Aldrich | C3032-100G |
| Custodiol | VK Siemens | 31268.00.00 |
| Cycloheximide (CHX) | Sigma Aldrich | C7698-1G |
| D-(+)-Glucose | Sigma Aldrich | G7528-250G |
| D-(+)-Saccharose | Carl Roth | 4621.1 |
| Developer concentrate | Adefodur | 00176 |
| Dimethyl sulfoxide (DMSO) | Sigma Aldrich | D8418 |
| Direct PCR Tail | Viagen | 102-T |
| DNA ladder, 100 bp | New England biolabs | N3231S |
| dNTP mix | Promega | U1511 |
| Ethylenediaminetetraacetic acid (EDTA) | AppliChem | A1104,0500 |
| Ethyleneglycoltetraacetic acid (EGTA) | Sigma Aldrich | E4378 |
| Ethanol, Rotipuran, >99.8% p.a. | Carl Roth | 9065.2 |
| Ethanol, 70% vergällt | Chemsolute | 2202.5000 |
| Fixer concentrate | Adefodur | 01176 |
| Forskolin | Sigma Aldrich | F6886 |
| Glycerol | Sigma Aldrich | G5516-100ML |
| Glycine | Carl Roth | 3908.2 |

| | | |
|---|---|---|
| GoTaq Hot Start Polymerase | Promega | M5001 |
| Green buffer (GoTaq reaction buffer) | Promega | M7911 |
| HCl, 37% | Carl Roth | 9277.1 |
| Heparin-Natrium, 25.000 I.E./5 mL | Leo Pharma AS | 050618 |
| 4-(2-hydroxyethyl)-1-piperazineethanesulfonic acid (HEPES) | AppliChem | A1069,0500 |
| Immersion liquid type F | Leica | 11515859 |
| 3-Isobutyl-1-Methylxanthine (IBMX) | AppliChem | A0695-0001 |
| Isoflurane (Forene) | Abbvie | B506 |
| KCl | Merck | 1.04933.0500 |
| $KHCO_3$ | Merck | 1.04854.0500 |
| $KH_2PO_4$ | Merck | 1.04873.0250 |
| Methanol | Carl Roth | 4627.24 |
| $MgCl_2$ x 6 $H_2O$ | Sigma Aldrich | M2670 |
| $MgSO_4$ x 7 $H_2O$ | Merck | 1.05886.0500 |
| Midori Green | Nippon Genetic | MG04 |
| Milchpulver | Carl Roth | T145.1 |
| $Na_2HPO_4$ x $2H_2O$ | Merck | 1.06580.0500 |
| NaCl | Merck | 3957.1 |
| $NaHCO_3$ | Merck | 1.06329.0500 |
| $NaN_3$ | Sigma Aldrich | S2002-25G |
| NaOH | Chemsolute | 1340.1000 |
| Na-Pyruvate | Sigma Aldrich | P8574 |
| NKH 477, 6-[3-(dimethylamino) propionyl]-forskolin | Sigma Aldrich | N3290 |
| ODQ, 1H-[1,2,4]oxa-diazolo [4,3-a]quinoxalin-1-one | Sigma Aldrich | O3636 |
| Polyethylene Glycol 8000 (PEG 8000) | Th.Geyer | RO/00002632/001000 |
| Ponceau S solution | Sigma Aldrich | P7170 |
| 2-Propanol | Chemsolute | 1136.1000 |
| Protein Marker V peqGold | Peqlab | 27-2210 |

| | | |
|---|---|---|
| RNase ERASE | MP Biomedicals | 821682 |
| RNase-free water | GE Healthcare | B-003000-WB-100 |
| SDS, Sodium dodecyl sulfate | Sigma Aldrich | 05030 |
| SDS-Solution, 20% | AppliChem | A0675,0500 |
| Sildenafil | Molekula | 8271 4520 |
| SNAP, S-Nitroso-N-acetyl-DL-penicillamine | Cayman | 82250 |
| Sodium deoxycholate, SOD | Sigma Aldrich | D6750 |
| Tris-acetate-EDTA (TAE) buffer | AppliChem | A1691 |
| Taurine | AppliChem | A1141,1000 |
| TEMED, Tetramethylethylenediamine | Sigma Aldrich | T9281-100ML |
| Tris-(hydroxymethyl)-aminomethan (TRIS) | Carl Roth | 4855.2 |
| Triton X-100 Solution, 10% | AppliChem | A1287,0100 |
| Tween 20 | Sigma Aldrich | P1379-500ML |

### 2.1.7 Cell Culture

Reagents used for cell culture are listed in Table 2.9.

**Table 2.9:     Cell Culture.**

| Chemical | Manufacturer | Catalogue number |
|---|---|---|
| Antibiotic-Antimycotic, 100 x | Gibco | 15240062 |
| Bovine serum albumin (BSA) | Sigma Aldrich | A6003-25G |
| Dulbecco's Modified Eagle's Medium (DMEM) | Biochrom | F0445 |
| FCS, fetal calf serum | Merck | S0615 |
| Iscove Modified Dulbecco Media (IMDM) | Gibco | 42200-014 |
| Iscove Basal Medium | Biochrom | FG 0465 |
| Insulin-Transferrin Selenium (ITS) X, 100 x, | Gibco | 51500-056 |

| Laminin | Sigma Aldrich | L2020 |
| Lipofectamine 2000 | Invitrogen | 11668-027 |
| L-Glutamine, 200 mM | Merck | K0282 |
| Minimum essential medium (MEM) without L-glutamine | Gibco | 51200-046 |
| MEM with L-glutamine | Sigma Aldrich | M4780 |
| Phosphate buffered saline (PBS) | Merck | L182-01 |
| Penicillin/Streptomycin, 100 x | Merck | A2212 |

**2.1.8 Enzymes and Kits**

Enzymes and kits used in this work are listed in Table 2.10.

**Table 2.10:    Enzymes and kits.**

| Chemical | Manufacturer | Catalogue number |
| --- | --- | --- |
| Collagenase Type 1 (ACT 323 u/mg) | Worthington | LS 004197 |
| cGMP Enzyme Immunoassay Kit | Sigma Aldrich | CG200 |
| DNase I | Roche | 11284932001 |
| Iscript cDNA synthesis kit | BioRad | 170-8890 |
| LDH Glo™ Cytotoxicity Assay | Promega | J2380 |
| Liberase DH | Roche | 05401089001 |
| PCR purification kit Qiaquick | Qiagen | 28104 |
| Phosphatase inhibitor cocktail | Roche | 04 906 837 001 |
| Pierce BCA Protein assay kit | Thermo Scientific | 23227 |
| Pierce Coomassie protein assay kit | Thermo Scientific | 23200 |
| Protease inhibitor cocktail | Roche | 04 693 116 001 |
| Protease inhibitor w/o EDTA | Roche | 11 836 170 001 |
| Proteinase, bacterial | Sigma Aldrich | P8038-1G |
| Proteinase K | Appli Chem | A3830,0500 |
| QIAprep Spin Miniprep Kit | Qiagen | 27106 |
| RNeasy fibrous tissue mini kit | Qiagen | 74704 |

| | | |
|---|---|---|
| RNeasy plus micro kit | Qiagen | 74034 |
| Rotor-Gene Multiplex PCR Kit | Qiagen | 204772 |
| Rotor-Gene SYBR Green PCR Kit | Qiagen | 204074 |
| SuperSignal West Pico PLUS | Thermo Fisher | 34580 |
| Trypsin/EDTA-Solution (0.05/0.02%) | Biochrom | L2143 |
| Trypsin, 2.5% | Gibco | 15090-046 |

### 2.1.9 Consumables

Consumables used in this work are listed in Table 2.11.

**Table 2.11:    Consumables.**

| Consumable | Manufacturer | Catalogue number |
|---|---|---|
| 20 G Sterican | Braun | 4657519 |
| 6-well plates | Falcon A-corning | 351146 |
| 96-well plates | Thermo Scientific | 167008 |
| Bacillol 30 Foam | Hartmann | ANY8.1 |
| Combi-tips advanced, 5 mL | Eppendorf | 0030 089.456 |
| Cryo Tube Vials | Thermo Scientific | 363401 |
| Dialysis Tubing, 1 Inf Dia 8/32-6.3 mm | Medicell Int. Ltd | DTV 12000.01.000 |
| EasyFill Cell Factory Nunclon, 2 trays | Thermo Fisher | 140250 |
| EasyFill Cell Factory Nunclon, 4 trays | Thermo Fisher | 140360 |
| Filterpapier, Type 598 | Hahnemühle | 5984657 |
| Filtropur S 0,2 | Sarstedt | 83.1826.001 |
| Gauze | Th Geyer | 9.068291 |
| Gelloader Pipette Tips | Sarstedt | 70.1190.100 |
| Glass bottom dish Cellvis | IBL | D29-10-0-N |
| Gloves S (Nitrile, powder free) | Ansell | 700122 |
| Kimtech | Kimberley Clark | 7558 |
| Laboratory film | Parafilm | PM-996 |

| | | |
|---|---|---|
| Lens cleaning tissue | Whatman | 2105-841 |
| Luer-Lok Syringes, 20 mL | BD Plastipak | 300629 |
| Luer-Lok Syringes, 30 mL | Braun | 4616308F |
| Microcentrifuge tube | Roth | 4190.1 |
| Multiply µStrip Pro 8-strip | Sarstedt | 72.991.002 |
| Needle 18G x 1 ½ 1,20 x 40 mm | Th.Geyer | 6070031 |
| Needle 20G x 2 ¾, 0,9 x 70 mm | Th.Geyer | 4657705 |
| Needle 21G x 1 ½ 0.8 x 40 mm | Th.Geyer | 6076221 |
| Needle 23G x 1 ¼ 0.6 x 30 mm | Th.Geyer | SAP80387 |
| Nitrocellulose Membrane, 0.45 µM | Amersham | 10600002 |
| Nonabsorbable Braided Silk Suture | FST | 18020-507 |
| Omnican 40, Insulin syringe | Braun | 9161635 |
| PCR 0.1 mL 4-tube & 4-cap strips | Biozym | 711200 |
| Pipette tips 10 µL | Sarstedt | 70.1130.105 |
| Pipette tips 100 µL | Sarstedt | 70.760.107 |
| Pipette tips 1000 µL | Sarstedt | 70.762.105 |
| Quick-Seal Centrifuge Tubes 5/8 x 3 | Beckmann | 342413 |
| Rotilabo reaction vials 5 mL | Carl Roth | PE68.1 |
| Round glass cover slips 24 mm | VWR | 631-0161 |
| Round glass cover slips 25 mm | VWR | 631-0171 |
| Safe Seal Reaktionsgefäße | Sarstedt | 72.706.400 |
| Serological pipette 2 mL | Sarstedt | 86.1252.001 |
| Serological pipette 5 mL | Sarstedt | 86.1253.001 |
| Serological pipette 10 mL | Sarstedt | 86.1254.025 |
| Serological pipette 25 mL | Sarstedt | 86.1685.001 |
| Serological pipette 50 mL | Sarstedt | 86.1256.001 |
| Softa-Man acute | Braun | 19114 |
| Sterilium | Bode | 975512 |
| Steritop 0.22 µM, 1000 mL | Merck | SCGPT10RE |
| Surgical scalpels, disposable | Braun | 5518083 |
| Syringe, 2 mL, BD Discardit II | BD | 300928 |

| | | |
|---|---|---|
| TC-Schale, 100 Cell+ | Sarstedt | 83.3902.300 |
| TC-Schale, 150 Cell + | Sarstedt | 83.3903.300 |
| Transfer pipette | Sarstedt | 86.1171.010 |
| Tube 15 mL | Sarstedt | 62.554.002 |
| Tube 50 mL | Sarstedt | 62.574.004 |
| U-40 Insulin, 30Gx1/2 | Braun | 4001525 |
| U-40 Insulin, Omnifix | Braun | 9161309 |
| UVette | Eppendorf | 9529 10051 |
| Vernichtungsbeutel | Labsolute | 796994 |
| Verschlussklammern SpectraPor | Carl Roth | 2781.1 |
| Waschlotion | Schülke | 112006 |
| X-ray film (Super RX) | Fujifilm | 7410 19230 |
| Zellkulturflasche T175 | Greiner | 660175 |

### 2.1.10 Microscope devices

Microscopic devices used in this work are listed in Table 2.12.

**Table 2.12:    Microscope devices.**

| Microscope device | Manufacturer |
|---|---|
| Arduino digital-to-analog input-output board | Arduino |
| CMOS camera (OptiMOS) | QImaging |
| DV2 Cube 05-EM, (505 dcxr, D480/30m, D535/40m) | Photometrics |
| DV2 Cube 11-EM, (565dcxr, 520/30m, D630/50m) | Photometrics |
| LED pE-100, 400 nM and 440 nM | CoolLED |
| LED pE-100 controller s/n 10949 | CoolLED |
| Leica DMi1 microscope | Leica |
| Leica DMI 3000 B microscope | Leica |
| Leica M165FC microscope | Leica |

| | |
|---|---|
| Leica M50 microscope | Leica |
| Nikon eclipse Ti-4 microscope | Nikon |
| Nikon SMZ 745T microscope | Nikon |
| Strahlenteiler 455 LP | AHF Analysetechnik |

### 2.1.11 General devices

General devices used in this work are listed in Table 2.13.

**Table 2.13:    General devices.**

| General device | Manufacturer |
|---|---|
| Accu-jet pro | Brand |
| Centrifuge 5810R | Eppendorf |
| Centrifuge Hareus Fresco 17 | Thermo Scientific |
| Centrifuge Hareus Megafuge 8R | Thermo Scientific |
| Centrifuge Hareus Pico 17 | Thermo Scientific |
| Centrifuge myFuge | Benchmark |
| Centrifuge XC-450 | Premiere |
| $CO_2$-Incubator MCO-5AC | Sanyo |
| Dual flow meter (HMIC3D) | Billups Rothenberg |
| E-Box Gel documentation | Vilber |
| FlexStation 3 | Molecular devices |
| Freezer Comfort | Liebherr |
| Fridge Comfort | Liebherr |
| Gene Touch | Bioer |
| Glacier Ultralow Temperature Freezer | Nuaire |
| GOX 100 Sauerstoffmessgerät | Greisinger |
| Harvard apparatus | Hugo Sachs Elektronik |
| ISM831C | Ismatec |
| KL1600 LED | Schott |
| Laboklav | HSP |

| | |
|---|---|
| LX320A scs | Precisa |
| Magnetic stirrer color squid | IKA |
| Medical film processor (SRX-101A) | Konica Minolta |
| MIC cycler | Biomolecular systems |
| Micro Ultracentrifuge CS150 FNX | Hitachi |
| Microwave | Panasonic |
| Mini-PROTEAN Tetra Cell, Mini Trans-Blot Module, PowerPac Basic Power Supply | Biorad, 1658033 |
| Modular Incubator Chamber, MIC-101 | Billups Rothenberg |
| Mupid-One | Advance |
| My FUGE | Benchmark |
| pH Level 1 | neoLab |
| Powerlab 8/35 | AD Instruments |
| PowerPac | Bio Rad |
| Power supply EC 200 XL | Thermo Scientific |
| Präzisionswaage PCB1000-2 | Kern |
| Precisa 321 | Swiss made |
| Research plus (10 µL – 10 mL) | Eppendorf |
| Rotor Gene Q | Qiagen |
| RCT standard Magnetrührer | IKA |
| Scanner LiDE 220 | Canon |
| Shaker DRS-12 | ELMI |
| Safety cabinet (class II) | ibs technomara |
| Spectrophotometer DS-11 | Denovix |
| STG 4002 | Multi Channel Systems |
| Thermomixer C | Eppendorf |
| Tube sealer STF3 | Hitachi |
| Ultra Turrax T-10 basic | IKA |
| Vibramax 100 | Heidolph |
| Visi Light LED3 | VWR |

| | |
|---|---|
| Vortex-2 genie | Scientific industries |
| Water bath | GFL |
| Water bath TC120 | Grant |
| Water bath | Julabo |

### 2.1.12 Software

Software used in this work is listed in Table 2.14.

**Table 2.14:    Software.**

| Software | Manufacturer |
|---|---|
| GraphPadPrism 6, 6.01 | GraphPad |
| ImageJ, 1.44n9 | National Institutes of Health |
| Endnote, X8.2 | Web of Science Group |
| Labchart | ADInstruments |
| Mic qPCR Software | Bio Molecular Systems |
| Micro-Manager, 1.4.5 | Open Imaging |
| Microsoft Office Professional Plus 2013 | Microsoft |
| Powerlab 8/30 | ADInstruments |
| Tbase, 4D v17.1 | 4D SAS |
| R, 3.3.2 | The R Foundation |
| Rotor Gene Q analysis software | Qiagen |
| SoftMax Pro, 5.4.6.005 | Molecular Devices |
| E-box gel documentation software | Vilber |

**2.1.13 Buffers**

*2.1.13.1 Buffers and solutions for isolation and culture of primary cardiomyocytes*

In this work, primary cardiomyocytes were isolated from mouse hearts, human atrial tissue samples, and human ventricular tissue samples.

*Isolation and culture of murine ventricular cardiomyocytes*

The buffers and solutions for isolation and culture of primary murine ventricular cardiomyocytes are listed in Tables 2.15 – Table 2.23.

**Table 2.15:** **Stock perfusion buffer, 1 x.** Dissolved in $H_2O$ Ampuwa, sterile filtered. Aliquots of 35 mL stored at -20°C.

| Compound | $C_{final}$ |
| --- | --- |
| NaCl | 113 mM |
| KCl | 4.7 mM |
| $KH_2PO_4$ | 0.6 mM |
| $Na_2HPO_4$ x 2 $H_2O$ | 0.6 mM |
| $MgSO_4$ x 7 $H_2O$ | 1.2 mM |
| $NaHCO_3$ | 12 mM |
| $KHCO_3$ | 10 mM |
| HEPES | 10 mM |
| Taurine | 30 mM |
| D-(+) Glucose | 5.6 mM |
| BDM | 9.9 mM |

**Table 2.16:** **BDM stock solution.** Dissolved in $H_2O$ Ampuwa, sterile filtered. Aliquots of 1 mL stored at -20°C.

| Compound | $C_{final}$ |
| --- | --- |
| BDM | 500 mM |

**Table 2.17:** **Calcium chloride solution, 100 mM.** Dissolved in $H_2O$ Ampuwa, sterile filtered. Stored at 4°C.

| Compound | $C_{final}$ |
| --- | --- |
| $CaCl_2$ x 2 $H_2O$ | 100 mM |

**Table 2.18:** **Liberase solution.** Prepared under sterile conditions. Reconstituted on ice for 20 min. Aliquots of 300 µL (= 1.25 mg Liberase) stored at -20°C.

| Compound | Mass/Volume |
| --- | --- |
| Liberase DH | 50 mg |
| $H_2O$ Ampuwa | 12 mL |

**Table 2.19:** **Digestion buffer.** Prepared freshly before every usage.

| Compound | Volume |
| --- | --- |
| Perfusion buffer, 1 x | 29.5 mL |
| $CaCl_2$, 100 mM | 3.75 µL |
| Liberase DH | 300 µL (= 1.25 mg) |
| Trypsin, 2.5% | 100 µL |

**Table 2.20:** **Stop buffer 1.** Prepared freshly before every usage.

| Compound | Volume |
| --- | --- |
| Perfusion buffer, 1 x | 2.25 mL |
| FCS solution | 250 µL |
| $CaCl_2$, 100 mM | 1.25 µL |

**Table 2.21:** **Stop buffer 2.** Prepared freshly before every usage. For isolation of cardiomyocytes for Immunoblot analysis, Stop buffer 2 was prepared without FCS.

| Compound | Volume |
|---|---|
| Perfusion buffer, 1 x | 9.5 mL |
| FCS solution | 500 µL |
| CaCl$_2$, 100 mM | 3.75 µL |

**Table 2.22:** **BSA stock solution, 10%.** Dissolved in H$_2$O Ampuwa, sterile filtered. Aliquots of 500 µL stored at -20°C.

| Compound | C$_{final}$ |
|---|---|
| BSA | 10% |

**Table 2.23:** **Myocyte culture medium.** Prepared freshly on the day of usage.

| Compound | Volume |
|---|---|
| MEM, without L-glutamine | 47.5 mL |
| BSA, 10% | 500 µL |
| Penicillin/Streptomycin | 500 µL |
| L-glutamine | 500 µL |
| BDM, 500 mM | 1 mL |
| ITS-Supplement, 100 x | 500 µL |

*Isolation and culture of human atrial and ventricular cardiomyocytes*

The buffers and solutions for isolation and culture of primary human atrial and ventricular cardiomyocytes are listed in Tables 2.24 – Table 2.31.

**Table 2.24:** **$Ca^{2+}$-free Tyrode solution.** Dissolved in $ddH_2O$, pH 7.4. Aliquots of 200 mL stored at - 20°C.

| Compound | $C_{final}$ |
|---|---|
| Sucrose | 88 mM |
| NaCl | 88 mM |
| KCl | 5.4 mM |
| $NaHCO_3$ | 4 mM |
| $NaH_2PO_4$ | 0.3 mM |
| $MgCl_2$ | 1.1 mM |
| HEPES | 10 mM |
| Taurine | 20 mM |

**Table 2.25:** **$Ca^{2+}$-free Tyrode solution, ready to use.** Sterile filtered, stored at 4°C, stable for maximal 2-3 days.

| Compound | Mass/Volume |
|---|---|
| $Ca^{2+}$-free Tyrode solution | 200 mL |
| Glucose | 0.36 g |
| Na-Pyruvate | 0.11 g |

**Table 2.26:** **Blebbistatin stock solution, 10 mM.** Dissolved in DMSO, aliquots of 40 µL stored at -20°C.

| Compound | $C_{final}$ |
|---|---|
| Blebbistatin, 5mg | 10 mM |

**Table 2.27:** **Stop Solution.** Sterile filtered, stored at 4°C. Stable for maximal 2-3 days.

| Compound | Mass/Volume/$C_{final}$ |
|---|---|
| $Ca^{2+}$-free Tyrode solution, ready to use | 100 mL |
| Blebbistatin (10 mM) | 12 µM for ventricle, 2 µM for atrium |
| BSA | 500 mg |

**Table 2.28:** **Enzymatic Solution I.** Sterile filtered, prepared freshly before every usage.

| Compound | Mass/Volume |
|---|---|
| $Ca^{2+}$-free Tyrode solution, ready to use" | 20 mL |
| Collagenase 323 | 0.5 mg/ml |
| BSA | 40 mg |
| Proteinase, bacterial | 0.5 mg/ml |

**Table 2.29:** **Enzymatic Solution II.** Sterile filtered, prepared freshly before every usage.

| Compound | Mass/Volume |
|---|---|
| $Ca^{2+}$-free Tyrode solution, ready to use | 30 mL |
| Collagenase 323 | 0.4 mg/ml |
| BSA | 80 mg |

**Table 2.30:** **Myocyte plating medium M2.** Stored at 4°C, sterile filtered 2 x before every usage.

| Compound | Mass/Volume |
|---|---|
| MEM, with L-glutamine | 500 mL |
| Creatine | 0.655 g |
| Taurine | 1.25 g |
| Penicillin/Streptomycin | 5 mL |
| L-Glutamine | 5 mL |
| BSA (10%) | 5 mL |
| Blebbistatin | 1.2 mL for ventricle, 200 µL for atria |

**Table 2.31:** **Myocyte plating medium M1.** Stored at 4°C, sterile filtered 2 x before every usage.

| Compound | Mass/Volume |
|---|---|
| Myocyte plating medium M2 | 50 mL |
| FCS | 2.5% |

*2.1.13.2 Buffers and solutions for cell culture of eukaryotic cell lines*

In this work, HEK293A cells were used as eukaryotic cell line. HEK293A cells were used for adenovirus amplification and FRET measurements for bleedthrough factor determination.

**Table 2.32:** **HEK293A culture medium.** Stored at 4°C.

| Compound | Volume/$C_{final}$ |
|---|---|
| DMEM | 500 mL |
| FCS | 10% |
| Glutamine | 1% |
| Penicillin/Streptomycin | 1% |

*2.1.13.3 Buffers and solutions for virus amplification, purification, and plaque assay*

Adenovirus encoding the FRET-based cGMP biosensor red-cGES-DE5 [216] was amplified and purified for the use in primary human atrial and ventricular cardiomyocytes. Buffers and solutions for virus amplification, purification, and plaque assay are listed in Table 2.33 – Table 2.40.

**Table 2.33:** **Virus amplification medium for HEK293A cells.** Stored at 4°C.

| Compound | Volume/$C_{final}$ |
|---|---|
| DMEM | 500 mL |
| FCS | 5% |
| Glutamine | 1% |
| Penicillin/Streptomycin | 1% |

**Table 2.34:    20% Triton/PBS.**  Sterile filtered, stored at 4°C.

| Compound | Volume |
| --- | --- |
| Triton-X-100 | 10 mL |
| PBS, warm | 40 mL |

**Table 2.35:    20% PEG 8000/2.5 M NaCl.**  Sterile filtered, stored at 4°C.

| Compound | Mass/Volume |
| --- | --- |
| NaCl | 292.6 g |
| 20% PEG 8000 | 400 g |
| ddH$_2$O | Ad 2 L |

**Table 2.36:    PBS, pH 8.0.**  pH 8.0, sterile filtered, stored at 4°C.

| Compound | Volume |
| --- | --- |
| PBS | 500 mL |

**Table 2.37:    10 x Sucrose-buffer, pH 8.0.**  pH 8.0, sterile filtered, stored at 4°C.

| Compound | Mass |
| --- | --- |
| Tris | 24.22 g |
| MgCl$_2$ x 6 H$_2$O | 8.13 g |
| D-(+)-Sucrose | 800 g |
| ddH$_2$O | Ad 2 L |

**Table 2.38:    2 x IMDM.** Sterile filtered, aliquots of 26 mL stored at -20°C.

| Compound | Volume/Mass |
| --- | --- |
| IMDM | Powder of two bottles |
| NaHCO$_3$ | 6.05 g |
| ddH$_2$O | Ad 1 L |

**Table 2.39:** **1.5% Agarose.** Autoclaved, stored at 4°C.

| Compound | Mass/Volume |
|---|---|
| Agarose | 1.5 g |
| ddH$_2$O | Ad 100 mL |

**Table 2.40:** **Plaque assay medium.** Stored at 4°C.

| Compound | Mass |
|---|---|
| Iscove basal medium | 500 mL |
| FCS | 5% |
| Antibiotic/Antimycotic | 1% |

*2.1.13.4 Buffers and solutions for microscopy techniques*

In this work, different microscope setups were used for FRET-based cGMP and cAMP measurements in isolated murine ventricular cardiomyocytes, isolated human ventricular cardiomyocytes, isolated human atrial cardiomyocytes, and murine whole hearts.

For FRET measurements of isolated murine ventricular cardiomyocytes, isolated human ventricular cardiomyocytes, and isolated human atrial cardiomyocytes FRET buffer was used (Table 2.41).

For FRET-based whole heart cGMP and cAMP measurements, modified Krebs-Henseleit solution was used (Table 2.42).

*FRET-based cGMP and cAMP measurements in isolated murine and human cardiomyocytes*

**Table 2.41:** **FRET buffer.** Dissolved in Ampuwa H$_2$O. pH 7.4, stored at room temperature (RT).

| Compound | C$_{final}$ |
|---|---|
| NaCl | 144 mM |
| KCl | 5.4 mM |
| MgCl$_2$ x 7 H$_2$O | 1 mM |
| CaCl$_2$ | 1 mM |
| HEPES | 10 mM |

*FRET-based cGMP and cAMP measurements in whole hearts*

**Table 2.42:** **Modified Krebs-Henseleit solution.** Sterile filtered, stored at 4°C. Stable for 2-3 days.

| Compound | $C_{final}$ |
|---|---|
| NaCl | 118 mM |
| KCl | 4.7 mM |
| $MgSO_4$ | 0.8 mM |
| $NaHCO_3$ | 25 mM |
| $KH_2PO_4$ | 1.2 mM |
| Glucose | 5 mM |
| Na Pyruvate | 24 mM |
| Dissolved in $ddH_2O$, gassed with carbogen for 15 min, pH 7.4 | |
| $CaCl_2$ | 2.5 mM |

*2.1.13.5 Buffers and solutions for protein biochemistry methods*

The buffers and solutions for the preparation of protein lysates from isolated murine cardiomyocytes, mouse hearts, and human atrial and ventricular tissue samples are listed in Table 2.43 – Table 2.45.

Buffers and solutions needed for SDS Polyacrylamide gel electrophoresis are listed in Table 2.46 – Table 2.56.

*Preparation of protein lysates*

**Table 2.43:** **Homogenization buffer, stock.** Dissolved in $ddH_2O$, pH 7.4. Aliquots of 9.0 mL stored at -20°C.

| Compound | $C_{final}$ |
|---|---|
| EGTA | 1 mM |
| HEPES | 10 mM |
| NaCl | 150 mM |
| Sucrose | 300 mM |

**Table 2.44:** **Homogenization buffer, ready to use.** Aliquots of 500 µL stored at -20°C.

| Compound | Volume |
| --- | --- |
| Homogenization buffer, stock | 9 mL |
| Triton X-100, 10% | 1 mL |
| Phosphatase inhibitor | According to manufacturer's instructions |
| Protease inhibitor | According to manufacturer's instructions |

**Table 2.45:** **RIPA buffer.** Dissolved in ddH$_2$O. Aliquots of 500 µL stored at -20°C.

| Compound | C$_{final}$ |
| --- | --- |
| NaCl | 150 mM |
| Triton-X-100 | 1% |
| SDS | 0.1% |
| SOD | 0.5% |
| Tris (1 M, pH 8.0) | 50 mM |
| Protease inhibitor | According to manufacturer's instructions |
| Phosphatase inhibitor | According to manufacturer's instructions |

*SDS Polyacrylamide gel electrophoresis*

**Table 2.46:** **SDS Stop, 3 x.** Dissolved in ddH$_2$O. pH 6.7, stored at RT.

| Compound | C$_{final}$ |
| --- | --- |
| Tris | 200 mM |
| SDS | 6% (v/v) |
| Glycerin | 15% (v/v) |
| Bromphenolblue | decide on colour |
| $\beta$-Mercaptoethanol | 10% (v/v) |

**Table 2.47:** **4 x Tris/SDS, pH 6.8.** Dissolved in ddH$_2$O. pH 6.8, stored at RT.

| Compound | C$_{final}$ |
| --- | --- |
| Tris | 500 mM |
| SDS | 0.4% (v/v) |

**Table 2.48:** **4 x Tris/SDS pH 8.8.** Dissolved in ddH$_2$O. pH 8.8, stored at RT.

| Compound | C$_{final}$ |
| --- | --- |
| Tris | 1.5 M |
| SDS | 0.4% (v/v) |

**Table 2.49:** **APS solution.** Dissolved in ddH$_2$O. Aliquots of 500 µL stored at -20°C.

| Compound | C$_{final}$ |
| --- | --- |
| APS | 10% |

**Table 2.50:** **10 x SDS Running buffer.** Dissolved in ddH$_2$O. pH 8.3, stored at RT.

| Compound | C$_{final}$ |
| --- | --- |
| Tris | 250 mM |
| Glycine | 1.9 M |
| SDS | 1% (v/v) |

**Table 2.51:** **10 x Transferbuffer.** Dissolved in ddH$_2$O. Stored at RT.

| Compound | C$_{final}$ |
| --- | --- |
| Tris | 325 mM |
| Glycine | 1.9 M |

**Table 2.52:** **1 x Transferbuffer.** Dissolved in ddH$_2$O. Stored at 4°C.

| Compound | C$_{final}$ |
| --- | --- |
| Transferbuffer, 10 x | 1 x |
| Methanol | 10% (v/v) |

**Table 2.53:** **10 x TBS Buffer.** Dissolved in ddH$_2$O. pH 7.5, stored at RT.

| Compound | C$_{final}$ |
| --- | --- |
| Tris | 100 mM |
| NaCl | 1.5 M |

**Table 2.54:** **1 x TBS-Tween Buffer.** Dissolved in ddH$_2$O. Stored at RT.

| Compound | C$_{final}$ |
| --- | --- |
| TBS Buffer, 10 x | 1 x |
| Tween 20 | 0.1% (v/v) |

**Table 2.55:** **Stacking Gel.** Volume for preparation of two mini gels (1.0 mm).

| Compound | Volume |
| --- | --- |
| Acrylamide | 500 µL |
| 4 x Tris/SDS, pH 6.8 | 940 µL |
| ddH$_2$O | 2.31 mL |
| APS, 10% | 18.8 µL |
| TEMED | 7.5 µL |

**Table 2.56:** **Separating Gel.** Volume for preparation of two mini gels (1.0 mm).

| Compound | 8% | 10% | 15% |
|---|---|---|---|
| Acrylamide | 3.2 mL | 4.0 mL | 6.0 mL |
| 4 x Tris/SDS, pH 8.8 | 3.0 mL | 3.0 mL | 3.0 mL |
| ddH$_2$O | 5.8 mL | 5.0 mL | 3.0 mL |
| APS, 10% | 48 µL | 48 µL | 48 µL |
| TEMED | 18 µL | 18 µL | 18 µL |

## 2.2 Methods

### 2.2.1 Experimental animals, mouse breeding

Mice were bred and accommodated in the animal facility of the University Medical Centre Hamburg-Eppendorf (UKE). Mice were maintained at 12 h light, 12 h dark cycle. Drinking water and normal chow were provided *ad libitum*. Mouse lines were managed using Tbase software. Tail biopsies were used for genotyping by Polymerase chain reaction (PCR) (section 2.2.3.4). If possible, equal numbers of female and male mice were used for experiments, aged between 2-6 months. All animal work was performed according to institutional and governmental guidelines.

### 2.2.2 Tissue collection of human atrial and ventricular samples

Human heart tissue samples were collected from patients undergoing cardiac surgery at the UKE. Specimens of right and left atrial tissues were taken from patients in sinus rhythm (SR) or with atrial fibrillation (AF), subjected to atrial cannulation for extracorporeal circulation and/or with ablation. Ventricular samples were collected from patients with or without heart failure at the time of transplantation, valvular surgeries, myectomy or catheter biopsy. All samples were taken with informed consent of the donors.

The study was conducted in accordance with the Declaration of Helsinki principles, and approved by the Ethical Committees of the UKE and the Ärztekammer Hamburg (WF-088/18).

### 2.2.3 Nucleic acid techniques

*2.2.3.1 DNA isolation*

In order to extract DNA for genotyping and TaqMan PCR from mouse tail biopsies, the biopsies were digested o.n. in Direct PCR-Tail buffer (200 µL) containing Proteinase K (500 µg/mL) at 55°C and 1.000 rotations per minute (rpm) in a thermo cycler (Eppendorf). The next morning, samples were incubated at 85°C for 45 min to stop the reaction. Lysate containing DNA was directly used for polymerase chain reaction (PCR) as described in section 2.2.3.4.

*2.2.3.2 Isolation of total RNA from murine cardiomyocytes*

Total RNA was isolated from murine cardiomyocytes in order to analyse gene expression level of hypoxia/reoxygenation and Normoxia treated cardiomyocytes by quantitative reverse

transcriptase polymerase chain reaction (qRT PCR) (section 2.2.3.6). Hypoxia/reoxygenation or Normoxia treated isolated murine cardiomyocytes (section 2.2.7.1) were harvested by centrifugation (3.000 rpm, 3 min, 4°C) and snap frozen in liquid nitrogen. Cell pellets were stored at -80°C until further usage. For RNA isolation from murine cardiomyocytes, RNeasy fibrous tissue mini kit (Qiagen) was used according to the manufacturer's instructions. RNA was eluted in 30 µL of RNase-free ddH$_2$O. For very low amounts of cells (less than 10.000 cells), RNeasy plus micro kit (Qiagen) was used according to the manufacturer's instructions and RNA was eluted in 10 µL of RNase-free ddH$_2$O. RNA concentration was measured on a spectrophotometer DS-11 (Denovix). RNA samples were stored at -80°C.

*2.2.3.3 Complementary DNA production*

Reverse transcriptase is an enzyme that transcribes RNA into complementary DNA (cDNA) [237]. In order to analyse gene expression levels of hypoxia/reoxygenation- and Normoxia-treated cardiomyocytes, isolated RNA (section 2.2.3.2) was transcribed into cDNA using reverse transcriptase. For cDNA production iScript cDNA synthesis kit (BioRad) was used according to the manufacturer's instructions. 200 ng of RNA were used per reaction. The reaction setup is shown in Table 2.57.

**Table 2.57:** **cDNA production reaction setup.** cDNA was produced using iScript cDNA synthesis kit (BioRad).

| Component | Volume |
|---|---|
| 5 x iScript reaction mix | 4 µL |
| iScript reverse transcriptase | 1 µL |
| Nuclease free H$_2$O | Ad 20 µL |
| RNA template (200 ng) | Volume needed for 200 ng |
| Total volume | **20 µL** |

cDNA synthesis was performed in a Gene Touch thermal cycler (Bioer). The reaction protocol is shown in Table 2.58. cDNA was stored at -20°C for subsequent analyses.

**Table 2.58:** **Programme for cDNA production.** cDNA production was performed in a Gene Touch thermal cycler (Bioer).

| Step | Temperature | Duration |
|---|---|---|
| 1 | 25°C | 5 min |
| 2 | 42°C | 30 min |
| 3 | 85°C | 5 min |
| 4 (optional) | 4°C | hold |

*2.2.3.4 Polymerase chain reaction*

PCR is a method to amplify specific DNA sequences using specific primer pairs, nucleotides, and DNA polymerase [238]. In this work, PCR was used for genotyping of the mouse lines. DNA for PCR was extracted from tail biopsies as described in section 2.2.3.1. The setup of the PCR reaction is summarized in Table 2.59.

**Table 2.59:** **Setup of PCR reaction.** PCR reaction was used for genotyping of the mouse lines used in this work.

| Component | Volume /reaction |
|---|---|
| 5 x Green Buffer Promega | 4 µL |
| dNTPs Promega | 0.5 µL |
| Forward Primer | 0.05 µL |
| Reverse Primer | 0.05 µL |
| DNA | 0.5 µL |
| $H_2O$ Ampuwa | 14.7 µL |
| GO Taq Polymerase | 0.2 µL |
| Total volume | **20 µL** |

PCR reaction was performed in a Gene Touch thermal cycler (Bioer). The reaction protocol is shown in Table 2.60.

**Table 2.60:** **PCR Programme.** PCR was performed in a Gene Touch thermal cycler (Bioer).

| Step | Temperature | Duration |
| --- | --- | --- |
| Preincubation | 94°C | 4 min |
| 3-step cycling | | |
|     Denaturation | 94°C | 30 sec |
|     Annealing | 56°C | 30 sec |
|     Synthesis | 72°C | 50 sec |
| Number of cycles | 35 | |
| Extension | 72°C | 7 min |
| Hold Temperature | 4°C | Forever |

PCR products were analysed on 2% agarose gels in 1 x TAE buffer using a 100-base pair (bp) DNA ladder (New England Biolabs) as molecular weight standard. Gel pictures were taken with the E-box gel documentation system (Vilber).

### 2.2.3.5 TaqMan polymerase chain reaction

In the original red-cGES-DE5 transgenic mice, which had been generated by Götz and colleagues, the expression of the red-cGES-DE5 biosensor was quite weak due to heterozygous expression of the biosensor gene (+/T) [136]. In order to facilitate FRET-based cGMP measurements in cardiomyocytes from red-cGES-DE5 transgenic mice [136] for this work, mice with homozygous expression of the sensor gene (T/T) were generated by mating two heterozygous mice together. In order to discriminate between homozygous (T/T) and heterozygous (T/+) sensor expression of the so generated mice, TaqMan PCR was performed.

TaqMan PCR is a quantitative PCR method, with very high specificity, which allows to distinguish between heterozygous and homozygous gene expression. For TaqMan PCR an oligonucleotide probe with a fluorophore covalently attached at the 5'-end and a quencher at the 3'-end, as well as a specific primer pair are needed [239]. During the PCR reaction, the TaqMan probe anneals with the DNA. If quencher and fluorophore are at close proximity to each other, the quencher inhibits the fluorescent signal of the fluorophore. However, when the *Taq* Polymerase synthesizes the new DNA strand, its exonuclease activity degrades the TaqMan probe, which releases the fluorophore, whose fluorescence can then be detected.

The probes used in this study were labelled with fluorescein (FAM) at the 5'-end and a dark quencher dye at the 3'-end. A primer pair and a probe for the reference gene Interleukin 2

(IL32) (probe #32), and a primer pair and a probe for the target gene red-cGES-DE5 (probe #161) were used in this study. Probes and primers for TaqMan PCR were designed at the Roche Assay Design Centre (https://lifescience.roche.com/en_de/brands/universal-probe-library.html).

For TaqMan PCR reaction, the Rotor-Gene Multiplex PCR Kit (Qiagen) was used according to the manufacturer's instructions. Samples were measured in triplicates. Wildtype DNA (+/+), and heterozygous DNA (T/+) were used as controls. Additionally, a non-template control was run. IL32 was used as reference gene. TaqMan PCR reaction setup is shown in Table 2.61.

**Table 2.61: TaqMan PCR reaction setup.** Rotor-Gene Multiplex PCR Kit (Qiagen) was used for TaqMan PCR.

| Compound | Volume/reaction | $C_{final}$ |
|---|---|---|
| 2 x Rotor-Gene Multiplex PCR Master Mix | 12.5 µL | 1 x |
| Primer forward (10 µM primer stock) | 1.25 µL | 0.5 µM |
| Primer reverse (10 µM primer stock) | 1.25 µL | 0.5 µM |
| Probe (10 µM stock) | 0.5 µL | 0.2 µM |
| DNA (100 ng/µL) | 2 µL | 200 ng |
| RNase-free water | 7.5 µL | |
| Total reaction volume | **25 µL** | |

Taqman PCR was performed in a mic cycler (biomolecular systems). The TaqMan PCR programme used in this work is shown in table 2.62.

**Table 2.62: TaqMan PCR programme.** PCR was performed in a mic cycler (biomolecular systems).

| Step | Time | Temperature |
|---|---|---|
| Initial activation | 5 min | 95°C |
| 2-step cycling | | |
| Denaturation | 15 sec | 95°C |
| Annealing/extension | 15 sec | 60°C |
| Number of cycles | 40 | |

Data analysis was done in the MIC analysis programme. Obtained $C_T$ values were further evaluated manually using the $\Delta\Delta C_T$ method [240].

$\Delta C_T = C_T$ (target gene) – $C_T$ (housekeeping gene)

$\Delta\Delta C_T = \Delta C_T$ (unknown genotype) – $\Delta C_T$ (reference genotype)

Ratio = $2^{(-\Delta\Delta C_T)}$

### 2.2.3.6 Quantitative reverse transcriptase polymerase chain reaction

Quantitative reverse transcriptase polymerase chain reaction (qRT PCR) is a method to analyse gene expression level. Therefore, a fluorescent dye (SYBR Green), which can bind double stranded DNA by intercalating between the bases, is added to the PCR reaction. The SYBR Green fluorescence can be measured at the end of each amplification cycle to determine how much DNA has been amplified [241].

In this study, qRT PCR was used in order to determine gene expression levels in murine cardiomyocytes exposed to hypoxia/reoxygenation injury (section 2.2.7.1). Primer pairs for qRT PCR were designed using the primer blast tool from the national centre for biotechnology information (NCBI) (https://www.ncbi.nlm.nih.gov/tools/primer-blast/). The following criteria were considered for primer design: PCR product size had to be between 70-200 bps, melting temperature of the primers had to be in the range of 57 – 63°C and primer pairs must span an exon-exon junction.

In order to perform qRT PCR, RNA was isolated from murine cardiomyocytes (section 2.2.3.2) and transcribed into cDNA (section 2.2.3.3). qRT PCR was done in 0.1 mL tubes in a 72-well rotor using the cycler Rotor Gene Q (Qiagen). qRT PCR reaction setup is shown in Table 2.63.

**Table 2.63: qRT PCR reaction setup.** Rotor-Gene Multiplex PCR Kit (Qiagen) was used for qRT PCR reaction.

| Component | Master Mix 1 x |
|---|---|
| SYBR Green | 5 µL |
| Primer forward (5 nM) | 0.5 µL |
| Primer reverse (5 nM) | 0.5 µL |
| cDNA (1:1 dilution) | 1 µL |
| RNAase free $H_2O$ | 3 µL |
| Total volume | **10 µL** |

Samples were run in triplicates. For each sample, a negative control (ddH$_2$O) was run. *Gapdh* was used as housekeeping gene [242, 243]. Gain optimization was done before the first acquisition. qRT PCR programme is shown in Table 2.64.

**Table 2.64:**  **qRT PCR programme.**  qRT PCR was performed in the cycler Rotor Gene Q (Qiagen).

| Step | Temperature | Duration |
|---|---|---|
| 1: Hold | 95°C | 10 min |
| 2: Cycling | 95°C | 10 sec |
| | 60°C | 15 sec |
| | 72°C | 20 sec |
| 3: Repeat Step 2 | 39 x | |
| 4: Melting Curve | 72°C – 95°C | 0.5°C steps |

Rotor Gene Q software (Qiagen) was used for data analysis. Obtained C$_T$ values were further evaluated manually using the $\Delta\Delta$C$_T$ method [240].

$\Delta$C$_T$ = C$_T$ (target gene) – C$_T$ (housekeeping gene)

Ratio = $2^{(-\Delta C_T)}$

$\Delta\Delta$C$_T$ = $\Delta$C$_T$ (treatment) – $\Delta$C$_T$ (control average)

Ratio = $2^{(-\Delta\Delta C_T)}$

### 2.2.4 Isolation and culture of primary cardiomyocytes

In this work, primary cardiomyocytes were isolated from murine hearts, human atrial tissue samples, and human ventricular tissue samples.

*2.2.4.1 Isolation and culture of adult murine cardiomyocytes*

The Langendorff method was used for isolation of adult murine cardiomyocytes [244]. Mice were sacrificed by cervical dislocation and the heart was dissected in ice cold PBS. Then, the heart was fixed to a blunted cannula (21 G cannula) *via* ligature, connecting aorta and cannula and attached to the Langendorff apparatus. A schematic illustration of how proper cannulation should look like is shown in Figure 2.1 (A). A perfusion system consisting of a peristaltic pump (perfusion speed 2.5 – 3.5 mL/min), a water bath (temperature of the

perfusion buffer should be 37°C when reaching the heart), and plastic tubing, was used to perfuse the heart. A schematic illustration of the perfusion system is shown in Figure 2.1 (B).
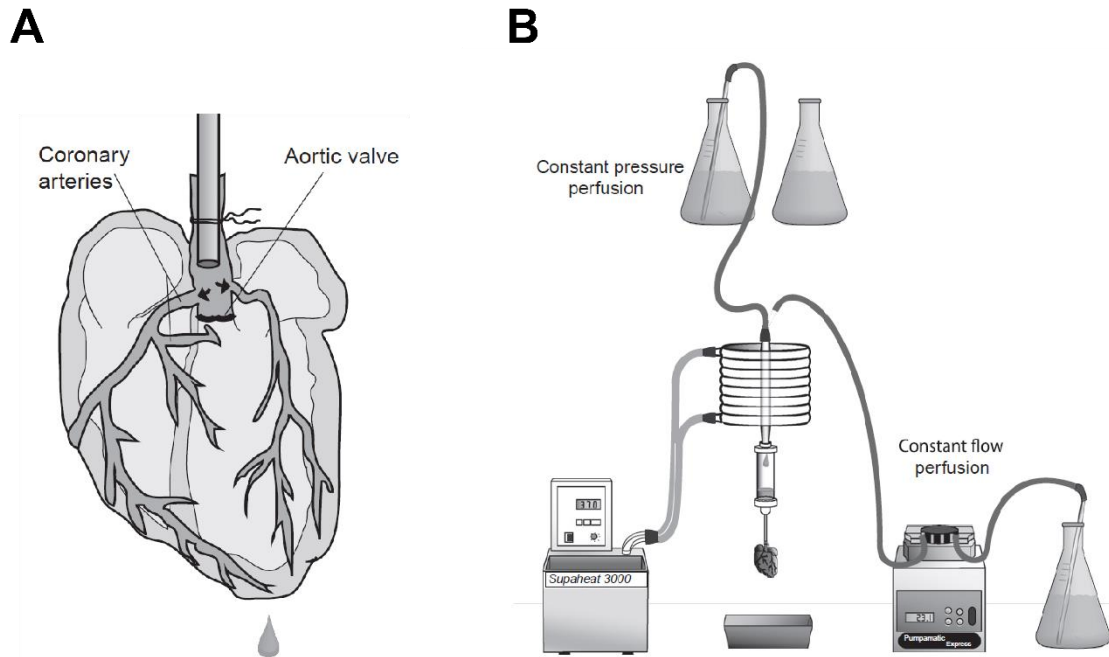


**Figure 2.1: Langendorff method. A)** Proper cannulation for isolation of adult murine cardiomyocytes. It is very important to place the cannula not too deep in the aorta in order to not passing through the aortic valve since this will prevent adequate perfusion of the coronary arteries. **B)** Langendorff setup for murine cardiomyocyte isolation. The system consists of a peristaltic pump to ensure constant perfusion, a water bath, and plastic tubing. The Langendorff setup enables retrograde perfusion of the heart with enzymatic solution *via* the coronary circulation. Figure adapted from [244].

After perfusion of the heart for 3 min with 1 x perfusion buffer, the buffer was changed to digestion buffer containing Liberase and Trypsin and perfused until the buffer was used up completely. Afterwards, the atria were removed, and the heart was transferred into a beaker containing 2.5 mL of digestion buffer. After cutting the heart into small pieces for 30 seconds, 2.5 mL of Stop buffer 1 were added in order to stop the enzymatic digestion. After mechanical disaggregation by scissors following trituration of the suspension up and down using a 1 mL insulin syringe for 3 minutes, the suspension was filtered through a 150 µm gauze into a 15 mL tube and cells were let settle for 10 minutes. Supernatant was removed and pellet was resuspended in Stop buffer 2. When cells were used for Immunoblot analysis, Stop buffer 2 without FCS was used. Afterwards, a re-calcification process followed in order to increase $CaCl_2$ concentrations to 1 mM final concentration. Therefore, five re-calcification steps were performed by adding 100 mM $CaCl_2$ solution with 4 min break in between: 5 µL - 5 µL – 10 µL - 30 µL - 50 µL were added to the cell suspension.

Afterwards, cells were seeded on Laminin-coated round glass coverslips (25 mm) and after incubation for 1 h at 37°C and 5% $CO_2$, Myocyte culture medium was added. Cells were kept at 37°C and 5% $CO_2$ until usage.

### 2.2.4.2 Isolation and culture of human atrial and ventricular cardiomyocytes

Human atrial and ventricular tissue samples were put into ice cold Custodiol solution immediately after excision for their transport from the surgery to the laboratory. There, blood and fat were removed, and the tissue was cut into small pieces. Tissue pieces were digested in oxygenated Enzymatic solution I (200 rpm, 30 min, 36°C). Afterwards, tissue pieces were transferred from the enzymatic solution into a 15 mL reaction tube containing Stop solution and disaggregated with a Pasteur pipette. Several rounds of enzymatic digestion with Enzymatic solution II (200 rpm, 15 min, 37°C) and mechanical disaggregation followed. Cells were harvested by centrifugation (500 rpm, 4 min, RT) and resuspended in plating medium M1. Cells were plated on Laminin-coated dishes (Cellvis Glasbottom dish, 29 mm with 10 mm bottom well). After 2 h of culturing at 37°C and 5% $CO_2$, medium was changed to plating medium M2.

## 2.2.5 Cell culture techniques

### 2.2.5.1 Cell culture and transfection of HEK293A cells

HEK293A cells were cultivated in HEK293A culture medium at 37°C and 5% $CO_2$.

For transfection with the plasmids for bleedthrough factor determination (section 2.2.8.1), HEK293A cells were plated on 6-well plates with 25 mm round glass cover slips. After 24 h, when cells reached 70% confluency, cells were transfected with plasmid DNA. Therefore, the transfection reaction mix was prepared as shown in table 2.65. Lipofectamine 2000 (Invitrogen) was used for transfection.

**Table 2.65:  Transfection reaction mix.** Reaction mix for transfection of one 6-well plate.

| Component | Master Mix 1 x |
| --- | --- |
| DMEM | 300 µL |
| Plasmid DNA | 3 µg |
| Lipofectamine 2000 | 7 µL |

The transfection reaction mix was incubated for 20 min at RT. Then, 50 µL of the transfection reaction mix were added per well and cells were kept at 37°C and 5% $CO_2$. After 24 h, cells were used for FRET measurements.

## 2.2.6 Adenovirus amplification, purification, and infection of cardiomyocytes

### 2.2.6.1 Adenovirus amplification and purification

In this work, adenovirus encoding the FRET-based cGMP biosensor red-cGES-DE5 was used in order to transduce human atrial and ventricular cardiomyocytes (section 2.2.6.3). Adenovirus encoding red-cGES-DE5 was first amplified and then purified according to the following protocol. Figure 2.2 shows a schematic illustration of the working flow of adenovirus amplification and purification.
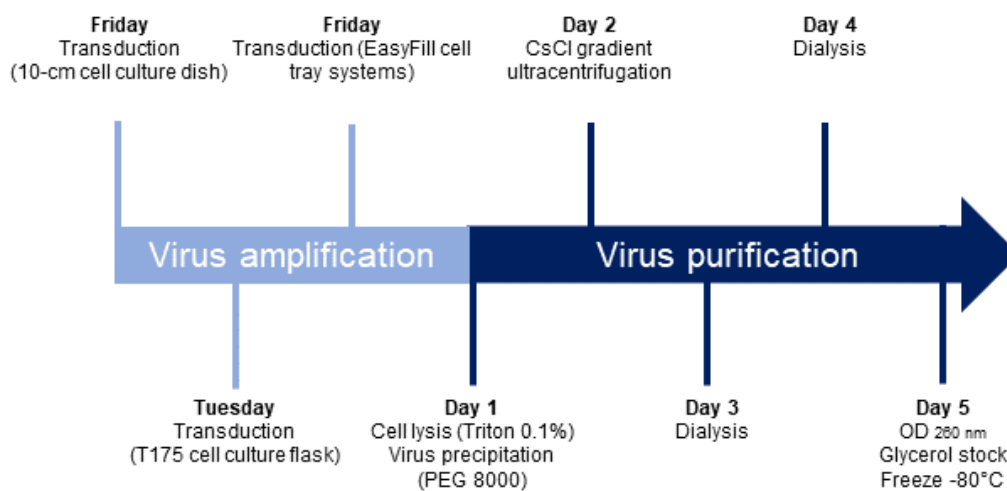


**Figure 2.2:** **Working flow of Adenovirus amplification and purification.** Adenovirus amplification required multiple rounds of amplification in different culture formats in order to generate high-titer virus for purification. Virus purification was done by CsCl gradient ultracentrifugation followed by dialysis. Virus glycerol stock was stored at -80°C.

For virus amplification, multiple rounds of amplifications in HEK293A are needed, in order to get enough high-titer virus for purification. At first, HEK293A cells grown in a 10-cm tissue culture dish were transduced with 2-5 µL of high-titer adenovirus encoding the biosensor red-cGES-DE5. 48 - 60 h post infection, the HEK293A cell culture supernatant was centrifuged (800 rpm, 5 min, RT), to remove the cells. The supernatant was transferred into a new 15 mL tube and pelleted cells were lysed in three rounds of freeze (in liquid nitrogen) and thaw cycles. Afterwards, lysed cells were resuspended in the supernatant taken before. The virus solution was centrifuged (800 rpm, 6 min, RT) to remove cell debris, and the supernatant

was stored at 4°C. Next, HEK293A cells grown in three T175 cell culture flasks were transduced. Therefore, the medium was removed from the T175 cell culture flasks. 25 ml of virus culture medium and 2 mL of virus (from the amplification on the 10-cm dish) were added per flask. Cells were grown at 37°C and 5% $CO_2$ and after 2.5 h medium was changed to fresh virus culture medium (35 mL). Cells should be lysed three to four days post infection. Next HEK293A cells grown on EasyFill Cell tray systems (2 trays and 4 trays) could be transduced with the virus amplified on the T175 flasks. Therefore, the cell culture supernatant of the transduced T175 cell culture flasks was centrifuged (800 rpm, 5 min, RT) to remove cell debris. The supernatant of all flasks was transferred into a new T175 flask and filled up to 300 mL with virus culture medium. HEK293A culture medium was removed from the EasyFill cell tray systems and virus solution was added (100 mL in 2 trays, 200 mL in 4 trays). After incubation at 37°C and 5% $CO_2$ for 2 h, medium was changed to fresh virus culture medium (150 mL in 2 trays, 300 mL in 4 trays). Cells should be lysed three days post infection. After virus amplification, virus purification followed.

The virus was purified *via* CsCl gradient ultracentrifugation. On day 1 of the purification, the virus was harvested from the EasyFill cell tray systems. Therefore, the cell culture supernatant from the cell trays was transferred equally into two centrifuge beakers (250 mL) and Triton-X-100/PBS solution was added ($C_{final,\ Triton}$ = 0.1%) in order to lyse the cells which had not been lysed yet. After incubation on a shaker for 30 min at 900 rpm, beakers were centrifuged (4.000 rpm, 60 min, 4°C). Supernatant was transferred equally into three new centrifuge beakers and ½ volume of 20% PEG 8000/2.5 M NaCl solution was added in order to precipitate the virus DNA. The solution was mixed well and incubated on ice o.n. at 4°C.

The next day (day 2) virus was harvested (60 min, 4.000 rpm, 4°C) and resuspended in a total volume of 11.5 mL PBS, pH 8.0. After pulling up of the solution in a 30 mL syringe with a 18G cannula, the cannula was changed to 23G and virus solution was transferred into a 15 mL tube. After incubation on a rotor at 4°C for 1.5 hours, the virus solution was centrifuged (2.000 rpm, 2 min, RT) and 5.02 g CsCl were resuspended in the supernatant. The mixture was kept at 37°C until CsCl was dissolved completely and CsCl concentration was adjusted to 1.33 g/ml. The virus-CsCl solution was transferred into ultracentrifuge tubes using a 30 mL syringe with 20G cannula, tubes were balanced and sealed. CsCl gradient centrifugation was done o.n. (40.000 rpm, 24 h, 16°C, acceleration 9, deceleration 4). On the following day (day 3), the virus band was removed from the CsCl gradient with a 2 mL syringe (21G cannula) and transferred into a dialysis tube. Dialysis tubing was closed by two knots at the ends. Then, a magnetic clamp was put on one side of the tubing and a plastic clamp on the other side. The tubing was rotated o.n. at 4°C in 1 x Sucrose buffer. On the next day, dialysis buffer was changed to fresh 1 x Sucrose buffer and incubated for one more day at 4°C. On day 5, the virus solution was removed from the dialysis tubing and optical

density ($OD_{260\,nm}$) was measured in order to determine the physical virus concentration. After adding sterile glycerol solution ($C_{final}$ = 10%), virus was aliquoted and frozen at -80°C until usage.

### 2.2.6.2 Determination of viral titers by plaque assay

Plaque assay was used to determine viral titer as plaque-forming units (PFUs) per mL. Therefore, virus was serial diluted 10-fold in plaque assay medium. Cell culture medium of confluent HEK293A cells grown on two 6-well plates was removed, and 1 mL of plaque assay medium was added per well. Then, virus dilutions were added to the wells in duplicates (1000 PFU, 100 PFU, 10 PFU). After incubation at 37°C for 2 h, medium was removed, cells were washed with plaque assay medium, and sterile Agarose/IMDM (mixed 1:2) was added (4 mL/per well). Agarose/IMDM was let solidified for 30 min at RT. After incubation at 37°C and 5% $CO_2$ for seven days, plaques were counted. Biological virus activities were calculated using the following formula.

$$Biological\ virus\ activity = \frac{Number\ of\ plaques}{Dilution\ factor} * physical\ virus\ concentration$$

### 2.2.6.3 Adenoviral transduction of isolated human atrial and ventricular cardiomyocytes

Since the Lipofectamine-based transfection technique (section 2.2.5.1) does not work for terminally differentiated adult cardiomyocytes [244], viral-based transduction was used in order to express the FRET-based cGMP biosensor red-cGES-DE5 in human atrial and ventricular cardiomyocytes. Adenovirus encoding the biosensor red-cGES-DE5 was amplified and purified as described in section 2.2.6.1. Isolated human atrial and ventricular cardiomyocytes (2.2.4.2) were seeded on Laminin-coated dishes in M1 culture medium and cultured at 37°C and 5% $CO_2$. After 2 h, medium was changed to M2 culture medium and cells were infected at multiplicity of infection (MOI) of 300 with adenovirus encoding red-cGES-DE5. Cell were cultured at 37°C and 5% $CO_2$. FRET measurements were performed 48 h after transduction.

### 2.2.7 Models of hypoxic injury

*2.2.7.1 In vitro model of hypoxia/reoxygenation in isolated mouse and human ventricular cardiomyocytes*

In order to induce hypoxic injury, freshly isolated mouse or human ventricular cardiomyocytes (section 2.2.4.1 and 2.2.4.2), plated in murine myocyte culture medium or human M2 plating medium, respectively, were placed in a modular incubator chamber (Billups Rothenberg). Then the chamber was flushed with a gaseous mixture of nitrogen ($N_2$) and carbon dioxide ($CO_2$), at a flow rate 20 to 1, respectively, until a final $O_2$ concentration of 1% was reached (94% $N_2$, 5% $CO_2$, 1% $O_2$). $O_2$ concentration in the modular incubator chamber was controlled by an oxygen detector (GOX-100, Greisinger). Flow rate of $N_2$ and $CO_2$ was controlled by a dual flow meter (Billups Rothenberg). Cells were kept in the modular incubator chamber at 37°C for different time periods (90 min and 4 h). Afterwards, cells were reoxygenated under standard conditions (5% $CO_2$, 37°C) for 2 h. Normoxic controls (Normoxia) were kept under standard conditions at 37°C and 5% $CO_2$. Cells were either used directly after hypoxia treatment or after hypoxia/reoxygenation treatment for further experiments. Hypoxia/reoxygenation protocol is shown in figure 2.3.
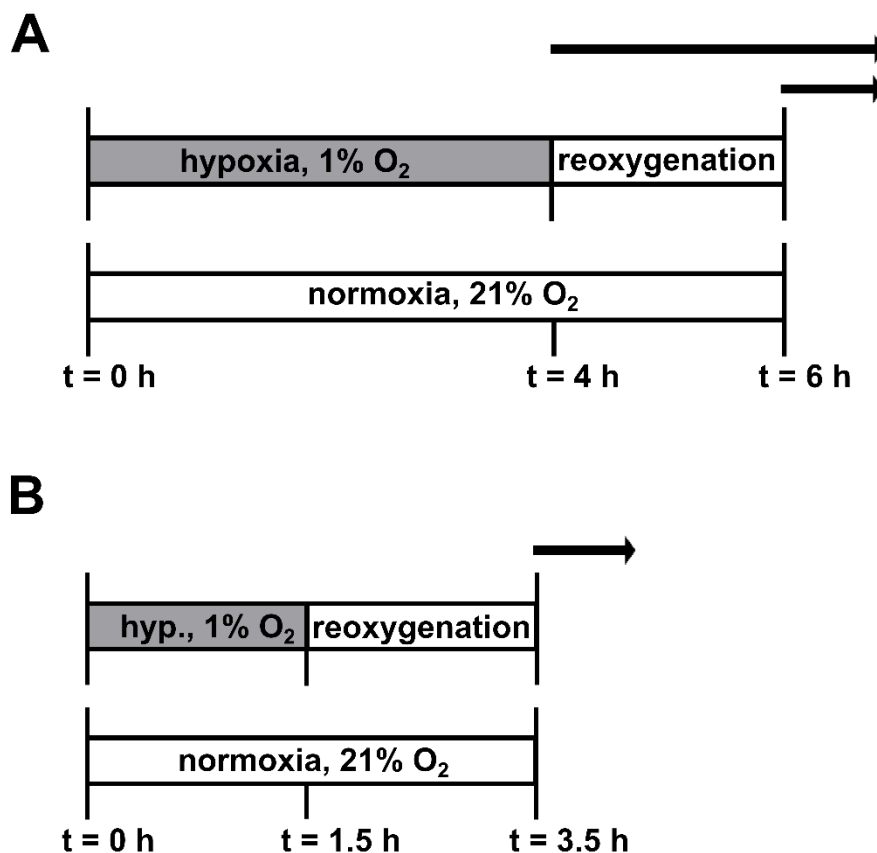


**Figure 2.3:** **Model of hypoxia/reoxygenation injury in isolated mouse and human ventricular cardiomyocytes.** Hypoxia was induced in a modular incubator chamber (Billups Rothenberg) with a gaseous mixture of $N_2$ and $CO_2$ with a flow rate 20:1 until a final $O_2$ concentration of 1% was reached

(94% $N_2$, 5% $CO_2$, and 1% $O_2$). Reoxygenation was performed under standard conditions at 37°C and 5% $CO_2$. Normoxic controls were kept at 37°C and 5% $CO_2$. Duration for hypoxia/reoxygenation was **A**) 4 hours of hypoxia followed by 2 hours of reoxygenation or **B**) 90 min of hypoxia, followed by 2 h of reoxygenation. Black arrows indicate the start of following experiments directly after hypoxia or after hypoxia/reoxygenation.

### 2.2.7.2 Ex vivo model of anoxic injury in Langendorff-perfused whole hearts

An *ex vivo* whole heart Langendorff model was used in order to induce anoxic injury in whole mouse hearts. Mice were heparinized and sacrificed by cervical dislocation. The heart was removed and dissected in ice cold modified Krebs-Henseleit solution. The aorta was cannulated, and the heart was attached to the Langendorff system (Harvard apparatus, Hugo Sachs Elektronik). There, the heart was perfused retrogradely with prewarmed (37°C) oxygenated Krebs-Henseleit solution at constant pressure (80 mm Hg). An octa polar electrophysiology catheter (2F, 0.5 mm electrode spacing) was inserted *via* the right atrium into the right ventricle and the heart was paced constantly at 530 beats per minute (BPM). Perfusion pressure, aortic flow, and heart rate were continuously recorded using a digital data acquisition system and corresponding software (Harvard Apparatus, Hugo Sachs Elektronik; STG 4002, Multi channel systems).

In order to induce anoxia in the hearts, the perfusion buffer was changed to non-oxygenated modified Krebs-Henseleit solution (37°C) for 30 min. Normoxic control hearts were perfused with oxygenated modified Krebs-Henseleit solution constantly. Figure 2.4 shows the model of anoxic injury in a whole-heart Langendorff system.
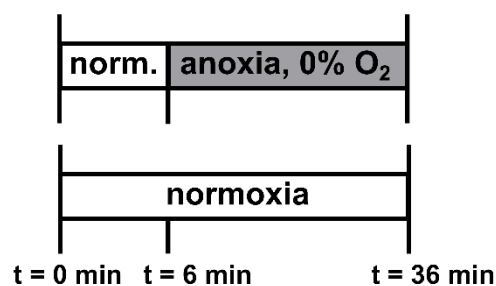


**Figure 2.4:**  **Model of anoxic injury in an *ex vivo* whole-heart Langendorff system.**  After 6 min of normoxic equilibration conditions, perfusion buffer was changed to non-oxygenated modified Krebs-Henseleit-solution for 30 min. Control hearts were perfused under normoxic conditions constantly. All hearts were perfused at constant pressure (80 mmHg) *via* retrograde perfusion and paced at 530 beats per minute (BPM).

*2.2.7.3 In vivo open-chest model of ischemia/reperfusion injury*

In order to induce ischemic injury in mouse hearts *in vivo*, an ischemia/reperfusion open-chest model was used. Surgeries were performed by Sandra Frankenreiter and Anna Kuret from the group of Prof. Robert Lukowski in Tübingen as described previously [168]. Ischemia was induced by occlusion of the left coronary artery. All hearts were subjected to 30 min ischemia followed by 10 min of reperfusion (Figure 2.5). For further experiments, tissue from non-infarcted regions of the heart ("Rest") was used as a control to compare with tissue from the infarcted region of the heart (I/R).
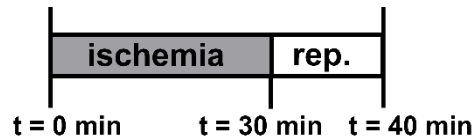


**Figure 2.5:** ***In vivo* open-chest model of ischemia/reperfusion injury.** An *in vivo* open chest model of myocardial infarction was done in mice. Ischemia was induced by occlusion of the left coronary artery for 30 min, followed by 10 min of reperfusion.

## 2.2.8 Microscopy techniques

*2.2.8.1 FRET-based cGMP and cAMP measurements in isolated cardiomyocytes and data analysis*

In this work FRET-based cGMP and cAMP measurements were performed in isolated mouse and human ventricular cardiomyocytes exposed to hypoxia/reoxygenation injury or normoxic control conditions, as well as in human atrial cardiomyocytes from right (RA) and left atria (LA) of patients in sinus rhythm (SR) and with atrial fibrillation (AF).

Therefore, a FRET system was used consisting of a light emitting diode (LED) light source (pE-100, CoolLED), to excite the donor fluorophore, a beamsplitter (DV2, Photometrics) to divide the emission light into two channels, and a camera (complementary metal oxide semiconductor (CMOS) camera optiMOS, QImaging) to detect donor and acceptor channel intensities simultaneously. A picture of the FRET system used for this work is shown in Figure 2.6.
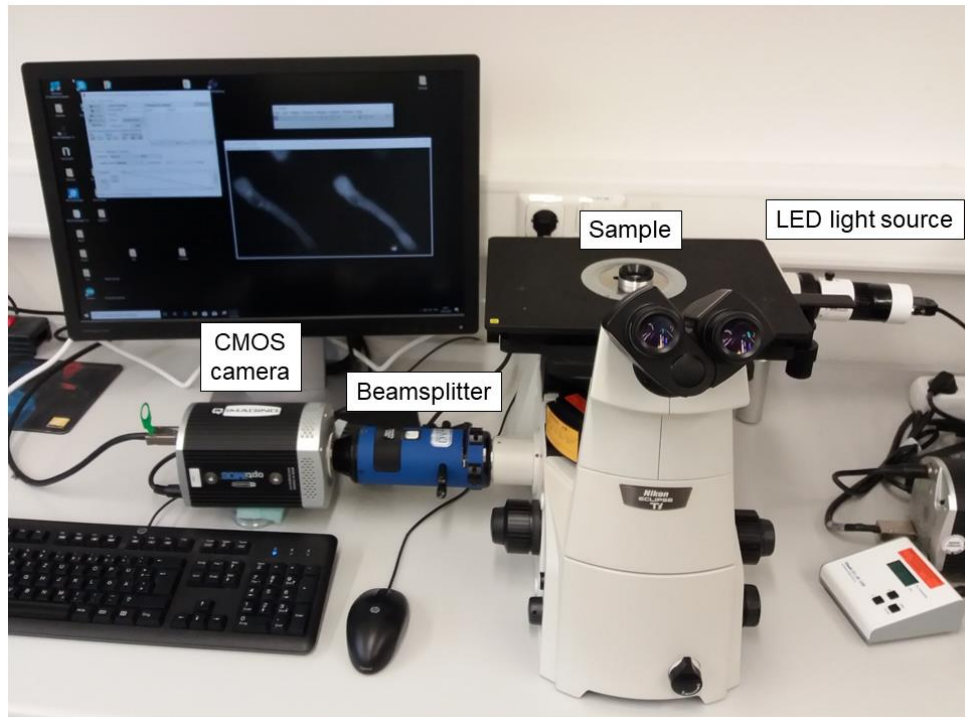
**Figure 2.6:**     **FRET system for cGMP and cAMP measurements in isolated cardiomyocytes.** The FRET system consisted of a light emitting diode (LED) light source to excite the donor fluorophore, a beamsplitter to divide the emission light into donor and acceptor channel, and a complementary metal oxide semiconductor (CMOS) camera to detect the two channel intensities.

A standard inverted microscope (Nikon eclipse Ti-4) with a 63 x/1.5 oil immersion objective was used for the FRET measurements. To excite the donor fluorophore (T-Sapphire for cGMP measurements, CFP for cAMP measurements) a single-wavelength LED (400 nm for cGMP measurements, 440 nm for cAMP measurements) was used. The LED was controlled by an Arduino digital-to-analogue input-output board (Arduino). A Dual View beamsplitter (Cube 11-EM, 565 dcxr, 520/30, D630/50 for cGMP measurements, Cube 05-EM, 505 dcxr, D480/30m, D535/40 m for cAMP measurements) was used to split the emission light into donor (T-Sapphire for cGMP measurements, CFP for cAMP measurements) and acceptor (Dimer2 for cGMP measurements, YFP for cAMP measurements) channels. Single channels intensities were recorded with a CMOS camera (QImaging). As software Micro Manager 1.4.5 was used to perform time-laps image acquisition.

For FRET measurements of mouse ventricular cardiomyocytes 25 mm round glass coverslips with laminin-coated cells were transferred into a FRET imaging chamber and medium was replaced by FRET buffer. FRET measurements of human atrial and ventricular cardiomyocytes were directly performed in the Glassbottom dishes on which cells were plated (Cellvis Glasbottom dish, 29 mm with 10 mm bottom well). Therefore, medium was replaced by FRET buffer.

FRET setup and drug application took place at RT without perfusion system. Images were taken every 5 seconds. For data analysis, Microsoft excel software was used. As the emission spectra of T-Sapphire and Dimer2 (for cGMP measurements) and of CFP and YFP (for cAMP measurements) overlap, bleedthrough factor (B) correction was necessary. In order to determine the bleedthrough factor coefficient B for cGMP measurements, T-Sapphire protein was expressed in HEK293A cells (section 2.2.5.1) and fluorescent intensity in the Dimer2 channel upon T-Sapphire excitation was measured. To determine the bleedthrough factor coefficient B for cAMP measurements, CFP protein was expressed in HEK293A cells (section 2.2.5.1) and fluorescent intensity in the YFP channel upon CFP excitation was measured.

The bleedthrough factor corrected FRET ratio was calculated as follows:

$$FRET\ ratio\ cGMP\ measurements = \frac{TSapphire}{Dimer2 - B * TSapphire}$$

$$FRET\ ratio\ cAMP\ measurements = \frac{YFP - B * CFP}{CFP}$$

Bleedthrough corrected FRET traces were normalized to baseline and FRET response was quantified using Microsoft Excel software.

*2.2.8.2 FRET-based cGMP and cAMP measurements in whole hearts and data analysis*

For monitoring FRET in whole mouse hearts, a Langendorff perfusion system was used (Harvard Apparatus, Hugo Sachs Elektronik). Hearts were prepared as described in section 2.2.7.2. After 20 min of equilibration, FRET recording was started. For FRET imaging, a self-build imaging system build around a stereomicroscope (M165FC, Leica) was used. It consisted of a LED (400 nm for cGMP measurements, 440 nm for cAMP measurements, CoolLED), a dual view beam splitter (Cube 11-EM, 565 dcxr, 520/30, D630/50 for cGMP measurements, Cube 05-EM, 505 dcxr, D480/30m, D535/40 m for cAMP measurements, Photometrics) and a CMOS camera (QImaging). LED was controlled by an Arduino digital-to-analogue input-output board (Arduino). As software Micro Mananger 1.4.5 was used to perform time-laps image acquisition. Images were taken every 30 seconds. Data analysis was done as described in section 2.2.8.1. Since mice with cardiomyocyte-specific expression of T-Sapphire protein (for cGMP) only or CFP protein (for cAMP) only were not available in the lab, bleedthrough factor could not be determined for this microscope. Therefore, the same bleedthrough factor as used for FRET measurements in isolated cardiomyocytes (see 2.2.8.1) was used for bleedthrough correction.

## 2.2.9 Protein biochemical methods

*2.2.9.1 Preparation of protein lysates*

In this work, protein lysates for immunoblot analysis (section 2.2.9.4) were prepared from isolated mouse ventricular cardiomyocytes, whole murine hearts, human ventricular tissue samples, and human atrial tissue samples.

Protein lysates for cGMP enzyme immunoassay (section 2.2.10) were prepared from isolated mouse ventricular cardiomyocytes, and whole murine hearts.

*Preparation of protein lysates from mouse ventricular cardiomyocytes for immunoblot analysis*

For preparation of protein lysates from isolated, cultured, murine ventricular cardiomyocytes, plated cells were washed with ice cold PBS, scratched with a cell scrapper and transferred into a 1.5 mL reagent tube. After centrifugation (3.000 rpm, 3 min, 4°C), supernatant was discarded, and cell pellet was resuspended in ready to use homogenization buffer. Suspension was pushed 10 x through an insulin syringe and incubated on ice for 30 min in order to lyse the cells. After centrifugation (13.000 rpm, 10 min, 4°C), supernatant was transferred into a new 1.5 mL reagent tube and lysate was stored at -20°C.

*Preparation of protein lysates from murine heart tissue for immunoblot analysis*

For preparation of protein lysates from murine hearts, snap frozen ventricular heart tissue was cut into small pieces. Ready to use homogenization buffer was added and tissue was homogenized three times for 20 sec using an Ultra Turrax (T-10 basic, IKA). In order to prevent the samples from warming they were cooled in liquid nitrogen in between. After incubation of the lysate on ice for 30 min, samples were centrifuged (13.000 rpm, 10 min, 4°C), supernatants were transferred into new reagent tubes, and stored at -20°C until usage.

*Preparation of protein lysates from human ventricular and atrial tissue samples for immunoblot analysis*

Preparation of protein lysates from human ventricular and atrial tissue samples was prepared as described in the section "*preparation of protein lysates from murine heart tissue for immunoblot analysis*" with some modifications. Homogenization was done in RIPA buffer instead of ready to use homogenization buffer and homogenization time was prolonged to 4 x 30 seconds.

71

*Preparation of protein lysates from mouse ventricular cardiomyocytes for cGMP immunoassay*

Preparation of protein lysates from mouse ventricular cardiomyocytes for cGMP immunoassay was done as described in the section "*Preparation of protein lysates from mouse ventricular cardiomyocytes for immunoblot analysis*" with some modifications. Instead of homogenization buffer, HCl (0.1 M) was used to lyse the cells. Samples were kept at RT, and incubation time of the lysate was reduced to 10 min at RT instead of 30 min on ice.

*Preparation of protein lysates from murine heart tissue for cGMP enzyme immunoassay*

Preparation of protein lysates from murine heart tissue for cGMP enzyme immunoassay was done as described in the section "*Preparation of protein lysates from murine heart tissue for immunoblot analysis*" with some modifications. Instead of homogenization buffer, HCl (0.1 M) was used to lyse the cells. Samples were kept at RT and no cooling of the samples in liquid nitrogen was performed in between. Incubation time of the lysate was reduced to 10 min at RT instead of 30 min on ice.

*2.2.9.2 Protein quantification*

In this work, protein quantification was necessary for different methods - immunoblot analysis and cGMP enzyme immunoassay. Depending on the lysis buffer used for preparation of the protein lysates, different quantification methods were used.

*Protein quantification for Immunoblot analysis*

Protein quantification of protein lysates prepared for Immunoblot analysis was done using the Pierce BCA protein assay kit (Thermo Scientific) according to the manufacturer's instructions. Microplate procedure was chosen with a working range of 20 – 2.000 µg/mL. Absorbance was measured in a FlexStation 3 plate reader (Molecular devices) and Soft Max Pro Software (Molecular devices) was used for analysis.

*Protein quantification for cGMP enzyme immunoassay*

Since protein lysates for cGMP enzyme immunoassay were prepared in HCl (section 2.2.9.1), Pierce Coomassie protein assay kit (Thermo Scientific) was used for protein concentration measurement. The assay was done according to the manufacturer's instructions. Microplate protocol with a working range 100 – 1.500 µg/mL was chosen. Absorbance was measured in a FlexStation 3 plate reader (Molecular devices) and Soft Max Pro Software (Molecular devices) was used for analysis.

*2.2.9.3 SDS polyacrylamide gel electrophoresis*

SDS polyacrylamide gel electrophoresis (SDS-PAGE) was used in order to separate proteins in an electrical field according to their molecular weight [245]. Therefore, 8 - 15% polyacrylamide gels were prepared as shown in section 2.1.13.5 (Tables 2.55 and 2.56) and stored at 4°C until usage, for maximal one day. Protein samples were incubated for 10 min at 70°C in a thermal cycler (Eppendorf). Depending on the antibody used, 10 - 30 µg of protein were loaded onto the polyacrylamide gel. Protein Marker V (Peqlab) (3 µL) was used as protein size standard. Gel electrophoresis was run at 80 - 110 V in the Mini-PROTEAN Tetra Cell system (Bio Rad). Mini Trans-Blot Cell (Bio Rad) was used to transfer the size-separated proteins on a nitrocellulose membrane (tank blot method). Membranes were then used for Immunoblot analysis (section 2.2.9.4).

*2.2.9.4 Immunoblot analysis*

In order to detect the proteins on the nitrocellulose membrane (section 2.2.9.3), membranes were blocked in blocking buffer (either 1 - 5% non-fat milk in TBS-T or 3% BSA in TBS-T, depending on the antibody) for 1 h at RT. Afterwards, primary antibodies were added. Dilutions and incubation conditions are shown in section 2.1.5.1 (Table 2.6). After incubation of the primary antibody, membranes were washed 3 x 10 min in TBS-T buffer and secondary antibodies were added, dilutions conditions are shown in section 2.1.5.2 (Table 2.7). After incubation for 1 h at RT, secondary antibodies were removed, and membranes were washed 3 x 10 min with TBS-T buffer at RT. For signal detection the SuperSignal West Pico PLUS kit (Thermo Fisher) was used according to the manufacturer's instructions. X-ray films were exposed and the medical film processor SRX-101A (Konica Minolta) was used to develop the films. Band densitometry analysis was performed using ImageJ software.

*2.2.9.5 Cycloheximide protein chase assay*

Cycloheximide (CHX) is a protein synthesis inhibitor and can be used to investigate protein stability [246]. In order to compare protein degradation between Normoxia and hypoxia/reoxygenation treated mouse ventricular cardiomyocytes, CHX protein chase assay was done. Therefore, the protein synthesis blocker CHX (50 µM) was added onto the plated cardiomyocytes before hypoxia/reoxygenation treatment (section 2.2.7.1). Afterwards, cells were harvested, and protein lysates were prepared as described in section 2.2.9.1. The

setup of the CHX treatment is shown in Figure 2.7. Protein degradation was analysed by immunoblot analysis as described in section 2.2.9.3 and section 2.2.9.4.
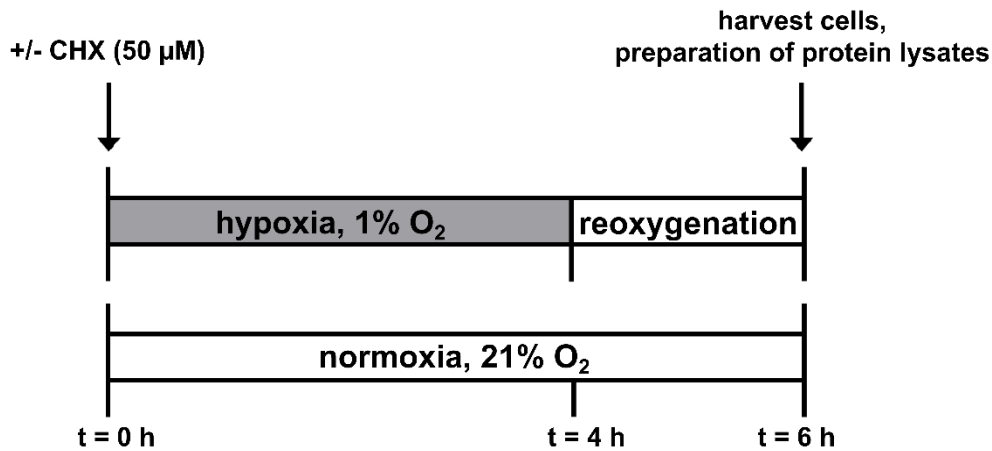


**Figure 2.7:** **Cycloheximide protein chase assay.** Cycloheximide (CHX) protein chase assay was done in order to compare protein degradation between Normoxia and hypoxia/reoxygenation treated mouse ventricular cardiomyocytes. CHX (50 µM) was added before hypoxia/reoxygenation or Normoxia treatment (t = 0 h). After 4 h of hypoxia (t = 4 h), followed by 2 h of reoxygenation (t = 6 h), protein lysates were prepared for further analysis as described in section 2.2.9.1. Control were kept under normoxic conditions (Normoxia).

### 2.2.10 cGMP immunoassay

For quantitative determination of cGMP levels in isolated mouse ventricular cardiomyocytes exposed to hypoxia/reoxygenation or mouse heart tissue samples of ischemia/reperfusion injury, a cGMP enzyme immunoassay kit (Sigma Aldrich) was used according to the manufacturer's instructions. The kit uses a polyclonal cGMP antibody to bind the cGMP in the sample or an alkaline phosphatase molecule covalently attached to cGMP in a competitive manner. At the end of the reaction, a yellow colour is generated which is inversely proportional to the cGMP concentration in the sample. The absorbance was measured in a FlexStation 3 plate reader (Molecular devices) and Soft Max Pro Software (Molecular devices) was used for analysis.

Lysates used for cGMP enzyme immunoassay were prepared in HCl (0.1 M) as described in section 2.2.9.1 and protein concentrations were measured with Pierce Coomassie protein assay kit (Thermo Scientific) as described in section 2.2.9.2. Lysates were acetylated in order to perform the acetylated version of the kit.

**2.2.11 LDH Glo Cytotoxicity assay**

In order to determine necrotic cell death in mouse ventricular cardiomyocytes after hypoxia/reoxygenation injury, a lactate dehydrogenase (LDH) assay was done. LDH is a soluble stable cytosolic enzyme which is rapidly released into the cell culture medium upon disruption of the plasma membrane [247]. LDH is widely used as a marker for cytotoxicity. In this work, the LDH Glo Cytotoxicity assay (Promega) was used according to the manufacturer's instructions.

Luminescence was measured after 60 min in a FlexStation 3 plate reader (Molecular devices) and Soft Max Pro Software (Molecular devices) was used for analysis.

**2.2.12 Statistical analysis**

All statistical evaluations in this study were carried out with GraphPad Prism 6 (version 6.01) and R 3.3.2 software. Data are presented as mean ± standard error of the mean (SEM). Normal distribution was tested with the Kolmogorov-Smirnov test. Differences between the groups were analysed using one-way ANOVA or Kruskal-Wallis test. For the analysis of the measurements in which several cells from different mice were used, mixed ANOVA followed by $\chi^2$ test was done. Statistical significance p was defined as * for $p < 0.05$, ** for $p < 0.01$ and *** for $p < 0.001$. Graphic illustrations were done using GraphPad Prism 6 software (version 6.01).

# 3. Results

The result part of this work is divided into two sections. In the first part, results of the project "Changes in mouse and human cardiomyocyte cGMP dynamics during hypoxic injury" are presented (section 3.1). In the second part, data of the project investigating "cGMP signalling in human atrium and its role in atrial fibrillation" are shown (section 3.2).

## 3.1 Changes in mouse and human cardiomyocyte cGMP dynamics during hypoxic injury

### 3.1.1 Enhancement of red-cGES-DE5 biosensor expression in transgenic red-cGES-DE5 mice

Some years ago, our group has generated a transgenic mouse line with cardiomyocyte-specific expression of the highly sensitive cytosolic FRET-based cGMP biosensor red-cGES-DE5 [136]. In those mice, the FRET sensor red-cGES-DE5 was uniformly expressed under control of the cardiac muscle-specific $\alpha$MHC promoter at high enough levels to allow reliable FRET measurements of cGMP dynamics in intact adult mouse cardiomyocytes [136]. However, even though FRET measurements were possible, weak sensor expression made cGMP measurements very challenging.

In order to facilitate FRET-based cGMP measurements with the biosensor red-cGES-DE5 for this work, transgenic mice with stronger expression of the biosensor were generated by mating together mice with heterozygous expression of the biosensor (T/+) in order generate mice with homozygous expression (T/T). After the genotype was confirmed by TaqMan PCR (section 2.2.3.5), whole-heart FRET measurements were performed in order to compare between heterozygous (T/+) and homozygous (T/T) sensor expression (Figure 3.1.1).

Biosensor expression was much stronger in the newly generated homozygous (T/T) mice compared to mice with heterozygous expression of the sensor (T/+), making FRET-based cGMP measurements much easier and more reliable because of less background noise.

**A**



**B**
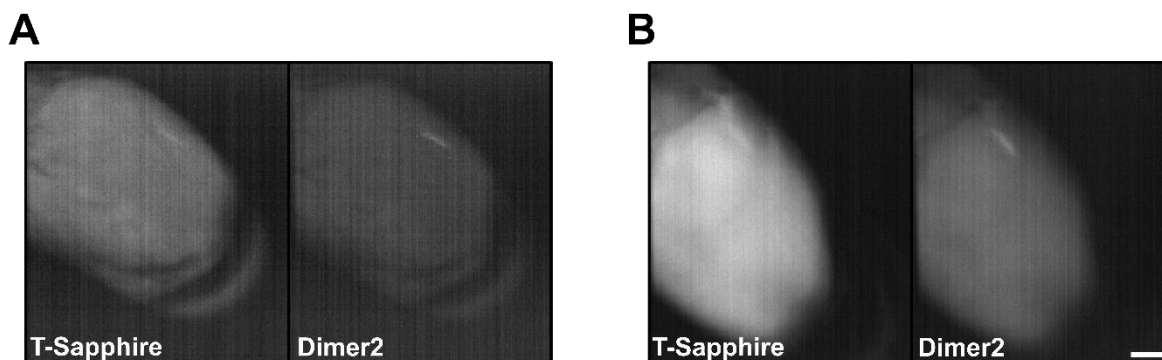


**Figure 3.1.1: Red-cGES-DE5 biosensor expression in different transgenic mouse lines.** Fluorescence of the 3',5'-cyclic guanosine monophosphate (cGMP) biosensor red-cGES-DE5 in T-Sapphire and Dimer2 channels during Förster resonance energy transfer (FRET) measurements in Langendorff-perfused whole hearts. **A**) Heart with heterozygous (T/+) expression of the biosensor red-cGES-DE5. **B**) Heart with homozygous biosensor expression (T/T). Images in both T-Sapphire and Dimer2 emission channels were taken with an exposure time of 500 msec. Scale bar, 1 mm.

### 3.1.2 Effects of *in vitro* hypoxia/reoxygenation on mouse ventricular cardiomyocytes

In the first series of experiments, it was tested whether the *in vitro* model of hypoxia/reoxygenation was functional. Therefore, different markers for hypoxic injury were analysed.

Cell death is one consequence of hypoxia/reoxygenation injury [248]. In order to quantify the amount of cell death during *in vitro* hypoxia/reoxygenation, images were taken from isolated ventricular mouse cardiomyocytes exposed to 4 h of hypoxia followed by 2 h of reoxygenation (4 h H/R) or normoxic control conditions (Normoxia). Images were taken before induction of hypoxia (t = 0 h), directly after 4 h of hypoxia (t = 4 h) and after 2 h of reoxygenation (t = 6 h). Quantification of cell death was done by counting the amount of living and dead cells. The data clearly showed a significant increase in cell death during 4 h of hypoxia (t = 4 h, living cells in %: 41.1 ± 4.0) as well as during 2 h of reoxygenation (t = 6 h, living cells in %: 28.1 ± 3.6) compared to normoxic controls (living cells in %: Normoxia t = 4 h: 67.5 ± 3.0; t = 6 h: 61.4 ± 5.4) (Figure 3.1.2 A and B).

The transcription factor HIF-1$\alpha$ is the master regulator of $O_2$ homeostasis. Upregulation of HIF-1$\alpha$ mRNA and protein level were shown to be a good marker for hypoxia [24, 39]. Gene expression analysis of HIF-1$\alpha$ in cells exposed to 4 h of hypoxia (Hypoxia) (fold of Normoxia: 1.37 ± 0.05) compared to Normoxia (0.99 ± 0.07) showed a significant upregulation of HIF-1$\alpha$ gene expression during Hypoxia (Figure 3.1.2, C).

LDH activity, which is a classical marker for necrosis [249], showed a tendency but not a significant increase in cells exposed to 4 h H/R (165.3 ± 14.7 mU/mL) compared to Normoxia (135.5 ± 24.2 mU/mL) (Figure 3.1.2, D).
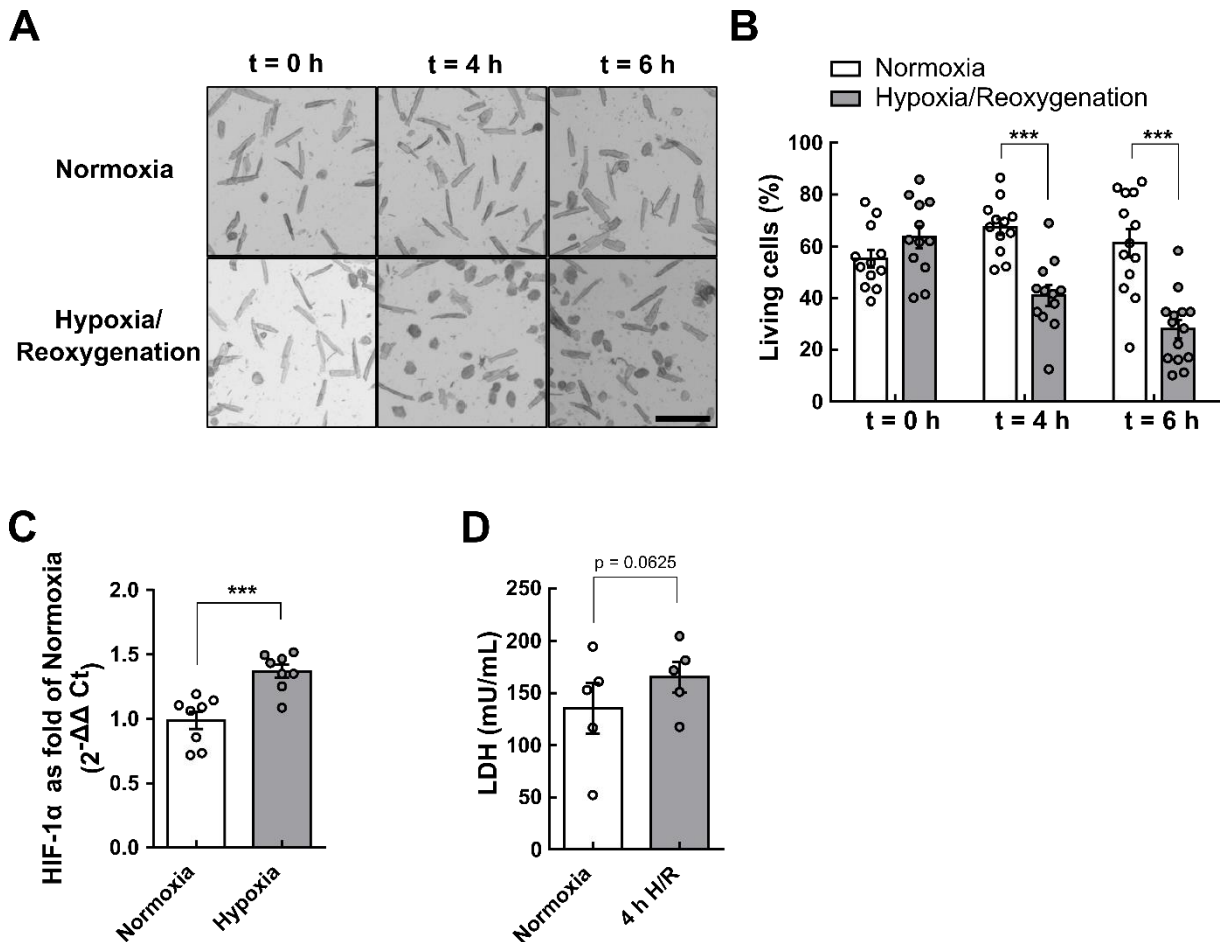


**Figure 3.1.2:** **Effects of *in vitro* hypoxia/reoxygenation on mouse ventricular cardiomyocytes.** The effects of hypoxia/reoxygenation on cardiomyocytes *in vitro* were investigated by different markers. **A**) Images of cardiomyocytes were used to quantify the amount of living and dead cells during hypoxic injury. Images were taken before induction of hypoxia (t = 0 h), directly after hypoxia treatment for 4 h (t = 4 h) and after 2 h of reoxygenation (t = 6 h). Controls were kept under normoxic conditions (Normoxia). Scale bar, 250 µm. **B**) Quantification of cell death. 4/5 pictures per mouse were analysed from 3 different mice. **C**) Hypoxia inducible factor 1α (HIF-1α) gene expression after 4 h of hypoxia (Hypoxia) compared to normoxic controls (Normoxia). **D**) Lactate dehydrogenase (LDH) activity as marker of necrotic cell death in cells exposed to 4 h of hypoxia followed by 2 h of reoxygenation (4 h H/R) and Normoxia. Data are presented as mean ± SEM, significant differences at * $p < 0.05$, ** $p < 0.01$, *** $p < 0.001$.

### 3.1.3 FRET measurements and cGMP immunoassay in red-cGES-DE5 cardiomyocytes reveal increased basal cGMP levels after hypoxia/reoxygenation

In order to analyse the effect of hypoxia/reoxygenation on basal cGMP levels, cGMP FRET recordings and cGMP immunoassay were conducted. Intracellular cyclic nucleotide concentrations can be calculated *via* FRET as described previously [250]. In this work, maximal FRET ratio values ($R_{max}$) were measured after maximal stimulation of GC-B with CNP (1 µM) and concurrent PDE inhibition with the broad range unselective PDE inhibitor IBMX (100 µM). Minimal FRET ratio values ($R_{min}$) were determined by inhibition of NO-GC with ODQ (50 µM) (Figure 3.1.3, A and B). Concomitant inhibition of NP-GCs was not necessary to determine $R_{min}$ values, since NO-GC is primarily responsible for basal cGMP production in mouse ventricular cardiomyocytes [136]. Calculation of basal cGMP levels *via* FRET was done using a concentration-response curve of red-cGES-DE5 protein to cGMP *in vitro* [216].

Basal cGMP levels in normoxic controls (Normoxia) were 32 nM. The FRET measurements revealed that with increasing durations of hypoxia, cGMP levels were increasing. 90 min of hypoxia followed by 2 h of reoxygenation (90 min H/R) led to an increase of basal cGMP to 76 nM. After 4 h of hypoxia followed by 2 h of reoxygenation (4 h H/R) basal cGMP levels were increased 4-fold compared to Normoxia (4 h H/R: 120 nM) (Figure 3.1.3, C). A significant reduction in the FRET response to CNP (1 µM) plus IBMX (100 µM) in 90 min H/R (6.7 ± 1.8%) and 4 h H/R treated cells (5.1 ± 0.5%) compared to Normoxia (12.6 ± 1.2%) (Figure 3.1.3, A and B) but higher basal cGMP levels in 90 min H/R and 4 h H/R treated cells (Figure 3.1.3, C) indicated that the sensor saturation was reached in these measurements.

In addition to the determination of the basal cGMP concentrations using FRET, basal cGMP concentrations were determined with cGMP immunoassay. cGMP concentration measurements in cardiomyocytes from 5 different mice each exposed to 4 h H/R and Normoxia showed a 3-fold increase in basal cGMP levels after 4 h H/R ($302.7 ± 70.0$ fmol/$10^5$ cells) compared to Normoxia ($111.0 ± 20.6$ fmol/$10^5$ cells). Assuming that the volume of a cardiomyocyte is 20.000 fL [174, 251], this is a cGMP concentration of 55 nM in Normoxia treated cells which increases to 151 nM after 4 h H/R (Figure 3.1.3, D).
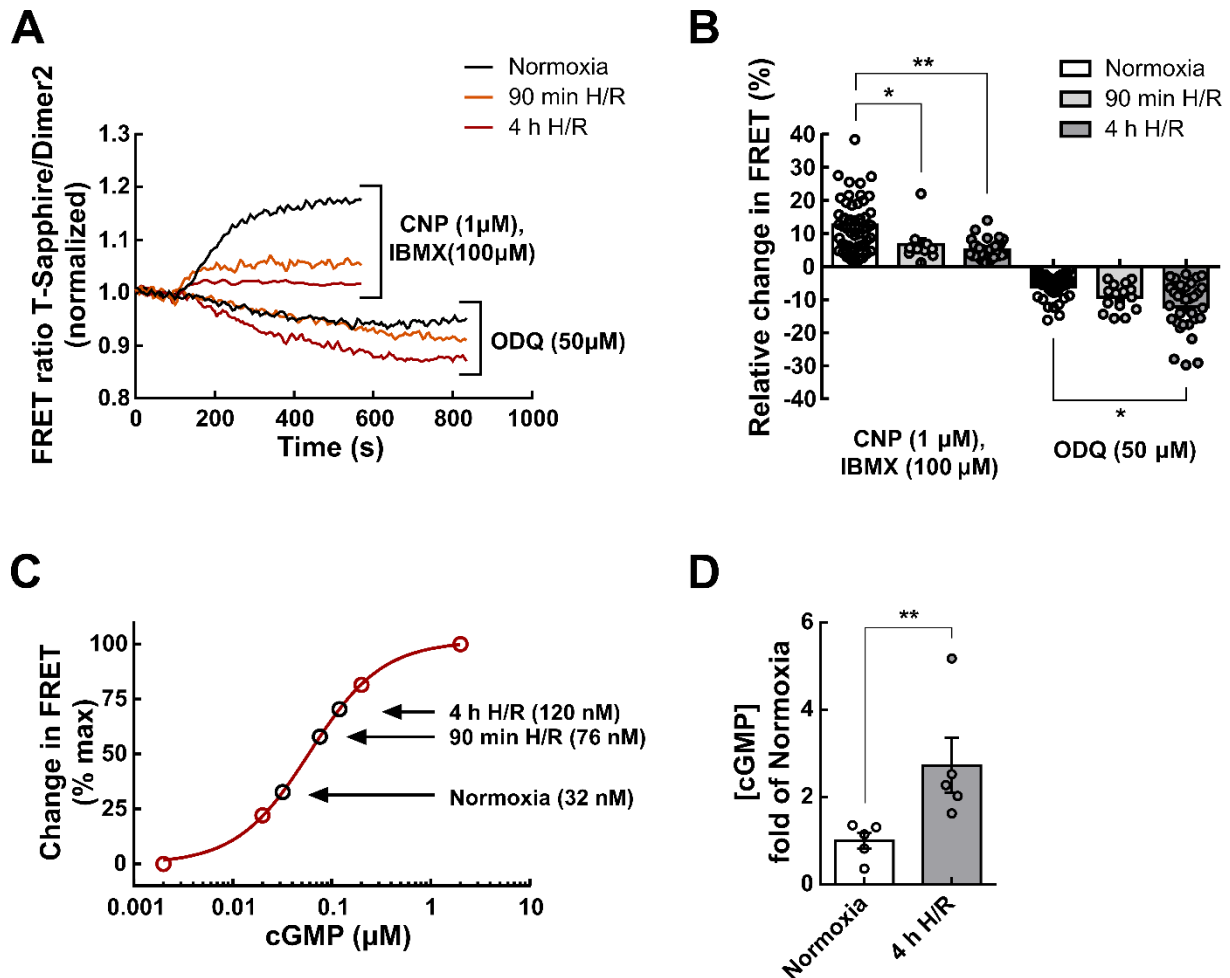
**Figure 3.1.3: Basal cGMP levels are increased in cardiomyocytes after hypoxia/reoxygenation.** **A**) Representative FRET traces from red-cGES-DE5 cardiomyocytes exposed to different durations of hypoxia, 90 min and 4 h, followed by 2 h of reoxygenation (90 min H/R, 4 h H/R) and normoxic controls (Normoxia). Maximal increase in cGMP levels was induced by stimulation of GC-B (CNP, 1 µM) with concurrent PDE inhibition (IBMX, 100 µM). Reduction in basal cGMP levels to minimum was reached by treating the cells with NO-GC inhibitor ODQ (50 µM). An increase in FRET ratio represents an increase in cytosolic cGMP, a decrease in FRET ratio represents a decrease in cytosolic cGMP. **B**) Quantification of the FRET experiments shown in A. **C**) Calculation of basal cGMP levels using dose-response titration *in vitro* and maximal FRET response [216, 250]. **D**) Determination of basal cGMP levels in cardiomyocytes exposed to Normoxia or 4 h H/R by cGMP immunoassay. cGMP immunoassay was done in cardiomyocytes from 5 different mice. Data are presented as mean ± SEM, significant differences at * $p < 0.05$, ** $p < 0.01$, *** $p < 0.001$.

In order to figure out, whether the increased basal cGMP levels after hypoxia/reoxygenation were produced during hypoxia or during reoxygenation period, additional FRET measurements were performed to calculate basal cGMP levels directly after 4 h of hypoxia without reoxygenation (4 h H w/o R) (Figure 3.1.4, A). Basal cGMP levels were clearly increased after 4 h H w/o R (78 nM) compared to Normoxia (32 nM). However, cGMP levels

increased even further during the two hours of reoxygenation (4 h H/R: 120 nM) (Figure 3.1.4, A and B).
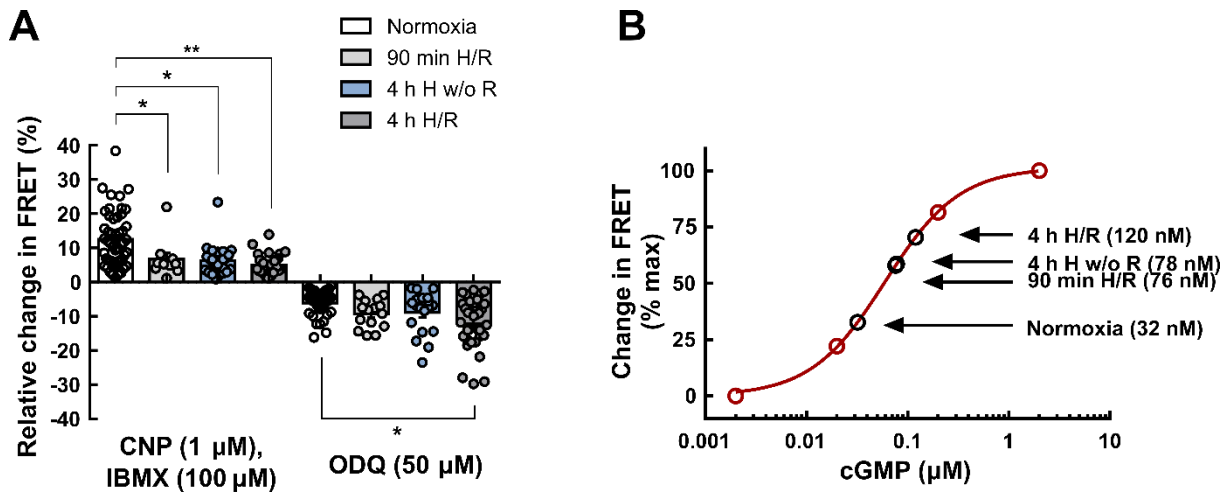


**Figure 3.1.4: Basal cGMP levels in cardiomyocytes increase during hypoxia and during reoxygenation.** Cardiomyocytes from transgenic red-cGES-DE5 mice were exposed to different durations of hypoxia, with and without reoxygenation: 90 min of hypoxia with 2 h of reoxygenation (90 min H/R), 4 h of hypoxia without reoxygenation (4 h H w/o R), and 4 h of hypoxia with 2 h of reoxygenation (4 h H/R). Controls were kept under normoxic conditions (Normoxia). In FRET measurements, maximal increase in cGMP levels was induced by stimulation of GC-B (CNP, 1 µM) with concurrent PDE inhibition (IBMX, 100 µM). Reduction in basal cGMP levels to minimum was reached by treating the cells with NO-GC inhibitor ODQ (50 µM). **A**) Quantification of FRET experiments. **B**) Calculation of basal cGMP levels using dose-response titration *in vitro* and maximal FRET response [216, 250]. Data are presented as mean ± SEM, significant differences at * $p < 0.05$, ** $p < 0.01$, *** $p < 0.001$.

### 3.1.4 cGMP degradation by PDE3A is impaired after hypoxia/reoxygenation

*3.1.4.1 Protein levels and mRNA expression of cGMP degrading phosphodiesterases in cardiomyocytes after hypoxia/reoxygenation*

As shown above (section 3.1.3), basal cGMP levels were significantly increased in adult mouse ventricular cardiomyocytes after hypoxia/reoxygenation. In order to figure out the mechanism that led to this raise in cGMP levels, the effect of hypoxia/reoxygenation on cGMP degradation by PDEs was investigated. PDEs involved in cGMP degradation in mouse cardiomyocytes are PDE1, PDE2, and PDE3 [136].

Protein levels of PDE1C, PDE2A, and PDE3A in mouse ventricular cardiomyocytes exposed to 4 h H/R or Normoxia were investigated with immunoblot analysis. PDE1C and PDE2A protein level remained unchanged after 4 h H/R compared to Normoxia. Interestingly, protein

levels of PDE3A were significantly reduced after 4 h H/R compared to Normoxia (Figure 3.1.5, A, B).

In order to figure out whether the downregulation of PDE3A protein after 4 h H/R was due to altered gene expression, mRNA was analysed. Gene expression analysis of *Pde1a*, *Pde1c*, *Pde2a*, and *Pde3a* showed a significant downregulation of *Pde2a* mRNA in 4 h H/R compared to Normoxia. However, *Pde3a* gene expression was not significantly changed after 4 h H/R (Figure 3.1.5, C).
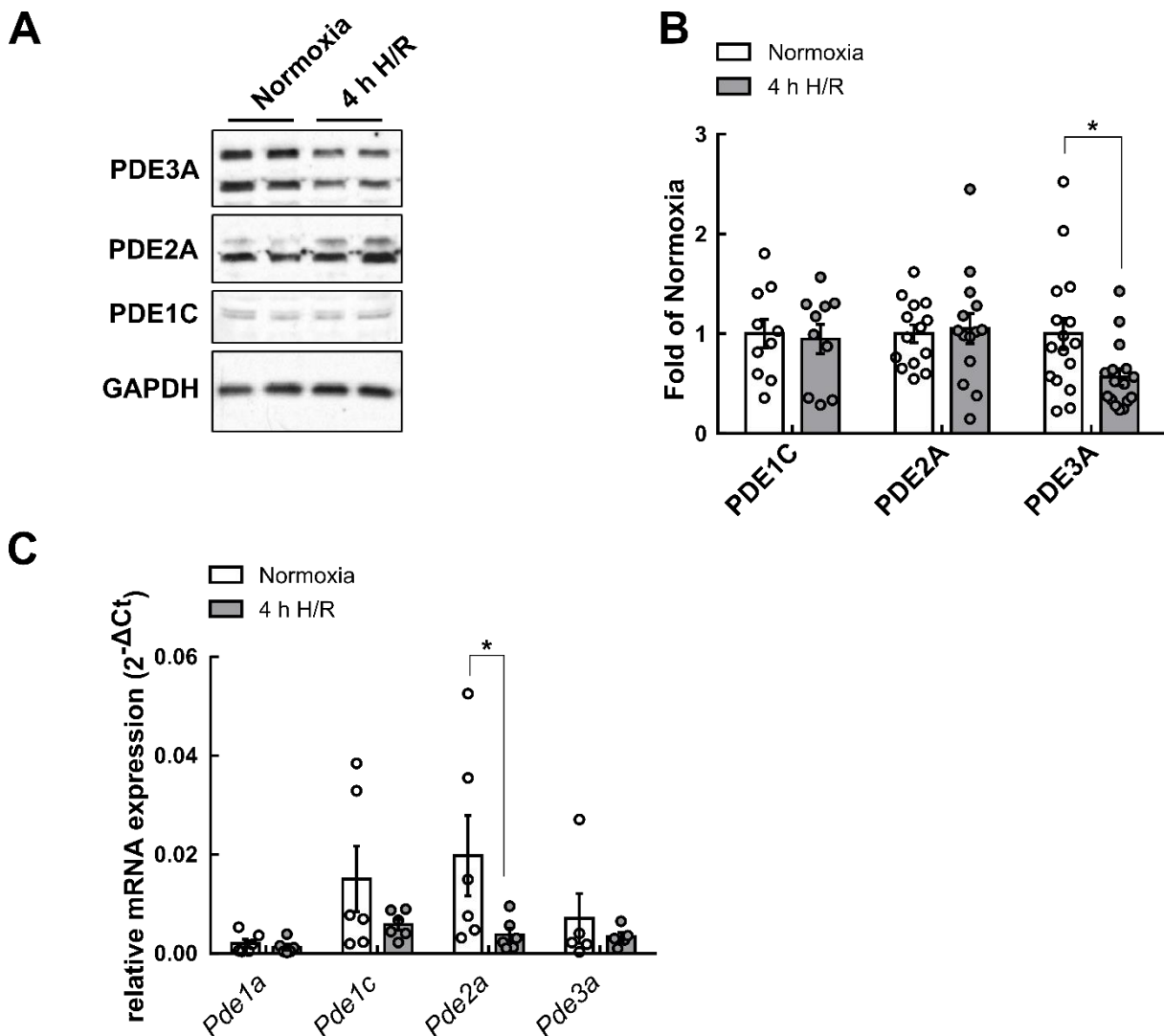


**Figure 3.1.5:    Protein levels and mRNA expression of cGMP degrading phosphodiesterases in cardiomyocytes after hypoxia/reoxygenation.  A**) Representative immunoblots of PDE1C, PDE2A and PDE3A protein in cardiomyocytes treated with 4 h of hypoxia followed by 2 h of reoxygenation (4 h H/R) compared to normoxic controls (Normoxia). GAPDH was used as a loading control. **B**) Quantification of the immunoblot experiments shown in A. **C**) Gene expression analysis of *Pde1a*, *Pde1c*, *Pde2a*, and *Pde3a* genes in cardiomyocytes treated with 4 h H/R or Normoxia. *Gapdh* was used as a housekeeping gene. Data are presented as mean ± SEM, significant differences at * $p < 0.05$, ** $p < 0.01$, *** $p < 0.001$.

*3.1.4.2 Analysis of PDE3A protein stability in cardiomyocytes exposed to hypoxia/reoxygenation by cycloheximide chase assay*

As shown above, reduced PDE3A protein level in 4 h H/R treated cardiomyocytes compared to Normoxia were not due to a reduction in gene expression of *Pde3a* (section 3.1.4.1). Thus, PDE3A protein stability in cardiomyocytes exposed to hypoxia/reoxygenation was analysed by cycloheximide (CHX) chase assay. Cardiomyocytes were treated with CHX (50 µM) directly before 4 h H/R or Normoxia treatment. Afterwards, PDE3A protein was analysed by immunoblot analysis. Whereas PDE3A protein level remained unchanged in Normoxia in CHX treated cardiomyocytes compared to untreated cardiomyocytes (Fold of untreated controls: Normoxia – CHX: 1.00 ± 0.14; Normoxia + CHX: 0.98 ± 0.06) (Figure 3.1.6, A and B), PDE3A protein expression was significantly reduced in CHX treated cardiomyocytes exposed to 4 h H/R compared to 4 h H/R cardiomyocytes which had not been treated with CHX (Fold of untreated controls: 4 h H/R - CHX: 1.00 ± 0.05; 4 h H/R + CHX: 0.72 ± 0.03) (Figure 3.1.6, A and C), indicating that PDE3A protein was unstable under hypoxic conditions.
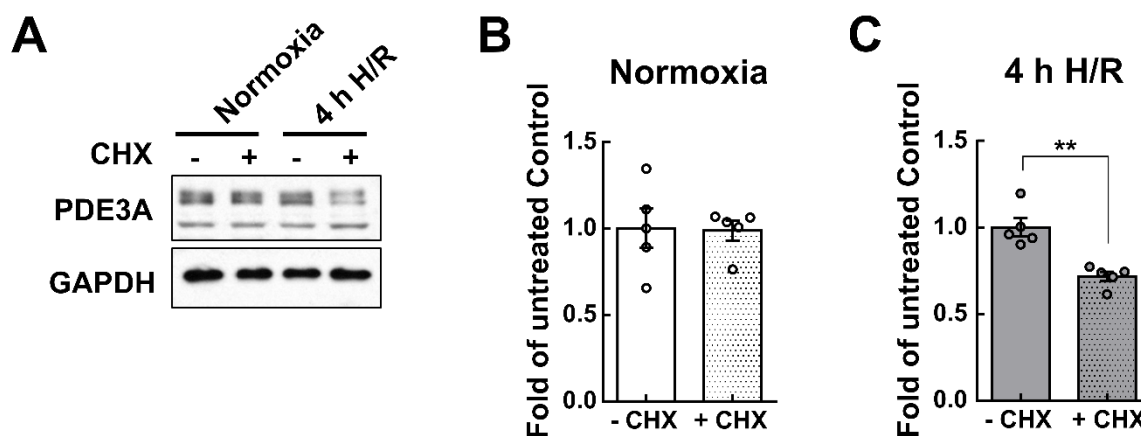


**Figure 3.1.6: Analysis of PDE3A protein stability in cardiomyocytes exposed to hypoxia/reoxygenation by cycloheximide chase assay.** Isolated cardiomyocytes were treated with the protein synthesis inhibitor cycloheximide (CHX, 50 µM) before exposure to 4 h hypoxia followed by 2 h of reoxygenation (4 h H/R) or normoxic conditions (Normoxia). As a control, CHX untreated cardiomyocytes were used. **A**) Representative immunoblot of PDE3A protein. GAPDH was used as loading control. **B**) Quantification of immunoblot experiments of Normoxia treated cardiomyocytes as fold of untreated controls. **C**) Quantification of immunoblot experiments of 4 h H/R treated cardiomyocytes as fold of untreated controls. Data are presented as mean ± SEM, significant differences at * p < 0.05, ** p< 0.01, *** p < 0.001.

*3.1.4.3 Phosphodiesterase inhibitor effects on basal cGMP degradation*

Immunoblot analysis could show a significant downregulation in PDE3A protein levels in cardiomyocytes after 4 h H/R compared to Normoxia (section 3.1.4.1) due to protein instability (section 3.1.4.2). In addition, the effects of PDE inhibition by selective PDE inhibitors in cardiomyocytes exposed to hypoxia/reoxygenation were investigated by FRET. Isolated cardiomyocytes from red-cGES-DE5 transgenic mice exposed to 4 h H/R or Normoxia were used for FRET analysis. Bay 60-7550 (Bay, 100 nM) was used as a selective inhibitor for PDE2, Cilostamide (Cilo, 10 µM) was used as a selective PDE3 inhibitor (Figure 3.1.7).
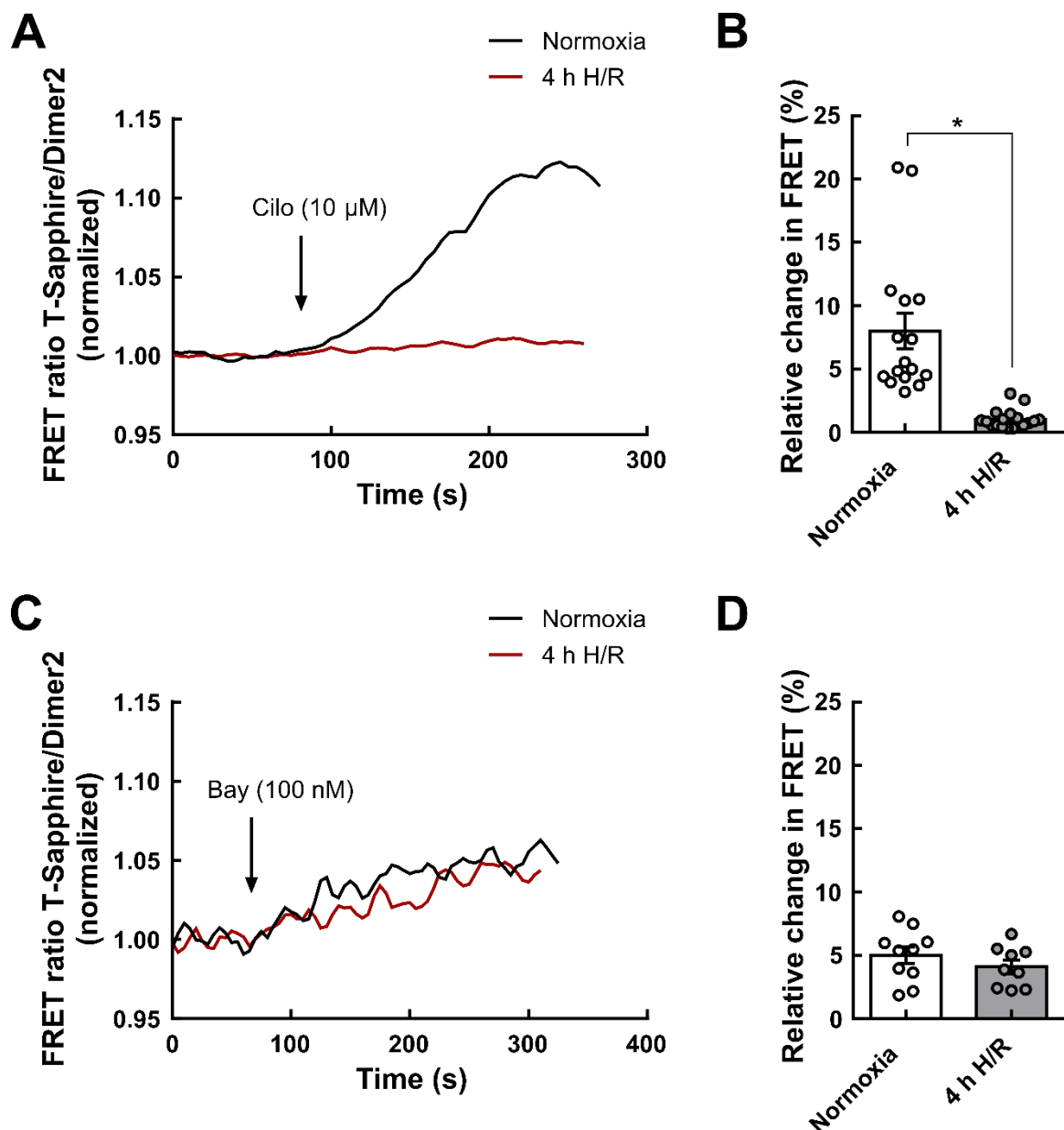


**Figure 3.1.7: FRET analysis of phosphodiesterase inhibitor effects in cardiomyocytes after hypoxia/reoxygenation.** Isolated cardiomyocytes from red-cGES-DE5 mice exposed to 4 h of hypoxia followed by 2 h of reoxygenation (4 h H/R) or normoxic control conditions (Normoxia) were used for FRET analysis with selective PDE inhibitors. **A**) Representative FRET traces from

cardiomyocytes exposed to PDE3 inhibitor Cilostamide (Cilo, 10 µM). **B**) Quantification of the FRET experiments shown in A. **C**) Representative FRET traces from cardiomyocytes exposed to PDE2 inhibitor Bay 60-7550 (Bay, 100 nM). **D**) Quantification of the FRET experiments shown in C. Data are presented as mean ± SEM, significant differences at * p < 0.05, ** p< 0.01, *** p < 0.001.

Interestingly, inhibition of PDE3 could raise cGMP levels in cardiomyocytes exposed to Normoxia (8.0 ± 1.4%) but not in cardiomyocytes exposed to 4 h H/R (1.0 ± 0.2%) (Figure 3.1.7, A and B), whereas PDE2 inhibition raised cGMP levels in both, Normoxia (5.0 ± 0.7%) and 4 h H/R (4.1 ± 0.5%) treated cells (Figure 3.1.7, C and D). In Normoxia cardiomyocytes, Bay increased cGMP levels to a much smaller extent than Cilo. This was due to the fact that PDE2 only plays a minor role in cGMP breakdown of mouse ventricular cardiomyocytes.

### 3.1.5 cGMP/cAMP crosstalk *via* PDE3 after natriuretic peptide stimulation is attenuated in cardiomyocytes exposed to hypoxia/reoxygenation

As the hydrolysis rate of PDE3 for cAMP ($V_{max}$ = 3.0 µmol/min/mg) is nearly 10-fold higher than the hydrolysis rate for cGMP ($V_{max}$ = 0.34 µmol/min/mg), PDE3 is known as the "cGMP-inhibited PDE". Therefore, cGMP can act as an inhibitor for cAMP hydrolysis [120]. Several years ago, it was shown by our group that PDE3 is involved in the cGMP/cAMP crosstalk after natriuretic peptide stimulation [136].

Since the effect of PDE3 inhibition by Cilostamide (Cilo, 10 µM) was significantly reduced in cardiomyocytes after hypoxia/reoxygenation as shown above in FRET-based cGMP measurements (section 3.1.4.3), the question was whether hypoxia/reoxygenation also affects the cGMP/cAMP crosstalk after natriuretic peptide stimulation *via* PDE3A. Cardiomyocytes from transgenic mice with expression of the cAMP-specific FRET biosensor Epac1-camps [236] were isolated and exposed to 4 h H/R or Normoxia. Afterwards single cell FRET measurements were done in order to measure cytosolic cAMP. β-AR stimulation with isoprenaline (ISO, 100 nM) increased cAMP. In cells exposed to Normoxia, further stimulation with CNP (100 nM) to stimulate cGMP generation by GC-B, significantly increased cAMP levels (Normoxia: 8.1 ± 0.7%). This effect was blocked by preincubation with the PDE3 inhibitor Cilostamide (Cilo, 10 µM), as expected (Normoxia + Cilo: 2.3 ± 0.6%) (Figure 3.1.8, A, B, and E). However, in cardiomyocytes exposed to 4 h H/R, cAMP increase after CNP stimulation was clearly reduced (4 h H/R: 2.6 ± 0.5%), demonstrating that the functional impairment of PDE3 caused by hypoxia/reoxygenation also affected cGMP/cAMP crosstalk after natriuretic peptide stimulation (Figure 3.1.8, C, D, and E).
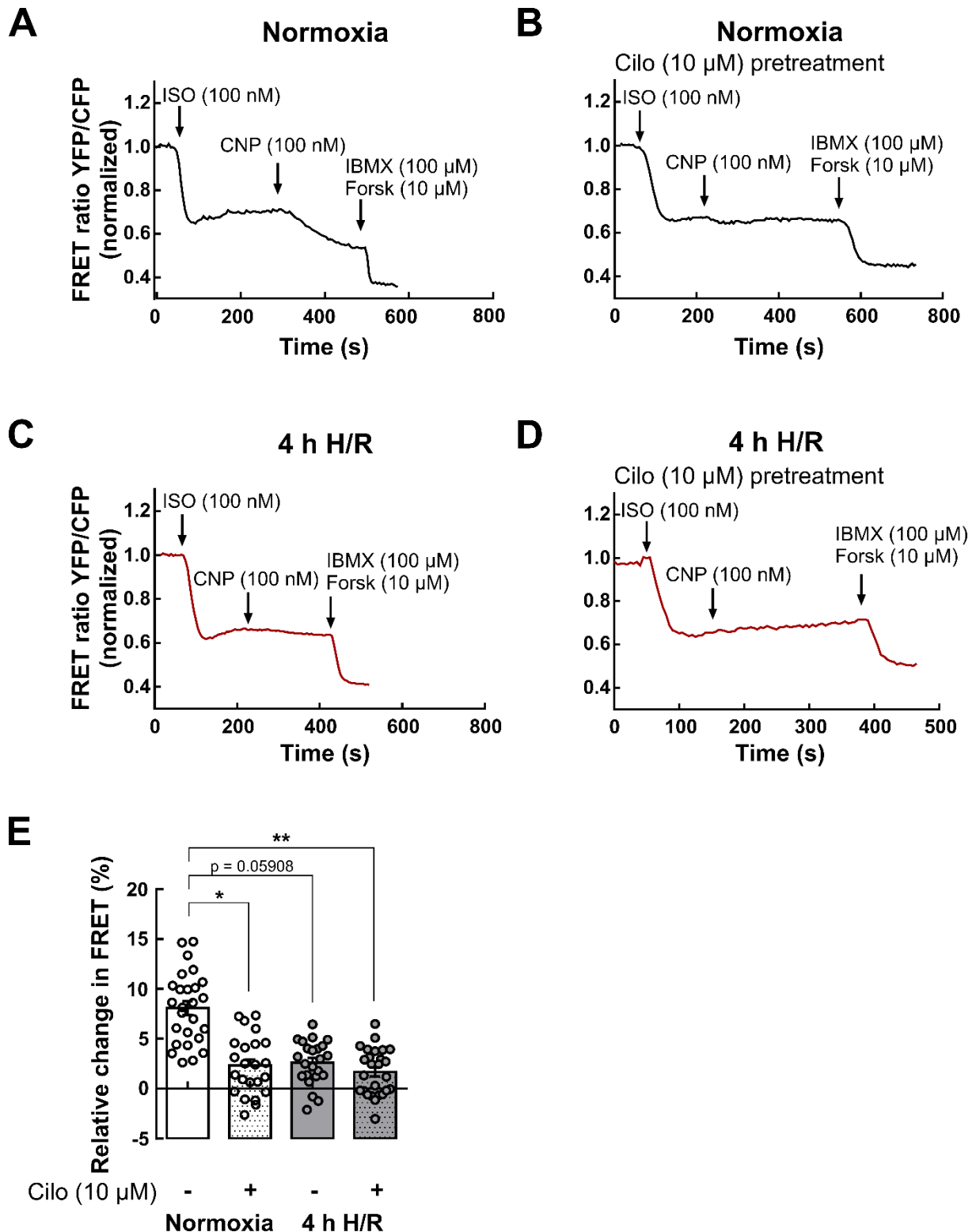
**Figure 3.1.8:** **cGMP/cAMP crosstalk** *via* **PDE3 after natriuretic peptide stimulation is attenuated in cardiomyocytes exposed to hypoxia/reoxygenation.** **A-D**) Representative FRET traces of cAMP measurements in cardiomyocytes from transgenic Epac1-camps mice [236]. β-adrenergic receptors (βARs) were stimulated with the agonist isoprenaline (ISO, 100 nM), followed by stimulation of GC-B with CNP (100 nM). Maximal FRET response was induced by stimulation of adenylyl cyclase (AC) by forskolin (Forsk, 10 µM) in combination with the unselective PDE inhibitor IBMX (100 µM). A decrease in FRET ratio represents an increase in cytosolic cAMP. Cardiomyocytes

were kept under normoxic control conditions (Normoxia) (A, B) or were exposed to 4 h of hypoxia followed by 2 h of reoxygenation (4 h H/R) (C, D) before FRET measurements. Pre-treatment of the cells with PDE3 inhibitor Cilostamide (Cilo, 10 µM) (B, D), attenuated CNP effects. **E**) Quantification of FRET response induced by CNP (100 nM) treatment after ISO (100 nM) stimulation shown in A-D. Data are presented as mean ± SEM, significant differences at * $p < 0.05$, ** $p < 0.01$, *** $p < 0.001$.

### 3.1.6 cGMP generating NO-GC is oxidized during hypoxia/reoxygenation

*3.1.6.1 Protein levels and mRNA expression of guanylyl cyclases in cardiomyocytes after hypoxia/reoxygenation*

After investigating the effects of hypoxia/reoxygenation on cGMP degrading PDEs, its effect on cGMP generating guanylyl cyclases (GCs) was analysed. Therefore, protein levels and mRNA expression of NO-GCs and NP-GCs in cardiomyocytes exposed to 4 h H/R or Normoxia were studied (Figure 3.1.9).
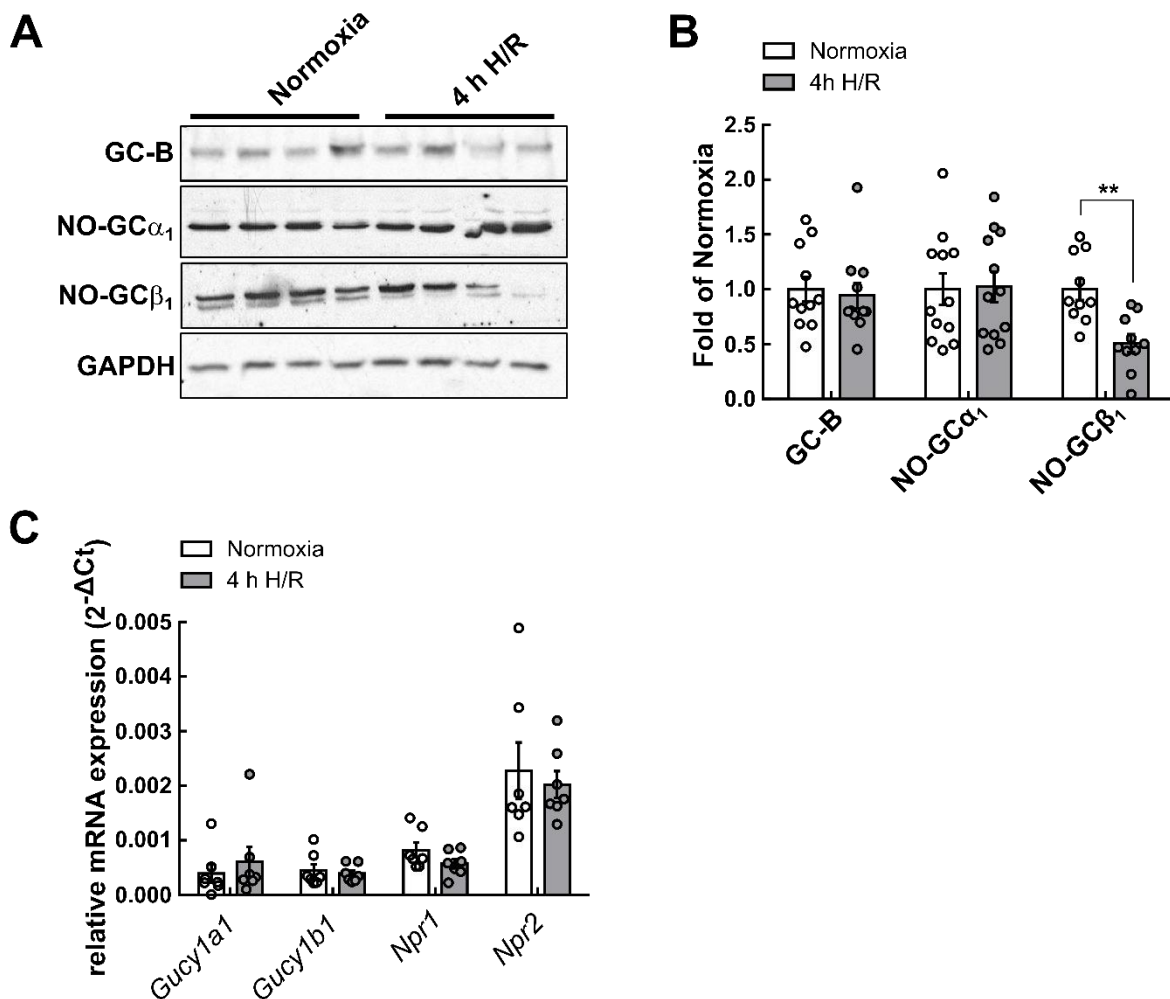


**Figure 3.1.9:    Protein levels and mRNA expression of cGMP generating guanylyl cyclases in cardiomyocytes after hypoxia/reoxygenation.  A**) Representative immunoblots of GC-B, NO-GC$\alpha_1$

and NO-GC$\beta_1$ protein in cardiomyocytes exposed to 4 h of hypoxia followed by 2 h of reoxygenation (4 h H/R) or normoxic control conditions (Normoxia). GAPDH was used as a loading control. **B**) Quantification of the immunoblot experiments shown in A. **C**) Analysis of *Gucy1a1*, *Gucy1b1*, *Npr1*, and *Npr2* gene expression in cardiomyocytes exposed to 4 h H/R or Normoxia. *Gapdh* was used as housekeeping gene. Data are presented as mean ± SEM, significant differences at * $p < 0.05$, ** $p < 0.01$, *** $p < 0.001$.

Protein levels of GC-B and NO-GC$\alpha_1$ remained unchanged after 4 h H/R compared to Normoxia. However, NO-GC$\beta_1$ was significantly reduced after 4 h H/R compared to Normoxia (Figure 3.1.9, A and B). RNA expression analysis revealed no significant alterations in gene expression of *Gucy1a1*, *Gucy1b1*, *Npr1*, and *Npr2* between Normoxia and 4 h H/R (Figure 3.1.9, C).

*3.1.6.2 Oxidation status of NO-GC in cardiomyocytes after hypoxia/reoxygenation*

Next, the oxidation status of NO-GC was investigated in cardiomyocytes exposed to 4 h H/R. Therefore, FRET response to NO-GC stimulator Bay 41-2272 (1 µM), which stimulates only the reduced form of NO-GC [252], and NO-GC activator Bay 60-2770 (1 µM), which stimulates both, the reduced and the oxidized form of NO-GC [252], in cardiomyocytes from red-cGES-DE5 transgenic mice was analysed. Unfortunately, both, NO-GC stimulator Bay 41-2272 (1 µM) and NO-GC activator Bay 60-2770 (1 µM) failed to evoke FRET signals in red-cGES-DE5 mouse ventricular cardiomyocytes (Figure 3.1.10). This had already been observed in previous measurements of our [136] and other groups [174].
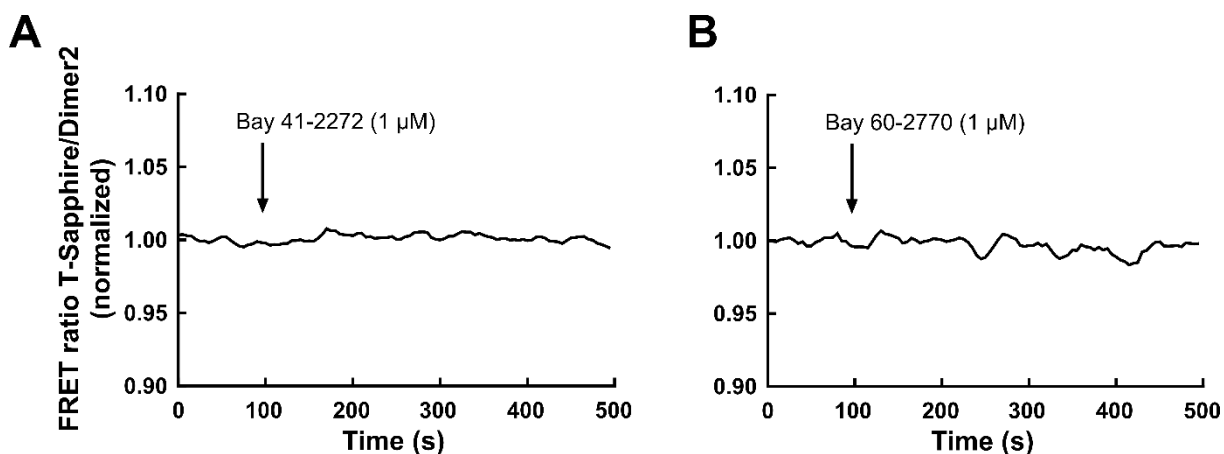


**Figure 3.1.10: NO-GC cannot be stimulated in mouse ventricular cardiomyocytes by NO-GC stimulators or activators.** Mouse ventricular cardiomyocytes from red-cGES-DE5 transgenic mice were used for FRET analysis with NO-GC stimulator Bay 41-2272 (1 µM) or NO-GC activator Bay 60-2770 (1 µM). In total, 6 cardiomyocytes per condition were measured. **A**) Representative FRET traces from mouse ventricular cardiomyocytes exposed to NO-GC stimulator Bay 41 2272 (1 µM) or **B**) NO-GC activator Bay 60-2770 (1 µM).

However, the establishment of FRET-based cGMP measurements in human ventricular cardiomyocytes, revealed that stimulation of human ventricular cardiomyocytes with the NO-donor SNAP could provoke an increase in cGMP levels (Supplemental Figure 5.2.1), which was not possible in mouse ventricular cardiomyocytes [136].

Therefore, in order to examine the oxidation status of NO-GC after hypoxia/reoxygenation, human ventricular cardiomyocytes were used. Human ventricular cardiomyocytes were isolated from left ventricular tissue samples and red-cGES-DE5 FRET sensor was expressed in those cells by adenovirus-mediated gene transfer. 48 h after transduction, the cGMP biosensor red-cGES-DE5 was uniformly expressed in human ventricular cardiomyocytes (Figure 3.1.11).
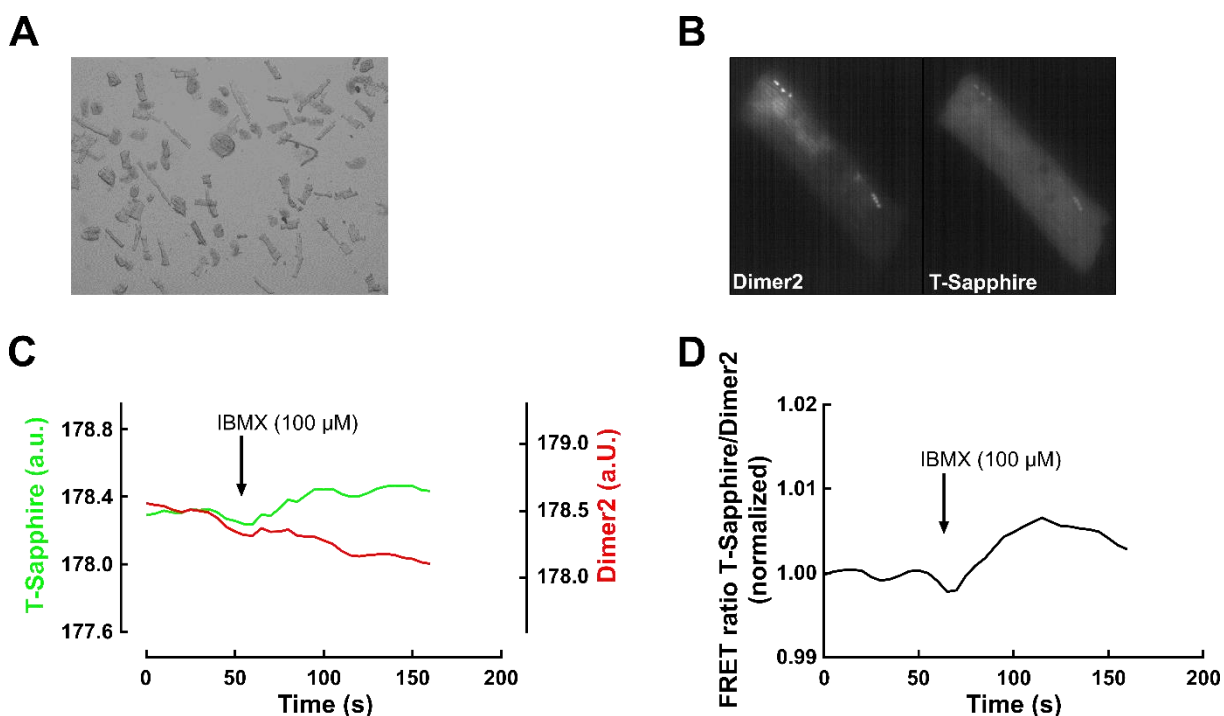


**Figure 3.1.11: Isolated human ventricular cardiomyocytes for FRET-based cGMP measurements.** Human ventricular cardiomyocytes **A**) directly after isolation, magnification 10 x, and **B**) 48 h after adenovirus-mediated gene transfer of the FRET-based cGMP sensor red-cGES-DE5. cGMP biosensor fluorescence in T-Sapphire and Dimer2 channels during single cell FRET measurements, magnification 63 x. **C**) Exemplary FRET trace, showing the change in fluorescence of the two fluorophores T-Sapphire and Dimer2 upon stimulation with the non-selective PDE inhibitor IBMX (100 µM). **D**) Normalized FRET ratio of the measurement shown in C). An increase in FRET ratio represents an increase in cGMP.

Clinical characteristics of patients whose left ventricular tissue samples were used for cardiomyocyte isolation and FRET-based cGMP measurements in this project are shown in Table 3.1. In total, left ventricular tissue samples of 12 different patients, aged 50 ± 5 years at the time of surgery were used. Coronary artery disease, valvular heart disease, or

transplantation were indications for surgery in these patients. A total of 96 human ventricular cardiomyocytes were used for FRET-based cGMP measurements in this project.

**Table 3.1:** **Clinical characteristics of patients whose left ventricular tissue samples were used for cardiomyocyte isolation and FRET-based cGMP measurements.** Data are presented as mean ± SEM. ACE, Angiotensin converting enzyme; AT1, Angiotensin II type 1; LVEF, left ventricular ejection fraction.

| | LV |
|---|---|
| **Patients (n)** | 12 |
| Male | 7 (58.3%) |
| Female | 5 (41.7%) |
| **Age at surgery (years)** | 50 ± 5 |
| **Indications for surgery** | |
| Coronary artery disease (n) | 0 (0.0%) |
| Valvular heart disease (n) | 9 (75.0%) |
| Both (n) | 2 (16.7%) |
| Transplant (n) | 1 (8.3%) |
| **Cardiovascular comorbidity** | |
| Arterial hypertension (n) | 3 (25.0%) |
| Diabetes mellitus (n) | 1 (8.3%) |
| Hyperlipoproteinemia (n) | 0 (0.0%) |
| **Echocardiography data** | |
| LVEF (%) | 53.7 ± 4.9 |
| **Medication** | |
| ACE inhibitor (n) | 0 (0.05%) |
| AT1 receptor antagonist (n) | 1 (8.3%) |
| Beta blocker (n) | 3 (25.0%) |
| $Ca^{2+}$ channel blocker (n) | 0 (0.0%) |
| Diuretics (n) | 1 (8.3%) |
| Digitalis (n) | 0 (0.0%) |
| Nitrates (n) | 0 (0.0%) |

After exposure of human ventricular cardiomyocytes to 4 h H/R or Normoxia, FRET-based cGMP measurements were done using either NO-GC stimulator Bay 41-2272 (1 µM) or NO-GC activator Bay 60-2770 (1 µM). While the NO-GC stimulator Bay 41-2272 (1 µM) led to a small increase in FRET ratio in both, Normoxia (2.4 ± 0.3%) and 4 h H/R treated cells (2.8 ± 0.7%) (Figure 3.1.12, A and C), NO-GC activator Bay 60-2770 (1 µM) evoked a much stronger increase in FRET in 4 h H/R treated cells (3.5 ± 0.4%) compared to Normoxia (2.5 ± 0.3%) (Figure 3.1.12, B and C). This clearly showed that NO-GC is oxidized under hypoxic conditions in human cardiomyocytes.
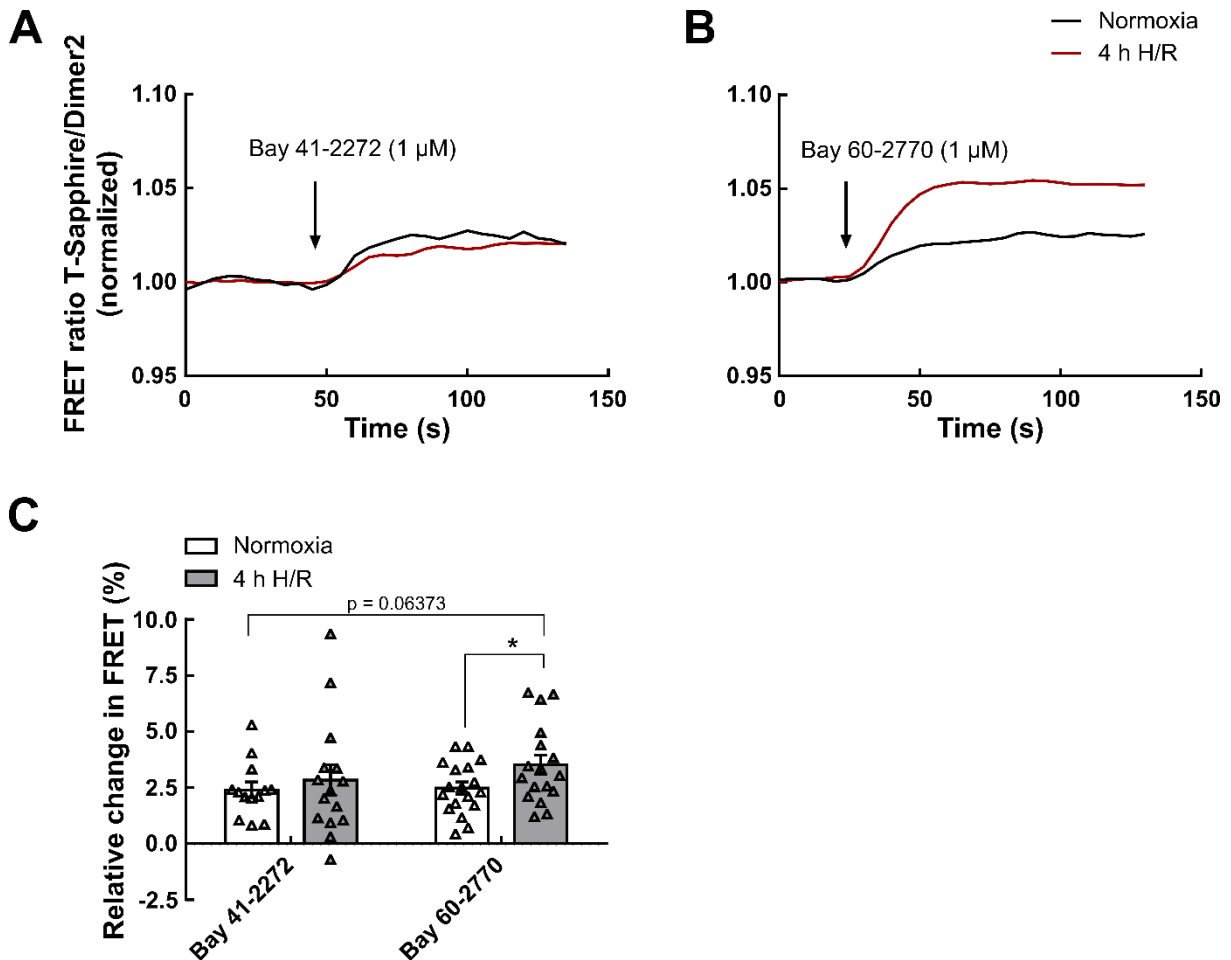


**Figure 3.1.12: cGMP generating NO-GC is oxidized in human ventricular cardiomyocytes exposed to hypoxia/reoxygenation.** Human ventricular cardiomyocytes expressing the FRET-based cGMP biosensor red-cGES-DE5 were exposed to 4 h of hypoxia followed by 2 h of reoxygenation (4 h H/R) or normoxic control conditions (Normoxia). Afterwards, they were used for FRET analysis with NO-GC stimulator Bay 41-2272 (1 µM) or NO-GC activator Bay 60-2770 (1 µM). **A**) Representative FRET traces from human ventricular cardiomyocytes exposed to NO-GC stimulator Bay 41 2272 (1 µM) or **B**) NO-GC activator Bay 60-2770 (1 µM). **C**) Quantification of the FRET experiments shown in A and B. Data are presented as mean ± SEM, significant differences at * p < 0.05, ** p< 0.01, *** p < 0.001.

**3.1.7 FRET response to PDE3 inhibitor Cilostamide is impaired in cardiomyocytes from cardiomyocyte-specific NO-GC knockout mice after hypoxia/reoxygenation**

*3.1.7.1 Cardiomyocyte-specific NO-GC knockout is functional*

It is known that NO-GC plays an essential role for basal cGMP generation in mouse [136], even if mouse ventricular cardiomyocytes cannot be stimulated with NO-GC stimulators and activators (Figure 3.1.10). In order to further investigate the role of NO-GC during hypoxia/reoxygenation, mice with cardiomyocyte-specific deletion of NO-GC [167] were crossed with red-cGES-DE5 transgenic mice to generate cardiomyocyte-specific NO-GC knockout mice with cardiomyocyte-specific expression of the FRET-based cGMP biosensor red-cGES-DE5. Immunoblot analysis of NO-GC$\beta_1$ protein in wildtype (WT) and NO-GC knockout (NO-GC KO) cardiomyocytes was done to confirm the NO-GC knockout. Although NO-GC$\beta_1$ protein was clearly reduced in NO-GC KO cardiomyocytes, a small residual amount of NO-GC$\beta_1$ protein was still detected (Figure 3.1.13, A). One possible explanation for this could be that the NO-GC KO was tamoxifen induced [167]. Tamoxifen-induced deletion of NO-GC leads to a gradual reduction of NO sensitivity, depending on the time of tamoxifen injection, and finally causes a complete loss of NO responsiveness [253]. For this project, mice were used fifty days after tamoxifen injection for subsequent experiments. This was maybe not enough for complete loss of NO-GC$\beta_1$ protein. Another and more reasonable explanation could be that the purity of the cardiomyocyte lysate used for immunoblot analysis was not high enough to completely avoid presence of other cell types with high NO-GC expression e.g. fibroblasts [174]. Since the NO-GC KO in this model was cardiomyocyte-specific, contamination of the cardiomyocyte cell lysate with fibroblasts could explain the small residual amount of NO-GC$\beta_1$ protein which was still detected in the NO-GC KO lysate.

FRET-based cGMP measurements in red-cGES-DE5 WT and NO-GC KO cardiomyocytes with the NO-GC specific inhibitor ODQ (50 µM), clearly showed that the knockout was functional. The FRET response to ODQ in NO-GC KO cardiomyocytes was completely diminished (WT: - 6.1 ± 0.6%; NO-GC KO: - 0.9 ± 0.1%) (Figure 3.1.13, B and C).
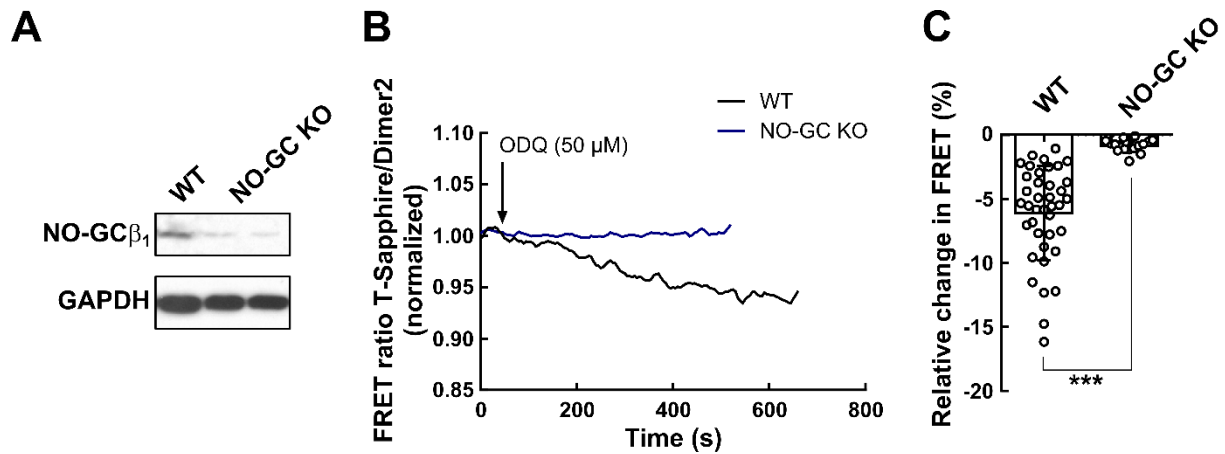
**Figure 3.1.13: Cardiomyocyte-specific NO-GC knockout is functional. A**) Immunoblot analysis of NO-GC$\beta_1$ protein in wildtype (WT) and NO-GC knockout (NO-GC KO) cardiomyocytes. GAPDH was used as a loading control. **B**) Representative FRET traces from WT and NO-GC KO red-cGES-DE5 cardiomyocytes exposed to the NO-GC inhibitor ODQ (50 µM). **C**) Quantification of FRET experiments shown in B). Data are presented as mean ± SEM, significant differences at * $p < 0.05$, ** $p < 0.01$, *** p 0.001.

*3.1.7.2 FRET response to PDE3 inhibitor Cilostamide is impaired in NO-GC knockout cardiomyocytes after hypoxia/reoxygenation*

In order to investigate the role of cGMP degrading PDE3 in NO-GC knockout cardiomyocytes exposed to hypoxia/reoxygenation, FRET-based cGMP measurements were done using the PDE3 specific inhibitor Cilostamide (Cilo, 10 µM). Cardiomyocytes from red-cGES-DE5 transgenic NO-GC knockout mice were exposed to 4 h H/R or Normoxia before FRET analysis. Inhibition of PDE3 could raise cGMP levels in Normoxia treated cardiomyocytes (8.5 ± 0.8%) but not in 4 h H/R treated cells (2.0 ± 0.3%) (Figure 3.1.14, A and B). This was in line with the results of the FRET measurements in wildtype mice, were the FRET response to PDE3 inhibitor Cilostamide was also significantly reduced in cardiomyocytes exposed to 4 h H/R compared to Normoxia treated cells (section 3.1.4.3).
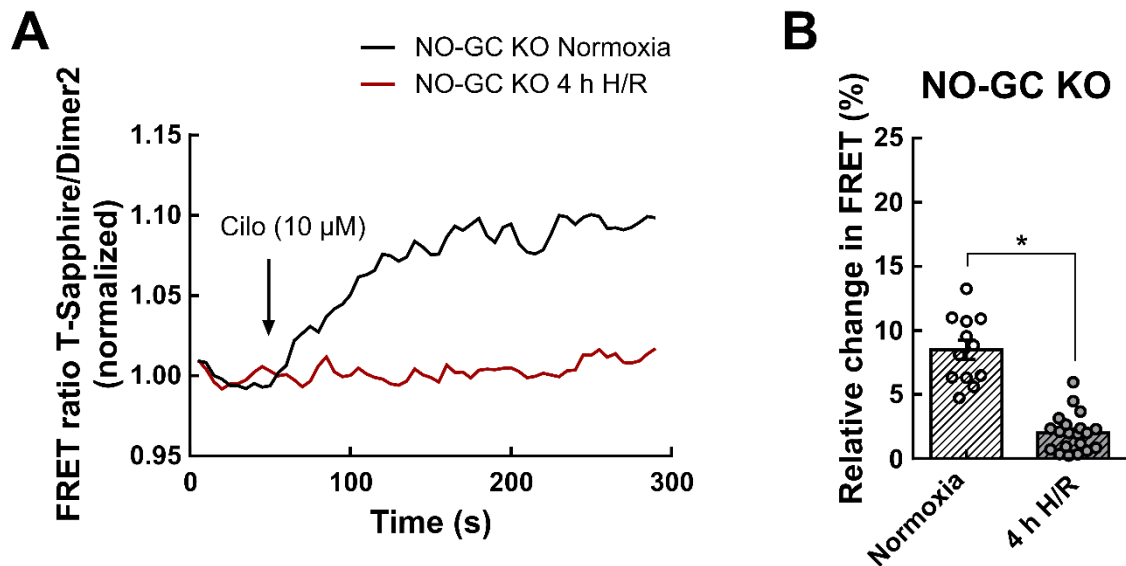
**Figure 3.1.14: FRET response to PDE3 inhibitor Cilostamide is reduced in NO-GC knockout cardiomyocytes after hypoxia/reoxygenation.** NO-GC knockout (NO-GC KO) cardiomyocytes from red-cGES-DE5 transgenic mice exposed to 4 h hypoxia followed by 2 h of reoxygenation (4 h H/R) or normoxic control conditions (Normoxia) were used for FRET analysis with the selective PDE3 inhibitor Cilostamide (Cilo, 10 µM). **A**) Representative FRET traces from NO-GC KO cardiomyocytes exposed to PDE3 inhibitor Cilostamide (Cilo, 10 µM). **B**) Quantification of the FRET experiments shown in A). Data are presented as mean ± SEM, significant differences at * $p < 0.05$, ** $p < 0.01$, *** $p < 0.001$.

In order to figure out, whether basal cGMP levels were also increased in cardiomyocytes of cardiomyocyte-specific NO-GC knockout mice after hypoxia/reoxygenation, basal cGMP levels were calculated *via* FRET as described previously [254]. FRET measurements to determine basal cGMP levels are shown in the supplemental information (Supplemental Figure 5.2.2).

Basal cGMP in Normoxia treated cardiomyocytes of NO-GC knockout mice were calculated 4 nM. 4 h H/R treatment could raise basal cGMP levels up to 12 nM. Furthermore, it was tried to measure basal cGMP levels with cGMP immunoassay. However, cGMP levels in NO-GC knockout cardiomyocytes were too low and outside the detection range of the assay.

### 3.1.8 cGMP stimulation can prevent from cardiomyocyte cell death during hypoxia/reoxygenation

PDE3 is known to be involved in the regulation of apoptosis and it was shown by several studies that a downregulation of PDE3A caused an increase in cardiomyocyte apoptosis [255, 256, 257]. In order to figure out whether increased cGMP levels before hypoxia/reoxygenation could prevent from cardiomyocyte cell death, mouse ventricular cardiomyocytes were treated with the GC-B stimulator CNP (100 nM) before induction of

hypoxia/reoxygenation. Quantification of cell death by counting the amount of living and dead cells before induction of hypoxia (t = 0 h), 4 h after hypoxia (t = 4 h), and 2 h after reoxygenation (t = 6 h), in Normoxia and 4 h H/R treated cardiomyocytes with and without CNP treatment, could show that upon CNP treatment, cell death was attenuated during hypoxia/reoxygenation (living cells in % in Normoxia + CNP: t = 0 h: 57.3 ± 5.5; t = 4 h: 69.9 ± 4.0; t = 6 h: 61.5 ± 5.2; living cells in % in 4 h H/R + CNP: t = 0 h: 66.3 ± 4.5; t = 4 h: 58.3 ± 4.9; t = 6 h: 56.8 ± 7.6) compared to cells which had not been treated with CNP before hypoxia/reoxygenation treatment (living cells in % in Normoxia: t = 0 h: 55.3 ± 3.5; t = 4 h: 67.5 ± 3.0; t = 6 h: 61.4 ± 5.4; living cells in % in 4 h H/R: t = 0 h: 63.5 ± 4.2; t = 4 h: 41.1 ± 4.0; t = 6 h: 28.1 ± 3.6) (Figure 3.1.15).
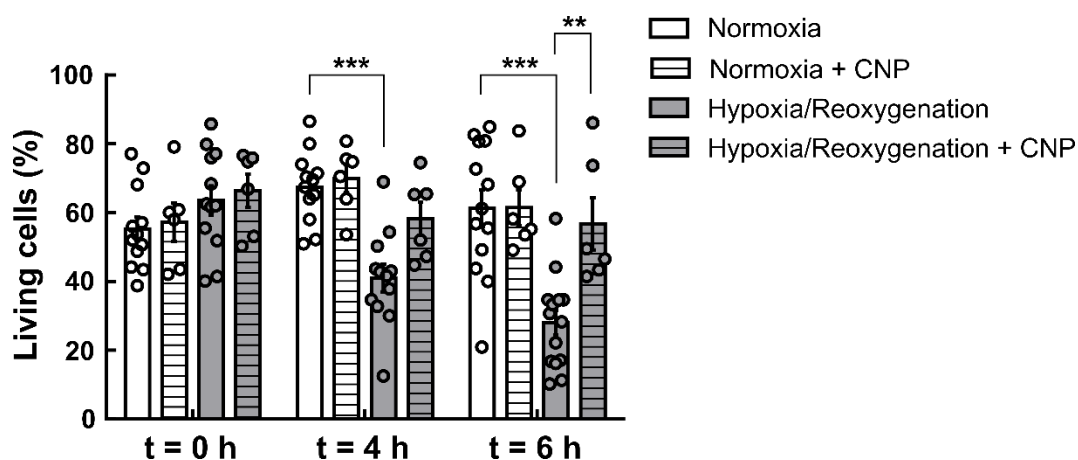


**Figure 3.1.15: Stimulation of cGMP synthesis before hypoxia/reoxygenation can prevent from cardiomyocyte cell death.** Isolated cardiomyocytes were treated with CNP (100 nM) before induction of 4 h of hypoxia followed by 2 h of reoxygenation (4 h H/R). As a control, CNP-untreated cells were used. Cell images were taken before induction of hypoxia (t = 0 h), directly after hypoxia treatment for 4 h (t = 4 h) and after 2 h of reoxygenation (t = 6 h). Controls were kept under normoxic conditions (Normoxia) with or without CNP treatment. For untreated cells, 4/5 pictures per mouse were analysed from 3 different mice, for CNP (100 nM) treated cells, 2 pictures per mouse were analysed from 3 different mice. Data are presented as mean ± SEM, significant differences at $^*$ p < 0.05, $^{**}$ p < 0.01, $^{***}$ p < 0.001.

### 3.1.9 Basal cGMP levels are increased during anoxic injury in an *ex vivo* whole heart Langendorff model

All results which have been shown so far were done in an *in vitro* model of hypoxia/reoxygenation. In order to figure out whether these findings could be reproduced in a more physiological context, an *ex vivo* whole heart Langendorff model of hypoxic injury was used. A self-built FRET imaging system enabled the direct monitoring of cGMP dynamics during hypoxic injury in red-cGES-DE5 transgenic mouse hearts. It needs to be mentioned

here that in the red-cGES-DE5 transgenic mice used for this work, the cGMP biosensor expression was under the $\alpha$MHC promoter and therefore cardiomyocyte-specific. Other cell types of the heart e.g. fibroblasts did not express the biosensor. Therefore, FRET recordings in the Langendorff setup monitored cardiomyocyte-specific changes in cGMP dynamics.

Most fluorescent proteins e.g. YFP are known to lose their fluorescence under acidic pH conditions [258, 259]. In order to rule out that changes in pH during anoxia would affect FRET measurements in red-cGES-DE5 transgenic hearts exposed to anoxia, biosensor fluorescence in T-Sapphire and Dimer2 channels were checked during FRET recordings. As the intensities of the two fluorophores T-Sapphire and Dimer2 still changed in opposite directions during anoxia treatment, it was assumed that the red-cGES-DE5 biosensor was not affected by changes in pH during Langendorff FRET recordings (Figure 3.1.16, B). As a comparison Langendorff anoxia experiments with hearts from transgenic Epac1-camps mice were done, since this FRET-based cAMP sensor is known to be pH sensitive. FRET recordings of hearts from transgenic Epac1-camps mice exposed to anoxia/reoxygenation clearly showed the impairment of this sensor by changes in pH (Supplemental Figure 5.2.3).

While normoxic red-cGES-DE5 control hearts showed no change in FRET ratio during the whole recording period (Figure 3.1.16, C), induction of anoxia caused an increase in cGMP levels (Figure 3.1.16, D). These results were in accordance with the results from the *in vitro* single cell measurements where basal cGMP levels were significantly increased after hypoxia/reoxygenation (section 3.1.3). Hearts of red-cGES-DE5 expressing NO-GC knockout mice were also used for anoxia treatment. Even in NO-GC knockout hearts, cGMP levels were increasing during anoxia (Figure 3.1.16, E), probably due to the reduction in the effect of PDE3A as shown before in FRET-based cGMP measurements with the PDE3-specific inhibitor Cilostamide (section 3.1.7.2).
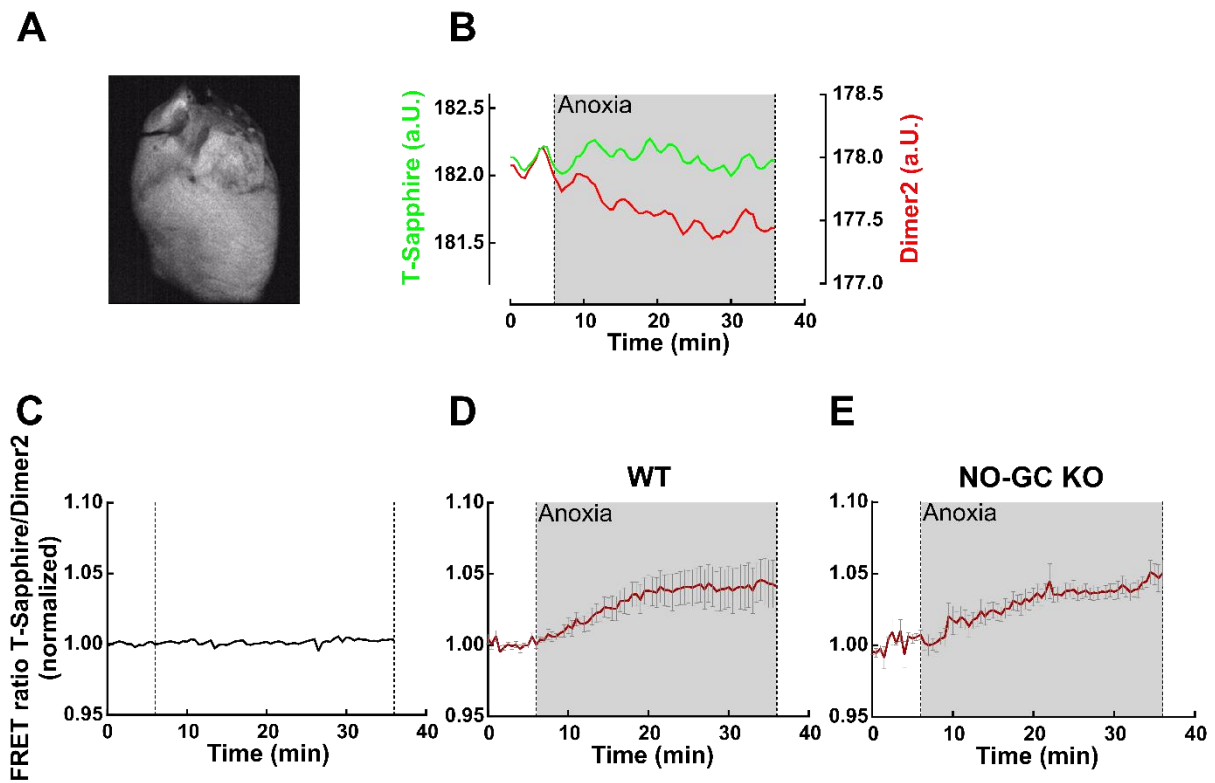
**Figure 3.1.16: Basal cGMP levels are increasing during anoxic injury in an *ex vivo* whole heart Langendorff model.** cGMP dynamics during anoxic injury were monitored in an *ex vivo* whole heart Langendorff model by FRET recordings. **A**) FRET image of a red-cGES-DE5 transgenic mouse heart used for whole-heart Langendorff experiments. **B**) cGMP biosensor fluorescence in T-Sapphire and Dimer2 channels during anoxia treatment. **C**) Representative FRET trace from a normoxic control heart. **D**) Mean of FRET traces from anoxia treated hearts of red-cGES-DE5 wildtype (WT) sensor mice. Mean of 7 hearts is shown. **E**) Mean of FRET traces from anoxia treated hearts of NO-GC knockout (NO-GC KO) red-cGES-DE5 sensor mice. Mean of 4 hearts is shown. Data are presented as mean ± SEM.

## 3.1.10 Basal cGMP levels are increased in mouse heart tissues after *in vivo* ischemia/reperfusion injury with a concomitant reduction of PDE3A protein

In addition to the *ex vivo* whole-heart Langendorff model, mouse heart tissues from an *in vivo* open chest model of ischemia/reperfusion were used to investigate cGMP dynamics during hypoxic injury (Figure 3.1.17). In this model, ischemic injury was induced by occlusion of the left coronary artery.
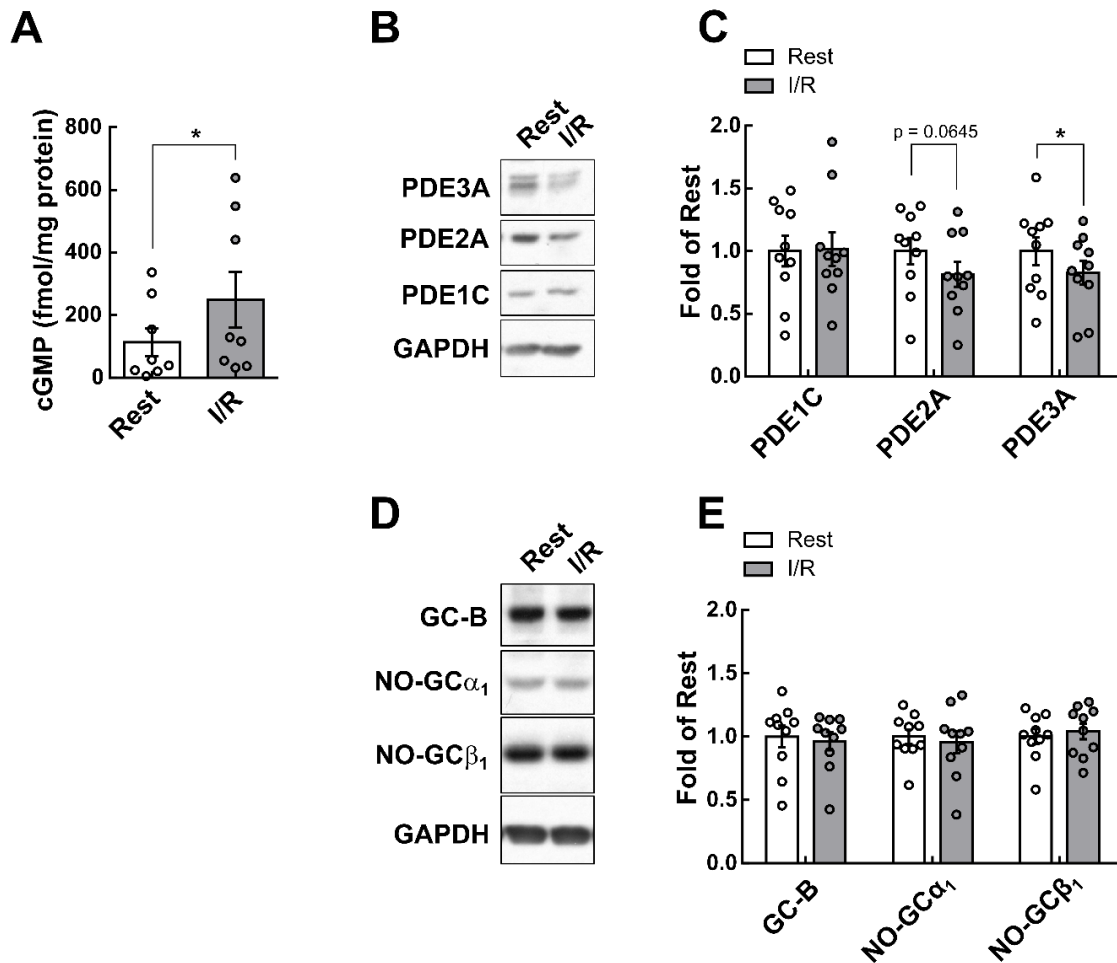
**Figure 3.1.17: Basal cGMP levels are increased in mouse heart tissues after *in vivo* ischemia/reperfusion injury with a concomitant reduction of PDE3A protein.** Ischemia/reperfusion injury was induced in mice in an *in vivo* open-chest model by occlusion of the left coronary artery [168]. Infarcted tissue (I/R) and non-infarcted control tissue (Rest) of the same hearts were analysed. **A**) cGMP immunoassay in Rest and I/R tissue to determine basal cGMP levels. **B**) Representative immunoblots of PDE1C, PDE2A, and PDE3A protein in I/R and Rest heart tissue. GAPDH was used as loading control. **C**) Quantification of the immunoblot experiments shown in B). **D**) Representative immunoblots of GC-B, NO-GC$\alpha_1$ and NO-GC$\beta_1$ protein in I/R and Rest heart tissue. GAPDH was used as loading control. **E**) Quantification of the immunoblot experiments shown in D). Data are presented as mean ± SEM, significant differences at * $p < 0.05$, ** $p < 0.01$, *** $p < 0.001$.

cGMP immunoassay of infarcted (I/R) and control (Rest) tissue of the same hearts showed that basal cGMP levels were significantly increased in I/R tissue (249.7 ± 88.6 fmol/mg protein) compared to control Rest tissue (113.6 ± 44.9 fmol/mg protein) (Figure 3.1.17, A). Immunoblot analysis of cGMP degrading PDE1C, PDE2A, and PDE3A revealed significant reduction of PDE3A protein level in I/R tissue compared to Rest control tissue (Figure 3.1.17, B and C). Protein levels of PDE1C and PDE2A were not significantly changed, nor were protein levels of cGMP generating GC-B, NO-GC$\alpha_1$, and NO-GC$\beta_1$ (Figure 3.1.17, D and E).

### 3.1.11 PDE3A is impaired in human ventricular myocytes after hypoxic injury as well as in human ventricular tissue samples of patients with ischemic cardiomyopathy

*3.1.11.1 FRET response to PDE3 inhibitor Cilostamide is impaired in human ventricular cardiomyocytes after hypoxia/reoxygenation*

In order to figure out whether the results from mouse experiments could be translated into the human situation, isolated human ventricular cardiomyocytes were transduced for 48 h with an adenovirus to express the red-cGES-DE5 biosensor and exposed to hypoxia/reoxygenation. Subsequently, FRET-based cGMP measurements were performed using the PDE3 specific inhibitor Cilostamide (Cilo, 10 µM). Clinical characteristics of patients whose left ventricular tissue samples were used for cardiomyocyte isolation were shown above in Table 3.1 (section 3.1.6).

Inhibition of PDE3 could raise cGMP levels in human ventricular cardiomyocytes exposed to Normoxia (2.7 ± 0.3%) but not in cardiomyocytes exposed to 4 h H/R (1.7 ± 0.2%) (Figure 3.1.18, A and B). This clearly showed that the FRET response to PDE3 inhibitor Cilostamide was also affected in human ventricular cardiomyocytes after hypoxia/reoxygenation.
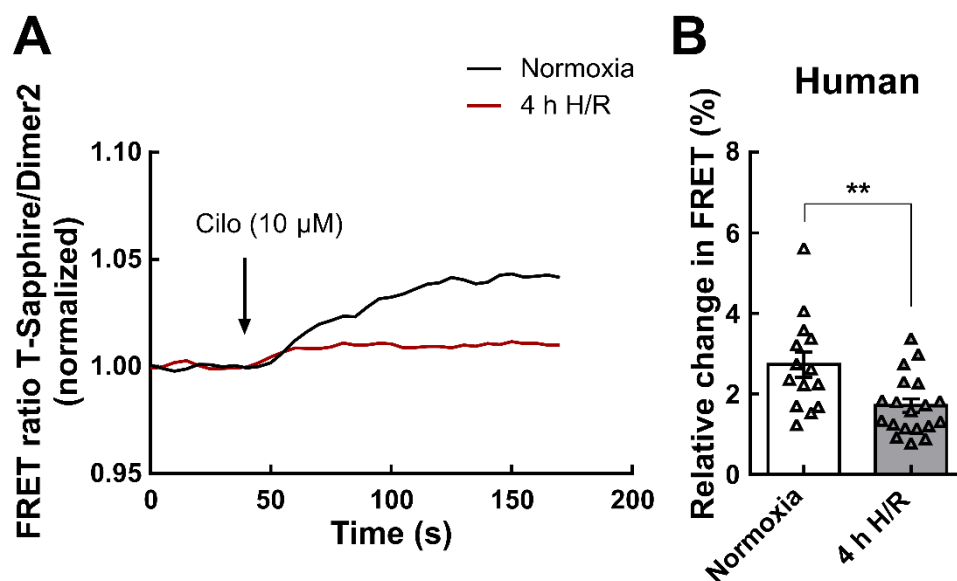


**Figure 3.1.18: FRET response to PDE3 inhibitor Cilostamide is impaired in human ventricular cardiomyocytes after hypoxia/reoxygenation.** Human ventricular cardiomyocytes expressing the FRET-based cGMP biosensor red-cGES-DE5 were exposed to 4 h of hypoxia followed by 2 h of reoxygenation (4 h H/R) or normoxic control conditions (Normoxia). Afterwards, cells were used for FRET analysis with the selective PDE3 inhibitor Cilostamide (Cilo, 10 µM). **A**) Representative FRET traces from human ventricular cardiomyocytes exposed to PDE3 inhibitor Cilostamide (Cilo, 10 µM). **B**) Quantification of the FRET experiments shown in A). Data are presented as mean ± SEM, significant differences at * p < 0.05, ** p< 0.01, *** p < 0.001.

*3.1.11.2 PDE3A protein is reduced in human ventricular tissue samples of patients with ischemic cardiomyopathy*

In addition to measure the cGMP FRET response to PDE3 inhibitor Cilostamide in human ventricular cardiomyocytes exposed to hypoxia/reoxygenation, PDE3A protein expression was investigated in human left ventricular tissue samples of patients suffering from dilated cardiomyopathy (DCM) as well as of patients suffering from ischemic cardiomyopathy (ICM) using immunoblot analysis. Tissue samples of patients with normal left ventricular ejection fraction (LVEF) without DCM or ICM were used as controls.

Clinical characteristics of patients whose left ventricular tissue samples were used for immunoblot analysis in this work are shown in Table 3.2.

**Table 3.2:** **Clinical characteristics of patients whose left ventricular tissue samples were used for immunoblot analysis.** Data are presented as mean ± SEM. DCM, dilated cardiomyopathy; ICM, ischemic cardiomyopathy; LVEDD, left ventricular end-diastolic diameter; LVEF, left ventricular ejection fraction.

|  | Control | DCM | ICM |
|---|---|---|---|
| **Patients (n)** | 5 | 6 | 5 |
| Male | 3 (60.0%) | 5 (83.3%) | 4 (80.0%) |
| Female | 2 (40.0%) | 1 (16.7%) | 1 (20.0%) |
| **Age at surgery (years)** | 45 ± 13 | 54 ± 4 | 64 ± 3 |
| **Indications for surgery** | | | |
| Coronary artery disease (n) | 0 (0.0%) | 0 (0.0%) | 0 (0.0%) |
| Valvular heart disease (n) | 4 (80.0%) | 2 (33.3%) | 2 (40.0%) |
| Both (n) | 0 (0.0%) | 0 (0.0%) | 2 (40.0%) |
| Transplant (n) | 0 (0.0%) | 3 (0.0%) | 0 (0.0%) |
| **Cardiovascular comorbidity** | | | |
| Arterial hypertension (n) | 0 (0.0%) | 2 (33.3%) | 3 (60.0%) |
| Diabetes mellitus (n) | 0 (0.0%) | 1 (16.7%) | 2 (40.0%) |
| Hyperlipoproteinemia (n) | 1 (20.0%) | 1 (16.7%) | 1 (20.0%) |
| **Echocardiography data** | | | |
| LVEF (%) | 60.2 ± 1.6 | 21.0 ± 1.7 | 24.8 ± 2.3 |
| LVEDD (mm) | 49.0 ± 4.9 | 67.2 ± 5.2 | 65.2 ± 2.7 |

| Coronary angiography | | | |
|---|---|---|---|
| Patients (n) with occluded vessels | 0 (0.0%) | 0 (0.0%) | 5 (100.0%) |

Immunoblot analysis of PDE3A protein revealed that in tissue samples of patients suffering from ICM, PDE3A protein was significantly reduced (Fold of control: 0.44 ± 0.10) compared to control tissue samples (1.00 ± 0.15). PDE3A protein also showed a tendency to be reduced in tissue samples of patients suffering from DCM (Fold of control: 0.61 ± 0.04) compared to controls, however this difference was not statistically significant. Comparing PDE3A protein levels in tissue samples of patients with DCM and ICM, PDE3A protein showed a tendency to be lower in ICM than in DCM, however this difference was not statistically significant.
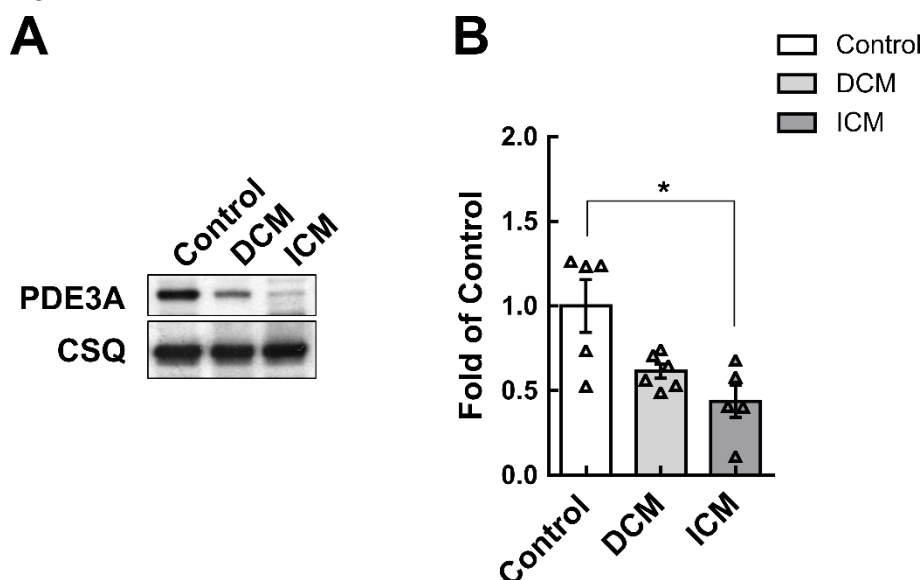


**Figure 3.1.19: PDE3A protein is reduced in human ventricular tissue samples from patients with ischemic cardiomyopathy.** Left ventricular tissue samples of patients suffering from dilated cardiomyopathy (DCM) and patients suffering from ischemic cardiomyopathy (ICM) as well as tissue samples of a control group were used to investigate PDE3A protein with immunoblot analysis. **A**) Representative immunoblots of PDE3A protein in human left ventricular tissue samples of control patients, patients with DCM and patients with ICM. CSQ (Calsequestrin) was used as loading control. **B**) Quantification of the immunoblot experiments shown in A. Data are presented as mean ± SEM, significant differences at * $p < 0.05$, ** $p < 0.01$, *** $p < 0.001$.

## 3.2 cGMP signalling in the human atrium and its role in atrial fibrillation

### 3.2.1 Establishment of FRET-based cGMP measurements in human atrial cardiomyocytes

In the first series of experiments for this project, FRET-based cGMP imaging in human atrial cardiomyocytes was established.

Since cGMP levels in adult cardiomyocytes are very low [136, 137], the cGMP biosensor red-cGES-DE5 [216] was chosen for FRET-based cGMP measurements in adult atrial cardiomyocytes. Adult cardiomyocytes that are fully differentiated are poor candidates for non-viral gene transfer, whereas viral-based techniques enable much more efficient and stable gene transfer [244]. Therefore, adenoviral transduction was used to express the cytosolic FRET-based cGMP sensor red-cGES-DE5 in human atrial cardiomyocytes. Different virus concentrations and expression times were tested in order figure out the optimal conditions for a good red-cGES-DE5 sensor expression. A multiplicity of infection (MOI) of 300 showed uniform sensor expression at high enough levels to allow FRET-based cGMP measurements in human atrial cardiomyocytes 48 h after transduction (Figure 3.2.1, A and B). FRET measurements revealed that the sensor was functional and usable for FRET-based cGMP measurements in human atrial cardiomyocytes (Figure 3.2.1, C and D).
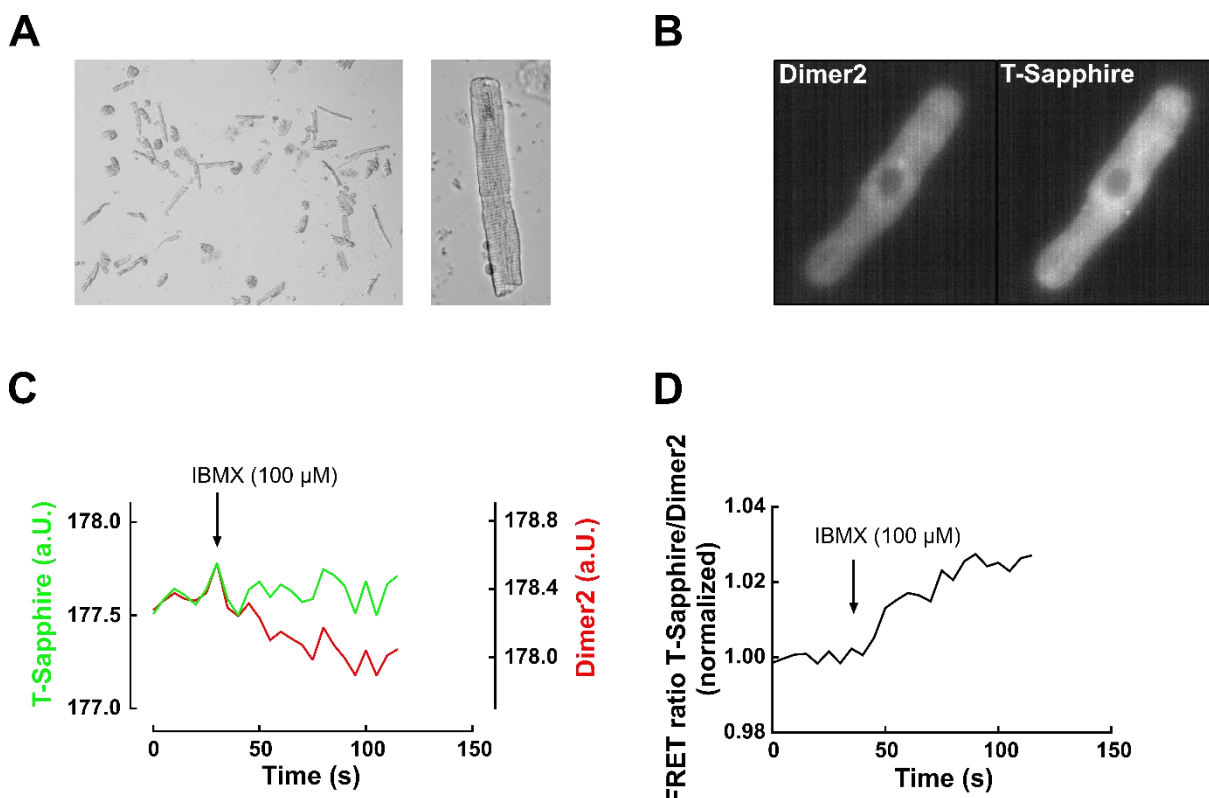


**Figure 3.2.1: FRET-based cGMP measurements in human atrial cardiomyocytes.** Human atrial cardiomyocytes **A**) directly after isolation, magnification 10 x and 63 x, and **B**) 48 h after red-cGES-DE5 adenovirus transduction using a multiplicity of infection (MOI) of 300. cGMP biosensor fluorescence in T-Sapphire and Dimer2 channels during FRET measurements in single

cardiomyocytes. The cytosolic biosensor red-cGES-DE5 is uniformly expressed in the cytosol at high enough levels to allow FRET measurements. Magnification 63 x. **C**) Exemplary FRET trace, showing the change in fluorescence of the two fluorophores T-Sapphire and Dimer2 upon stimulation with the non-selective PDE inhibitor IBMX (100 µM). **D**) Normalized FRET ratio of the measurement shown in C). An increase in FRET ratio represents an increase in cGMP.

After the establishment of FRET-based cGMP measurements in human atrial cardiomyocytes, the cGMP signalling cascade was investigated in right (RA) and left atria (LA) from patients in sinus rhythm (SR) and with atrial fibrillation (AF). Therefore, different kinds of FRET-based cGMP measurements in isolated atrial cardiomyocytes, as well as immunoblot analysis of atrial tissue samples were performed. The results of these experiments are shown in the following sections.

Clinical characteristics of patients whose atrial tissue samples were used for cardiomyocyte isolation and FRET-based cGMP measurements in this project are shown in Table 3.3. In total, 199 human atrial cardiomyocytes from 92 patients were used for FRET measurements. Clinical characteristics of patients whose atrial tissue samples were used for immunoblot analysis in this project are shown in Table 3.4.

**Table 3.3: Clinical characteristics of patients whose atrial tissue samples were used for cardiomyocyte isolation and FRET-based cGMP measurements.** Data are presented as mean ± SEM. ACE, Angiotensin converting enzyme; AF, atrial fibrillation; AT1, Angiotensin II type 1; LA, left atrium; LVEF, left ventricular ejection fraction; RA, right atrium; SR, sinus rhythm.

| | SR RA | SR LA | AF RA | AF LA |
|---|---|---|---|---|
| **Patients (n)** | 46 | 5 | 17 | 24 |
| Male | 37 (80.4%) | 3 (60.0%) | 11 (64.7%) | 14 (58.3%) |
| Female | 9 (19.6%) | 2 (40.0%) | 6 (35.3%) | 10 (41.7%) |
| **Age at surgery (years)** | 68 ± 1 | 66 ± 8 | 71 ± 3 | 71 ± 2 |
| **Indications for surgery** | | | | |
| Coronary artery disease (n) | 27 (58.7%) | 0 (0.0%) | 4 (23.5%) | 6 (25.0%) |
| Valvular heart disease (n) | 7 (15.2%) | 4 (80.0%) | 10 (58.8%) | 16 (66.7%) |
| Both (n) | 12 (26.1%) | 1 (20.0%) | 3 (17.6%) | 2 (8.3%) |
| Dilated Cardiomyopathy (n) | 18 (39.1%) | 3 (60.0%) | 3 (17.6%) | 12 (50.5%) |
| **Cardiovascular comorbidity** | | | | |
| Arterial hypertension (n) | 35 (76.1%) | 3 (60.0%) | 12 (70.6%) | 11 (45.8%) |

| | | | | |
|---|---|---|---|---|
| Diabetes mellitus (n) | 10 (21.7%) | 1 (20.0%) | 2 (11.8%) | 2 (8.3%) |
| Hyperlipoproteinemia (n) | 15 (32.6%) | 1 (20.0%) | 5 (29.4%) | 7 (29.2%) |
| **Echocardiography data** | | | | |
| LVEF (%) | 55.8 ± 1.6 | 49.3 ± 8.9 | 49.8 ± 4.9 | 49.1 ± 3.7 |
| **Medication** | | | | |
| ACE inhibitor (n) | 19 (41.3%) | 2 (40.0%) | 8 (47.1%) | 8 (33.3%) |
| AT1 receptor antagonist (n) | 5 (10.9%) | 0 (0.0%) | 1 (5.9%) | 0 (0.0%) |
| Beta blocker (n) | 17 (37.0%) | 5 (100.0%) | 12 (70.6%) | 14 (58.3%) |
| $Ca^{2+}$ channel blocker (n) | 6 (13.0%) | 0 (0.0%) | 2 (11.8%) | 2 (8.3%) |
| Diuretics (n) | 3 (6.5%) | 3 (60.0%) | 7 (41.2%) | 8 (33.3%) |
| Digitalis (n) | 0 (0.0%) | 0 (0.0%) | 0 (0.0%) | 2 (8.3%) |
| Nitrates (n) | 1 (2.2%) | 0 (0.0%) | 0 (0.0%) | 0 (0.0%) |

**Table 3.4:** **Clinical characteristics of patients whose atrial tissue samples were used for immunoblot analysis.** Data are presented as mean ± SEM. ACE, Angiotensin converting enzyme; AF, atrial fibrillation; AT1, Angiotensin II type 1; LVEF, left ventricular ejection fraction; RA, right atrium; SR, sinus rhythm.

| | SR RA | AF RA |
|---|---|---|
| **Patients (n)** | 7 | 7 |
| Male | 7 (100.0%) | 7 (100.0%) |
| Female | 0 (0.0%) | 0 (0.0%) |
| **Age at surgery (years)** | 59 ± 4 | 70 ± 4 |
| **Indications for surgery** | | |
| Coronary artery disease (n) | 3 (42.9%) | 0 (0.0%) |
| Valvular heart disease (n) | 2 (28.6%) | 5 (71.4%) |
| Both (n) | 1 (14.3%) | 2 (28.6%) |
| Dilated Cardiomyopathy (n) | 2 (28.6%) | 2 (28.6%) |
| **Cardiovascular comorbidity** | | |
| Arterial hypertension (n) | 4 (57.1%) | 4 (57.1%) |
| Diabetes mellitus (n) | 0 (0.0%) | 1 (14.3%) |

| | | |
|---|---|---|
| Hyperlipoproteinemia (n) | 1 (14.3%) | 1 (14.3%) |
| **Echocardiography data** | | |
| LVEF (%) | 60.0 ± 2.7 | 57.3 ± 2.5 |
| **Medication** | | |
| ACE inhibitor (n) | 4 (57.1%) | 4 (57.1%) |
| AT1 receptor antagonist (n) | 1 (14.3%) | 1 (14.3%) |
| Beta blocker (n) | 2 (26.6%) | 6 (85.7%) |
| $Ca^{2+}$ channel blocker (n) | 2 (26.6%) | 2 (26.6%) |
| Diuretics (n) | 0 (0.0%) | 2 (26.6%) |
| Digitalis (n) | 0 (0.0%) | 0 (0.0%) |
| Nitrates (n) | 1 (14.3%) | 0 (0.0%) |

### 3.2.2 Role of NO-GC and NP-GC in right and left atrium of patients in sinus rhythm and with atrial fibrillation

*3.2.2.1 NO-GC stimulation effects are equal in human atrial cardiomyocytes from right and left atria of patients in sinus rhythm and with atrial fibrillation*

In order to analyse the role of cGMP producing NO-GC in human atrium, FRET recordings were done with the NO-donor SNAP (100 µM). Atrial cardiomyocytes from right (RA) and left atrium (LA) of patients in sinus rhythm (SR) and with atrial fibrillation (AF) were stimulated with the NO-donor SNAP (100 µM) in single cell FRET measurements. SNAP stimulation evoked a nice increase in FRET which did not significantly differ, neither between cells from RA and LA, nor under pathological AF conditions (SNAP response in %: SR RA: 1.2 ± 0.2; AF RA: 1.5 ± 0.3; SR LA: 1.5 ± 0.2; AF LA: 1.0 ± 0.3). Stimulation of the cells with the unspecific PDE inhibitor IBMX (100 µM) could further increase cGMP levels in all conditions (SNAP + IBMX response in %: SR RA: 2.5 ± 0.3; AF RA: 2.7 ± 0.5; SR LA: 2.4 ± 0.4; AF LA: 1.9 ± 0.3) (Figure 3.2.2). These effects to IBMX treatment indicated that PDEs play an important role in cGMP degradation of NO-GC produced cGMP.
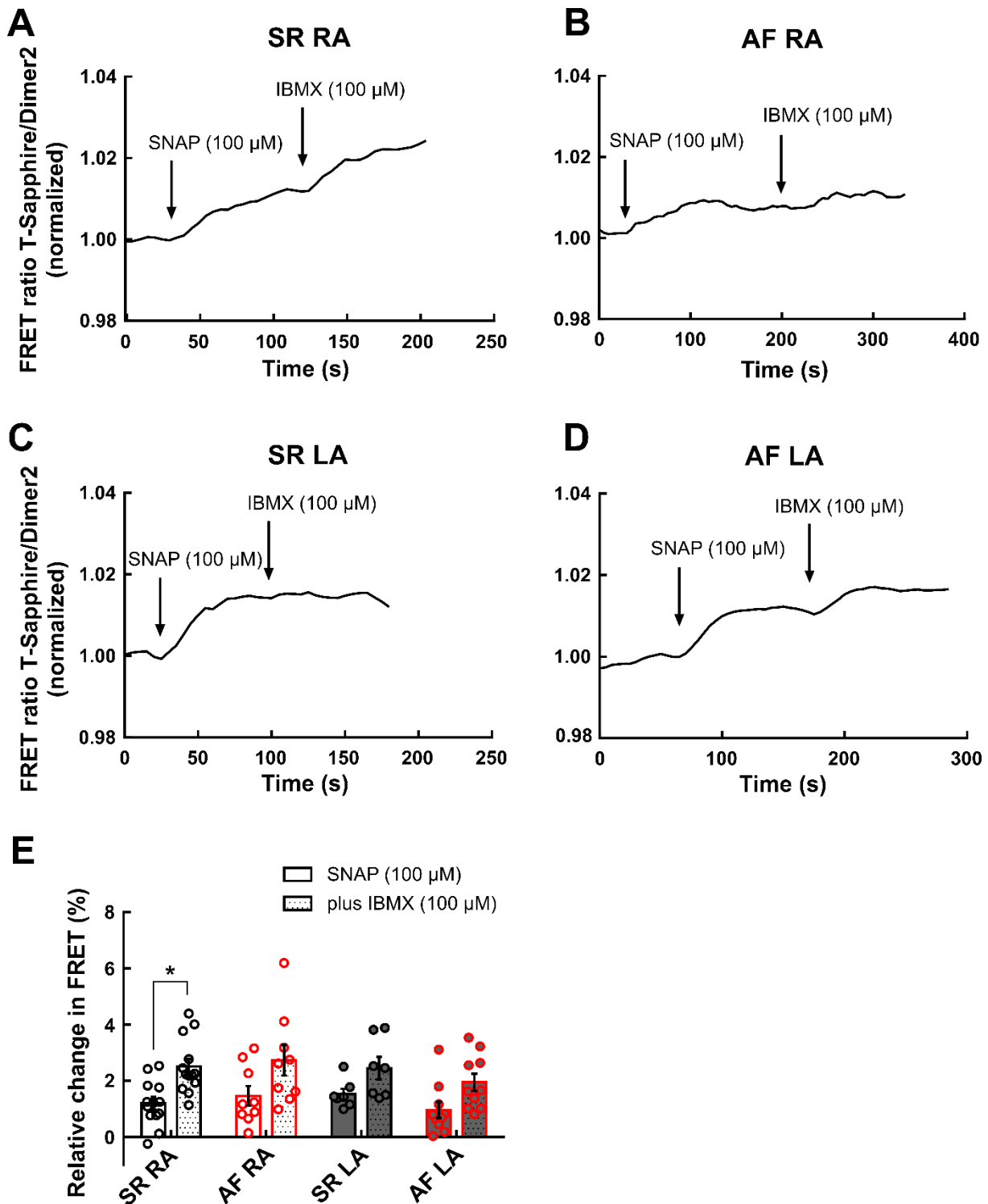
**Figure 3.2.2:    Effects of NO-GC stimulation on FRET-based cGMP measurements in human atrial cardiomyocytes from right (RA) and left atrium (LA) of patients in sinus rhythm (SR) and with atrial fibrillation (AF).**    Atrial cardiomyocytes were stimulated with the NO-donor SNAP (100 μM) followed by the unselective PDE inhibitor IBMX (100 μM). An increase in FRET ratio represents an increase in cytosolic cGMP. Representative FRET traces from RA cardiomyocytes from patients in **A**) SR, and **B**) with AF. Representative FRET traces from LA cardiomyocytes from patients in **C**) SR, and **D**) with AF. **E**) Quantification of the FRET experiments shown in A-D. Data are presented as mean ± SEM, significant differences at * $p < 0.05$, ** $p < 0.01$, *** $p < 0.001$.

*3.2.2.2 NO-GC protein levels are equal in right atrial tissue samples of patients in sinus rhythm and with atrial fibrillation*

In addition to FRET-based cGMP measurements of NO-GC stimulation effects, protein levels of NO-GC were analysed in RA tissue samples of patients in SR and with AF. Neither NO-GC$\alpha_1$, nor NO-GC$\beta_1$ protein levels were significantly changed between SR and AF tissue samples (Figure 3.2.3). However, NO-GC$\beta_1$ protein showed a tendency to be downregulated in AF tissue.
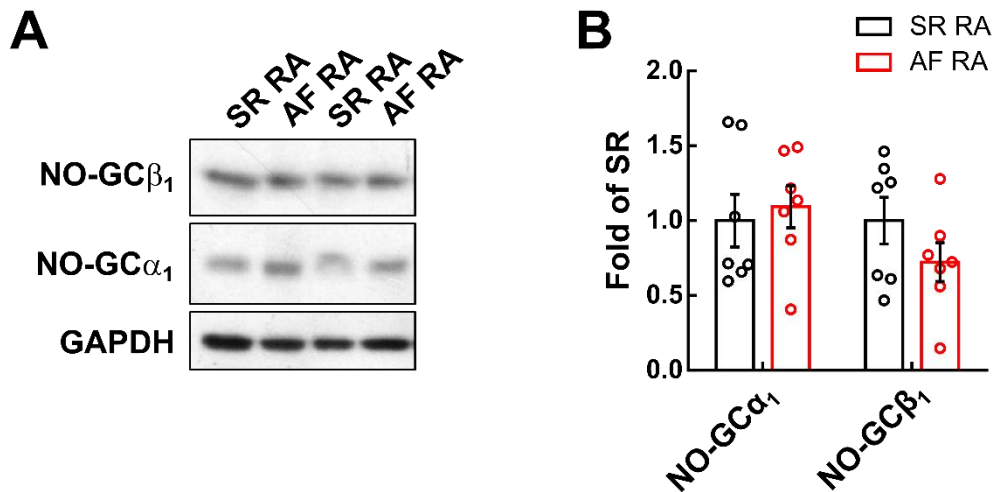


**Figure 3.2.3:** **Protein levels of cGMP-generating NO-GC in human atrial tissue samples from right atrium (RA) of patients in sinus rhythm (SR) and with atrial fibrillation (AF).** **A**) Representative immunoblots of NO-GC$\alpha_1$ and NO-GC$\beta_1$ protein in human atrial tissue. GAPDH was used as loading control. **B**) Quantification of the immunoblot experiments shown in A). Data are presented as mean ± SEM, significant differences at * $p < 0.05$, ** $p < 0.01$, *** $p < 0.001$.

*3.2.2.3 NP-GC stimulation effects are different in human atrial cardiomyocytes from right and left atria of patients in sinus rhythm and with atrial fibrillation*

The role of cGMP generating NP-GC in human atrium was also investigated. Cardiomyocytes from RA and LA of patients in SR and with AF were used for FRET measurements. Cells were stimulated with two different concentrations of CNP (100 nM, 1 µM) to stimulate GC-B, followed by the unspecific PDE inhibitor IBMX (100 µM) and change in FRET was recorded (Figure 3.2.4).
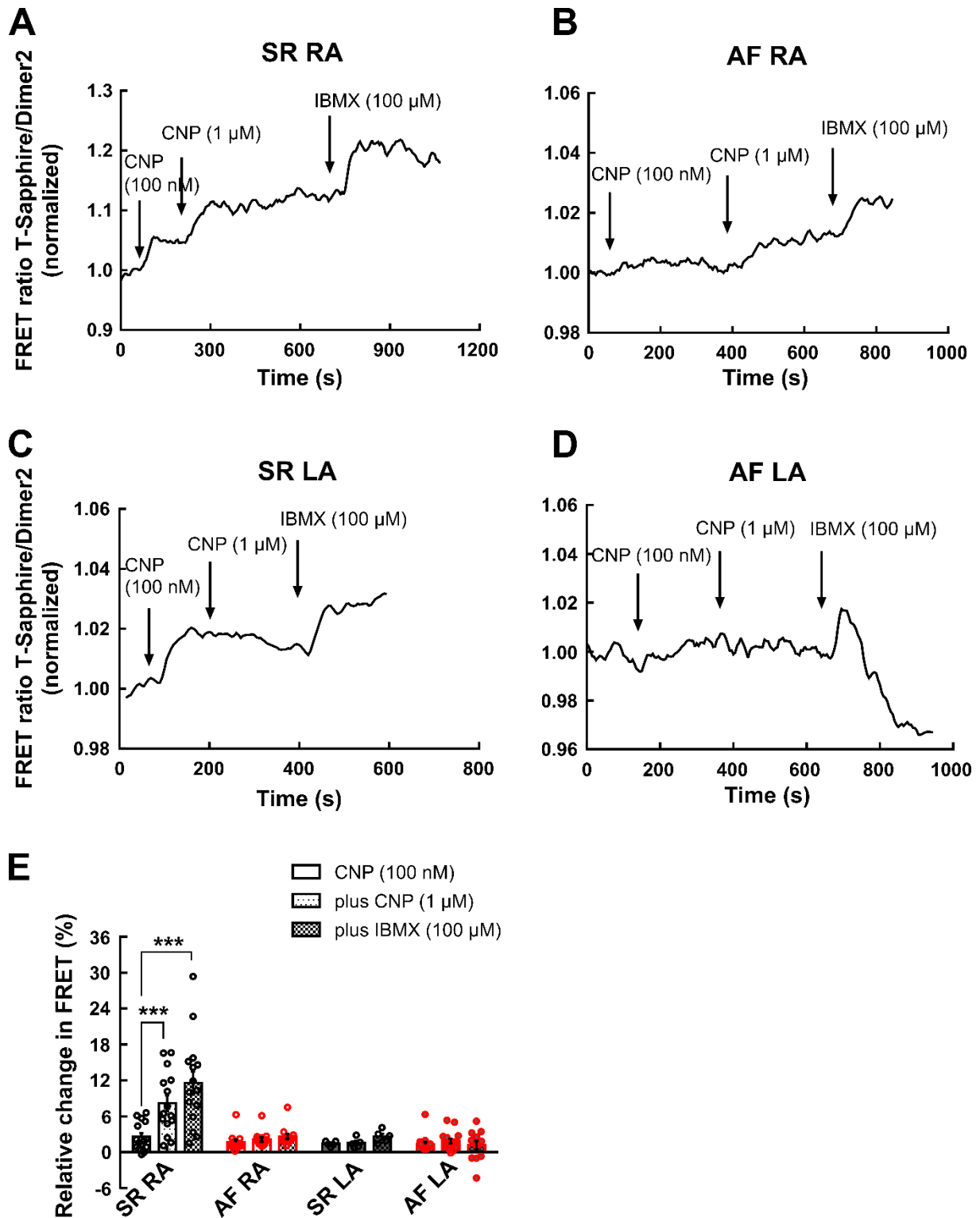
**Figure 3.2.4: Effects of NP-GC stimulation on FRET-based cGMP measurements in human atrial cardiomyocytes from right (RA) and left atrium (LA) of patients in sinus rhythm (SR) and with atrial fibrillation (AF).** Atrial cardiomyocytes were stimulated with the natriuretic peptide CNP (100 nM, 1 µM) to stimulate GC-B followed by the unselective PDE inhibitor IBMX (100 µM). Representative FRET traces from RA cardiomyocytes from patients in **A**) SR, and **B**) with AF. Representative FRET traces from LA cardiomyocytes from patients in **C**) SR, and **D**) with AF. **E**) Quantification of the FRET experiments shown in A-D. Data are presented as mean ± SEM, significant differences at * $p < 0.05$, ** $p < 0.01$, *** $p < 0.001$.

Interestingly, in contrast to the effects of NO-GC stimulation on cGMP dynamics (section 3.2.2.1), the effects of NP-GC stimulation on cGMP dynamics were completely different in RA and LA of patients in SR and with AF (Figure 3.2.4). The increase in FRET ratio upon CNP (100 nM, and 1 µM) and IBMX (100 µM) stimulation was much stronger in cardiomyocytes from SR RA than in cardiomyocytes from AF RA, SR LA, and AF LA. Stimulation with CNP (100 nM) could increase FRET ratio in cardiomyocytes of all conditions (CNP (100 nM) response in %: SR RA 2.6 ± 0.6; AF RA: 1.7 ± 0.4; SR LA: 1.4 ± 0.2; AF LA: 1.3 ± 0.4). However, whereas additional stimulation with higher concentrations of CNP (1 µM) could further increase cGMP levels in RA (CNP (100 nM) + CNP (1 µM) response in %: SR RA: 8.2 ± 1.3; AF RA: 2.1 ± 0.4), they could not be raised further in LA (CNP (100 nM) + CNP (1 µM) response in %: SR LA: 1.5 ± 0.4; AF LA: 1.9 ± 0.4). Inhibition of PDEs with the unspecific PDE inhibitor IBMX (100 µM) could raise cGMP levels in cardiomyocytes from SR RA (11.6 ± 1.9%), AF RA (2.6 ± 0.4%), and SR LA (2.6 ± 0.5%). Unexpectedly, IBMX treatment decreased cGMP levels in cells from AF LA (1.2 ± 0.7%).

Additional FRET measurements were done in order to investigate the role of GC-A in patients with AF compared to patients in SR. Therefore, cardiomyocytes of SR RA and AF LA were stimulated with ANP (100 nM, 1 µM) to stimulate GC-A. ANP (100 nM, 1 µM) treatment could raise cGMP levels in cardiomyocytes of SR RA but not in AF LA (Supplemental Figure 5.3.1).

These data of the effects of NO-GC and NP-GC stimulation on cGMP dynamics, analysed by FRET-based cGMP measurements, nicely showed that whereas the effects of NO-GC stimulation on cGMP FRET were equal between cardiomyocytes from RA and LA of patients in SR and with AF, the effects of NP-GC stimulation were very different between cardiomyocytes from RA and LA of patients in SR and with AF.

### 3.2.3 Role of cGMP degrading phosphodiesterases in right and left atrium of patients in sinus rhythm and with atrial fibrillation

In addition to cGMP generating GCs, the role of different PDEs involved in cGMP degradation was investigated in cardiomyocytes isolated from RA and LA of patients in SR and with AF. Therefore, FRET-based cGMP measurements with selective PDE inhibitors were performed. Furthermore, PDE protein levels were analysed by immunoblot analysis.

*3.2.3.1 FRET response to PDE2 inhibitor Bay 60-7550 is different in human atrial cardiomyocytes from right and left atria of patients in sinus rhythm and with atrial fibrillation*
The FRET response to the PDE2 selective inhibitor Bay 60-7550 (Bay, 100 nM) was investigated in isolated atrial cardiomyocytes (Figure 3.2.5).
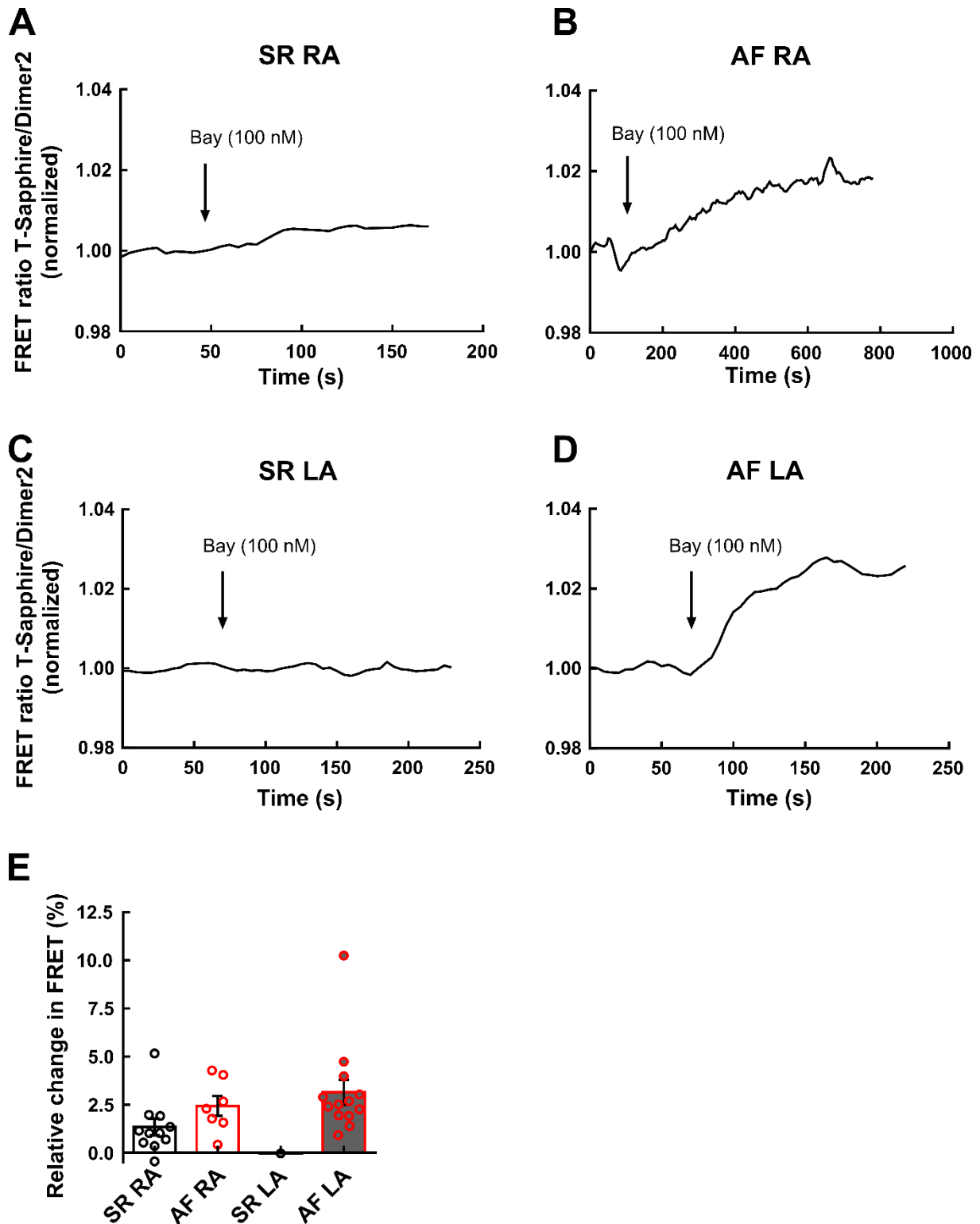


**Figure 3.2.5: FRET response to PDE2 inhibitor Bay 60-7550 in human atrial cardiomyocytes from right (RA) and left atrium (LA) of patients in sinus rhythm (SR) and with atrial fibrillation (AF).** Atrial cardiomyocytes were exposed to the PDE2-specific inhibitor Bay 60-7550 (Bay, 100 nM).

Representative FRET traces from RA cardiomyocytes from patients in **A**) SR, and **B**) with AF. Representative FRET traces from LA cardiomyocytes from patients in **C**) SR, and **D**) with AF. **E**) Quantification of the FRET experiments shown in A-D. Data are presented as mean ± SEM, significant differences at * $p < 0.05$, ** $p < 0.01$, *** $p < 0.001$.

Whereas inhibition of PDE2 only slightly increased cGMP levels in cardiomyocytes from RA and LA of patients in SR (Bay response in %: SR RA 1.3 ± 0.4; SR LA: -0.04), PDE2 inhibition caused a strong increase in cGMP levels in cardiomyocytes from RA and LA of patients with AF (Bay response in %: AF RA: 2.4 ± 0.5; AF LA: 3.1 ± 0.7). This effect was even stronger in AF cells from LA (AF LA), than in AF cells from RA (AF RA). Due to lack of SR LA tissue for cardiomyocyte isolation, only one FRET-based cGMP measurement of the effect of PDE2 inhibitor Bay 60-7550 could be recorded in SR LA cardiomyocytes.

### 3.2.3.2 PDE2A protein levels are equal in right atrial tissue samples of patients in sinus rhythm and with atrial fibrillation

In addition to FRET-based cGMP measurements of the effects to PDE2 inhibition, protein levels of PDE2A were analysed in RA tissue samples of patients in SR and with AF. Although the effect of PDE2 inhibition on FRET was much stronger in RA cardiomyocytes of patients with AF (AF RA) than in SR (SR RA) (section 3.2.3.1), PDE2A protein was not significantly changed. However, it showed a tendency to be downregulated in AF RA (Figure 3.2.6).
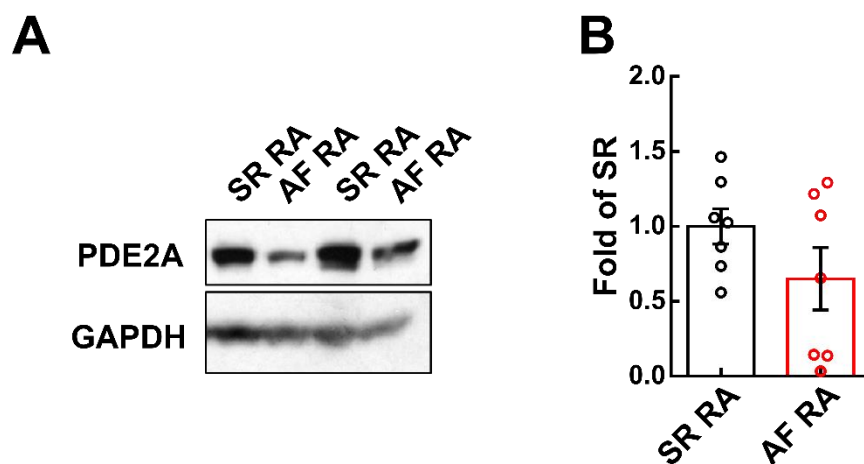


**Figure 3.2.6:   Protein levels of cGMP degrading PDE2A in human atrial tissue samples from right atrium (RA) of patients in sinus rhythm (SR) and with atrial fibrillation (AF). A**) Representative immunoblots of PDE2A protein in human atrial tissue. GAPDH was used as loading control. **B**) Quantification of the immunoblot experiments shown in A). Data are presented as mean ± SEM, significant differences at * $p < 0.05$, ** $p < 0.01$, *** $p < 0.001$.

*3.2.3.3 FRET response to PDE3 inhibitor Cilostamide is comparable in human atrial cardiomyocytes from right and left atria of patients in sinus rhythm and with atrial fibrillation*

The FRET response to the PDE3 selective inhibitor Cilostamide (Cilo, 10 µM) was investigated in isolated atrial cardiomyocytes. Interestingly, the effects of PDE3 inhibition on cGMP FRET were comparable in cardiomyocytes from RA and LA of patients in SR and with AF (Cilo response in %: SR RA: 1.6 ± 0.3; AF RA: 1.6 ± 0.2; SR LA: 1.9 ± 0.9; AF LA: 1.4 ± 0.2) (Figure 3.2.7).
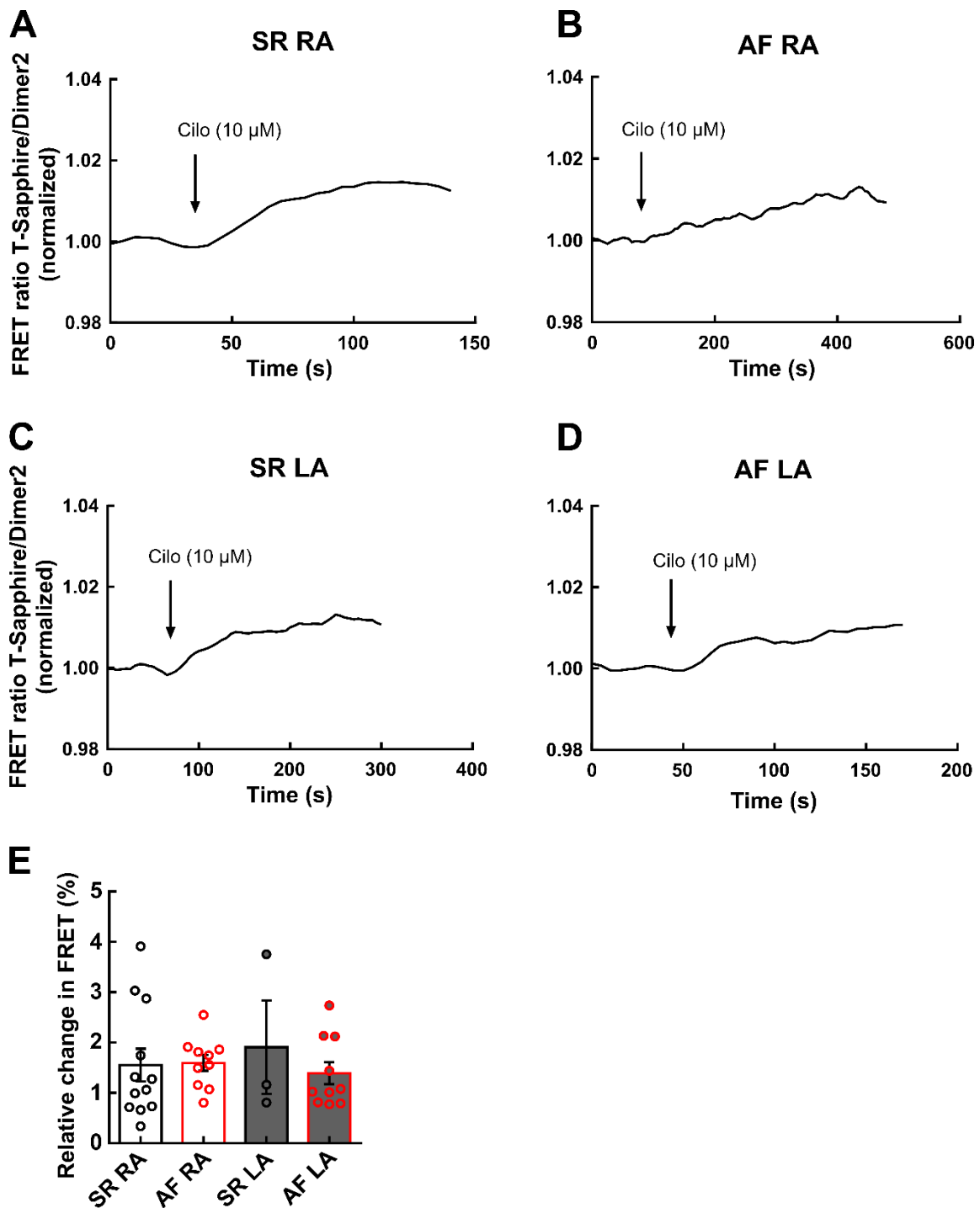


**Figure 3.2.7:** **FRET response to PDE3 inhibitor Cilostamide in human atrial cardiomyocytes from right (RA) and left atrium (LA) of patients in sinus rhythm (SR) and with atrial fibrillation**

**(AF).** Atrial cardiomyocytes were exposed to the selective PDE3 inhibitor Cilostamide (Cilo, 10 µM). Representative FRET traces from RA cardiomyocytes from patients in **A**) SR, and **B**) with AF. Representative FRET traces from LA cardiomyocytes from patients in **C**) SR, and **D**) with AF. **E**) Quantification of the FRET experiments shown in A-D. Data are presented as mean ± SEM, significant differences at * $p < 0.05$, ** $p < 0.01$, *** $p < 0.001$.

*3.2.3.4 PDE3A protein levels are equal in right atrial tissue samples of patients in sinus rhythm and with atrial fibrillation*

In addition to FRET-based cGMP measurements of the effects to PDE3 inhibition, protein levels of PDE3A were analysed in RA tissue samples of patients in SR and with AF. There was no significant change in PDE3 protein levels in RA tissues of patients in SR and with AF (Figure 3.2.8).
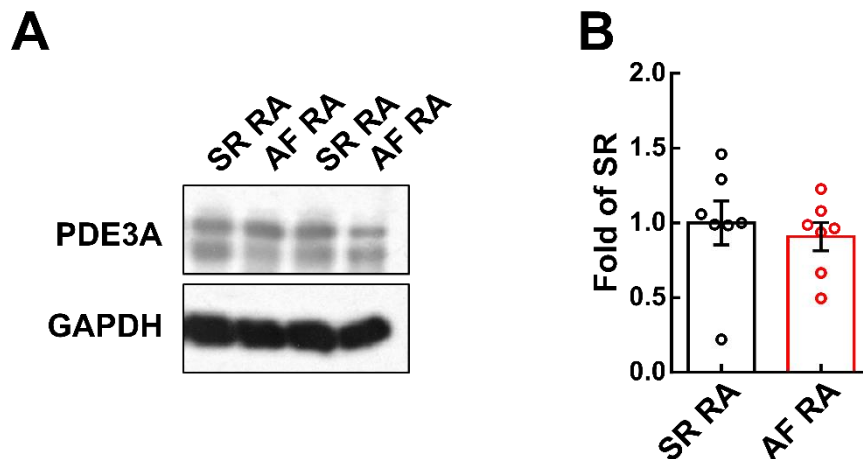


**Figure 3.2.8:** **Protein levels of cGMP degrading PDE3A in human atrial tissue samples from right atrium (RA) of patients in sinus rhythm (SR) and with atrial fibrillation (AF).** **A**) Representative immunoblots of PDE3A protein in human atrial tissue. GAPDH was used as loading control. **B**) Quantification of the immunoblot experiments shown in A). Data are presented as mean ± SEM, significant differences at * $p < 0.05$, ** $p < 0.01$, *** $p < 0.001$.

*3.2.3.5 FRET response to PDE5 inhibitor Sildenafil is different in human atrial cardiomyocytes from right and left atria of patients in sinus rhythm and with atrial fibrillation*

Next, the FRET response to the PDE5 selective inhibitor Sildenafil was investigated in isolated atrial cardiomyocytes. Sildenafil can also inhibit PDE1C at higher concentrations ($EC_{50\ PDE5} = 6.6$ nM; $EC_{50\ PDE1C} = 396$ nM) [260]. Therefore, two different concentrations of Sildenafil (Sil 100 nM and 1 µM) were used (Figure 3.2.9).
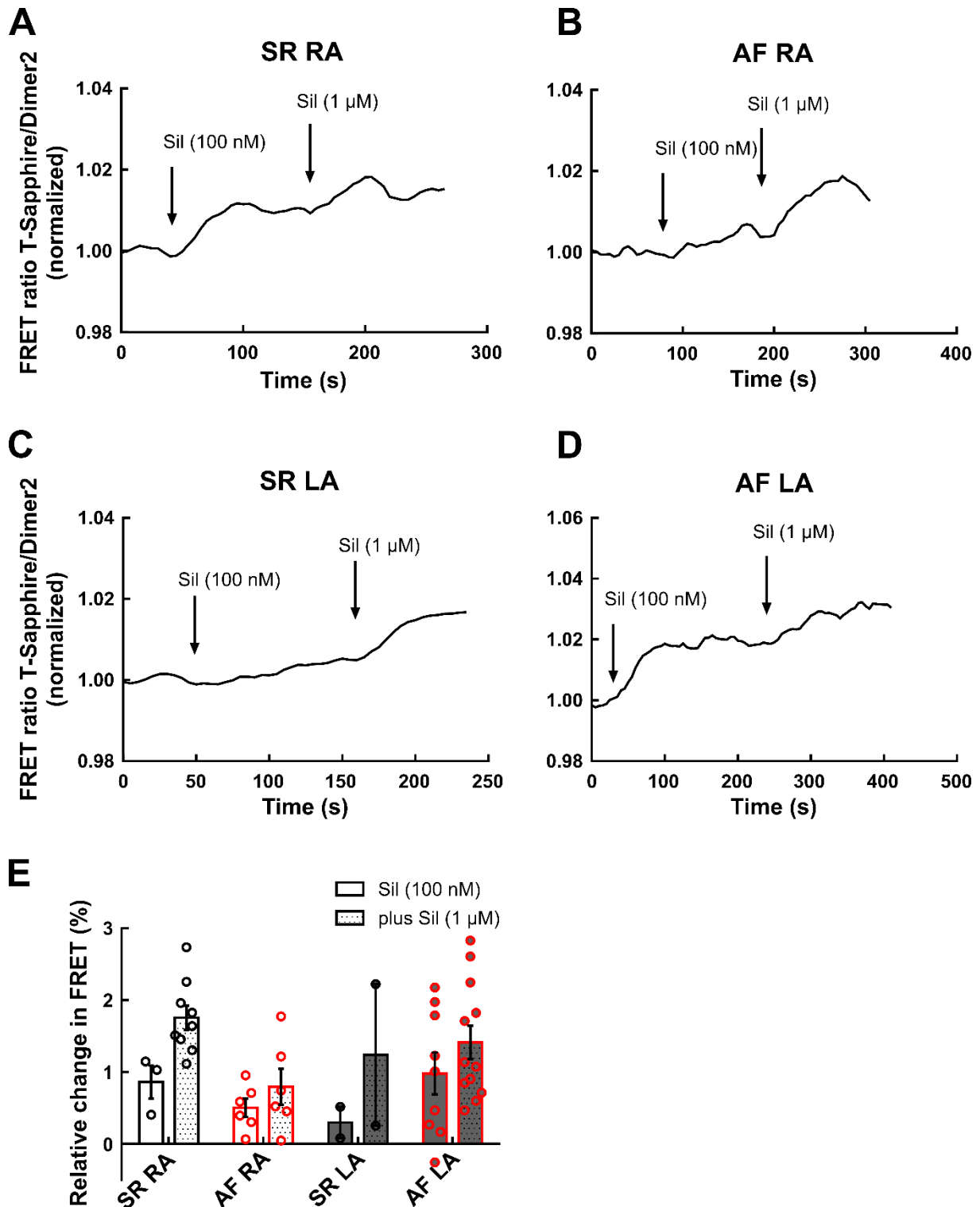
**Figure 3.2.9:** **FRET response to PDE5 inhibitor Sildenafil in human atrial cardiomyocytes from right (RA) and left atrium (LA) of patients in sinus rhythm (SR) and with atrial fibrillation (AF).** Atrial cardiomyocytes were exposed to the PDE5-specific inhibitor Sildenafil (Sil, 100 nM, and 1 µM). Representative FRET traces from RA cardiomyocytes from patients in **A**) SR, and **B**) with AF. Representative FRET traces from LA cardiomyocytes from patients in **C**) SR, and **D**) with AF. **E**) Quantification of the FRET experiments shown in A-D. Data are presented as mean ± SEM, significant differences at * $p < 0.05$, ** $p < 0.01$, *** $p < 0.001$.

In cardiomyocytes of RA there was a trend, however statistically not significant, that the increase in FRET ratio upon Sil (100 nM, and 1 µM) was stronger in cardiomyocytes from patients in SR (SR RA: 1.8 ± 0.2%) than with AF (AF RA: 0.8 ± 0.3%) (Figure 3.2.9). In LA, this trend was exactly the opposite, here, the increase in FRET ratio upon Sil (100 nM, and 1 µM) showed a tendency to be stronger in cardiomyocytes from patients with AF (AF LA: 1.4 ± 0.2%), than in patients in SR (SR LA: 1.2 ± 1.0%) (Figure 3.2.9). Inhibition of PDE5 with low concentrations of Sil (100 nM) caused an increase in FRET in cardiomyocytes from all conditions (Sil (100 nM) response in %: SR RA: 0.9 ± 0.2; AF RA: 0.5 ± 0.1; SR LA: 0.3 ± 0.2; AF LA: 1.0 ± 0.3). Upon stimulation of the cells with higher concentrations of Sil (1 µM), cGMP levels further increased.

### 3.2.4 Protein levels of cGMP effector protein PKG in right atrium of patients in sinus rhythm and with atrial fibrillation

Since PKG is an important downstream target of cGMP, protein levels of PKG in RA tissue of patients in SR and with AF were investigated as well. Immunoblot analysis revealed no significant changes between PKG protein in SR RA and AF RA tissue samples (Figure 3.2.10).
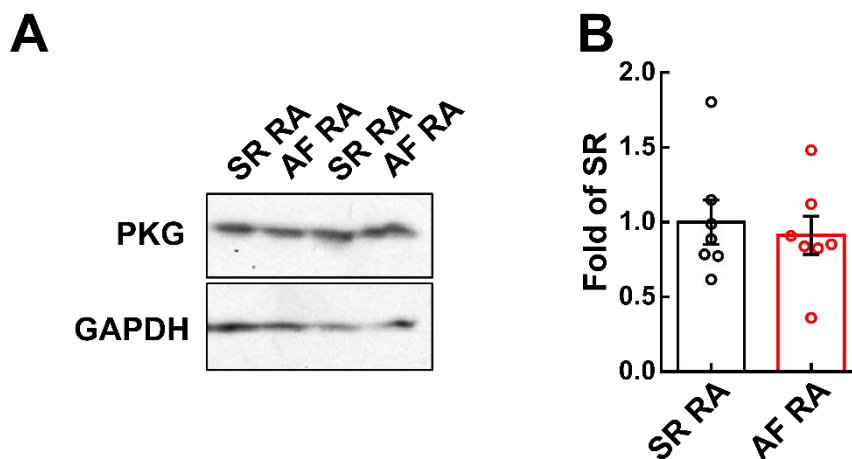


**Figure 3.2.10: Protein levels of cGMP effector protein kinase G (PKG) in human atrial tissue samples from right atrium (RA) of patients in sinus rhythm (SR) and with atrial fibrillation (AF).** **A**) Representative immunoblots of PKG protein in human atrial tissue. GAPDH was used as loading control. **B**) Quantification of the immunoblot experiments shown in A). Data are presented as mean ± SEM, significant differences at * p < 0.05, ** p< 0.01, *** p < 0.001.

# 4. Discussion

The discussion is divided into two sections. In the first part, the results of the project "Changes in mouse and human cardiomyocyte cGMP dynamics during hypoxic injury" are discussed (section 4.1). The second part of the discussion is based on the results the project "cGMP signalling in the human atrium and its role in atrial fibrillation" (section 4.2).

## 4.1 Changes in mouse and human cardiomyocyte cGMP dynamics during hypoxic injury

This part of the thesis aimed to uncover the changes in cardiomyocyte cGMP dynamics during hypoxic injury and to figure out whether the cGMP signalling cascade offers a potential therapeutic target for the treatment of hypoxic injury.

### 4.1.1 *In vitro* models of hypoxia/reoxygenation

In the first part of this project, an *in vitro* model of hypoxia/reoxygenation was used. *In vitro* models of hypoxic injury offer several advantages over *in vivo* models. *In vivo* models cover the whole complexity of the injury, however this makes it very difficult to uncouple the various interacting pathways [261]. *In vitro* models enable the control of individual external factors and isolated cardiomyocytes represent a powerful tool to distinguish between direct effects of the hypoxic injury on the cardiomyocyte itself and indirect mechanisms such as the influence of non-myocytes [261, 262].

Several studies have been done in the past using *in vitro* models of hypoxia/reoxygenation. Amongst them, most studies used immortalized cell lines such as embryonic rat ventricular H9c2 cardiomyoblasts [263, 264, 265] or mouse atrial HL-1 cells [266, 267]. However, these immortalized cell types do not fully reflect cardiac physiology. Besides differences in their cell death pathways and bioenergetics [261], these cells are not terminally differentiated as adult cardiomyocytes are and still continue to divide. In an adult heart, less than 1% of adult cardiomyocytes renew per year and during a normal life span less than 50% of cardiomyocytes are exchanged [268]. Furthermore, neonatal cardiomyocytes are more resistant to hypoxia compared to adult cardiomyocytes [262, 269, 270]. Since many cardiovascular diseases are present in the adult population, the use of adult cardiomyocytes can better reflect the physiological situation [262].

Most of the hypoxia/reoxygenation studies in isolated adult or neonatal cardiomyocytes were done in order to investigate different cardioprotective strategies against hypoxic injury such

as prevention of apoptosis [271, 272, 273] and $Ca^{2+}$ homoeostasis [274, 275, 276]. The cardioprotective second messenger cGMP has been shown to provide protection against ischemia/reperfusion injury in different *in vivo* models [166, 168, 182, 183], however not much is known about the cardioprotective role of cGMP during hypoxic injury alone. This has been due, at least in part, to the lack of suitable cGMP imaging and quantification techniques. Biochemical techniques such as immunoblot analysis, radioimmunoassay, and enzyme-linked immunosorbent assays which have been used in the past to investigate the cGMP signalling cascade all have the limitation that they do not allow to monitor real time cGMP dynamics under physiologically relevant conditions. Furthermore, they all require high amounts of cells or tissues [206].

In this thesis, transgenic mice with cardiomyocyte-specific expression of the FRET-based cGMP biosensor red-cGES-DE5 [136, 216] were used to isolate adult ventricular cardiomyocytes and monitor real time cGMP dynamics with high temporal and spatial resolution. Besides the cGMP-specific FRET sensors Yellow *Pf*PKG and Red *Pf*PKG [218], the red-cGES-DE5 biosensor [216] is the only so far available FRET sensor capable of measuring real time cGMP dynamics in adult cardiomyocytes. Other FRET-based cGMP biosensors such as the CGY-Del1 [219, 220], the Cynget sensors [221, 222] or the cGi family [223, 224, 225] are not usable in adult cardiomyocytes, either because they are not sensitive enough to detect the very low cGMP concentrations or because their cGMP/cAMP selectivity is too low. Until now the red-cGES-DE5 biosensor is the only sensor capable of measuring cGMP in adult cardiomyocytes for which transgenic sensor mice are available [136].

Transgenic mice with cardiomyocyte-specific cGMP FRET biosensor expression offer several advantages compared to adenovirus-mediated sensor expression [244, 277]. Usually, in order to achieve uniform biosensor expression by adenovirus-mediated gene transfer, cardiomyocytes need to be cultured for at least 48 h. Cardiomyocytes are well known to change during culturing. In addition to changes in cell morphology such as cell shortening, indistinct striations and reduction in t-tubule density, functional changes also occur, for example depolarization of the resting membrane potential [244, 278, 279]. An increased expression of the red-cGES-DE5 biosensor in the transgenic red-cGES-DE5 sensor mice in this work further facilitated the FRET based cGMP measurements in transgenic cardiomyocytes due to a reduction in the background noise (Figure 3.1.1).

At the beginning of the project it was shown that the *in vitro* hypoxia/reoxygenation model used for this work was functional. Hif-1$\alpha$, which is a clear marker for hypoxia [280] was significantly increased (Figure 3.1.2). However, one could argue that the upregulation of only 1.4-fold was too mild. There are two possible reasons for this. One could be the experimental setup. In order to induce hypoxia in the isolated ventricular cardiomyocytes, laminin-plated cardiomyocytes were put into a modular incubator chamber with low oxygen conditions

(1% $O_2$, 94% $N_2$, 5% $CO_2$). However, to be able to isolate RNA from those cells for gene expression analysis, the modular incubator chamber needs to be opened which starts reoxygenation. Harvesting the cells before lysis also takes some additional time. The regulation of hypoxia in the cell *via* Hif-1$\alpha$ is known to happen within a few minutes and the half-life time of HIF-1$\alpha$ protein is about 5 min [281, 282, 283, 284]. It could be possible that the time which was needed to harvest the cells and to lyse them was already long enough, to reduce Hif-1$\alpha$ mRNA level. Another explanation could be the so-called Hif-switch during chronic hypoxia. Besides Hif-1, Hif-2 and Hif-3 are also involved in hypoxia regulation. While Hif-1 is responsible for acute adaption to hypoxia, Hif-2 and Hif-3 expression begins during chronic hypoxia. Then, Hif-1 level is declining while Hif-2 and Hif-3 level increase [285, 286, 287]. It was shown in human umbilical vein endothelial cells exposed to 0.8% of $O_2$ that this switch between Hif-1$\alpha$ and Hif-2$\alpha$ started already after 2 h of hypoxia [285]. Therefore, it could be possible, that in the model used here, the Hif-switch started already during 4 h of hypoxia and Hif-1$\alpha$ level have already declined. Nevertheless, in addition to the significant increase in Hif-1$\alpha$ gene expression, the significant increase in cell death during hypoxia (Figure 3.1.2) clearly showed that the hypoxia/reoxygenation model used in this part of the thesis was functional.

### 4.1.2 Basal cGMP levels are increased after hypoxia/reoxygenation

In order to figure out whether hypoxia/reoxygenation affected the cGMP signalling cascade, basal cGMP levels were measured by two different methods, FRET and cGMP immunoassay. The significant increase in basal cGMP levels during hypoxia/reoxygenation (Figure 3.1.3) clearly showed that hypoxia/reoxygenation was causing a change in the regulation of cGMP signalling. cGMP concentration measurements in normoxic controls *via* FRET [250] (32 nM) as well as with cGMP immunoassay (55 nM) were in accordance with another study where the authors estimated basal cGMP levels to be ~10 nM in adult mouse cardiomyocytes [136].

Furthermore, it could be clearly shown in this work that the duration of hypoxia also plays an important role - the longer the hypoxia treatment, the more severe were the effects. The contradictory results of cGMP measurements done in two different studies in the past can now be explained with this finding. Whereas a model of anoxia in adult rat cardiomyocytes could show no change in cGMP levels neither after 30 min of anoxia, nor after 60 min of anoxia [188], a model of 2 h of sustained hypoxia in adult rat cardiomyocytes showed significantly increased cGMP levels [187]. It could be possible that the duration of hypoxia in the study of Geisbuhler and Schwager [188] was simply not long enough to increase cGMP levels, whereas the hypoxia duration in the study of Strijdom and colleagues was sufficient

[187]. Furthermore, both studies used radioimmunoassay as a method to determine cGMP concentrations. Radioimmunoassay requires high amounts of cells that need to be disrupted and measure only the total cyclic nucleotide concentrations [206, 250]. The FRET method can precisely report physiologically relevant free intracellular cGMP levels and is therefore more exact [250].

In order to understand the molecular mechanisms causing these severe increases in basal cGMP levels during hypoxia/reoxygenation, cGMP degrading PDEs as well as cGMP generating GCs were investigated. Several changes have been observed that are discussed in detail in the following sections.

**4.1.3 cGMP degradation by PDE3A is impaired after hypoxia/reoxygenation**

In this study, it could be shown for the first time that PDE3A protein levels are significantly reduced after hypoxia/reoxygenation (Figure 3.1.5) due to PDE3A protein instability (Figure 3.1.6). Furthermore, the cGMP-FRET response to PDE3 inhibition with Cilostamide was significantly impaired after hypoxia/reoxygenation (Figure 3.1.7).

PDE3 is the main PDE responsible for basal cGMP degradation in adult mouse ventricular cardiomyocytes [136] and it plays an important role in human cardiomyocytes as well [288, 289]. A significant downregulation of the cGMP-FRET response to PDE3 inhibition after hypoxia/reoxygenation indicates that PDE3 function is impaired which can cause detrimental changes in cGMP levels as shown in this work.

Several studies could demonstrate that administration of PDE3 inhibitors reduced infarct size when administered before ischemia/reperfusion injury [290, 291, 292]. Various signalling pathways have been proposed to explain the mechanism of how PDE3 inhibition can cause cardioprotection. One was the potentiation of the opening of cardioprotective mitochondrial $Ca^{2+}$-activated $K^+$ channels (mitoK$_{Ca}$) by PKA [293]. Interestingly, the cardioprotective role of the mitoK$_{Ca}$ channels [294, 295, 296] was also suggested to be linked to the cGMP/PKG signalling cascade [297]. Recently, the group of Robert Lukowski could show in an *in vivo* open chest model of ischemia/reperfusion injury, that increased cGMP levels provide cardioprotection *via* activation of mitochondrial mitoK$_{Ca}$ channels of the BK type by PKG [168].

Hypoxia/reoxygenation significantly increased cardiomyocyte cell death (Figure 3.1.2). It has been shown by multiple studies that apoptosis is increased in hypoxia/reoxygenation [271, 273, 298, 299]. A few years ago, PDE3 was shown to play a critical role in the regulation of cardiomyocyte apoptosis. A study by the group of Chen Yan could show that chronic inhibition of PDE3 activity by pharmacological agents or adenovirus-mediated knockdown of PDE3A in primary mouse cardiomyocytes promoted apoptosis. Isoprenaline or Angiotensin II

induced apoptosis caused by PDE3 downregulation could be completely blocked by restoring PDE3A *via* adenovirus-mediated gene delivery [255]. Furthermore, an *in vivo* model of ischemia/reperfusion injury demonstrated that transgenic mice with cardiomyocyte-specific overexpression of PDE3A1 were protected against ischemia/reperfusion injury by inhibition of cardiomyocyte apoptosis [257]. The authors suggested the so called PDE3A-ICER feedback loop as possible mechanism of how PDE3 reduction led to an increase in cellular apoptosis. The downregulation of PDE3A caused an upregulation of inducible cAMP early repressor (ICER), which in turn repressed PDE3A gene transcription. ICER plays a critical role in apoptosis regulation and can downregulate the apoptosis-regulating protein Bcl-2 which leads to increased apoptosis [256].

The question remains, which signalling pathway predominates at the end during hypoxia/reoxygenation injury, the cardioprotective cGMP/PKG signalling activated by the reduction of PDE3A or the increase in cardiomyocyte cell death probably caused by PDE3A reduction as well. The prevention of cell death during hypoxia/reoxygenation upon CNP pre-treatment (Figure 3.1.15) indicated that further increase in cardioprotective cGMP level could overrule the increase in cardiomyocyte apoptosis due to PDE3A downregulation. However, to be able to really answer this question in the future the use of cardiomyocyte-specific PDE3A knockout mice and a model of adenovirus-mediated cardiomyocyte-specific PDE3A overexpression could be very helpful.

Gene expression analysis revealed that *Pde3a* gene expression was not modulated during hypoxia/reoxygenation (Figure 3.1.5). Similar results were shown in primary superior cervical ganglia neuros. In those cells, *Pde3a* gene expression was not significantly changed after exposure to hypoxia compared to normoxic controls [300]. In contrast to that, another study showed that *PDE3A* gene expression was changed under hypoxic conditions. Transcriptomic analysis of right ventricular specimens of cyanotic children with tetralogy of Fallot exposed to chronic hypoxia during cardiac surgery revealed that *PDE3A* was more than 3-fold downregulated in cyanotic versus a-cyanotic children [301]. However, children with tetralogy of Fallot have severe congenital abnormalities which probably caused detrimental changes in the whole transcriptome already before exposure to hypoxia during surgery and it remains unclear how these changes affected *PDE3A* regulation.

cGMP and cAMP signalling can influence each other due to crosstalk regulation *via* dual-substrate PDEs such as PDE2 and PDE3 [66, 302]. It could be shown in this work, that the cGMP/cAMP crosstalk *via* PDE3 after natriuretic peptide stimulation was attenuated in cardiomyocytes exposed to hypoxia/reoxygenation due to impairment of PDE3 (Figure 3.1.8). This clearly showed that changes in cGMP dynamics during hypoxic injury could affect cAMP and consequently cAMP-related signalling pathways as well. However,

cGMP/cAMP crosstalk regulation is a very complex system involving many different factors which needs to be investigated in another project.

### 4.1.4 cGMP generating NO-GC is oxidized during hypoxia/reoxygenation

In this work, it was also found that hypoxia/reoxygenation caused oxidation of NO-GC in adult cardiomyocytes (Figure 3.1.12).

In mice NO-GC is responsible for basal cGMP production [136]. It is well established that a change in the redox equilibrium of NO-GC towards the oxidized form desensitizes NO-GC to NO, leading to a decrease in cGMP production [114]. The oxidation of NO-GC by oxidative stress has already been shown by several studies in the past. For example, it could be shown that NO-GC is oxidized to the NO-insensitive form in isolated monkey coronary arteries without endothelium exposed to hypoxia or hypoxia/reoxygenation [303]. Oxidative stress could also decrease NO-GC activity in rat aortic smooth muscle cells [304], and oxidative stress in a rat *in vivo* model could shift the redox equilibrium of NO-GC towards the oxidized form [252].

NO-GC$\beta_1$ protein was reduced after hypoxia/reoxygenation (Figure 3.1.9). A possible reason for this could be that oxidized NO-GC is prone to degradation [252, 305].

Several studies could observe a reduction in gene expression of *Gucy1a1* and *Gucy1b1* in addition to oxidation [252, 304, 306] which could not be seen in this project (Figure 3.1.9). One possible explanation for these discrepancies could be the duration of hypoxia and the severity of reactive oxygen species formation. In all studies in which a downregulation in NO-GC gene expression was shown, either direct administration of oxidative agents like ODQ [252] or $H_2O_2$ [304] or very long exposure to chronic hypoxia (72 h) [306] were used to induce oxidative stress. The relatively short hypoxia duration of 4 h in this study without concomitant administration of oxidative agents was probably not enough to decrease NO-GC gene expression.

### 4.1.5 FRET response to PDE3 inhibitor Cilostamide is impaired in cardiomyocytes from cardiomyocyte-specific NO-GC knockout mice after hypoxia/reoxygenation

Even in NO-GC knockout mice, were the main GC responsible for basal cGMP generation was knocked-out, cGMP levels were increased after hypoxia/reoxygenation. The reduced cGMP FRET response to PDE3 inhibitor Cilostamide in NO-GC knockout cardiomyocytes exposed to hypoxia/reoxygenation indicates that PDE3 activity is impaired after hypoxic injury (Figure 3.1.14). An additional reason for the increased basal cGMP levels could be the role of NP-GCs during hypoxia/reoxygenation. Under normoxic conditions, NP-GC only plays

a minor role in basal cGMP production [136]. However, hypoxia-sensitive elements were found in ANP, BNP, and CNP gene promoter sequences by several groups. Chen and colleagues reported a hypoxia stimulated increase in ANP gene expression and secretion in cultured atrial myocytes (AT-1 cells) [307]. Likewise, Chun and colleagues demonstrated that the activity of the ANP promoter was induced by hypoxia in H9c2 and neonatal cardiomyocytes [308]. Furthermore, Weidemann and colleagues could show that CNP is a specific HIF-1$\alpha$ target gene in a model of cultured rat cardiomyocytes exposed to hypoxia [309]. Therefore, it could be possible that increased natriuretic peptide production during hypoxia raises the cGMP production *via* NP-GC.

### 4.1.6 Validation of the results in an *ex vivo* whole heart Langendorff model of anoxic injury and an *in vivo* open chest model of ischemia/reperfusion injury

As already mentioned above, the use of an *in vitro* model of hypoxia/reoxygenation in isolated adult cardiomyocytes facilitated the investigation of the effects of hypoxia/reoxygenation on cGMP dynamics by eliminating other factors such as the influence of non-myocytes. All experiments discussed in the previous sections led to the conclusion that the cGMP signalling cascade is altered by hypoxia/reoxygenation due to impairment of PDE3 and the oxidation of NO-GC.

In order to figure out whether these findings could be validated in a more physiological context, an *ex vivo* whole heart Langendorff model of anoxic injury as well as an *in vivo* open chest model of ischemia/reperfusion injury were used. In both models, cGMP levels were increased after hypoxic injury (Figure 3.1.16 and Figure 3.1.17), and the impairment of PDE3 could be confirmed in the *in vivo* open chest model of ischemia/reperfusion injury (Figure 3.1.17). Both models offered several advantages which made them very useful for this study.

The *ex vivo* whole heart Langendorff model enabled the direct visualization of cGMP dynamics during anoxic injury, which was not possible in the *in vitro* model of hypoxia/reoxygenation. This was for the first time that cGMP dynamics were monitored in real time during hypoxic injury and offers a promising basis for further investigations.

However, this model also had several disadvantages. In the traditional Langendorff technique, which was used in this project, the mouse heart is exposed to the air during perfusion which can cause ischemia and changes in tissue temperature [310]. However, to enable FRET recordings during anoxic injury this setup was necessary. Furthermore, the stereomicroscope which was used for FRET recordings could only measure cGMP dynamics at the surface of the heart, but not deeper inside. It would be very interesting to be able to measure cGMP dynamics in different cell layers in the heart during anoxic injury. Another

highly discussed issue is the pH sensitivity of several FRET sensors limiting their use to setups with a physiological pH. For example, it is known that the fluorophores CFP and YFP are very sensitive to changes in pH [258, 259]. Unfortunately, it was not clear how big the pH change in the heart was during anoxia. However, the dramatic artificial effects of anoxia on Epac1-camps transgenic hearts (Supplemental Figure 5.2.3) indicated that there were some changes in pH inside the heart during anoxia. Unit now, it is not completely clear whether the FRET biosensor red-cGES-DE5 [216] is sensitive to changes in pH as well. However, it was shown that the absorption spectrum of T-Sapphire is very pH stable [311]. The influence of pH on Dimer2 remains unknown until now. Dimer2 is a mutational variant of DsRed [312] and at least for DsRed pH resistance has been shown [313].

The in *vivo-open* chest model of ischemia/reperfusion injury illustrated the whole complexity of the cardiovascular system. Unfortunately, so far, it was not possible to monitor cGMP dynamics directly during ischemia/reperfusion injury *in vivo*. In the future, it would be very interesting to establish a FRET setup which enables monitoring of real time cGMP dynamics during ischemia/reperfusion injury *in vivo*.

### 4.1.7 Translatability of the findings from mouse to human situation

Neither *in vitro* models of hypoxia/reoxygenation in adult mouse cardiomyocytes, nor *ex vivo* or *in vivo* mouse models of ischemic injury can recapitulate the human physiology [261]. Animal and human cardiomyocytes differ in many aspects, such as beating rate, myosin isoform predominance, and electrophysiological properties [261, 314]. These differences can affect cardiomyocyte response to hypoxia/reoxygenation and make it difficult to extrapolate results from animals to the human situation. [261].

The establishment of FRET-based cGMP measurements in human ventricular cardiomyocytes in this work (Figure 3.1.11) made it possible to check whether the findings of the effects of hypoxia/reoxygenation on the cGMP signalling cascade could be translated from mouse to human situation.

Several differences in the regulation of the cGMP signalling cascade between mouse and human were found. One difference was the ability of NO-donors like SNAP or NO-GC stimulators/activators to evoke a change in FRET ratio. Whereas NO donors as well as NO-GC stimulators/activators could evoke an increase in cGMP FRET in human ventricular cardiomyocytes (Figure 3.1.12 and Supplemental Figure 5.2.1), this was not possible in mouse cardiomyocytes (Figure 3.1.10) [136, 174], indicating a different role of distinct GCs in mouse and human.

Another difference between mouse and human ventricular cardiomyocytes which was not shown in this thesis is the PDE distribution. Whereas it is still highly discussed whether the

cGMP specific PDE5 is expressed in mouse ventricular cardiomyocytes or not [137, 171, 172], PDE5 could be shown to be expressed in human ventricular tissue [289]. Interestingly, whereas cGMP FRET measurements with PDE5 inhibitors such as Sildenafil in isolated mouse ventricular cardiomyocytes did not show any change in FRET signal [136], Sildenafil could evoke a clear increase cGMP FRET in human ventricular cardiomyocytes (Supplemental Figure 5.2.4).

Nevertheless, despite the differences in the cGMP signalling cascade between mouse and human, the detrimental effects of hypoxia/reoxygenation on PDE3 could be reproduced in human ventricular cardiomyocytes (Figure 3.1.18). The fact that PDE3A protein levels are also reduced in patients with ICM (Figure 3.1.19) makes the cGMP signalling cascade a promising target in the treatment of hypoxia/reoxygenation injury in the clinics.


### 4.1.8 Summary and conclusion

In summary, hypoxia/reoxygenation causes a significant increase in basal cGMP levels. Significant reduction of PDE3A protein levels due to protein instability under hypoxic conditions led to a reduction in the cGMP FRET response to the PDE3 specific inhibitor Cilostamide. Furthermore, NO-GC was oxidized during hypoxic injury. A schematic illustration of the effects of hypoxic injury on the cGMP signalling cascade in ventricular cardiomyocytes is shown in Figure 4.1.

These basic findings from an *in vitro* model of hypoxia/reoxygenation in isolated adult mouse ventricular cardiomyocytes could be validated in an *ex vivo* whole heart Langendorff model of anoxic injury as well as in an *in vivo* open chest model of ischemia/reperfusion injury. This clearly proves the physiological relevance of these findings. Reproducibility of the results in human ventricular cardiomyocytes demonstrated the potential of the cGMP signalling cascade as a potential target for the treatment of hypoxic injury in the clinics.

In conclusion it could be shown in this project that the cGMP signalling cascade could be a promising therapeutic target to treat hypoxia/reoxygenation injury in the clinics.
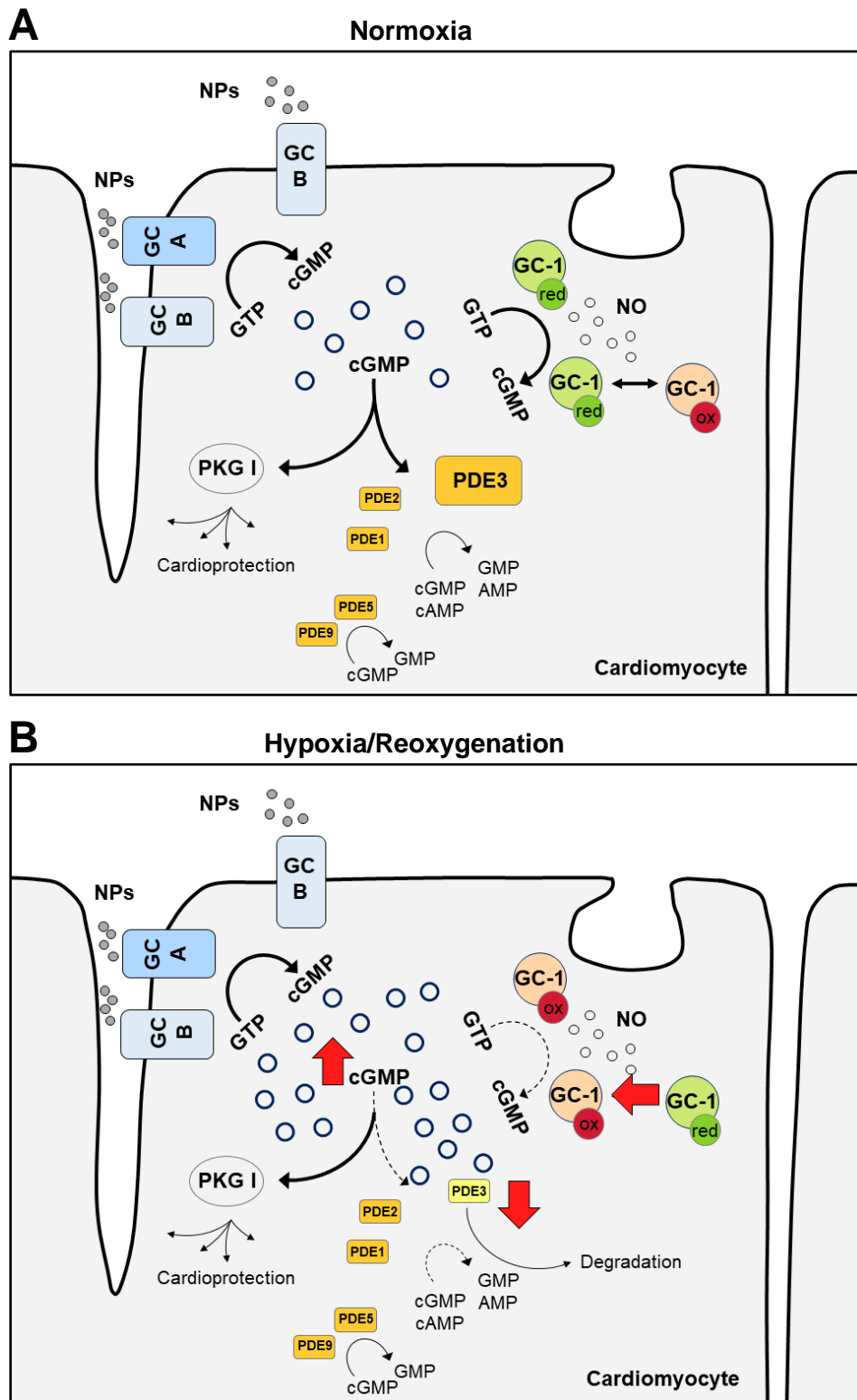
**Figure 4.1** **Schematic illustration of the effects of hypoxic injury on the cGMP signalling cascade in adult cardiomyocytes.** **A**) Under normoxic conditions, 3',5'-cyclic guanosine monophosphate (cGMP) is generated from guanosine triphosphate (GTP) by the natriuretic peptide (NP) stimulated guanylyl cyclases (NP-GCs) GC-A and GC-B, as well as by the nitric oxide (NO)-stimulated NO-GC GC-1. GC-1 can be present in the cardiomyocyte in a reduced (red) or oxidized (ox) state and is the main GC responsible for basal cGMP production. Phosphodiesterases (PDEs) degrade cGMP to guanosine monophosphate (GMP). Some of them are cGMP-specific, whereas

125

others are dual substrate PDEs and degrade both, cGMP and 3',5'-cyclic adoneosine monophosphate (cAMP). Under normoxic conditions, PDE3 is the main PDE responsible for basal cGMP degradation. Protein kinase G (PKG) is an important cGMP effector protein which has several phosphorylation targets in the cell that are known for their cardioprotective function. **B**) During hypoxia/reoxygenation, basal cGMP levels are increasing due to a reduction of PDE3A caused by protein instability. In addition to that, the redox equilibrium of GC-1 is shifted towards the oxidized, NO-insensitive form.

## 4.2 cGMP signalling in the human atrium and its role in atrial fibrillation

This part of the thesis was aimed to characterize the cGMP signalling cascade in human cardiomyocytes from RA and LA of patients in SR and with AF. The goal was to uncover the role of cGMP in AF and to answer the question whether the cGMP signalling cascade could be a potential therapeutic target for the treatment of AF.

### 4.2.1 Successful establishment of FRET-based cGMP measurements in human atrial cardiomyocytes

The FRET-based cGMP biosensor red-cGES-DE5 was initially developed to measure cGMP dynamics in adult cardiomyocytes under real time conditions with high temporal and spatial resolution [136, 216]. This sensor enabled several studies of global cGMP changes under physiologically relevant conditions in the cytosol [136, 172, 216, 217] as well as in the submembrane microdomain [228] of ventricular cardiomyocytes.

However, until now, cGMP dynamics in atrial cardiomyocytes are mostly unknown. Approximately 2500 genes are differentially regulated in atria and ventricle. Whereas ventricular cardiomyocytes preferentially express genes required for contraction and energy consumption, genes required for neurohumoral function are expressed more in atrial cardiomyocytes [315, 316, 317].

Furthermore, right and left atria also differ. Besides differences in shape [318], and structure, e.g. extracellular matrix proteins are higher expressed in the right atrium, whereas the microvascular density is higher in the left atrium [319], action potential durations are also different between right and left atrial cardiomyocytes [320]. In addition, there are indications that the differences in the gene expression pattern between right and left atria may be also relevant in atrial pathophysiology [321].

In this part of the thesis, FRET-based cGMP measurements were established in human atrial cardiomyocytes (Figure 3.2.1). Therefore, adenovirus-mediated red-cGES-DE5 biosensor expression was used. One might argue that the use of adenovirus-mediated gene transfer to express the red-cGES-DE5 biosensor in human atrial cardiomyocytes has several disadvantages e.g. long culture duration compared to the use of atrial cardiomyocytes from transgenic sensor mice. However, the use of primary human atrial cardiomyocytes offers several advantages compared to the use of mouse atrial cardiomyocytes. The most obvious one are the interspecies differences [261, 314]. As already mentioned above, one example are the differences in PDE distribution in mouse and human [128, 289]. Another reason is the limitation of good mouse models for AF. The pathophysiology of human AF is very complex, involving many factors such as patient status, genetics, and environmental influences [322].

Differences in size and electrophysiological properties of the mouse heart make it very difficult to reproduce the complex pathophysiology of clinical AF [322, 323, 324].

In order to reveal differences or similarities the cGMP signalling cascade regulation in cardiomyocytes of RA and LA of patients in SR and with AF, cGMP generating GCs, cGMP degrading PDEs, and cGMP effector protein PKG were investigated. Several changes have been observed that are discussed in detail in the following sections.

### 4.2.2 Role of NO-GC and NP-GC in right and left atrium of patients in sinus rhythm and with atrial fibrillation

First, cGMP production was analysed by treating atrial cardiomyocytes from RA and LA of patients in SR and with AF with the NO donor SNAP to stimulate NO-GC. Interestingly, stimulation with SNAP could equally increase cytosolic cGMP levels in cardiomyocytes from RA and LA of patients in SR and with AF (Figure 3.2.2).

A few years ago, Rotzmaritsa and colleagues investigated the effects of SNAP on L-type $Ca^{2+}$ currents ($I_{Ca, L}$) in atrial cardiomyocytes of patients in SR and with AF and could show that the cGMP induced increase in $I_{Ca,L}$ was attenuated in AF compared to SR [205]. One possible explanation for the different findings in SNAP response could be that cGMP signalling in cardiomyocytes is regulated in so-called microdomains to enable precise signalling [96, 152]. Whereas global cGMP changes in the bulk cytosol upon SNAP treatment were monitored in this work, Rozmaritsa and colleagues investigated the functional effects of SNAP induced cGMP increase on LTCCs [205] and it could be possible that this microdomain around the LTCCs is regulated differently.

It is known that NO levels are reduced in AF due to decreased NOS expression and change in subcellular NOS localization [203, 204, 325]. Maintaining NO levels to normal was suggested as one possible treatment option for AF [326, 327, 328]. The results of the FRET-based cGMP measurements in response to SNAP indicated that NO-GC is functional in AF and maintaining NO levels to normal in AF would definitely have an effect on NO-GC.

Immunoblot analysis of NO-GC$\alpha_1$ and NO-GC$\beta_1$ revealed a tendency towards downregulation of NO-GC$\beta_1$ protein (Figure 3.2.3). This could be a sign for oxidation of NO-GC during AF since oxidized NO-GC is prone for degradation [252, 305]. Oxidative stress has been associated with the development of AF in patients and animal models [329, 330, 331]. However, a clinical trial with systemic antioxidant therapy for arrhythmias failed [332]. Nevertheless, more targeted antioxidants such as mitochondria targeted antioxidants rather than general antioxidants seemed to be more promising in animal models of AF [333, 334, 335]. NO-GC activators have been shown to be cardioprotective in many different disease models in ventricular cardiomyocytes [165, 167, 168, 336]. However, until now their role in

the prevention of AF remains unknown. Thus, assuming that NO-GC is oxidized during AF, treatment with NO-GC activators would be a better treatment option to influence the cGMP signalling cascade than maintaining NO levels to normal since oxidized NO-GC is insensitive to NO.

The fact that human atrial cardiomyocytes responded to SNAP also indicated that there could be differences in the cGMP signalling regulation between mouse and human. It is known at least for ventricular cardiomyocytes that stimulation of NO-GC with NO donors like SNAP or NO-GC stimulators/activators could not evoke any increase in cytosolic cGMP levels measurable by either the cGMP sensor red-cGES-DE5 [136] (Figure 3.1.10), or the cGMP sensor cGi500 [174], whereas stimulation of human ventricular cardiomyocytes with SNAP or NO-GC stimulators/activators could evoke a cGMP FRET response (Figure 3.1.12 and Supplemental Figure 5.2.1). Unfortunately, it has never been tested whether NO donors or NO-GC stimulators/activators can evoke a change in cGMP FRET in mouse atrial cardiomyocytes. Therefore, the assumption that there are differences between mouse and human atrial cardiomyocytes in response to NO donors and NO-GC stimulators/activators remains speculative.

Treatment of cardiomyocytes from RA and LA of patients in SR and with AF with the natriuretic peptide CNP to stimulate GC-B revealed that in contrast to NO-GC, the cGMP FRET response of GC-B was different (Figure 3.2.4).

The CNP receptor GC-B was shown to play a protective role in the development of Angiotensin II induced AF [337] and GC-B knockout mice had increased susceptibility to develop AF [338]. Interestingly, GC-B stimulation by CNP was much stronger in cardiomyocytes from RA compared to LA from patients in SR. However, studies analysing gene expression analysis could not reveal any significant changes in *Npr1*, *Npr2*, and *Npr3* gene expression in right and left atria of mice [337], rat and human heart [339]. GC-A and GC-B receptors can be desensitized under high natriuretic peptide concentrations [340, 341, 342]. Unfortunately, it is not known whether CNP concentrations differ between cardiomyocytes from RA and LA. Higher CNP levels in LA compared to RA could explain the reduced cGMP FRET response to CNP in SR LA by desensitization of GC-B.

Nevertheless, AF is associated with high ANP and BNP levels [343, 344, 345, 346] and N-terminal proBNP can be used a predictor of incident AF [343]. Interestingly, in cardiomyocytes from AF LA stimulation of GC-A with ANP could not evoke any increase in intracellular cGMP, whereas it could in cardiomyocytes from SR RA (Supplemental Figure 5.3.1). This could be due to desensitization of GC-A in AF caused by high natriuretic peptide concentrations.

Another very interesting finding was that in cardiomyocytes from patients with AF, blocking of PDEs with the unspecific PDE inhibitor IBMX after CNP stimulation could further raise cGMP levels in AF RA cardiomyocytes whereas it reduced cGMP levels in cardiomyocytes from AF LA. IBMX is a broadband unselective PDE inhibitor, however it does not inhibit PDE8 and PDE9 [120]. The regulation of cGMP levels *via* PDEs is very complex, since dual-substrate PDEs cause a crosstalk regulation between cGMP and cAMP [66]. More experiments would be necessary in the future to understand the molecular mechanism leading to the different effects of IBMX after CNP stimulation in AF RA and AF LA. However, many molecular changes that confer AF are known to be more pronounced in the left atrial tissue [324], and this could be one of them.

### 4.2.3 Role of cGMP degrading phosphodiesterases in right and left atrium of patients in sinus rhythm and with atrial fibrillation

This part of the discussion will focus on the differences in cGMP degrading PDEs between right and left atria first before continuing with the differences in PDEs between SR and AF.

Analysis of the cGMP FRET response to different PDE inhibitors in human atrial cardiomyocytes from RA and LA of patients in SR revealed that whereas FRET response to PDE3 inhibitor Cilostamide was equal between RA and LA (Figure 3.2.7), FRET response to PDE5 inhibitor Sildenafil was higher in RA than in LA (Figure 3.2.9). Unfortunately, because of the low availability of SR LA tissue, not enough measurements could be done with the PDE2 selective inhibitor Bay 60-7550 to be able to make a clear statement about the role of PDE2 in SR LA cardiomyocytes. However, FRET response to PDE2 inhibitor was measurable in SR RA (Figure 3.2.5).

Until now, not much is known about the differences in cGMP hydrolysing PDE activity between right and left human atria. The group of Rodolphe Fischmeister could show with patch-clamp recordings in human atrial cardiomyocytes that both, PDE2 [347], and PDE3 [348] control basal L-type $Ca^{2+}$ current ($I_{Ca,L}$) and that both contribute to keep the cyclic nucleotide concentration at minimum in the absence of AC or GC stimulation [347]. Another group could confirm the role of PDE3 in $I_{Ca,L}$ regulation [205].

Gene expression analysis of *PDE1A*, *PDE1C*, *PDE3A*, and *PDE3B* could show no differences between RA and LA of patients in SR. However, *PDE2A* was significantly upregulated in LA compared to RA (Garnier, Bork et al., 2020, in preparation). Unfortunately, no gene expression studies on *PDE5* expression have ever been done yet in human atria. However, it could be shown at least in human ventricular tissue samples, that PDE5 is expressed. Here, PDE1 and PDE3 were shown to be primarily responsible for cGMP hydrolysing activity, whereas the effect of PDE5 was only minor [288, 289].

The increase in cGMP FRET ratio upon stimulation of the cells with the PDE3 specific inhibitor Cilostamide was preserved in AF in both RA and LA cardiomyocytes (Figure 3.2.7). Berk and colleagues could show the same in contractile force measurements in trabeculae from patients in SR or with paroxysmal and persistent AF. PDE3 inhibition with PDE3 inhibitor Cilostamide similarly potentiated the inotropic effects of Serotonin in all three groups [349]. The effect of PDE3 inhibition to enhance $I_{Ca,L}$ current in human atrial cardiomyocytes could also be shown to be preserved in AF [205]. In this work, PDE3 protein remained unchanged in RA of patients in SR and with AF (Figure 3.2.8). Contrary to that, *PDE3A* gene expression was shown to be reduced in human atria with AF compared to SR (Garnier, Bork et al., 2020, in preparation).

The cGMP FRET response to PDE2 inhibition was higher in both, AF RA and AF LA compared to SR RA (Figure 3.2.5). However, gene expression analysis of *PDE2A* could reveal no differences between SR and AF (Garnier, Bork et al., 2020, in preparation).

The increase in cytosolic cGMP upon PDE5 inhibition with the PDE5 selective inhibitor Sildenafil was regulated differently between RA and LA. Whereas the increase in cGMP FRET ratio in AF RA was lower than in SR RA, it was higher in AF LA than in SR LA (Figure 3.2.9). It is known that Sildenafil can inhibit PDE1C at higher concentrations [260] and PDE1 is known to be expressed in the human atrium [350]. Unfortunately, there was no PDE1 selective inhibitor available in the lab to investigate the effects of PDE1 inhibition on basal cGMP levels. However, the trend in FRET response was the same at low concentrations of Sildenafil which inhibited only PDE5 and at high concentrations were PDE1C was inhibited as well. This indicated that PDE1 activity was not significantly changed between SR and AF.

As already mentioned above, many molecular changes that confer AF are known to be more pronounced in the left atrial tissue [324]. Here, it could be shown that the change in cGMP FRET upon PDE2 as well as PDE5 inhibition was much higher in AF LA than in AF RA cardiomyocytes, indicating that they could be involved in the regulation of AF.

### 4.2.4 cGMP effector protein PKG in right atrium of patients in sinus rhythm and with atrial fibrillation

No differences in PKG protein level were found between SR RA and AF RA (Figure 3.2.10). Another study could show that PKG is strongly expressed in human atrial cardiomyocytes, however, the authors did not investigate changes between RA and LA [351]. In rabbit atrial cardiomyocytes, PKG was shown to mediate the stimulation of LTCC current ($I_{Ca,L}$) [352]. $I_{Ca;L}$ has been shown to be modified as a consequence of AF [353, 354, 355, 356]. However, whether and how PKG could modify $I_{Ca,L}$ in human AF remains unknown until now.

**4.2.5 Summary and conclusion**

In summary, the characterization of the cGMP signalling cascade in human atrial cardiomyocytes of RA and LA from patients in SR and with AF provided important insights about cGMP regulation.

It could be shown that both, NO-GC and NP-GC are involved in cGMP generation in human atrial cardiomyocytes. Whereas the increase in cytosolic cGMP levels upon NO-GC stimulation was comparable between RA and LA of patients in SR and with AF, the cGMP FRET response upon stimulation of NP-GC with CNP was different. PDE2, PDE3, PDE5, and possibly PDE1 are involved in cGMP degradation in human atrial cardiomyocytes. The increase in cytosolic cGMP levels upon treatment with a PDE3 specific inhibitor was shown to be equal between RA and LA of patients in SR and with AF. In contrast to that, the FRET response to PDE2 and PDE5 inhibition was very different. A schematic illustration of the cGMP signalling cascade in human RA and LA cardiomyocytes from patients in SR and with AF is shown in Figure 4.2.

In conclusion it could be shown in this project that the cGMP signalling cascade might offer promising therapeutic targets in the treatment of AF.
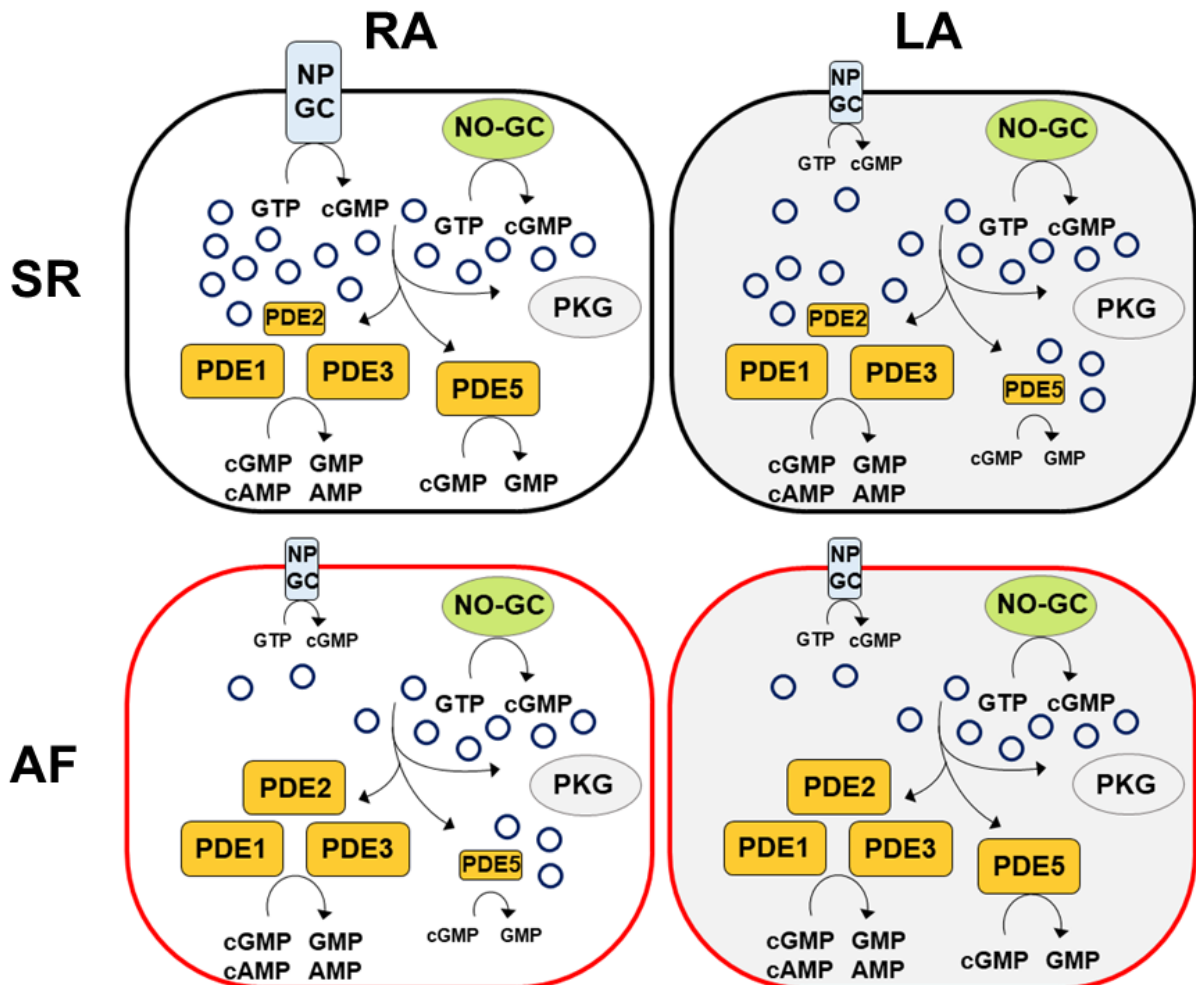
**Figure 4.2** **Schematic illustration of cGMP signalling in the human atrium and its role in atrial fibrillation.** It could be shown in this project, that 3',5'-cyclic guanosine monophosphate (cGMP, shown as blue circles in the figure) in cardiomyocytes of right (RA) and left atria (LA) of patients in sinus rhythm (SR) and with atrial fibrillation (AF) is generated from guanosine triphosphate (GTP) by two different types of guanylyl cyclases (GCs), the membrane bound, natriuretic peptide-stimulated-GCs (NP-GCs), and the soluble, nitric oxide (NO)-stimulated GCs (NO-GCs). However, whereas the increase in cytosolic cGMP levels upon NO-GC stimulation is comparable in cardiomyocytes of RA and LA of patients in SR and with AF (indicated by equal sizes of NO-GC in the schematic illustration), the effects on cGMP levels upon NP-GC stimulation are different (indicated by different sizes of NP-GC in the schematic illustration). cGMP is degraded to guanosine monophosphate (GMP) by phosphodiesterases (PDEs). It could be shown here, that PDE1, PDE2, PDE3, and PDE5 are involved in cGMP degradation in human atrial cardiomyocytes. Whereas the increase in basal cGMP levels upon PDE3 inhibition is comparable in all the conditions (indicated by equal sizes of PDE3 in the schematic illustration), the cGMP FRET responses upon PDE2 and PDE5 inhibition are different (indicated by different sizes of PDE2 and PDE5 in the schematic illustration).

# Bibliography

[1] Collaborators GBDCoD. Global, regional, and national age-sex-specific mortality for 282 causes of death in 195 countries and territories, 1980-2017: a systematic analysis for the Global Burden of Disease Study 2017. Lancet. 2018;392(10159):1736-1788.

[2] Group WCRCW. World Health Organization cardiovascular disease risk charts: revised models to estimate risk in 21 global regions. Lancet Glob Health. 2019;7(10):e1332-e1345.

[3] Timmis A, Townsend N, Gale CP, Torbica A, Lettino M, Petersen SE, et al. European Society of Cardiology: Cardiovascular Disease Statistics 2019. Eur Heart J. 2020;41(1):12-85.

[4] Roth GA, Johnson C, Abajobir A, Abd-Allah F, Abera SF, Abyu G, et al. Global, Regional, and National Burden of Cardiovascular Diseases for 10 Causes, 1990 to 2015. J Am Coll Cardiol. 2017;70(1):1-25.

[5] Collaborators GMaCoD. Global, regional, and national age-sex specific all-cause and cause-specific mortality for 240 causes of death, 1990-2013: a systematic analysis for the Global Burden of Disease Study 2013. Lancet. 2015;385(9963):117-171.

[6] Criteria IoMUCoSSCD.  Cardiovascular Disability: Updating the Social Security Listings. Washington (DC)2010.

[7] Ahmadi A, Stone GW, Leipsic J, Shaw LJ, Villines TC, Kern MJ, et al. Prognostic Determinants of Coronary Atherosclerosis in Stable Ischemic Heart Disease. Circ Res. 2016;119(2):317-329.

[8] Morley RL, Sharma A, Horsch AD, Hinchliffe RJ. Peripheral artery disease. BMJ. 2018;360:j5842.

[9] Criqui MH, Aboyans V. Epidemiology of Peripheral Artery Disease. Circ Res. 2015;116(9):1509-1526.

[10] Hoffman J. The global burden of congenital heart disease. Cardiovasc J Afr. 2013;24(4):141-145.

[11] Mrsic Z, Hopkins SP, Antevil JL, Mullenix PS. Valvular Heart Disease. Prim Care. 2018;45(1):81-94.

[12] Maheshwari V, Barr B, Srivastava M. Acute Valvular Heart Disease. Cardiol Clin. 2018;36(1):115-127.

[13] Tanai E, Frantz S. Pathophysiology of Heart Failure. Compr Physiol. 2015;6(1):187-214.

[14] McMurray JJ, Pfeffer MA. Heart failure. Lancet. 2005;365(9474):1877-1889.

[15] Lu L, Sun R, Liu M, Zheng Y, Zhang P. The Inflammatory Heart Diseases: Causes, Symptoms, and Treatments. Cell Biochem Biophys. 2015;72(3):851-855.

[16] Fung G, Luo H, Qiu Y, Yang D, McManus B. Myocarditis. Circ Res. 2016;118(3):496-514.

[17] Heijman J, Guichard JB, Dobrev D, Nattel S. Translational Challenges in Atrial Fibrillation. Circ Res. 2018;122(5):752-773.

[18] Ferreira C, Providencia R, Ferreira MJ, Goncalves LM. Atrial Fibrillation and Non-cardiovascular Diseases: A Systematic Review. Arq Bras Cardiol. 2015;105(5):519-526.

[19] (IHME). IfHMaE. Findings from the Global Burden of Disease Study 2017. IHME. 2018.

[20] Ostadal B, Ostadalova I, Kolar F, Sedmera D. Developmental determinants of cardiac sensitivity to hypoxia. Can J Physiol Pharm. 2014;92(7):566-574.

[21] Kolar F, Ostadal B. Molecular mechanisms of cardiac protection by adaptation to chronic hypoxia. Physiol Res. 2004;53 Suppl 1:S3-13.

[22] Handley MG, Medina RA, Nagel E, Blower PJ, Southworth R. PET imaging of cardiac hypoxia: opportunities and challenges. J Mol Cell Cardiol. 2011;51(5):640-650.

[23] Azzouzi HE, Leptidis S, Doevendans PA, De Windt LJ. HypoxamiRs: regulators of cardiac hypoxia and energy metabolism. Trends Endocrinol Metab. 2015;26(9):502-508.

[24] Semenza GL. Hypoxia-Inducible Factor 1 and Cardiovascular Disease. Annu Rev Physiol. 2014;76(1):39-56.

[25] Gupta N, Ashraf MZ. Hyoxia Signalling in Cardiovascular Diseases2018.

[26] Lee JW, Ko J, Ju C, Eltzschig HK. Hypoxia signaling in human diseases and therapeutic targets. Exp Mol Med. 2019;51(6):68.

[27]     Lopaschuk GD, Collins-Nakai RL, Itoi T. Developmental changes in energy substrate use by the heart. Cardiovasc Res. 1992;26(12):1172-1180.

[28]     Pei JM, Kravtsov GM, Wu S, Das R, Fung ML, Wong TM. Calcium homeostasis in rat cardiomyocytes during chronic hypoxia: a time course study. Am J Physiol Cell Physiol. 2003;285(6):C1420-1428.

[29]     Pei J-M, Zhou J-J, Bian J-S, Yu X-C, Fung M-L, Wong T-M. Impaired [Ca2+]i and pHi responses to κ-opioid receptor stimulation in the heart of chronically hypoxic rats. Am J Physiol Cell Physiol. 2000;279(5):C1483-C1494.

[30]     Gauthier LD, Greenstein JL, Cortassa S, O'Rourke B, Winslow RL. A computational model of reactive oxygen species and redox balance in cardiac mitochondria. Biophys J. 2013;105(4):1045-1056.

[31]     Giordano FJ. Oxygen, oxidative stress, hypoxia, and heart failure. J Clin Invest. 2005;115(3):500-508.

[32]     NobelMedia AB. The Nobel Prize in Physiology or Medicine 2019. . Nobel Media AB. 2019;Sat. 15 Feb 2020.

[33]     Abe H, Semba H, Takeda N. The Roles of Hypoxia Signaling in the Pathogenesis of Cardiovascular Diseases. J Atheroscler Thromb. 2017;24(9):884-894.

[34]     Bishop T, Ratcliffe PJ. HIF hydroxylase pathways in cardiovascular physiology and medicine. Circ Res. 2015;117(1):65-79.

[35]     D'Ignazio L, Batie M, Rocha S. Hypoxia and Inflammation in Cancer, Focus on HIF and NF-kappaB. Biomedicines. 2017;5(2).

[36]     Dengler VL, Galbraith M, Espinosa JM. Transcriptional regulation by hypoxia inducible factors. Crit Rev Biochem Mol Biol. 2014;49(1):1-15.

[37]     Nakayama K, Kataoka N. Regulation of Gene Expression under Hypoxic Conditions. Int J Mol Sci. 2019;20(13).

[38]     Fukuda R, Zhang H, Kim JW, Shimoda L, Dang CV, Semenza GL. HIF-1 regulates cytochrome oxidase subunits to optimize efficiency of respiration in hypoxic cells. Cell. 2007;129(1):111-122.

[39]     Semenza GL. Regulation of metabolism by hypoxia-inducible factor 1. Cold Spring Harb Symp Quant Biol. 2011;76:347-353.

[40]     D'Ignazio L, Rocha S. Hypoxia Induced NF-kappaB. Cells. 2016;5(1).

[41]     Koong AC, Chen EY, Giaccia AJ. Hypoxia causes the activation of nuclear factor kappa B through the phosphorylation of I kappa B alpha on tyrosine residues. Cancer Res. 1994;54(6):1425-1430.

[42]     Culver C, Sundqvist A, Mudie S, Melvin A, Xirodimas D, Rocha S. Mechanism of hypoxia-induced NF-kappaB. Mol Cell Biol. 2010;30(20):4901-4921.

[43]     Chugh SS, Havmoeller R, Narayanan K, Singh D, Rienstra M, Benjamin EJ, et al. Worldwide epidemiology of atrial fibrillation: a Global Burden of Disease 2010 Study. Circulation. 2014;129(8):837-847.

[44]     Andrade JG, Macle L, Nattel S, Verma A, Cairns J. Contemporary Atrial Fibrillation Management: A Comparison of the Current AHA/ACC/HRS, CCS, and ESC Guidelines. Can J Cardiol. 2017;33(8):965-976.

[45]     Lubitz SA, Benjamin EJ, Ruskin JN, Fuster V, Ellinor PT. Challenges in the classification of atrial fibrillation. Nat Rev Cardiol. 2010;7(8):451-460.

[46]     Wakili R, Voigt N, Kaab S, Dobrev D, Nattel S. Recent advances in the molecular pathophysiology of atrial fibrillation. J Clin Invest. 2011;121(8):2955-2968.

[47]     Nattel S, Burstein B, Dobrev D. Atrial remodeling and atrial fibrillation: mechanisms and implications. Circ Arrhythm Electrophysiol. 2008;1(1):62-73.

[48]     Nattel S. New ideas about atrial fibrillation 50 years on. Nature. 2002;415(6868):219-226.

[49]     Chaudhry GM, Haffajee CI. Antiarrhythmic agents and proarrhythmia. Crit Care Med. 2000;28(10 Suppl):N158-164.

[50]   Barman M. Proarrhythmic Effects Of Antiarrhythmic Drugs: Case Study Of Flecainide Induced Ventricular Arrhythmias During Treatment Of Atrial Fibrillation. J Atr Fibrillation. 2015;8(4):1091.

[51]   Miller JM, Olgin JE, Das MK. Atrial fibrillation: what are the targets for intervention? J Interv Card Electrophysiol. 2003;9(2):249-257.

[52]   Maan A, Mansour M, McManus DD, Patel VV, Cheng A, Ruskin JN, et al. Novel therapeutic targets in the management of atrial fibrillation. Am J Cardiovasc Drugs. 2014;14(6):403-421.

[53]   Newton AC, Bootman MD, Scott JD. Second Messengers. Cold Spring Harb Perspect Biol. 2016;8(8).

[54]   Beavo JA, Brunton LL. Cyclic nucleotide research -- still expanding after half a century. Nat Rev Mol Cell Biol. 2002;3(9):710-718.

[55]   Eisner DA, Caldwell JL, Kistamas K, Trafford AW. Calcium and Excitation-Contraction Coupling in the Heart. Circ Res. 2017;121(2):181-195.

[56]   Neef S, Maier LS. Remodeling of excitation-contraction coupling in the heart: inhibition of sarcoplasmic reticulum Ca(2+) leak as a novel therapeutic approach. Curr Heart Fail Rep. 2007;4(1):11-17.

[57]   Bers DM. Cardiac excitation-contraction coupling. Nature. 2002;415(6868):198-205.

[58]   Bers DM. Calcium cycling and signaling in cardiac myocytes. Annu Rev Physiol. 2008;70:23-49.

[59]   Anderson ME, Braun AP, Schulman H, Premack BA. Multifunctional Ca2+/calmodulin-dependent protein kinase mediates Ca(2+)-induced enhancement of the L-type Ca2+ current in rabbit ventricular myocytes. Circ Res. 1994;75(5):854-861.

[60]   Davis BA, Schwartz A, Samaha FJ, Kranias EG. Regulation of cardiac sarcoplasmic reticulum calcium transport by calcium-calmodulin-dependent phosphorylation. J Biol Chem. 1983;258(22):13587-13591.

[61]   Witcher DR, Kovacs RJ, Schulman H, Cefali DC, Jones LR. Unique phosphorylation site on the cardiac ryanodine receptor regulates calcium channel activity. J Biol Chem. 1991;266(17):11144-11152.

[62]   Wagner S, Dybkova N, Rasenack EC, Jacobshagen C, Fabritz L, Kirchhof P, et al. Ca2+/calmodulin-dependent protein kinase II regulates cardiac Na+ channels. J Clin Invest. 2006;116(12):3127-3138.

[63]   Bers DM. Adrenergic Fight-or-Flight: S-NO Falls on PKA Targets. Circ Res. 2015;117(9):747-749.

[64]   Scott JD, Santana LF. A-kinase anchoring proteins: getting to the heart of the matter. Circulation. 2010;121(10):1264-1271.

[65]   Zaccolo M. cAMP signal transduction in the heart: understanding spatial control for the development of novel therapeutic strategies. Br J Pharmacol. 2009;158(1):50-60.

[66]   Zaccolo M, Movsesian MA. cAMP and cGMP Signaling Cross-Talk: Role of Phosphodiesterases and Implications for Cardiac Pathophysiology. Circ Res. 2007;100(11):1569-1578.

[67]   Zhang M, Kass DA. Phosphodiesterases and cardiac cGMP: evolving roles and controversies. Trends Pharmacol Sci. 2011;32(6):360-365.

[68]   Hartzell HC, Fischmeister R. Opposite effects of cyclic GMP and cyclic AMP on Ca2+ current in single heart cells. Nature. 1986;323(6085):273-275.

[69]   Lalli MJ, Shimizu S, Sutliff RL, Kranias EG, Paul RJ. [Ca2+]i homeostasis and cyclic nucleotide relaxation in aorta of phospholamban-deficient mice. Am J Physiol. 1999;277(3):H963-970.

[70]   Colyer J. Phosphorylation states of phospholamban. Ann N Y Acad Sci. 1998;853:79-91.

[71]   Blumenthal DK, Stull JT, Gill GN. Phosphorylation of cardiac troponin by guanosine 3':5'-monophosphate-dependent protein kinase. J Biol Chem. 1978;253(2):324-326.

[72]   Layland J, Solaro RJ, Shah AM. Regulation of cardiac contractile function by troponin I phosphorylation. Cardiovasc Res. 2005;66(1):12-21.

[73]   Burgoyne JR, Eaton P. Oxidant sensing by protein kinases a and g enables integration of cell redox state with phosphoregulation. Sensors (Basel). 2010;10(4):2731-2751.

[74]    Conti M, Beavo J. Biochemistry and physiology of cyclic nucleotide phosphodiesterases: essential components in cyclic nucleotide signaling. Annu Rev Biochem. 2007;76:481-511.

[75]    Lukowski R, Krieg T, Rybalkin SD, Beavo J, Hofmann F. Turning on cGMP-dependent pathways to treat cardiac dysfunctions: boom, bust, and beyond. Trends Pharmacol Sci. 2014;35(8):404-413.

[76]    Frantz S, Klaiber M, Baba HA, Oberwinkler H, Volker K, Gabetaner B, et al. Stress-dependent dilated cardiomyopathy in mice with cardiomyocyte-restricted inactivation of cyclic GMP-dependent protein kinase I. Eur Heart J. 2013;34(16):1233-1244.

[77]    Mohan P, Brutsaert DL, Paulus WJ, Sys SU. Myocardial contractile response to nitric oxide and cGMP. Circulation. 1996;93(6):1223-1229.

[78]    Klabunde RE, Tse J, Weiss HR. Guanylyl cyclase inhibition reduces contractility and decreases cGMP and cAMP in isolated rat hearts. Cardiovasc Res. 1998;37(3):676-683.

[79]    Oliver PM, Fox JE, Kim R, Rockman HA, Kim HS, Reddick RL, et al. Hypertension, cardiac hypertrophy, and sudden death in mice lacking natriuretic peptide receptor A. Proc Natl Acad Sci U S A. 1997;94(26):14730-14735.

[80]    Lopez MJ, Wong SK, Kishimoto I, Dubois S, Mach V, Friesen J, et al. Salt-resistant hypertension in mice lacking the guanylyl cyclase-A receptor for atrial natriuretic peptide. Nature. 1995;378(6552):65-68.

[81]    Friebe A, Sandner P, Schmidtko A. cGMP: a unique 2nd messenger molecule - recent developments in cGMP research and development. Naunyn Schmiedebergs Arch Pharmacol. 2019.

[82]    Tsai EJ, Kass DA. Cyclic GMP signaling in cardiovascular pathophysiology and therapeutics. Pharmacol Ther. 2009;122(3):216-238.

[83]    Ashman DF, Lipton R, Melicow MM, Price TD. Isolation of adenosine 3', 5'-monophosphate and guanosine 3', 5'-monophosphate from rat urine. Biochem Biophys Res Commun. 1963;11:330-334.

[84]    Hardman JG, Sutherland EW. Guanyl cyclase, an enzyme catalyzing the formation of guanosine 3',5'-monophosphate from guanosine trihosphate. J Biol Chem. 1969;244(23):6363-6370.

[85]    Schultz G, Bohme E, Munske K. Guanyl cyclase. Determination of enzyme activity. Life Sci. 1969;8(24):1323-1332.

[86]    White AA, Aurbach GD. Detection of guanyl cyclase in mammalian tissues. Biochim Biophys Acta. 1969;191(3):686-697.

[87]    Potter LR, Abbey-Hosch S, Dickey DM. Natriuretic peptides, their receptors, and cyclic guanosine monophosphate-dependent signaling functions. Endocr Rev. 2006;27(1):47-72.

[88]    Montfort WR, Wales JA, Weichsel A. Structure and Activation of Soluble Guanylyl Cyclase, the Nitric Oxide Sensor. Antioxid Redox Signal. 2017;26(3):107-121.

[89]    Kuhn M. Molecular Physiology of Membrane Guanylyl Cyclase Receptors. Physiol Rev. 2016;96(2):751-804.

[90]    Kuhn M. Structure, regulation, and function of mammalian membrane guanylyl cyclase receptors, with a focus on guanylyl cyclase-A. Circ Res. 2003;93(8):700-709.

[91]    Nishizawa H, Matsuda M, Yamada Y, Kawai K, Suzuki E, Makishima M, et al. Musclin, a novel skeletal muscle-derived secretory factor. J Biol Chem. 2004;279(19):19391-19395.

[92]    Thomas G, Moffatt P, Salois P, Gaumond MH, Gingras R, Godin E, et al. Osteocrin, a novel bone-specific secreted protein that modulates the osteoblast phenotype. J Biol Chem. 2003;278(50):50563-50571.

[93]    Woods RL. Cardioprotective functions of atrial natriuretic peptide and B-type natriuretic peptide: a brief review. Clin Exp Pharmacol Physiol. 2004;31(11):791-794.

[94]    de Bold AJ, Bruneau BG, Kuroski de Bold ML. Mechanical and neuroendocrine regulation of the endocrine heart. Cardiovasc Res. 1996;31(1):7-18.

[95]    Del Ry S, Cabiati M, Lionetti V, Emdin M, Recchia FA, Giannessi D. Expression of C-type natriuretic peptide and of its receptor NPR-B in normal and failing heart. Peptides. 2008;29(12):2208-2215.

[96]    Bork NI, Molina CE, Nikolaev VO. cGMP signalling in cardiomyocyte microdomains. Biochem Soc Trans. 2019;47(5):1327-1339.

[97]    McFarlane SI, Winer N, Sowers JR. Role of the Natriuretic Peptide System in Cardiorenal Protection. Arch Intern Med. 2003;163(22):2696-2704.

[98]    Hayashi D, Kudoh S, Shiojima I, Zou Y, Harada K, Shimoyama M, et al. Atrial natriuretic peptide inhibits cardiomyocyte hypertrophy through mitogen-activated protein kinase phosphatase-1. Biochem Biophys Res Commun. 2004;322(1):310-319.

[99]    Holtwick R, van Eickels M, Skryabin BV, Baba HA, Bubikat A, Begrow F, et al. Pressure-independent cardiac hypertrophy in mice with cardiomyocyte-restricted inactivation of the atrial natriuretic peptide receptor guanylyl cyclase-A. J Clin Invest. 2003;111(9):1399-1407.

[100]   Kishimoto I, Rossi K, Garbers DL. A genetic model provides evidence that the receptor for atrial natriuretic peptide (guanylyl cyclase-A) inhibits cardiac ventricular myocyte hypertrophy. Proc Natl Acad Sci U S A. 2001;98(5):2703-2706.

[101]   Rosenkranz AC, Woods RL, Dusting GJ, Ritchie RH. Antihypertrophic actions of the natriuretic peptides in adult rat cardiomyocytes: importance of cyclic GMP. Cardiovasc Res. 2003;57(2):515-522.

[102]   Rosenkranz AC, Hood SG, Woods RL, Dusting GJ, Ritchie RH. B-type natriuretic peptide prevents acute hypertrophic responses in the diabetic rat heart: importance of cyclic GMP. Diabetes. 2003;52(9):2389-2395.

[103]   Soeki T, Kishimoto I, Okumura H, Tokudome T, Horio T, Mori K, et al. C-type natriuretic peptide, a novel antifibrotic and antihypertrophic agent, prevents cardiac remodeling after myocardial infarction. J Am Coll Cardiol. 2005;45(4):608-616.

[104]   Ponikowski P, Voors AA, Anker SD, Bueno H, Cleland JGF, Coats AJS, et al. 2016 ESC Guidelines for the diagnosis and treatment of acute and chronic heart failure: The Task Force for the diagnosis and treatment of acute and chronic heart failure of the European Society of Cardiology (ESC)Developed with the special contribution of the Heart Failure Association (HFA) of the ESC. European Heart Journal. 2016;37(27):2129-2200.

[105]   Kita S, Nishizawa H, Okuno Y, Tanaka M, Yasui A, Matsuda M, et al. Competitive binding of musclin to natriuretic peptide receptor 3 with atrial natriuretic peptide. J Endocrinol. 2009;201(2):287-295.

[106]   Jhund PS, McMurray JJ. The neprilysin pathway in heart failure: a review and guide on the use of sacubitril/valsartan. Heart. 2016;102(17):1342-1347.

[107]   Evgenov OV, Pacher P, Schmidt PM, Hasko G, Schmidt HH, Stasch JP. NO-independent stimulators and activators of soluble guanylate cyclase: discovery and therapeutic potential. Nat Rev Drug Discov. 2006;5(9):755-768.

[108]   Friebe A, Koesling D. Regulation of Nitric Oxide-Sensitive Guanylyl Cyclase. Circ Res. 2003;93(2):96.

[109]   Russwurm M, Wittau N, Koesling D. Guanylyl cyclase/PSD-95 interaction: targeting of the nitric oxide-sensitive alpha2beta1 guanylyl cyclase to synaptic membranes. J Biol Chem. 2001;276(48):44647-44652.

[110]   Russwurm M, Behrends S, Harteneck C, Koesling D. Functional properties of a naturally occurring isoform of soluble guanylyl cyclase. Biochemical Journal. 1998;335(1):125.

[111]   Zabel U, Hausler C, Weeger M, Schmidt HH. Homodimerization of soluble guanylyl cyclase subunits. Dimerization analysis using a glutathione s-transferase affinity tag. J Biol Chem. 1999;274(26):18149-18152.

[112]   Koglin M, Vehse K, Budaeus L, Scholz H, Behrends S. Nitric oxide activates the beta 2 subunit of soluble guanylyl cyclase in the absence of a second subunit. J Biol Chem. 2001;276(33):30737-30743.

[113] Wagner C, Russwurm M, Jager R, Friebe A, Koesling D. Dimerization of nitric oxide-sensitive guanylyl cyclase requires the alpha 1 N terminus. J Biol Chem. 2005;280(18):17687-17693.

[114] Shah RC, Sanker S, Wood KC, Durgin BG, Straub AC. Redox regulation of soluble guanylyl cyclase. Nitric Oxide. 2018;76:97-104.

[115] Shah AM, MacCarthy PA. Paracrine and autocrine effects of nitric oxide on myocardial function. Pharmacol Ther. 2000;86(1):49-86.

[116] Carnicer R, Crabtree MJ, Sivakumaran V, Casadei B, Kass DA. Nitric oxide synthases in heart failure. Antioxid Redox Signal. 2013;18(9):1078-1099.

[117] Baillie GS, Tejeda GS, Kelly MP. Therapeutic targeting of 3',5'-cyclic nucleotide phosphodiesterases: inhibition and beyond. Nat Rev Drug Discov. 2019;18(10):770-796.

[118] Sutherland EW, Rall TW. Fractionation and characterization of a cyclic adenine ribonucleotide formed by tissue particles. J Biol Chem. 1958;232(2):1077-1091.

[119] Butcher RW, Sutherland EW. Adenosine 3',5'-phosphate in biological materials. I. Purification and properties of cyclic 3',5'-nucleotide phosphodiesterase and use of this enzyme to characterize adenosine 3',5'-phosphate in human urine. J Biol Chem. 1962;237:1244-1250.

[120] Bender AT, Beavo JA. Cyclic nucleotide phosphodiesterases: molecular regulation to clinical use. Pharmacol Rev. 2006;58(3):488-520.

[121] Miller CL, Yan C. Targeting cyclic nucleotide phosphodiesterase in the heart: therapeutic implications. J Cardiovasc Transl Res. 2010;3(5):507-515.

[122] Rybalkin SD, Hinds TR, Beavo JA. Enzyme assays for cGMP hydrolyzing phosphodiesterases. Methods Mol Biol. 2013;1020:51-62.

[123] Bobin P, Belacel-Ouari M, Bedioune I, Zhang L, Leroy J, Leblais V, et al. Cyclic nucleotide phosphodiesterases in heart and vessels: A therapeutic perspective. Arch Cardiovasc Dis. 2016;109(6-7):431-443.

[124] Chen S, Zhang Y, Lighthouse JK, Mickelsen DM, Wu J, Yao P, et al. A Novel Role of Cyclic Nucleotide Phosphodiesterase 10A in Pathological Cardiac Remodeling and Dysfunction. Circulation. 2019.

[125] Goraya TA, Cooper DM. Ca2+-calmodulin-dependent phosphodiesterase (PDE1): current perspectives. Cell Signal. 2005;17(7):789-797.

[126] Fischmeister R, Castro L, Abi-Gerges A, Rochais F, Vandecasteele G. Species- and tissue-dependent effects of NO and cyclic GMP on cardiac ion channels. Comparative Biochemistry and Physiology Part A: Molecular & Integrative Physiology. 2005;142(2):136-143.

[127] Patrucco E, Albergine MS, Santana LF, Beavo JA. Phosphodiesterase 8A (PDE8A) regulates excitation-contraction coupling in ventricular myocytes. J Mol Cell Cardiol. 2010;49(2):330-333.

[128] Richter W, Xie M, Scheitrum C, Krall J, Movsesian MA, Conti M. Conserved expression and functions of PDE4 in rodent and human heart. Basic Res Cardiol. 2011;106(2):249-262.

[129] Knight WE, Yan C. Cardiac cyclic nucleotide phosphodiesterases: function, regulation, and therapeutic prospects. Horm Metab Res. 2012;44(10):766-775.

[130] Lee DI, Zhu G, Sasaki T, Cho G-S, Hamdani N, Holewinski R, et al. Phosphodiesterase 9A controls nitric-oxide-independent cGMP and hypertrophic heart disease. Nature. 2015;519(7544):472-476.

[131] Sonnenburg WK, Seger D, Beavo JA. Molecular cloning of a cDNA encoding the "61-kDa" calmodulin-stimulated cyclic nucleotide phosphodiesterase. Tissue-specific expression of structurally related isoforms. J Biol Chem. 1993;268(1):645-652.

[132] Kincaid RL, Stith-Coleman IE, Vaughan M. Proteolytic activation of calmodulin-dependent cyclic nucleotide phosphodiesterase. J Biol Chem. 1985;260(15):9009-9015.

[133] Lee DI, Kass DA. Phosphodiesterases and cyclic GMP regulation in heart muscle. Physiology (Bethesda). 2012;27(4):248-258.

[134] Mongillo M, Tocchetti CG, Terrin A, Lissandron V, Cheung YF, Dostmann WR, et al. Compartmentalized phosphodiesterase-2 activity blunts beta-adrenergic cardiac inotropy via an NO/cGMP-dependent pathway. Circ Res. 2006;98(2):226-234.

[135]   Houslay MD, Milligan G. Tailoring cAMP-signalling responses through isoform multiplicity. Trends Biochem Sci. 1997;22(6):217-224.

[136]   Götz K, Sprenger J, Perera RK, Steinbrecher JH, Lehnart SE, Kuhn M, et al. Transgenic Mice for Real Time Visualization of cGMP in Intact Adult Cardiomyocytes. Circ Res. 2014.

[137]   Lukowski R, Rybalkin SD, Loga F, Leiss V, Beavo JA, Hofmann F. Cardiac hypertrophy is not amplified by deletion of cGMP-dependent protein kinase I in cardiomyocytes. Proc Natl Acad Sci U S A. 2010;107(12):5646-5651.

[138]   Hofmann F. A concise discussion of the regulatory role of cGMP kinase I in cardiac physiology and pathology. Basic Res Cardiol. 2018;113(4):31.

[139]   Layland J, Li JM, Shah AM. Role of cyclic GMP-dependent protein kinase in the contractile response to exogenous nitric oxide in rat cardiac myocytes. J Physiol. 2002;540(Pt 2):457-467.

[140]   Heximer SP, Watson N, Linder ME, Blumer KJ, Hepler JR. RGS2/G0S8 is a selective inhibitor of Gqalpha function. Proc Natl Acad Sci U S A. 1997;94(26):14389-14393.

[141]   Tang M, Wang G, Lu P, Karas RH, Aronovitz M, Heximer SP, et al. Regulator of G-protein signaling-2 mediates vascular smooth muscle relaxation and blood pressure. Nat Med. 2003;9(12):1506-1512.

[142]   Takimoto E, Koitabashi N, Hsu S, Ketner EA, Zhang M, Nagayama T, et al. Regulator of G protein signaling 2 mediates cardiac compensation to pressure overload and antihypertrophic effects of PDE5 inhibition in mice. J Clin Invest. 2009;119(2):408-420.

[143]   Heximer SP, Knutsen RH, Sun X, Kaltenbronn KM, Rhee MH, Peng N, et al. Hypertension and prolonged vasoconstrictor signaling in RGS2-deficient mice. J Clin Invest. 2003;111(4):445-452.

[144]   Surks HK, Mochizuki N, Kasai Y, Georgescu SP, Tang KM, Ito M, et al. Regulation of myosin phosphatase by a specific interaction with cGMP- dependent protein kinase Ialpha. Science. 1999;286(5444):1583-1587.

[145]   Fukao M, Mason HS, Britton FC, Kenyon JL, Horowitz B, Keef KD. Cyclic GMP-dependent protein kinase activates cloned BKCa channels expressed in mammalian cells by direct phosphorylation at serine 1072. J Biol Chem. 1999;274(16):10927-10935.

[146]   Schlossmann J, Ammendola A, Ashman K, Zong X, Huber A, Neubauer G, et al. Regulation of intracellular calcium by a signalling complex of IRAG, IP3 receptor and cGMP kinase Ibeta. Nature. 2000;404(6774):197-201.

[147]   Rybalkin SD, Yan C, Bornfeldt KE, Beavo JA. Cyclic GMP Phosphodiesterases and Regulation of Smooth Muscle Function. Circ Res. 2003;93(4):280-291.

[148]   Samuel S, Zhang K, Tang YD, Gerdes AM, Carrillo-Sepulveda MA. Triiodothyronine Potentiates Vasorelaxation via PKG/VASP Signaling in Vascular Smooth Muscle Cells. Cell Physiol Biochem. 2017;41(5):1894-1904.

[149]   Shi W, Wymore R, Yu H, Wu J, Wymore RT, Pan Z, et al. Distribution and prevalence of hyperpolarization-activated cation channel (HCN) mRNA expression in cardiac tissues. Circ Res. 1999;85(1):e1-6.

[150]   Scicchitano P, Carbonara S, Ricci G, Mandurino C, Locorotondo M, Bulzis G, et al. HCN channels and heart rate. Molecules. 2012;17(4):4225-4235.

[151]   Mazzolini M, Arcangeletti M, Marchesi A, Napolitano LMR, Grosa D, Maity S, et al. The gating mechanism in cyclic nucleotide-gated ion channels. Sci Rep. 2018;8(1):45.

[152]   Bork NI, Nikolaev VO. cGMP Signaling in the Cardiovascular System-The Role of Compartmentation and Its Live Cell Imaging. Int J Mol Sci. 2018;19(3).

[153]   Colucci WS, Elkayam U, Horton DP, Abraham WT, Bourge RC, Johnson AD, et al. Intravenous nesiritide, a natriuretic peptide, in the treatment of decompensated congestive heart failure. Nesiritide Study Group. N Engl J Med. 2000;343(4):246-253.

[154]   O'Connor CM, Starling RC, Hernandez AF, Armstrong PW, Dickstein K, Hasselblad V, et al. Effect of nesiritide in patients with acute decompensated heart failure. N Engl J Med. 2011;365(1):32-43.

[155] Dickey DM, Dries DL, Margulies KB, Potter LR. Guanylyl cyclase (GC)-A and GC-B activities in ventricles and cardiomyocytes from failed and non-failed human hearts: GC-A is inactive in the failed cardiomyocyte. J Mol Cell Cardiol. 2012;52(3):727-732.

[156] Jourdain P, Jondeau G, Funck F, Gueffet P, Le Helloco A, Donal E, et al. Plasma brain natriuretic peptide-guided therapy to improve outcome in heart failure: the STARS-BNP Multicenter Study. J Am Coll Cardiol. 2007;49(16):1733-1739.

[157] Lainchbury JG, Troughton RW, Strangman KM, Frampton CM, Pilbrow A, Yandle TG, et al. N-terminal pro-B-type natriuretic peptide-guided treatment for chronic heart failure: results from the BATTLESCARRED (NT-proBNP-Assisted Treatment To Lessen Serial Cardiac Readmissions and Death) trial. J Am Coll Cardiol. 2009;55(1):53-60.

[158] Tokudome T, Horio T, Soeki T, Mori K, Kishimoto I, Suga S, et al. Inhibitory effect of C-type natriuretic peptide (CNP) on cultured cardiac myocyte hypertrophy: interference between CNP and endothelin-1 signaling pathways. Endocrinology. 2004;145(5):2131-2140.

[159] Izumiya Y, Araki S, Usuku H, Rokutanda T, Hanatani S, Ogawa H. Chronic C-Type Natriuretic Peptide Infusion Attenuates Angiotensin II-Induced Myocardial Superoxide Production and Cardiac Remodeling. Int J Vasc Med. 2012;2012:246058.

[160] Eiringhaus J, Wuensche C, Herting J, Hasenfuss G, Sossalla S, Fischer T. P3829Antiarrhythmic effects of Sacubitrilat (LBQ657) on Ca2+ homeostasis in ventricular cardiomyocytes. European Heart Journal. 2019;40(Supplement_1).

[161] McMurray JJ, Packer M, Desai AS, Gong J, Lefkowitz MP, Rizkala AR, et al. Angiotensin-neprilysin inhibition versus enalapril in heart failure. N Engl J Med. 2014;371(11):993-1004.

[162] McMurray JJ, Packer M, Desai AS, Gong J, Lefkowitz MP, Rizkala AR, et al. Dual angiotensin receptor and neprilysin inhibition as an alternative to angiotensin-converting enzyme inhibition in patients with chronic systolic heart failure: rationale for and design of the Prospective comparison of ARNI with ACEI to Determine Impact on Global Mortality and morbidity in Heart Failure trial (PARADIGM-HF). Eur J Heart Fail. 2013;15(9):1062-1073.

[163] McMurray JJ, Packer M, Desai AS, Gong J, Lefkowitz M, Rizkala AR, et al. Baseline characteristics and treatment of patients in prospective comparison of ARNI with ACEI to determine impact on global mortality and morbidity in heart failure trial (PARADIGM-HF). Eur J Heart Fail. 2014;16(7):817-825.

[164] Sandner P, Zimmer DP, Milne GT, Follmann M, Hobbs A, Stasch JP. Soluble Guanylate Cyclase Stimulators and Activators. Handb Exp Pharmacol. 2019.

[165] Irvine JC, Ganthavee V, Love JE, Alexander AE, Horowitz JD, Stasch JP, et al. The soluble guanylyl cyclase activator bay 58-2667 selectively limits cardiomyocyte hypertrophy. PLoS One. 2012;7(11):e44481.

[166] Bice JS, Keim Y, Stasch JP, Baxter GF. NO-independent stimulation or activation of soluble guanylyl cyclase during early reperfusion limits infarct size. Cardiovasc Res. 2014;101(2):220-228.

[167] Frankenreiter S, Groneberg D, Kuret A, Krieg T, Ruth P, Friebe A, et al. Cardioprotection by ischemic postconditioning and cyclic guanosine monophosphate-elevating agents involves cardiomyocyte nitric oxide-sensitive guanylyl cyclase. Cardiovascular Research. 2018;114(6):822-829.

[168] Frankenreiter S, Bednarczyk P, Kniess A, Bork NI, Straubinger J, Koprowski P, et al. cGMP-Elevating Compounds and Ischemic Conditioning Provide Cardioprotection Against Ischemia and Reperfusion Injury via Cardiomyocyte-Specific BK Channels. Circulation. 2017;136(24):2337-2355.

[169] Takimoto E, Champion HC, Li M, Belardi D, Ren S, Rodriguez ER, et al. Chronic inhibition of cyclic GMP phosphodiesterase 5A prevents and reverses cardiac hypertrophy. Nat Med. 2005;11(2):214-222.

[170] Hsu S, Nagayama T, Koitabashi N, Zhang M, Zhou L, Bedja D, et al. Phosphodiesterase 5 inhibition blocks pressure overload-induced cardiac hypertrophy independent of the calcineurin pathway. Cardiovasc Res. 2009;81(2):301-309.

[171] Rybalkin SD, Shimizu M, Rybalkina IG, Patrucco E, Bible K, Minami E, et al. Differential effects of PDE5 inhibitors on cardiac dysfunction in the MDX ouse model of Duchenne muscular dystrophy. BMC Pharmacol Toxico. 2013;14(Suppl 1):O38-O38.

[172] Straubinger J, Schottle V, Bork N, Subramanian H, Dunnes S, Russwurm M, et al. Sildenafil Does Not Prevent Heart Hypertrophy and Fibrosis Induced by Cardiomyocyte Angiotensin II Type 1 Receptor Signaling. J Pharmacol Exp Ther. 2015;354(3):406-416.

[173] Shuhaibar LC, Egbert JR, Norris RP, Lampe PD, Nikolaev VO, Thunemann M, et al. Intercellular signaling via cyclic GMP diffusion through gap junctions restarts meiosis in mouse ovarian follicles. Proc Natl Acad Sci U S A. 2015;112(17):5527-5532.

[174] Menges L, Krawutschke C, Fuchtbauer EM, Fuchtbauer A, Sandner P, Koesling D, et al. Mind the gap (junction): cGMP induced by nitric oxide in cardiac myocytes originates from cardiac fibroblasts. Br J Pharmacol. 2019;176(24):4696-4707.

[175] Redfield MM, Chen HH, Borlaug BA, Semigran MJ, Lee KL, Lewis G, et al. Effect of phosphodiesterase-5 inhibition on exercise capacity and clinical status in heart failure with preserved ejection fraction: a randomized clinical trial. JAMA. 2013;309(12):1268-1277.

[176] Andersen MJ, Ersboll M, Axelsson A, Gustafsson F, Hassager C, Kober L, et al. Sildenafil and diastolic dysfunction after acute myocardial infarction in patients with preserved ejection fraction: the Sildenafil and Diastolic Dysfunction After Acute Myocardial Infarction (SIDAMI) trial. Circulation. 2013;127(11):1200-1208.

[177] Knight WE, Chen S, Zhang Y, Oikawa M, Wu M, Zhou Q, et al. PDE1C deficiency antagonizes pathological cardiac remodeling and dysfunction. Proc Natl Acad Sci U S A. 2016;113(45):E7116-E7125.

[178] Miller CL, Oikawa M, Cai Y, Wojtovich AP, Nagel DJ, Xu X, et al. Role of Ca2+/calmodulin-stimulated cyclic nucleotide phosphodiesterase 1 in mediating cardiomyocyte hypertrophy. Circ Res. 2009;105(10):956-964.

[179] Miller CL, Cai Y, Oikawa M, Thomas T, Dostmann WR, Zaccolo M, et al. Cyclic nucleotide phosphodiesterase 1A: a key regulator of cardiac fibroblast activation and extracellular matrix remodeling in the heart. Basic Res Cardiol. 2011;106(6):1023-1039.

[180] Baliga RS, Preedy MEJ, Dukinfield MS, Chu SM, Aubdool AA, Bubb KJ, et al. Phosphodiesterase 2 inhibition preferentially promotes NO/guanylyl cyclase/cGMP signaling to reverse the development of heart failure. Proc Natl Acad Sci U S A. 2018;115(31):E7428-E7437.

[181] Nakamura T, Ranek MJ, Lee DI, Shalkey Hahn V, Kim C, Eaton P, et al. Prevention of PKG1alpha oxidation augments cardioprotection in the stressed heart. J Clin Invest. 2015;125(6):2468-2472.

[182] Methner C, Buonincontri G, Hu CH, Vujic A, Kretschmer A, Sawiak S, et al. Riociguat reduces infarct size and post-infarct heart failure in mouse hearts: insights from MRI/PET imaging. PLoS One. 2013;8(12):e83910.

[183] Salloum FN, Das A, Samidurai A, Hoke NN, Chau VQ, Ockaili RA, et al. Cinaciguat, a novel activator of soluble guanylate cyclase, protects against ischemia/reperfusion injury: role of hydrogen sulfide. Am J Physiol Heart Circ Physiol. 2012;302(6):H1347-1354.

[184] Depré C, Hue L. Cyclic GMP in the perfused rat heart Effect of ischaemia, anoxia and nitric oxide synthase inhibitor. FEBS Letters. 1994;345(2–3):241-245.

[185] Nesher R, Robinson WF, Gibb L, Bishop SP, Kruger FA. Cyclic nucleotide levels in the perfused rat heart subjected to hypoxia. Experientia. 1977;33(2):215-217.

[186] Agullo L, Garcia-Dorado D, Inserte J, Paniagua A, Pyrhonen P, Llevadot J, et al. L-arginine limits myocardial cell death secondary to hypoxia-reoxygenation by a cGMP-dependent mechanism. Am J Physiol. 1999;276(5 Pt 2):H1574-1580.

[187] Strijdom H, Genade S, Lochner A. Nitric Oxide synthase (NOS) does not contribute to simulated ischaemic preconditioning in an isolated rat cardiomyocyte model. Cardiovasc Drugs Ther. 2004;18(2):99-112.

[188]   Geisbuhler TP, Schwager TL. Effect of anoxia on cyclic nucleotides and inositol phosphate turnover in cardiac myocytes. J Mol Cell Cardiol. 1996;28(9):1857-1866.

[189]   Mizuno K, Ogawa K. Increased concentration of plasma cyclic GMP during aconitine-induced atrial fibrillation in dogs and paroxysmal atrial fibrillation in patients. J Cardiovasc Pharmacol. 1981;3(6):1211-1220.

[190]   Ogawa K, Mizuno K. Increased concentration of plasma cyclic GMP from aconitine-induced atrial fibrillation in dogs and patients with paroxysmal atrial fibrillation. Adv Myocardiol. 1982;3:177-183.

[191]   Hirata Y, Nozaki A, Toda I, Murakawa Y, Sugimoto T, Matsuoka H, et al. Plasma concentration of atrial natriuretic polypeptide in patients with atrial tachycardia. Jpn Heart J. 1987;28(1):53-61.

[192]   Nakaoka H, Imataka K, Kitahara Y, Fujii J, Ishibashi M, Yamaji T. Relationship between plasma levels of atrial natriuretic peptide and cyclic guanosine monophosphate in patients with heart diseases. Jpn Circ J. 1988;52(1):30-34.

[193]   Czekalski S, Widecka K, Gozdzik J, Ciechanowski K, Krzyzanowska-Swiniarska B, Gromniak E, et al. Atrial natriuretic peptide and cyclic guanosine monophosphate plasma concentrations in patients with thyrotoxicosis and atrial fibrillation. Effect of short-term methimazole therapy. J Endocrinol Invest. 1994;17(5):341-346.

[194]   Lechleitner P, Genser N, Hauptlorenz S, Putensen C, Mitterschiffthaler G, Artner-Dworzak E, et al. [Values of atrial natriuretic peptide (ANP) and cyclic guanosine monophosphate (cGMP) in cardioversion]. Z Kardiol. 1991;80(9):574-579.

[195]   Hodgson-Zingman DM, Karst ML, Zingman LV, Heublein DM, Darbar D, Herron KJ, et al. Atrial natriuretic peptide frameshift mutation in familial atrial fibrillation. N Engl J Med. 2008;359(2):158-165.

[196]   Menon A, Hong L, Savio-Galimberti E, Sridhar A, Youn SW, Zhang M, et al. Electrophysiologic and molecular mechanisms of a frameshift NPPA mutation linked with familial atrial fibrillation. J Mol Cell Cardiol. 2019;132:24-35.

[197]   Cheng C, Liu H, Tan C, Tong D, Zhao Y, Liu X, et al. Mutation in NPPA causes atrial fibrillation by activating inflammation and cardiac fibrosis in a knock-in rat model. FASEB J. 2019;33(8):8878-8891.

[198]   Pérez-Hernández M, Matamoros M, Barana A, Amorós I, Gómez R, Núñez M, et al. Pitx2c increases in atrial myocytes from chronic atrial fibrillation patients enhancing IKs and decreasing ICa,L. Cardiovasc Res. 2015;109(3):431-441.

[199]   Gudbjartsson DF, Arnar DO, Helgadottir A, Gretarsdottir S, Holm H, Sigurdsson A, et al. Variants conferring risk of atrial fibrillation on chromosome 4q25. Nature. 2007;448(7151):353-357.

[200]   Gore-Panter SR, Hsu J, Hanna P, Gillinov AM, Pettersson G, Newton DW, et al. Atrial Fibrillation associated chromosome 4q25 variants are not associated with PITX2c expression in human adult left atrial appendages. PLoS One. 2014;9(1):e86245.

[201]   Chinchilla A, Daimi H, Lozano-Velasco E, Dominguez JN, Caballero R, Delpon E, et al. PITX2 insufficiency leads to atrial electrical and structural remodeling linked to arrhythmogenesis. Circ Cardiovasc Genet. 2011;4(3):269-279.

[202]   Suffee N, Moore-Morris T, Farahmand P, Rucker-Martin C, Dilanian G, Fradet M, et al. Atrial natriuretic peptide regulates adipose tissue accumulation in adult atria. Proc Natl Acad Sci U S A. 2017;114(5):E771-E780.

[203]   Cai H, Li Z, Goette A, Mera F, Honeycutt C, Feterik K, et al. Downregulation of endocardial nitric oxide synthase expression and nitric oxide production in atrial fibrillation: potential mechanisms for atrial thrombosis and stroke. Circulation. 2002;106(22):2854-2858.

[204]   Reilly SN, Liu X, Carnicer R, Recalde A, Muszkiewicz A, Jayaram R, et al. Up-regulation of miR-31 in human atrial fibrillation begets the arrhythmia by depleting dystrophin and neuronal nitric oxide synthase. Sci Transl Med. 2016;8(340):340ra374.

[205]   Rozmaritsa N, Christ T, Van Wagoner DR, Haase H, Stasch JP, Matschke K, et al. Attenuated response of L-type calcium current to nitric oxide in atrial fibrillation. Cardiovasc Res. 2014;101(3):533-542.

[206]   Sprenger JU, Nikolaev VO. Biophysical techniques for detection of cAMP and cGMP in living cells. Int J Mol Sci. 2013;14(4):8025-8046.

[207]   Piggott LA, Hassell KA, Berkova Z, Morris AP, Silberbach M, Rich TC. Natriuretic peptides and nitric oxide stimulate cGMP synthesis in different cellular compartments. J Gen Physiol. 2006;128(1):3-14.

[208]   Castro LR, Verde I, Cooper DM, Fischmeister R. Cyclic guanosine monophosphate compartmentation in rat cardiac myocytes. Circulation. 2006;113(18):2221-2228.

[209]   Bork NI, Nikolaev VO. Receptor-Cyclic Nucleotide Microdomains in the Heart. In: Nikolaev V, Zaccolo M, editors. Microdomains in the Cardiovascular System. Cham: Springer International Publishing; 2017. p. 3-15.

[210]   Förster T. Zwischenmolekulare Energiewanderung und Fluoreszenz. Annalen der Physik. 1948;437(1-2):55-75.

[211]   Zaccolo M. Use of chimeric fluorescent proteins and fluorescence resonance energy transfer to monitor cellular responses. Circ Res. 2004;94(7):866-873.

[212]   Wu P, Brand L. Resonance energy transfer: methods and applications. Anal Biochem. 1994;218(1):1-13.

[213]   Clegg RM. Fluorescence resonance energy transfer. Curr Opin Biotechnol. 1995;6(1):103-110.

[214]   Hochreiter B, Garcia AP, Schmid JA. Fluorescent proteins as genetically encoded FRET biosensors in life sciences. Sensors (Basel). 2015;15(10):26281-26314.

[215]   Iancu RV, Ramamurthy G, Warrier S, Nikolaev VO, Lohse MJ, Jones SW, et al. Cytoplasmic cAMP concentrations in intact cardiac myocytes. Am J Physiol Cell Physiol. 2008;295(2):C414-422.

[216]   Niino Y, Hotta K, Oka K. Simultaneous Live Cell Imaging Using Dual FRET Sensors with a Single Excitation Light. PLoS ONE. 2009;4(6):e6036.

[217]   Belge C, Hammond J, Dubois-Deruy E, Manoury B, Hamelet J, Beauloye C, et al. Enhanced expression of beta3-adrenoceptors in cardiac myocytes attenuates neurohormone-induced hypertrophic remodeling through nitric oxide synthase. Circulation. 2014;129(4):451-462.

[218]   Calamera G, Li D, Ulsund AH, Kim JJ, Neely OC, Moltzau LR, et al. FRET-based cyclic GMP biosensors measure low cGMP concentrations in cardiomyocytes and neurons. Commun Biol. 2019;2:394.

[219]   Sato M, Hida N, Ozawa T, Umezawa Y. Fluorescent indicators for cyclic GMP based on cyclic GMP-dependent protein kinase Ialpha and green fluorescent proteins. Anal Chem. 2000;72(24):5918-5924.

[220]   Nikolaev VO, Gambaryan S, Lohse MJ. Fluorescent sensors for rapid monitoring of intracellular cGMP. Nat Methods. 2006;3(1):23-25.

[221]   Honda A, Adams SR, Sawyer CL, Lev-Ram V, Tsien RY, Dostmann WR. Spatiotemporal dynamics of guanosine 3',5'-cyclic monophosphate revealed by a genetically encoded, fluorescent indicator. Proc Natl Acad Sci U S A. 2001;98(5):2437-2442.

[222]   Stangherlin A, Gesellchen F, Zoccarato A, Terrin A, Fields LA, Berrera M, et al. cGMP signals modulate cAMP levels in a compartment-specific manner to regulate catecholamine-dependent signaling in cardiac myocytes. Circ Res. 2011;108(8):929-939.

[223]   Couto A, Oda S, Nikolaev VO, Soltesz Z, de Bono M. In vivo genetic dissection of O2-evoked cGMP dynamics in a Caenorhabditis elegans gas sensor. Proc Natl Acad Sci U S A. 2013;110(35):E3301-3310.

[224]   Russwurm M, Mullershausen F, Friebe A, Jager R, Russwurm C, Koesling D. Design of fluorescence resonance energy transfer (FRET)-based cGMP indicators: a systematic approach. Biochem J. 2007;407(1):69-77.

[225]   Thunemann M, Wen L, Hillenbrand M, Vachaviolos A, Feil S, Ott T, et al. Transgenic mice for cGMP imaging. Circ Res. 2013;113(4):365-371.

[226] Herget S, Lohse MJ, Nikolaev VO. Real-time monitoring of phosphodiesterase inhibition in intact cells. Cell Signal. 2008;20(8):1423-1431.

[227] Jäger R, Schwede F, Genieser HG, Koesling D, Russwurm M. Activation of PDE2 and PDE5 by specific GAF ligands: delayed activation of PDE5. Br J Pharmacol. 2010;161(7):1645-1660.

[228] Subramanian H, Froese A, Jonsson P, Schmidt H, Gorelik J, Nikolaev VO. Distinct submembrane localisation compartmentalises cardiac NPR1 and NPR2 signalling to cGMP. Nat Commun. 2018;9(1):2446.

[229] Ros O, Zagar Y, Ribes S, Baudet S, Loulier K, Couvet S, et al. SponGee: A Genetic Tool for Subcellular and Cell-Specific cGMP Manipulation. Cell Rep. 2019;27(13):4003-4012 e4006.

[230] Biswas KH, Sopory S, Visweswariah SS. The GAF domain of the cGMP-binding, cGMP-specific phosphodiesterase (PDE5) is a sensor and a sink for cGMP. Biochemistry. 2008;47(11):3534-3543.

[231] Nausch LW, Ledoux J, Bonev AD, Nelson MT, Dostmann WR. Differential patterning of cGMP in vascular smooth muscle cells revealed by single GFP-linked biosensors. Proc Natl Acad Sci U S A. 2008;105(1):365-370.

[232] Bhargava Y, Hampden-Smith K, Chachlaki K, Wood KC, Vernon J, Allerston CK, et al. Improved genetically-encoded, FlincG-type fluorescent biosensors for neural cGMP imaging. Front Mol Neurosci. 2013;6:26.

[233] Woldemariam S, Nagpal J, Hill T, Li J, Schneider MW, Shankar R, et al. Using a Robust and Sensitive GFP-Based cGMP Sensor for Real-Time Imaging in Intact Caenorhabditis elegans. Genetics. 2019;213(1):59-77.

[234] Niino Y, Hotta K, Oka K. Blue fluorescent cGMP sensor for multiparameter fluorescence imaging. PLoS One. 2010;5(2):e9164.

[235] Matsuda S, Harada K, Ito M, Takizawa M, Wongso D, Tsuboi T, et al. Generation of a cGMP Indicator with an Expanded Dynamic Range by Optimization of Amino Acid Linkers between a Fluorescent Protein and PDE5α. ACS Sensors. 2017;2(1):46-51.

[236] Calebiro D, Nikolaev VO, Gagliani MC, de Filippis T, Dees C, Tacchetti C, et al. Persistent cAMP-signals triggered by internalized G-protein-coupled receptors. PLoS Biol. 2009;7(8):e1000172.

[237] Gerard GF, Fox DK, Nathan M, D'Alessio JM. Reverse Transcriptase. Mol Biotechnol. 1997;8(1):61-77.

[238] Garibyan L, Avashia N. Polymerase chain reaction. J Invest Dermatol. 2013;133(3):1-4.

[239] Tajadini M, Panjehpour M, Javanmard SH. Comparison of SYBR Green and TaqMan methods in quantitative real-time polymerase chain reaction analysis of four adenosine receptor subtypes. Adv Biomed Res. 2014;3:85.

[240] Livak KJ, Schmittgen TD. Analysis of relative gene expression data using real-time quantitative PCR and the 2(-Delta Delta C(T)) Method. Methods. 2001;25(4):402-408.

[241] Nolan T, Hands RE, Bustin SA. Quantification of mRNA using real-time RT-PCR. Nat Protoc. 2006;1(3):1559-1582.

[242] Moein S, Javanmard SH, Abedi M, Izadpanahi MH, Gheisari Y. Identification of Appropriate Housekeeping Genes for Gene Expression Analysis in Long-term Hypoxia-treated Kidney Cells. Adv Biomed Res. 2017;6:15.

[243] Julian GS, Oliveira RW, Tufik S, Chagas JR. Analysis of the stability of housekeeping gene expression in the left cardiac ventricle of rats submitted to chronic intermittent hypoxia. J Bras Pneumol. 2016;42(3):211-214.

[244] Louch WE, Sheehan KA, Wolska BM. Methods in cardiomyocyte isolation, culture, and gene transfer. J Mol Cell Cardiol. 2011;51(3):288-298.

[245] Sambrook J, Russell DW. SDS-Polyacrylamide Gel Electrophoresis of Proteins. CSH Protoc. 2006;2006(4).

[246] Schneider-Poetsch T, Ju J, Eyler DE, Dang Y, Bhat S, Merrick WC, et al. Inhibition of eukaryotic translation elongation by cycloheximide and lactimidomycin. Nat Chem Biol. 2010;6(3):209-217.

[247]   Allen M, Millett P, Dawes E, Rushton N. Lactate dehydrogenase activity as a rapid and sensitive test for the quantification of cell numbers in vitro. Clin Mater. 1994;16(4):189-194.

[248]   Sendoel A, Hengartner MO. Apoptotic Cell Death Under Hypoxia. Physiology. 2014;29(3):168-176.

[249]   Marshall KD, Edwards MA, Krenz M, Davis JW, Baines CP. Proteomic mapping of proteins released during necrosis and apoptosis from cultured neonatal cardiac myocytes. Am J Physiol Cell Physiol. 2014;306(7):C639-647.

[250]   Börner S, Schwede F, Schlipp A, Berisha F, Calebiro D, Lohse MJ, et al. FRET measurements of intracellular cAMP concentrations and cAMP analog permeability in intact cells. Nat Protoc. 2011;6(4):427-438.

[251]   Bensley JG, De Matteo R, Harding R, Black MJ. Three-dimensional direct measurement of cardiomyocyte volume, nuclearity, and ploidy in thick histological sections. Sci Rep. 2016;6(1):23756.

[252]   Stasch JP, Schmidt PM, Nedvetsky PI, Nedvetskaya TY, H SA, Meurer S, et al. Targeting the heme-oxidized nitric oxide receptor for selective vasodilatation of diseased blood vessels. J Clin Invest. 2006;116(9):2552-2561.

[253]   Groneberg D, Konig P, Wirth A, Offermanns S, Koesling D, Friebe A. Smooth muscle-specific deletion of nitric oxide-sensitive guanylyl cyclase is sufficient to induce hypertension in mice. Circulation. 2010;121(3):401-409.

[254]   Borner S, Schwede F, Schlipp A, Berisha F, Calebiro D, Lohse MJ, et al. FRET measurements of intracellular cAMP concentrations and cAMP analog permeability in intact cells. Nat Protoc. 2011;6(4):427-438.

[255]   Ding B, Abe J, Wei H, Huang Q, Walsh RA, Molina CA, et al. Functional role of phosphodiesterase 3 in cardiomyocyte apoptosis: implication in heart failure. Circulation. 2005;111(19):2469-2476.

[256]   Ding B, Abe J, Wei H, Xu H, Che W, Aizawa T, et al. A positive feedback loop of phosphodiesterase 3 (PDE3) and inducible cAMP early repressor (ICER) leads to cardiomyocyte apoptosis. Proc Natl Acad Sci U S A. 2005;102(41):14771-14776.

[257]   Oikawa M, Wu M, Lim S, Knight WE, Miller CL, Cai Y, et al. Cyclic nucleotide phosphodiesterase 3A1 protects the heart against ischemia-reperfusion injury. J Mol Cell Cardiol. 2013;64:11-19.

[258]   Shinoda H, Shannon M, Nagai T. Fluorescent Proteins for Investigating Biological Events in Acidic Environments. Int J Mol Sci. 2018;19(6).

[259]   Betolngar DB, Erard M, Pasquier H, Bousmah Y, Diop-Sy A, Guiot E, et al. pH sensitivity of FRET reporters based on cyan and yellow fluorescent proteins. Anal Bioanal Chem. 2015;407(14):4183-4193.

[260]   Saenz de Tejada I, Angulo J, Cuevas P, Fernandez A, Moncada I, Allona A, et al. The phosphodiesterase inhibitory selectivity and the in vitro and in vivo potency of the new PDE5 inhibitor vardenafil. Int J Impot Res. 2001;13(5):282-290.

[261]   Chen T, Vunjak-Novakovic G. In vitro Models of Ischemia-Reperfusion Injury. Regen Eng Transl Med. 2018;4(3):142-153.

[262]   Portal L, Martin V, Assaly R, d'Anglemont de Tassigny A, Michineau S, Berdeaux A, et al. A model of hypoxia-reoxygenation on isolated adult mouse cardiomyocytes: characterization, comparison with ischemia-reperfusion, and application to the cardioprotective effect of regular treadmill exercise. J Cardiovasc Pharmacol Ther. 2013;18(4):367-375.

[263]   Cao X, Wang X, Ling Y, Song X, Yang P, Liu Y, et al. Comparison of the degree of autophagy in neonatal rat cardiomyocytes and H9c2 cells exposed to hypoxia/reoxygenation. Clin Lab. 2014;60(5):809-814.

[264]   Chang G, Zhang D, Liu J, Zhang P, Ye L, Lu K, et al. Exenatide protects against hypoxia/reoxygenation-induced apoptosis by improving mitochondrial function in H9c2 cells. Exp Biol Med (Maywood). 2014;239(4):414-422.

[265] Bonavita F, Stefanelli C, Giordano E, Columbaro M, Facchini A, Bonafe F, et al. H9c2 cardiac myoblasts undergo apoptosis in a model of ischemia consisting of serum deprivation and hypoxia: inhibition by PMA. FEBS Lett. 2003;536(1-3):85-91.

[266] Teixeira G, Abrial M, Portier K, Chiari P, Couture-Lepetit E, Tourneur Y, et al. Synergistic protective effect of cyclosporin A and rotenone against hypoxia-reoxygenation in cardiomyocytes. J Mol Cell Cardiol. 2013;56:55-62.

[267] Kuznetsov AV, Javadov S, Sickinger S, Frotschnig S, Grimm M. H9c2 and HL-1 cells demonstrate distinct features of energy metabolism, mitochondrial function and sensitivity to hypoxia-reoxygenation. Biochim Biophys Acta. 2015;1853(2):276-284.

[268] Bergmann O, Bhardwaj RD, Bernard S, Zdunek S, Barnabe-Heider F, Walsh S, et al. Evidence for cardiomyocyte renewal in humans. Science. 2009;324(5923):98-102.

[269] Riva E, Hearse DJ. Age-dependent changes in myocardial susceptibility to ischemic injury. Cardioscience. 1993;4(2):85-92.

[270] Ostadalova I, Ostadal B, Kolar F, Parratt JR, Wilson S. Tolerance to ischaemia and ischaemic preconditioning in neonatal rat heart. J Mol Cell Cardiol. 1998;30(4):857-865.

[271] Shang L, Ananthakrishnan R, Li Q, Quadri N, Abdillahi M, Zhu Z, et al. RAGE modulates hypoxia/reoxygenation injury in adult murine cardiomyocytes via JNK and GSK-3beta signaling pathways. PLoS One. 2010;5(4):e10092.

[272] Kang PM, Haunstetter A, Aoki H, Usheva A, Izumo S. Morphological and Molecular Characterization of Adult Cardiomyocyte Apoptosis During Hypoxia and Reoxygenation. Circ Res. 2000;87(2):118-125.

[273] Webster KA, Discher DJ, Kaiser S, Hernandez O, Sato B, Bishopric NH. Hypoxia-activated apoptosis of cardiac myocytes requires reoxygenation or a pH shift and is independent of p53. J Clin Invest. 1999;104(3):239-252.

[274] Griffiths EJ, Ocampo CJ, Savage JS, Rutter GA, Hansford RG, Stern MD, et al. Mitochondrial calcium transporting pathways during hypoxia and reoxygenation in single rat cardiomyocytes. Cardiovasc Res. 1998;39(2):423-433.

[275] Kim HS, Hwang KC, Park WK. Cardioprotection via modulation of calcium homeostasis by thiopental in hypoxia-reoxygenated neonatal rat cardiomyocytes. Yonsei Med J. 2010;51(2):187-196.

[276] Lu FH, Tian Z, Zhang WH, Zhao YJ, Li HL, Ren H, et al. Calcium-sensing receptors regulate cardiomyocyte Ca2+ signaling via the sarcoplasmic reticulum-mitochondrion interface during hypoxia/reoxygenation. J Biomed Sci. 2010;17:50.

[277] Kass-Eisler A, Falck-Pedersen E, Alvira M, Rivera J, Buttrick PM, Wittenberg BA, et al. Quantitative determination of adenovirus-mediated gene delivery to rat cardiac myocytes in vitro and in vivo. Proc Natl Acad Sci U S A. 1993;90(24):11498-11502.

[278] Decker ML, Behnke-Barclay M, Cook MG, La Pres JJ, Clark WA, Decker RS. Cell shape and organization of the contractile apparatus in cultured adult cardiac myocytes. J Mol Cell Cardiol. 1991;23(7):817-832.

[279] Pavlovic D, McLatchie LM, Shattock MJ. The rate of loss of T-tubules in cultured adult ventricular myocytes is species dependent. Exp Physiol. 2010;95(4):518-527.

[280] Semenza GL. HIF-1: mediator of physiological and pathophysiological responses to hypoxia. J Appl Physiol (1985). 2000;88(4):1474-1480.

[281] Masoud GN, Li W. HIF-1alpha pathway: role, regulation and intervention for cancer therapy. Acta Pharm Sin B. 2015;5(5):378-389.

[282] Salceda S, Caro J. Hypoxia-inducible factor 1alpha (HIF-1alpha) protein is rapidly degraded by the ubiquitin-proteasome system under normoxic conditions. Its stabilization by hypoxia depends on redox-induced changes. J Biol Chem. 1997;272(36):22642-22647.

[283] Moroz E, Carlin S, Dyomina K, Burke S, Thaler HT, Blasberg R, et al. Real-time imaging of HIF-1alpha stabilization and degradation. PLoS One. 2009;4(4):e5077.

[284] Marxsen JH, Stengel P, Doege K, Heikkinen P, Jokilehto T, Wagner T, et al. Hypoxia-inducible factor-1 (HIF-1) promotes its degradation by induction of HIF-alpha-prolyl-4-hydroxylases. Biochem J. 2004;381(Pt 3):761-767.

[285] Serocki M, Bartoszewska S, Janaszak-Jasiecka A, Ochocka RJ, Collawn JF, Bartoszewski R. miRNAs regulate the HIF switch during hypoxia: a novel therapeutic target. Angiogenesis. 2018;21(2):183-202.

[286] Koh MY, Powis G. Passing the baton: the HIF switch. Trends Biochem Sci. 2012;37(9):364-372.

[287] Lin Q, Cong X, Yun Z. Differential hypoxic regulation of hypoxia-inducible factors 1alpha and 2alpha. Mol Cancer Res. 2011;9(6):757-765.

[288] Vandeput F, Wolda SL, Krall J, Hambleton R, Uher L, McCaw KN, et al. Cyclic nucleotide phosphodiesterase PDE1C1 in human cardiac myocytes. J Biol Chem. 2007;282(45):32749-32757.

[289] Vandeput F, Krall J, Ockaili R, Salloum FN, Florio V, Corbin JD, et al. cGMP-hydrolytic activity and its inhibition by sildenafil in normal and failing human and mouse myocardium. J Pharmacol Exp Ther. 2009;330(3):884-891.

[290] Sanada S, Kitakaze M, Papst PJ, Asanuma H, Node K, Takashima S, et al. Cardioprotective effect afforded by transient exposure to phosphodiesterase III inhibitors: the role of protein kinase A and p38 mitogen-activated protein kinase. Circulation. 2001;104(6):705-710.

[291] Lochner A, Genade S, Tromp E, Podzuweit T, Moolman JA. Ischemic Preconditioning and the &#x3b2;-Adrenergic Signal Transduction Pathway. Circulation. 1999;100(9):958-966.

[292] Tong H, Bernstein D, Murphy E, Steenbergen C. The role of beta-adrenergic receptor signaling in cardioprotection. FASEB J. 2005;19(8):983-985.

[293] Fukasawa M, Nishida H, Sato T, Miyazaki M, Nakaya H. 6-[4-(1-Cyclohexyl-1H-tetrazol-5-yl)butoxy]-3,4-dihydro-2-(1H)quinolinone (cilostazol), a phosphodiesterase type 3 inhibitor, reduces infarct size via activation of mitochondrial Ca2+-activated K+ channels in rabbit hearts. J Pharmacol Exp Ther. 2008;326(1):100-104.

[294] Costa AD, Pierre SV, Cohen MV, Downey JM, Garlid KD. cGMP signalling in pre- and post-conditioning: the role of mitochondria. Cardiovasc Res. 2008;77(2):344-352.

[295] Costa ADT, Pierre SV, Cohen MV, Downey JM, Garlid KD. cGMP signalling in pre- and post-conditioning: the role of mitochondria. Cardiovasc Res. 2007;77(2):344-352.

[296] Oldenburg O, Qin Q, Krieg T, Yang X-M, Philipp S, Critz SD, et al. Bradykinin induces mitochondrial ROS generation via NO, cGMP, PKG, and mitoKATP channel opening and leads to cardioprotection. Am J Physiol Heart Circ Physiol. 2004;286(1):H468-H476.

[297] Costa AD, Garlid KD, West IC, Lincoln TM, Downey JM, Cohen MV, et al. Protein kinase G transmits the cardioprotective signal from cytosol to mitochondria. Circ Res. 2005;97(4):329-336.

[298] Kang PM, Haunstetter A, Aoki H, Usheva A, Izumo S. Morphological and Molecular Characterization of Adult Cardiomyocyte Apoptosis During Hypoxia and Reoxygenation. Circulation Research. 2000;87(2):118-125.

[299] Yuan Y, Wang Y-y, Liu X, Luo B, Zhang L, Zheng F, et al. KPC1 alleviates hypoxia/reoxygenation-induced apoptosis in rat cardiomyocyte cells though BAX degradation. Journal of Cellular Physiology. 2019;234(12):22921-22934.

[300] Nunes AR, Sample V, Xiang YK, Monteiro EC, Gauda E, Zhang J. Effect of oxygen on phosphodiesterases (PDE) 3 and 4 isoforms and PKA activity in the superior cervical ganglia. Adv Exp Med Biol. 2012;758:287-294.

[301] Ghorbel MT, Cherif M, Jenkins E, Mokhtari A, Kenny D, Angelini GD, et al. Transcriptomic analysis of patients with tetralogy of Fallot reveals the effect of chronic hypoxia on myocardial gene expression. J Thorac Cardiovasc Surg. 2010;140(2):337-345 e326.

[302] Zhao CY, Greenstein JL, Winslow RL. Roles of phosphodiesterases in the regulation of the cardiac cyclic nucleotide cross-talk signaling network. J Mol Cell Cardiol. 2016;91:215-227.

[303] Tawa M, Geddawy A, Shimosato T, Iwasaki H, Imamura T, Okamura T. Soluble guanylate cyclase redox state under hypoxia or hypoxia/reoxygenation in isolated monkey coronary arteries. J Pharmacol Sci. 2014;125(2):169-175.

[304] Gerassimou C, Kotanidou A, Zhou Z, Simoes DC, Roussos C, Papapetropoulos A. Regulation of the expression of soluble guanylyl cyclase by reactive oxygen species. Br J Pharmacol. 2007;150(8):1084-1091.

[305] Mergia E, Friebe A, Dangel O, Russwurm M, Koesling D. Spare guanylyl cyclase NO receptors ensure high NO sensitivity in the vascular system. J Clin Invest. 2006;116(6):1731-1737.

[306] Xu X, Wang S, Liu J, Dou D, Liu L, Chen Z, et al. Hypoxia induces downregulation of soluble guanylyl cyclase beta1 by miR-34c-5p. J Cell Sci. 2012;125(Pt 24):6117-6126.

[307] Chen Y-F, Durand J, Claycomb WC. Hypoxia Stimulates Atrial Natriuretic Peptide Gene Expression in Cultured Atrial Cardiocytes. Hypertension. 1997;29(1):75-82.

[308] Chun YS, Hyun JY, Kwak YG, Kim IS, Kim CH, Choi E, et al. Hypoxic activation of the atrial natriuretic peptide gene promoter through direct and indirect actions of hypoxia-inducible factor-1. Biochem J. 2003;370(Pt 1):149-157.

[309] Weidemann A, Klanke B, Wagner M, Volk T, Willam C, Wiesener MS, et al. Hypoxia, via stabilization of the hypoxia-inducible factor HIF-1alpha, is a direct and sufficient stimulus for brain-type natriuretic peptide induction. Biochem J. 2008;409(1):233-242.

[310] Motayagheni N. Modified Langendorff technique for mouse heart cannulation: Improved heart quality and decreased risk of ischemia. MethodsX. 2017;4:508-512.

[311] Zapata-Hommer O, Griesbeck O. Efficiently folding and circularly permuted variants of the Sapphire mutant of GFP. BMC Biotechnol. 2003;3:5.

[312] Campbell RE, Tour O, Palmer AE, Steinbach PA, Baird GS, Zacharias DA, et al. A monomeric red fluorescent protein. Proc Natl Acad Sci U S A. 2002;99(12):7877-7882.

[313] Baird GS, Zacharias DA, Tsien RY. Biochemistry, mutagenesis, and oligomerization of DsRed, a red fluorescent protein from coral. Proc Natl Acad Sci U S A. 2000;97(22):11984-11989.

[314] Lu HR, Marien R, Saels A, De Clerck F. Species plays an important role in drug-induced prolongation of action potential duration and early afterdepolarizations in isolated Purkinje fibers. J Cardiovasc Electrophysiol. 2001;12(1):93-102.

[315] Brandenburg S, Arakel EC, Schwappach B, Lehnart SE. The molecular and functional identities of atrial cardiomyocytes in health and disease. Biochim Biophys Acta. 2016;1863(7, Part B):1882-1893.

[316] Barth AS, Merk S, Arnoldi E, Zwermann L, Kloos P, Gebauer M, et al. Functional profiling of human atrial and ventricular gene expression. Pflugers Arch. 2005;450(4):201-208.

[317] Tabibiazar R, Wagner RA, Liao A, Quertermous T. Transcriptional profiling of the heart reveals chamber-specific gene expression patterns. Circ Res. 2003;93(12):1193-1201.

[318] Anderson RH, Cook AC. The structure and components of the atrial chambers. Europace. 2007;9 Suppl 6:vi3-9.

[319] Smorodinova N, Lantova L, Blaha M, Melenovsky V, Hanzelka J, Pirk J, et al. Bioptic Study of Left and Right Atrial Interstitium in Cardiac Patients with and without Atrial Fibrillation: Interatrial but Not Rhythm-Based Differences. PLoS One. 2015;10(6):e0129124.

[320] Lomax AE, Kondo CS, Giles WR. Comparison of time- and voltage-dependent K+ currents in myocytes from left and right atria of adult mice. Am J Physiol Heart Circ Physiol. 2003;285(5):H1837-1848.

[321] Kahr PC, Piccini I, Fabritz L, Greber B, Scholer H, Scheld HH, et al. Systematic analysis of gene expression differences between left and right atria in different mouse strains and in human atrial tissue. PLoS One. 2011;6(10):e26389.

[322] Nishida K, Michael G, Dobrev D, Nattel S. Animal models for atrial fibrillation: clinical insights and scientific opportunities. EP Europace. 2009;12(2):160-172.

[323] Milan DJ, MacRae CA. Animal models for arrhythmias. Cardiovasc Res. 2005;67(3):426-437.

[324] Riley G, Syeda F, Kirchhof P, Fabritz L. An Introduction to Murine Models of Atrial Fibrillation. Frontiers in physiology. 2012;3:296.

[325] Knobloch K, Brendel J, Peukert S, Rosenstein B, Busch AE, Wirth KJ. Electrophysiological and antiarrhythmic effects of the novel I(Kur) channel blockers, S9947 and S20951, on left vs. right pig atrium in vivo in comparison with the I(Kr) blockers dofetilide, azimilide, d,l-sotalol and ibutilide. Naunyn Schmiedebergs Arch Pharmacol. 2002;366(5):482-487.

[326] Baró I. Atrial fibrillation: Is NO an answer for refractoriness? Cardiovasc Res. 2006;72(1):7-8.

[327] Nunez L, Vaquero M, Gomez R, Caballero R, Mateos-Caceres P, Macaya C, et al. Nitric oxide blocks hKv1.5 channels by S-nitrosylation and by a cyclic GMP-dependent mechanism. Cardiovasc Res. 2006;72(1):80-89.

[328] Rubart M, Zipes DP. NO Hope for Patients With Atrial Fibrillation. Circulation. 2002;106(22):2764-2766.

[329] Huang CX, Liu Y, Xia WF, Tang YH, Huang H. Oxidative stress: a possible pathogenesis of atrial fibrillation. Med Hypotheses. 2009;72(4):466-467.

[330] Xie W, Santulli G, Reiken SR, Yuan Q, Osborne BW, Chen B-X, et al. Mitochondrial oxidative stress promotes atrial fibrillation. Sci Rep. 2015;5(1):11427.

[331] Mihm MJ, Yu F, Carnes CA, Reiser PJ, McCarthy PM, Van Wagoner DR, et al. Impaired myofibrillar energetics and oxidative injury during human atrial fibrillation. Circulation. 2001;104(2):174-180.

[332] Negi S, Shukrullah I, Veledar E, Bloom HL, Jones DP, Dudley SC. Statin therapy for the prevention of atrial fibrillation trial (SToP AF trial). J Cardiovasc Electrophysiol. 2011;22(4):414-419.

[333] Yang K-C, Dudley SC. Oxidative Stress and Atrial Fibrillation. Circulation. 2013;128(16):1724-1726.

[334] Sovari AA, Rutledge CA, Jeong E-M, Dolmatova E, Arasu D, Liu H, et al. Mitochondria oxidative stress, connexin43 remodeling, and sudden cardiac death. Circ Arrhythm Electrophysiol. 2013;6(3):623-631.

[335] Purohit A, Rokita AG, Guan X, Chen B, Koval OM, Voigt N, et al. Oxidized Ca(2+)/calmodulin-dependent protein kinase II triggers atrial fibrillation. Circulation. 2013;128(16):1748-1757.

[336] Bice JS, Burley DS, Baxter GF. Novel approaches and opportunities for cardioprotective signaling through 3',5'-cyclic guanosine monophosphate manipulation. J Cardiovasc Pharmacol Ther. 2014;19(3):269-282.

[337] Jansen H, Mackasey M, Moghtadaei M, Liu Y, Kaur J, Egom E, et al. NPR-C (Natriuretic Peptide Receptor-C) Modulates the Progression of Angiotensin II–Mediated Atrial Fibrillation and Atrial Remodeling in Mice. Circulation: Arrhythmia and Electrophysiology. 2019;12.

[338] Egom EE, Vella K, Hua R, Jansen HJ, Moghtadaei M, Polina I, et al. Impaired sinoatrial node function and increased susceptibility to atrial fibrillation in mice lacking natriuretic peptide receptor C. J Physiol. 2015;593(5):1127-1146.

[339] Nunez DJ, Dickson MC, Brown MJ. Natriuretic peptide receptor mRNAs in the rat and human heart. J Clin Invest. 1992;90(5):1966-1971.

[340] Fan D, Bryan PM, Antos LK, Potthast RJ, Potter LR. Down-regulation does not mediate natriuretic peptide-dependent desensitization of natriuretic peptide receptor (NPR)-A or NPR-B: guanylyl cyclase-linked natriuretic peptide receptors do not internalize. Mol Pharmacol. 2005;67(1):174-183.

[341] Schröter J, Zahedi RP, Hartmann M, Gassner B, Gazinski A, Waschke J, et al. Homologous desensitization of guanylyl cyclase A, the receptor for atrial natriuretic peptide, is associated with a complex phosphorylation pattern. FEBS J. 2010;277(11):2440-2453.

[342] Müller D, Cortes-Dericks L, Budnik LT, Brunswig-Spickenheier Br, Pancratius M, Speth RC, et al. Homologous and Lysophosphatidic Acid-Induced Desensitization of the Atrial Natriuretic Peptide Receptor, Guanylyl Cyclase-A, in MA-10 Leydig Cells. Endocrinology. 2006;147(6):2974-2985.

[343] Patton KK, Ellinor PT, Heckbert SR, Christenson RH, DeFilippi C, Gottdiener JS, et al. N-terminal pro-B-type natriuretic peptide is a major predictor of the development of atrial fibrillation: the Cardiovascular Health Study. Circulation. 2009;120(18):1768-1774.

[344]    Richards M, Di Somma S, Mueller C, Nowak R, Peacock WF, Ponikowski P, et al. Atrial fibrillation impairs the diagnostic performance of cardiac natriuretic peptides in dyspneic patients: results from the BACH Study (Biomarkers in ACute Heart Failure). JACC Heart Fail. 2013;1(3):192-199.

[345]    Wozakowska-Kaplon B. Effect of sinus rhythm restoration on plasma brain natriuretic peptide in patients with atrial fibrillation. Am J Cardiol. 2004;93(12):1555-1558.

[346]    Rossi A, Enriquez-Sarano M, Burnett JC, Lerman A, Abel MD, Seward JB. Natriuretic peptide levels in atrial fibrillation: A prospective hormonal and Doppler-echocardiographic study. J Am Coll Cardiol. 2000;35(5):1256-1262.

[347]    Rivet-Bastide M, Vandecasteele G, Hatem S, Verde I, Benardeau A, Mercadier JJ, et al. cGMP-stimulated cyclic nucleotide phosphodiesterase regulates the basal calcium current in human atrial myocytes. J Clin Invest. 1997;99(11):2710-2718.

[348]    Kirstein M, Rivet-Bastide M, Hatem S, Benardeau A, Mercadier JJ, Fischmeister R. Nitric oxide regulates the calcium current in isolated human atrial myocytes. J Clin Invest. 1995;95(2):794-802.

[349]    Berk E, Christ T, Schwarz S, Ravens U, Knaut M, Kaumann AJ. In permanent atrial fibrillation, PDE3 reduces force responses to 5-HT, but PDE3 and PDE4 do not cause the blunting of atrial arrhythmias. Br J Pharmacol. 2016;173(16):2478-2489.

[350]    Molina CE, Leroy J, Richter W, Xie M, Scheitrum C, Lee IO, et al. Cyclic adenosine monophosphate phosphodiesterase type 4 protects against atrial arrhythmias. J Am Coll Cardiol. 2012;59(24):2182-2190.

[351]    Mishra M, Wagner MB, Wang Y-g, Joyner RW, Kumar R. Expression of cGMP-dependent Protein Kinase in Human Atrium. J Mol Cell Cardiol. 2001;33(8):1467-1476.

[352]    Wang Y-g, Wagner MB, Joyner RW, Kumar R. cGMP-dependent protein kinase mediates stimulation of L-type calcium current by cGMP in rabbit atrial cells. Cardiovasc Res. 2000;48(2):310-322.

[353]    Yue L, Feng J, Gaspo R, Li G-R, Wang Z, Nattel S. Ionic Remodeling Underlying Action Potential Changes in a Canine Model of Atrial Fibrillation. Circulation Research. 1997;81(4):512-525.

[354]    Ling T-Y, Wang X-L, Chai Q, Lu T, Stulak JM, Joyce LD, et al. Regulation of cardiac CACNB2 by microRNA-499: Potential role in atrial fibrillation. BBA Clinical. 2017;7:78-84.

[355]    Van Wagoner DR, Pond AL, Lamorgese M, Rossie SS, McCarthy PM, Nerbonne JM. Atrial L-type Ca2+ currents and human atrial fibrillation. Circ Res. 1999;85(5):428-436.

[356]    Klein G, Schröder F, Vogler D, Schaefer A, Haverich A, Schieffer B, et al. Increased open probability of single cardiac L-type calcium channels in patients with chronic atrial fibrillation: Role of phosphatase 2A. Cardiovasc Res. 2003;59(1):37-45.

[357]    Hazard Pictograms [Internet].  [cited March 09 2020]. Available from: https://www.conceptdraw.com/How-To-Guide/hazard-pictograms.

# 5. Appendix

## 5.1 Chemicals categorized to GHS

**Table 5.1:** **Chemicals categorized according to GHS.** GHS, globally harmonized system of classification and labelling of chemicals.

| Chemical | H Statement | P Statement | Hazard Pictograms |
|---|---|---|---|
| Acrylamide (Rotiphorese Gel 40) | H302, H315, H317, H319, H340, H350, H361f, H372 | P201 P280.7 P301+P312.0 P302+P352.1 P305+P351+P338 P308+P313 i | 07, 08 |
| Agarose universal peqGold | | | |
| Agarose, Plaque GP | | | |
| Ammonium persulfate (APS) | H272, H302, H315, H317, H319, H334, H335 | P210, P280, P301 + P012 + P030, P302+P352, P305 + P351 + P338 | 02, 07, 08 |
| Ampuwa | | | |
| Antibiotic-Antimycotic, 100x | H317, H334, H360 | P201, P202, P261, P280, P284, P272, P302 + P352, P304 + P340, P333 + P313, P342 + P311, P308 + P313 | 07, 08 |
| ANP, human | | | |
| BAY 41-2272 | | | |
| BAY 58-2667 (Cinaciguat) | | | |
| BAY 60-7550 | | | |
| BAY 60-2770 | | | |
| β-Mercaptoethanol | H301 + H331, H310, H315, H317, H318, H361fd, H373, H410 | P201, P262, P280, P301 + P310 + P330, P302 + P352 + P310, P305 + P351 + P338 + P310 | 05, 06, 08, 09 |

| | | | |
|---|---|---|---|
| Blebbistatin | H302, H312, H315, H317, H319, H332, H335 | P280, P305 + P351 + P338 | 07 |
| Bovine serum albumin (BSA) | | | |
| Bromphenolblue | | | |
| 2,3-Butandione monoxime (BDM) | H302, H312, H315, H319, H332, H335 | P261, P264, P270, P271, P280, P301 + P312, P302 + P352, P304 + P312, P304 + P340, P305 + P351 + P338, P312, P321, P322, P330, P332 + P313, P337 + P313, P362, P363, P403 + P233, P405, P501 | 07 |
| CaCl$_2$ x 2 H$_2$O | H319 | P305 + P351 + P338 | 07 |
| cGMP Enzyme Immunoassay Kit | H302 + H312 + H332, H314 | P280, P305 + P351 + P338, P310 | 05, 07 |
| C-type natriuretic peptide (CNP) | | | |
| Cilostamide | | | |
| Collagenase Type 1 | H315, H317, H319, H335 | P280, P302 + P352, P304 + P340, P305 + P351 + P338 | 07 |
| CsCl | H361f | P201, P308 + P313 | 08 |
| Custodiol | | | |
| Cycloheximide | H300, H341, H360D, H411 | P201, P273, P301 + P310 + P330 | 06, 08, 09 |
| D-(+)-Glucose | | | |
| D-(+)-Saccharose | | | |
| Developer concentrate | H315, H318, H317, H341, H351, H400 | P273, P280, P305 + P351 + P338, P310, P333 + P313, P501 | 05, 07, 08, 09 |
| Dimethyl sulfoxide (DMSO) | | | |

| | | | |
|---|---|---|---|
| Direct PCR Tail | | | |
| DMEM | | | |
| DNA ladder, 100 bp | | | |
| DNase I | | | |
| dNTP mix | | | |
| EDTA | H332, H373 | P260, P271, P304 + P340, P312, P314, P501 | 07, 08 |
| EGTA | | | |
| Ethanol, Rotipuran, >99.8% p.a. | H225, H319 | P210, P233, P305 + P351 + P338 | 02, 07 |
| Ethanol, 70% vergällt | H225, H319 | P210, P233, P305 + P351 + P338 | 02, 07 |
| FCS, fetal calf serum | | | |
| Fixer concentrate | H290, H315, H318 | P280, P305 + P351 + P338, P310, P390, P501 | 05 |
| Forskolin | H312 | P280 | 07 |
| Glycerol | | | |
| Glycine | | | |
| GoTaq Hot Start Polymerase | | | |
| Green buffer (GoTaq reaction buffer) | | | |
| HCl, 37 % | H290, H314, H335 | P280, P303 + P361 + P353, P304 + P340, P305 + P351 + P338, P310 | 05, 07 |
| Heparin-Natrium | | | |
| HEPES | | | |
| IMDM | | | |
| Immersion liquid type F | H315, H412 | P273, P280, P302 + P352 | 07 |
| Insulin-Transferrin Selenium (ITS) X, 100 x | | | |

| | | | |
|---|---|---|---|
| Iscove Basal Medium | | | |
| Iscript cDNA synthesis kit | H319 | P280, P264, P305 + P351 + P338, P337 + P313 | 07 |
| 3-Isobutyl-1-Methylxanthine (IBMX) | H302 | P313, P301 + P330 + P331 | 07 |
| Isoflurane (Forene) | H336 | P261, P271, P303 + P340, P312, P403 + P233, P405, P501 | 07, 08 |
| KCl | | | |
| KHCO$_3$ | | | |
| KH$_2$PO$_4$ | H315, H319 | P264, P280, P305 + P351 + P338, P321, P332 + P313, P337 + P313 | 07 |
| Laminin | | | |
| LDH Glo™ Cytotoxicity Assay | H319, H412 | P264, P273, P280, P305 + P351 + P338, P337 + P313, P501 | 07 |
| L-Glutamine | | | |
| Liberase DH | H315, H319, H334 | P261, P264, P280, P285, P302 + P352, P304 + P341, P305 + P351 + P338, P332 + P313, P342 + P311, P362, P501 | 08 |
| Lipofectamine 2000 | | | |
| MEM without L-glutamine | | | |
| MEM with L-glutamine | | | |
| Methanol | H225, H301, H311, H331, H370 | P210.3, P270, P280.7, P303 + P361 + P353, P304 + P340, P308 + P311 | 02, 06, 08 |

| | | | |
|---|---|---|---|
| MgCl$_2$ x 6 H$_2$O | | | |
| MgSO$_4$ x 7 H$_2$O | | | |
| Midori Green | | P261, P280 | |
| Milchpulver | | | |
| Na$_2$HPO$_4$ x 2H$_2$O | | | |
| NaCl | | | |
| NaHCO$_3$ | | | |
| NaN$_3$ | H300 + H310 + H330, H373, H410 | P262, P273, P280, P301 + P310 + P330, P302 + P352 + P310, P304 + P340 + P310 | 06, 08, 09 |
| NaOH | H290, H314 | P233, P280, P303 + P361 + P353, P305 + P351 + P338, P310 | 05 |
| Na-Pyruvate | H317, H319 | P280, P302 + P352, P305 + P351 + P338 | 07 |
| NKH 477 | H300 | P264, P301 + P310 | 06 |
| ODQ | | | |
| PBS | | | |
| PCR purification kit Qiaquick | H225, H315, H319, H336 | P210, P280 | 02, 07 |
| Penicillin/Streptomycin | H302, H317, H361 | P280, P302 + P352, P308 + P313 | 07, 08 |
| Phosphatase inhibitor cocktail | | P280 | |
| Pierce BCA Protein assay kit | | | |
| Pierce Coomassie protein assay kit | H314, H371 | P280, P260, P304 + P340, P301 + P310, P331, P303 + P361 + P353, P305, P310 | 05, 08 |
| Polyethylene Glycol 8000 (PEG 8000) | | | |
| Ponceau S solution | | | |

| | | | |
|---|---|---|---|
| 2-Propanol | H225, H319, H336 | P210, P280, P305 + P351 + P338, P337 + P313 | 02, 07 |
| Protease inhibitor cocktail | H319 | P305 + P338 | 07 |
| Protease inhibitor w/o EDTA | H319 | P305 + P338 | 07 |
| Proteinase, bacterial | H302, H315, H318, H334, H335, H410 | P273, P280, P301 + P312 + P330, P302 + P352, P305 + P351 + P338 + P310 | 05, 07, 08, 09 |
| Proteinase K | H315, H319, H334, H335 | P261, P284, P305 + P351 + P338, P342 + P311, P405, P501 | 07, 08 |
| Protein Marker V peqGold | | | |
| QIAprep Spin Miniprep Kit | H225, H290, H315, H317, H319, H334, H336 | P210, P261, P280, P284, P304 + P340, P342 + P311 | 02, 05, 07, 08 |
| RNase ERASE | | | |
| RNase-free water | | | |
| RNeasy fibrous tissue mini kit | H226, H302, H314, H317, H318, H334, H412 | P210, P261, P264, P280, P284, P384, P304 + P340, P305 + P351 + P338 + P310, P342 + P311 | 02, 05, 07, 08 |
| RNeasy plus micro kit | H226, H302, H314, H318, H412 | P210, P264, P280, P305 + P351 + P338 + P30 | 02, 05, 07 |
| Rotor-Gene Multiplex PCR Kit | H361 | P280 | 08 |
| Rotor-Gene SYBR Green PCR Kit | | | |
| SDS, Sodium dodecyl sulfate | H315, H318, H335 | P261, P280, P302 + P352, P304 + P340 + P312, P305 + P351 + P338 + P310 | 05, 07 |

| SDS-Solution, 20 % | H315, H318 | P305 + P351 + P338 | 05 |
|---|---|---|---|
| Sildenafil | H315, H319, H335 | P261, P280, P304 + P340, P305 + P351 + P338, P405, P501 | 07 |
| SNAP, S-Nitroso-N-acetyl-DL-penicillamine | H315, H319, H335 | P261, P264, P280, P302 + P352, P304 + P340, P312, P332 + P313, P337 + P313, P362 + P364 | 07 |
| Sodium deoxycholate, SOD | H302, H412 | P273, P301 + P312 + P330 | 07 |
| SuperSignal West Pico PLUS | | | |
| TAE buffer | | | |
| Taurine | | | |
| TEMED, Tetramethylethylene diamine | H225, H302 + H332, H314 | P210, P280, P301 + P330 + P331, P303 + P361 + P353, P304 + P340 + P312, P305 + P351 + P338 | 02, 05, 07 |
| Tris-(hydroxymethyl)-aminomethan (TRIS) | | | |
| Triton X-100 Solution, 10% | H318 | P280, P305 + P351 + P338, P313 | 05 |
| Tween 20 | | | |
| Trypsin/EDTA-Solution | | | |
| Trypsin, 2.5% | H334 | P261, P284, P304 + P340, P342 + P311, P501 | 08 |

**Figure 5.1.1:** **Hazard Pictograms according to GHS.** Diagram adapted from [357].

## 5.2 Supplemental information for the project "Changes in mouse and human cardiomyocyte cGMP dynamics during hypoxic injury"

### 5.2.1 FRET-based cGMP measurements in human ventricular cardiomyocytes

FRET-based cGMP measurements with the NO-donor SNAP (100 µM) in human ventricular cardiomyocytes expressing the cGMP biosensor red-cGES-DE5 could show an increase in cytosolic cGMP upon NO-GC stimulation.
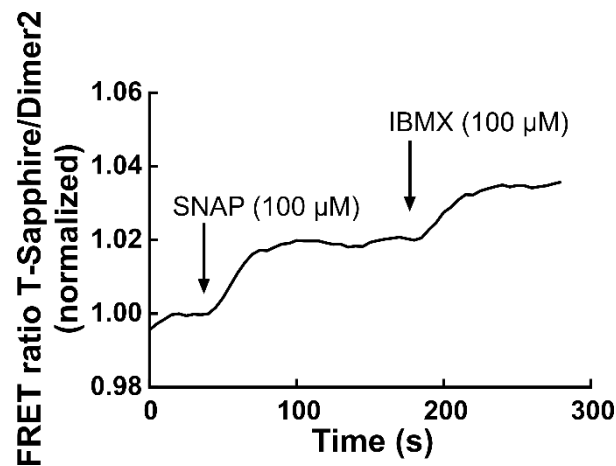


**Figure 5.2.1:   FRET-based cGMP measurements in human ventricular cardiomyocytes.** Human ventricular cardiomyocytes expressing the FRET-based cGMP biosensor red-cGES-DE5 were stimulated with NO-donor SNAP (100 µM) to stimulate NO-GC followed by the unspecific PDE inhibitor IBMX (100 µM). An increase in FRET ratio represents an increase in cytosolic cGMP.

### 5.2.2 Determination of basal cGMP levels in NO-GC knockout cardiomyocytes *via* FRET

cGMP concentrations in Normoxia or 4 h H/R treated NO-GC knockout cardiomyocytes were calculated *via* FRET as described previously [250].
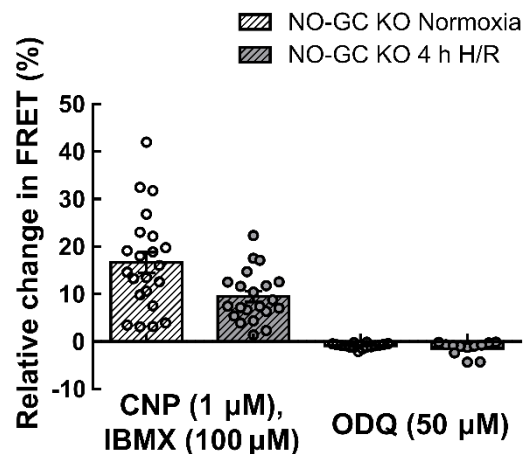


**Figure 5.2.2:   Determination of basal cGMP levels in NO-GC knockout cardiomyocytes *via* FRET.**   NO-GC knockout (NO-GC KO) cardiomyocytes exposed to normoxic control conditions

(Normoxia) or 4 h of hypoxia followed by 2 h of reoxygenation (4 h H/R) were used for FRET measurements. Maximal increase in cGMP levels was induced by stimulation of GC-B (CNP, 1 µM) with concurrent PDE inhibition (IBMX, 100 µM). Reduction in basal cGMP levels to minimum was reached by treating the cells with NO-GC inhibitor ODQ (50 µM). Quantification of FRET measurements are shown. Data are presented as mean ± SEM. FRET response in % in NO-GC KO Normoxia treated cells: CNP + IBMX response = 16.6 ± 2.2; ODQ response = -0.9 ± 0.1. FRET response in % in NO-GC KO 4 h H/R treated cells: CNP + IBMX response = 9.5 ± 1.2; ODQ response = -1.4 ± 0.4.

### 5.2.3 pH sensitivity of Epac1-camps sensor during anoxia

Langendorff experiments with hearts from transgenic Epac1-camps mice clearly showed that the Epac1-camps FRET biosensor is affected by changes in pH.
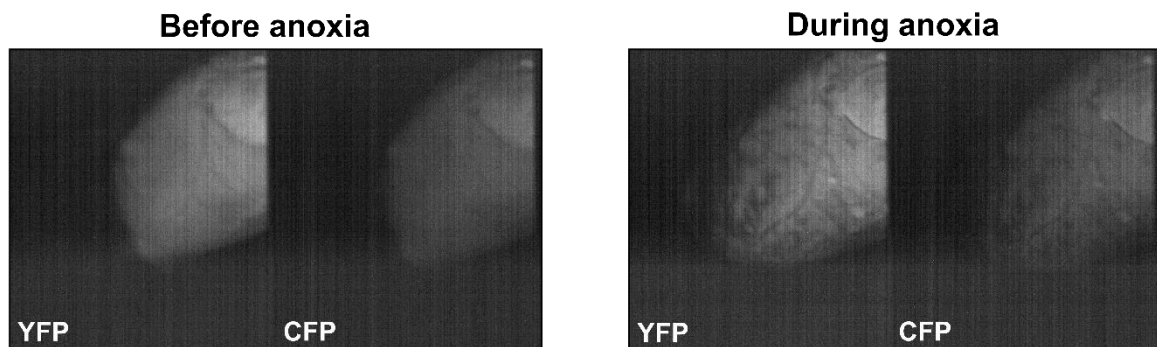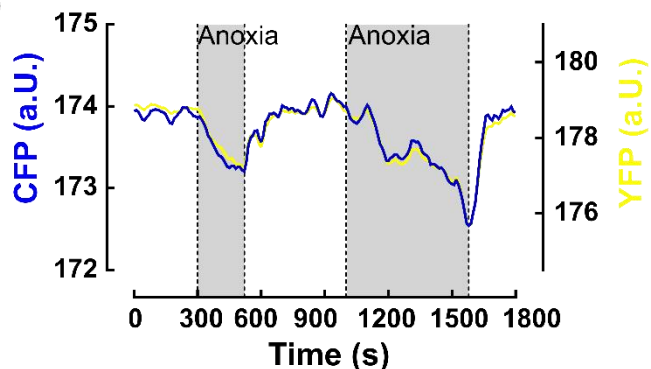


**Figure 5.2.3: pH sensitivity of Epac1-camps sensor during anoxia. A)** Influence of pH on Epac1-camps fluorescence in Langendorff perfused hearts before and during anoxia treatment. Impairment of the fluorescence in YFP and CFP can be seen by dark areas in the fluorescent images during anoxia. **B)** Epac1-camps biosensor fluorescence in CFP and YFP channels during anoxia treatment.

## 5.2.4 FRET response to PDE5 inhibitor Sildenafil in isolated human ventricular cardiomyocytes

FRET-based cGMP measurements with the selective PDE5 inhibitor Sildenafil (Sil, 100 nM and 1 µM) in human ventricular cardiomyocytes expressing the cGMP biosensor red-cGES-DE5 could raise cytosolic cGMP levels.
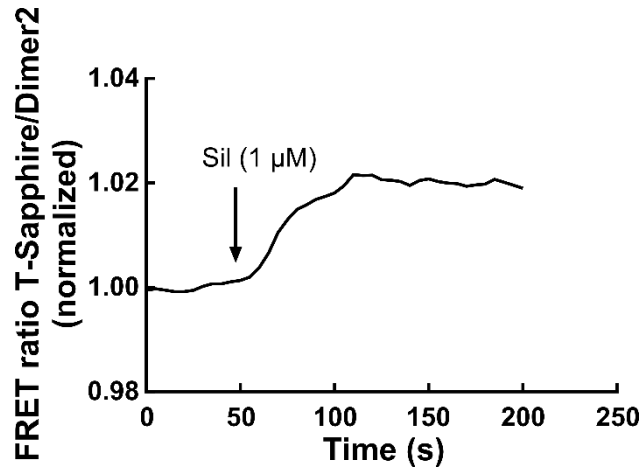


**Figure 5.2.4: FRET response to PDE5 inhibitor Sildenafil in human ventricular cardiomyocytes.** Human ventricular cardiomyocytes expressing the FRET-based cGMP biosensor red-cGES-DE5 were exposed to the PDE5-specific inhibitor Sildenafil (Sil, 1 µM). An increase in FRET ratio represents an increase in cytosolic cGMP.

## 5.3 Supplemental information for the project "cGMP signalling in the human atrium and its role in atrial fibrillation"

Stimulation of GC-A with ANP (100 nM, 1 µM) could raise cGMP levels in cardiomyocytes of SR RA but not in AF LA.
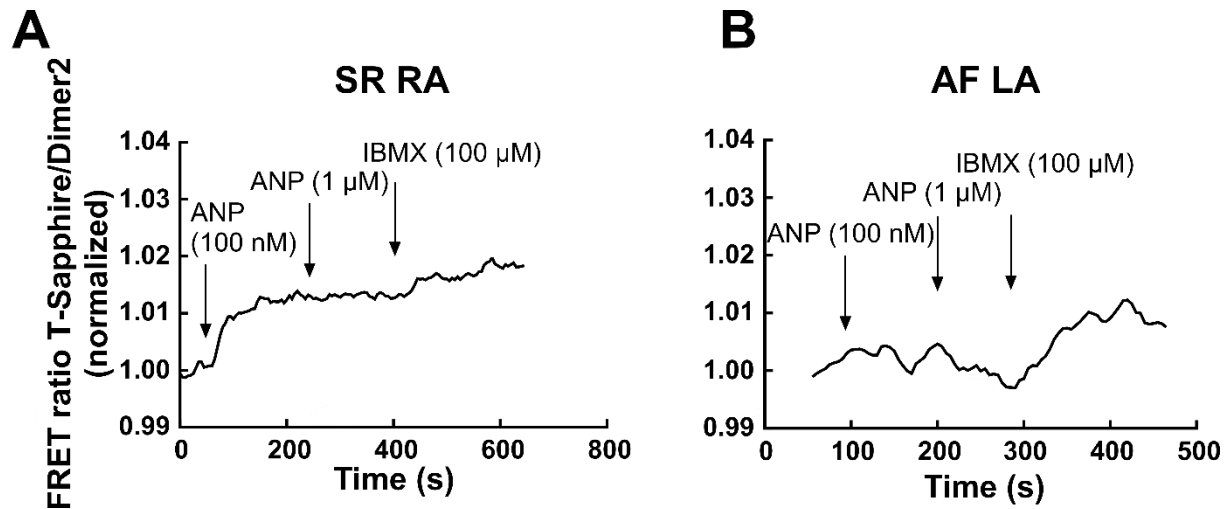


**Figure 5.3.1:** **Effects of NP-GC stimulation with ANP on FRET-based cGMP measurements in human atrial cardiomyocytes from right (RA) and left atrium (LA) of patients in sinus rhythm (SR) and with atrial fibrillation (AF).** Atrial cardiomyocytes were stimulated with the natriuretic peptide ANP (100 nM, 1 µM) to stimulate GC-A followed by the unselective PDE inhibitor IBMX (100 µM). Representative FRET traces from atrial cardiomyocytes from **A**) SR RA, and **B**) AF LA. An increase in FRET ratio represents an increase in cytosolic cGMP.

# Acknowledgements

## Affidavit

Hiermit versichere ich an Eides statt, die vorliegende Dissertation selbst verfasst und keine anderen als die angegebenen Hilfsmittel benutzt zu haben. Die eingereichte schriftliche Fassung entspricht der auf dem elektronischen Speichermedium. Ich versichere, dass diese Dissertation nicht in einem früheren Promotionsverfahren eingereicht wurde.

Hamburg, den 24.03.2020.